EFFECT OF TEMPERATURE ON MAGNETORHEOLOGICAL FLUID AND ITS PERFORMANCE IN MAGNETORHEOLOGICAL FLUID DAMPER AND MAGNETORHEOLOGICAL FLUID BRAKE

Thesis

Submitted in partial fulfillment of the requirements for the degree of

DOCTOR OF PHILOSOPHY

By

ASHOK KUMAR K

DEPARTMENT OF MECHANICAL ENGINEERING

NATIONAL INSTITUTE OF TECHNOLOGY KARNATAKA,

SURATHKAL, MANGALORE – 575025

APRIL 2023

EFFECT OF TEMPERATURE ON MAGNETORHEOLOGICAL FLUID AND ITS PERFORMANCE IN MAGNETORHEOLOGICAL FLUID DAMPER AND MAGNETORHEOLOGICAL FLUID BRAKE

Thesis

Submitted in partial fulfillment of the requirements for the degree of

DOCTOR OF PHILOSOPHY

By

ASHOK KUMAR K

(**177151ME027**)

Under the guidance of

Dr. Hemantha Kumar
Associate Professor

Dr. Arun M.
Associate Professor

DEPARTMENT OF MECHANICAL ENGINEERING

NATIONAL INSTITUTE OF TECHNOLOGY KARNATAKA,

SURATHKAL, MANGALORE – 575025

APRIL 2023

D E C L A R A T I O N

I hereby *declare* that the Research Thesis entitled "**Effect of Temperature on Magnetorheological Fluid and its Performance in Magnetorheological Fluid Damper and Magnetorheological Fluid Brake**" which is being submitted to the **National Institute of Technology Karnataka, Surathkal** in partial fulfillment of the requirements for the award of the Degree of **Doctor of Philosophy** in **Department of Mechanical Engineering** is a *bonafide report of the research work carried out by me*. The material contained in this Research work has not been submitted to any University or Institution for the award of any degree.

Register Number   **: 177151 177ME027**

Name of the Research Scholar   **: ASHOK KUMAR K.**

Signature of the Research Scholar   :

Department of Mechanical Engineering

Place   **: NITK, Surathkal**

Date   **:**

C E R T I F I C A T E

This is to *certify* that the Research Thesis entitled "**Effect of Temperature on Magnetorheological Fluid and its Performance in Magnetorheological Fluid Damper and Magnetorheological Fluid Brake**" submitted by **Mr. ASHOK KUMAR K. (Register Number: 177151ME027)** as the record of the research work carried out by him, is *accepted as the Research thesis submission* in partial fulfillment of the requirements for the award of degree of **Doctor of Philosophy.**

Research Guide[s]

Dr. HEMANTHA KUMAR
Associate Professor

Dr. ARUN M.
Associate Professor

Chairman – DRPC

Department of Mechanical Engineering

NITK Surathkal

ACKNOWLEDGEMENTS

Lastly, I thank my parents, **Mr. Gopalappa Kariganaur** and **Mrs. Sumithramma Kariganaur**. Last, my wife, **Mrs. Anusha,** and my son **Arjun,** for their undying love, encouragement, and moral support throughout my research. Without them and their blessings, achieving this goal would not have been possible.

I wish to thank all other individuals who have helped me complete my research work.

(Ashok Kumar Kariganaur)

ABSTRACT

Magnetorheological fluid (MRF) is the dispersion of magnetic particles in a base liquid. They are controllable fluids whose flow properties can be changed by applying an external magnetic field. The design of the MR system and composition of MR fluid significantly impact the performance. Sedimentation stability and high yield stress of an MRF are essential parameters for better damping performance for any practical MR application. Initially, investigations have been carried out on carbonyl iron particles to determine the morphology, particle size, crystal structure, and saturation magnetization for their feasibility of synthesizing magnetorheological fluids in-house.

In the first section of the study, the synthesis of various MRFs from commonly used carrier fluids and additives was carried out. The MRF samples were prepared for 25 % volume fractions of carbonyl iron (CI) powder in either silicone oil (350 cSt) or hydraulic oil (50 cSt) and by using lithium or calcium-based additives or a combination of both additives. The sedimentation stability and yield behaviour at different temperatures show a remarkable drop in sedimentation rate and yield stress for all the MR fluid samples. The characterization of the prepared MR fluids reveals that silicone oil fluid samples are more stable and have high yield stress values. One of the samples among the silicone oil based MRF is selected to further characterize its dynamic performance in magnetorheological fluid damper fabricated based on geometric dimensions obtained from the response surface optimization technique. The results indicate a 164.45 % and 135.48 % increase in damping force at higher amplitude and frequencies at 0 A and 1 A currents.

Further, similar tests have been carried out by synthesizing one more MRF with silicone oil (50 cSt) + lithium base grease as the additive. The samples stability and yield stress with temperature are carried out, and performance analysis shows a remarkable change in damping force than earlier MRFs in the present study. The dynamic range obtained is practically more viable in 50 cSt silicone oil carrier fluid MRF than 350 cSt and 50 cSt in MRF samples, with less variability.

The second part of the study aims to evaluate the temperature effect of MR fluid on performance while the damper is working. The range of critical parameters used to fabricate the MR damper is selected using the Technique for Order of Preference by Similarity to Ideal Solution performance score (TOPSIS). The temperature of the MR fluid is measured using an embedded thermocouple while the damper is operating at different loading parameters. The results reveal that the fluid temperature rises significantly from atmospheric to 125.39 °C, decreasing damping force by 66.32 % at higher loading parameters. The theoretical model predicts a temperature increase similar to the experimental values, with an average error of 10.24 % in the on-state condition. Particle characterization after dynamic testing reveals particle morphology has not changed, but the saturation magnetization of the particles reduced by 57 % at higher temperatures (127 °C). It is observed through thermogravimetric analysis (TGA) that the fluid's life is reduced by 0.25 %, which is negligible after dynamic testing of the liquid for approximately 85000 cycles. Finally, to imitate the temperature effect on the particle, particles were heat-treated at 200 °C, 400 °C, and 600 °C. Through scanning electron microscope (SEM) images, it is confirmed that deterioration of the particle starts after 200 °C if the fluid is operated for a prolonged amount of time.

Along similar lines, the better MR fluid, which gives good sedimentation and yield stress, is further used to study the torque generation in two-rotor MR brake. The objective of this study is to know the torque generation capacity of the MR brake (Total mass=1.62 kg). The fabrication of MR brake is based on the Finite Element Method Magnetics (FEMM), which shows approximately 0.145 T magnetic flux density in the shearing gap. The MR brake's characterization shows an increase in torque with increased current and speed. Lastly, the tests have been carried out to identify the effect of sedimentation on torque generation at 52 °C after 15 hours of sedimentation. TGA and SEM analysis of the MR fluid and particles shows that 322 °C is the start of destabilization of the fluid, and after complete destabilization, the particle starts to melt at 400 °C, which acts as critical point in controlling the MR fluid system input parameters.

TABLE OF CONTENTS

CHAPTER 3 EFFECT OF TEMPERATURE ON SEDIMENTATION STABILITY OF MAGNETORHEOLOGICAL FLUID WITH DAMPER AS THE PERFORMANCE ANALYSER

CHAPTER 4 INFLUENCE OF TEMPERATURE ON MAGNETORHEOLOGICAL FLUIDS AND DAMPING PERFORMANCE

CHAPTER 5 PERFORMANCE ANALYSIS OF TWO PLATE ROTOR MAGNETORHEOLOGICAL BRAKE WITH INHOUSE MR FLUID

CHAPTER 6 SUMMARY AND CONCLUSIONS

LIST OF FIGURES

xviii

xxiii

LIST OF TABLES

ABBREVIATIONS

AWG	American wire gauge
CI	Carbonyl iron (powder)
DAQ	Data Acquisition
DC	Direct Current
DOF	Degrees of freedom
ER	Electro-rheological
FE	Finite Element
FEMM	Finite Element Method Magnetics
FESEM	Field Emission Scanning Electron Microscope
GA	Genetic Algorithm
HB	Herschel-Bulkley
HP	Horse Power
LVDT	Linear Variable Differential Transformer
MR	Magneto-rheological
PC	Personal Computer
PSA	Particle size analyser
RMS	Root Mean Square
SEM	Scanning Electron Microscopy
TGA	Thermogravimetric analysis

CHAPTER 1

INTRODUCTION

1.1 INTRODUCTION

Intelligent materials are gradually employed in various technologies due to their inherent benefits over contemporary technologies. Changes in flow properties of the smart materials to the external electrical field, magnetic field, etc., can be programmed in a controllable way. The various intelligent or smart materials types include controllable magnetorheological (MR) and electrorheological (ER) fluids, MR elastomers, shape memory alloys, piezoelectric, electro-active polymers, etc. The potential application of smart materials can be seen in vibration control, health monitoring of mechanical systems with special applications in the automobile industry, aerospace, mechanical and civil engineering structures, prosthetic technology, etc. (Gołdasz and Bogdan (2014)).

Winslow and Rabinow (1947-48) first reported the magnetic and electrorheological fluids, where magnetic particles were dispersed in a non-conducting liquid medium that can be activated through magnetic and electric fields. However, due to technical limits, commercialization was hindered. Although in the past 20 years, many researchers successfully implemented mechanical devices such as damper, brake, and clutch applications using MR fluid. The inherent disadvantages of the ER fluid, like more voltage consumption, sensitivity at lower temperatures, and lesser performance, create less importance when compared to MR fluids.

This chapter includes the basic terminologies related to magnetorheological fluids flow behaviour, a brief introduction to the MR damper and MR brake, and its controllable behaviour. Finally, a few mathematical models of the MR fluid and MR dampers are disclosed.

1.2 MAGNETORHEOLOGICAL (MR) FLUID

These are the class of smart fluids that consist of magnetic particles suspended in the base fluid. Generally, the magnetic particles are pure carbonyl (CI) iron or cobalt powder and the base liquid may be silicone or fork oil. The additives were added in small percentages to minimize the settling rate of the magnetic particles. In the absence of a magnetic field, the particles were dispersed in a carrier fluid, as shown in figure 1.1(a). However, using a magnetic field introduces a dipole moment in the particles and tends to align in the direction of the external magnetic field, as illustrated in figure 1.1(b). The formation of the chain in the direction of the magnetic field is reversible, and this reversible yield stress in MR fluid can be controlled based on the increase in the applied magnetic field.

Formation of chain in the direction of magnetic field lines

Magnetic particles

B = 0, magnetic field

B > 0, magnetic field

(a)Without magnetic field   (b) With magnetic field
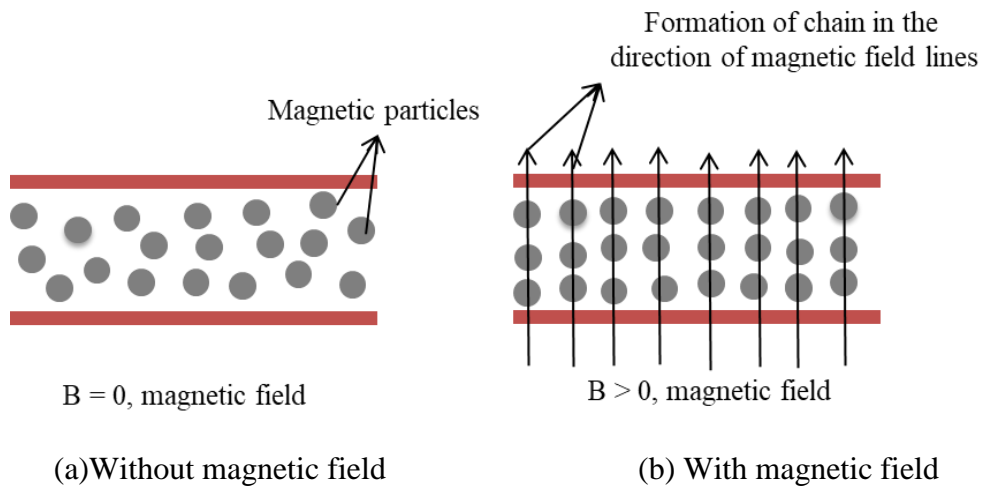
Figure 1.1 Magnetorheological fluid behaviour with and without magnetic field

The MR fluid in without magnetic field shows Newtonian behaviour, and with the application of a magnetic field, MR fluid shows non-Newtonian behaviour. Flow property study of MR fluid is carried out in pre and post-yield stress regions through constitutive models, which is given by Jolly et al. (1999) and is shown in equation (1.1) and (1.2).

$$\tau = G^{*}. \, \dot{\gamma}, \text{ when } \tau < \tau_{B, \, yield} \qquad (1.1)$$

$$\tau = \tau. \, \tau_{B, \, yield} + \mu. \, \dot{\gamma}, \text{ when } \tau > \tau_{B, \, yield} \qquad (1.2)$$

Where, $\dot{\gamma}$ = shear rate (s^{-1}), $\tau_{(B)}$= yield stress (Pa) μ = viscosity (Pa-s), B = magnetic flux density (T), G* = shear modulus, and τ = shear stress (Pa)

2

1.2.1 MR fluid models

The factors which affect MR fluid properties are magnetic particle concentration, base liquid viscosity, additive, and external magnetic field etc. The induction of yield stress or viscosity change due to application of magnetic field is also called MR effect. Due to this magnetic effect, MR fluid behaves as a semi-solid like in the pre-yield region with absence of flow. When the applied shear crosses yield stress the MR fluid starts to flow creating a post-yield region where MR fluids mainly work. The non-linear flow characteristics of the MR fluids can be evaluated using various mathematical models (Mitsoulis et al. (2007)). The design of MR fluid technology will be based on rheological models. Some of the most suitably reported non-linear rheological models for MR fluids are discussed below.

a. *Bingham – Plastic model:* The present model describes Newtonian viscosity in equivalence with variable shear stress parameters. The characteristics of the flow of fluid and shear stress can be using equation (1.3) is shown in figure 1.2(a).

$$\tau = \tau_B + \eta\dot{\gamma} \ , \ |\tau| > \tau_B \tag{1.3}$$

Where, τ_B = yield stress dependent on magnetic field, η = apparent viscosity and $\dot{\gamma}$ = shear rate

b. *Herschel – Bulkley (HB) model:* The post-yield shear thinning nature of MR fluids was considered in this model. The variation in shear stress with respect to shear rate is expressed as shown in figure 1.2a and equation 1.4.

$$\tau = \tau_B + K(\dot{\gamma})^n, \ |\tau| > \tau_B \tag{1.4}$$

Where τ_B = yield stress depends on the magnetic field, n and K is flow and consistency index and $\dot{\gamma}$ = shear rate

c. *Casson model:* The behaviour of the fluid is shown in figure 1.2(a), and the fluid shear stress can be modelled according to the equation Mitsoulis (2007)

$$\sqrt{\tau} = \sqrt{\tau_B} + \sqrt{\eta\dot{\gamma}} \ , \qquad |\tau| > \tau_B \tag{1.5}$$

d. Biviscous model: In this model, the rheology of MR fluids is characterized in terms of pre-yield and post-yield behaviour, as shown in Figure 1.2(b). The shear stress can be estimated by the following equation Goldasz and Sapiński (2015)

$$\tau = \begin{cases} \eta_r \dot{\gamma} \\ \tau_B + \eta \dot{\gamma} \end{cases} \qquad \tau \leq \tau_1 \tag{1.6}$$

Here, η_r and η are the elastic and viscous fluid properties. It can be noticed that in a limiting case of $\eta_r \to \infty$, this model tends to be the Bingham model. Ghaffari et al. (2015) shows the detailed view of all the rheological models that can be referred.
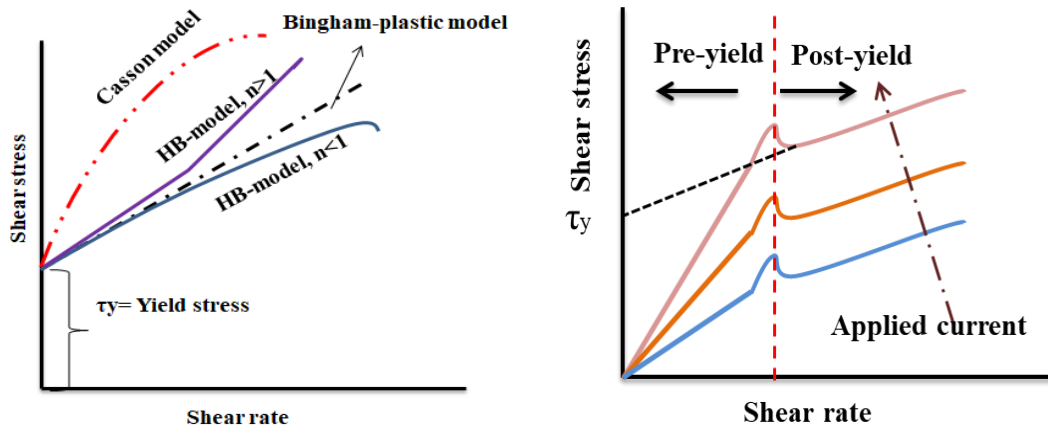
Figure 1.2 (a) Non-linear models (b) shear stress versus shear strain for different MR fluid models

The dynamic yield shear stress increases with an increment in a magnetic field. In the absence of a magnetic field, the shear stress of the fluid is due to its own viscosity and is termed viscous-induced shear stress. In the presence of a magnetic field, the fluid shear stress comprises two components: viscous-induced shear stress and field-dependent yield shear stress. The field-dependent yield shear stress of MR fluid is evaluated by adopting two rheological regimes of MR fluid, as shown in figure 1.2(b). In the pre-yield region, MR fluid behaves like a linear viscoelastic material, a nonlinear viscoelastic material in the yield region and plastic material in the post-yield part. The rheological property in the post-yield area, field-dependent dynamic yield shear stress, is considered in the design of MR fluid devices like dampers, brakes, clutches, etc. In the design of smart structures such as MR fluid sandwich beams and

MR elastomer sandwich beams for vibration control, the field-dependent complex modulus in the pre-yield region is a significant property considered Choi and Han (2012).

1.2.2 MR fluid operating modes

There are four Modes of operation MR fluid: There are four main operating modes of the MR damper. They are

a. Flow mode: the fluid flows between two stationaries planar (or concentric) surfaces due to a pressure difference. The changes in the rheology of the fluid are controlled by an external field that is normal to the direction of the flow.

b. Shear mode: the fluid flows between two surfaces that move relative to each other. Again, the external magnetic field is normal to the direction of the fluid flow, thus causing changes in the rheology of the fluid.

c. Squeeze mode: the fluid is sandwiched between two planar parallel surfaces. The distance between the poles varies according to the prescribed displacement or force input.

d. Pinch mode: the MR valve features magnetic poles in an axial arrangement along the flow channel. The magnetic field controls the effective diameter of the semi-orifice—the fluid is solidified at the fluid layers near the magnetic poles. Figure 1.3(a)-(d) shows the various operational modes.
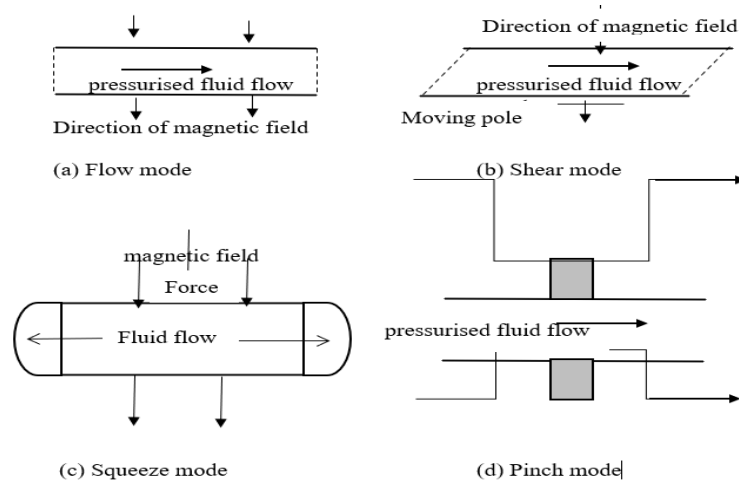
Figure 1.3 Operating modes of the MR fluids

1.3 MAGNETORHEOLOGICAL DAMPER

MR damper is an energy dissipating device which semi-active that uses MR fluid to induce governable damping force. The MR damper consists of a reciprocating electromagnetic piston having an electromagnetic coil which is also called an electromagnetic circuit. The piston glides inside a cylinder, separating the cylindrical compartment into upper and lower segments. When the piston rod moves, the MR fluid flows through the annular gap. When the current is supplied to the coil, a magnetic field is generated around the piston creating resistance to the flow of fluid in the gap. The force produced by the MR damper is divided into three components they are viscous force and frictional force which is uncontrollable in nature and the third one controllable force which is dependent on the magnetic field. The variation in the damping force can be decided by the application magnetic field. Prabhakar et al. (2009) carried out experimental studies on performance of the MR damper and figure 1.4 depicts the magnetorheological damper and its parts. Using the control strategy, the desired magnitude of the current is provided to the coil so that the magnetic field produced will induce the necessary damping force in the system.
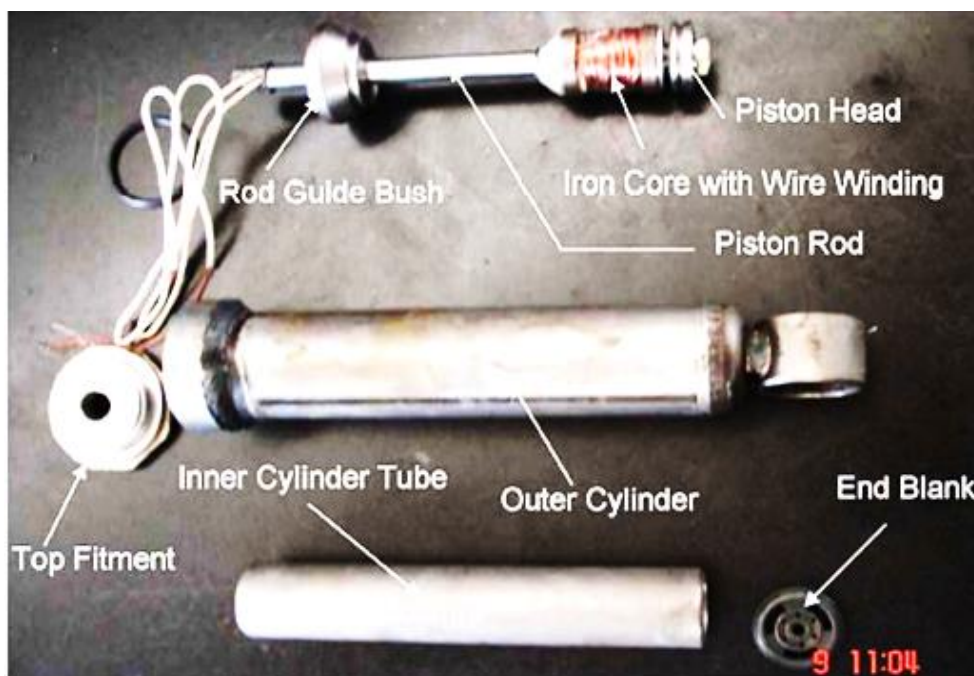
Figure 1.4 MR damper and its components (Prabhakar et al. (2009))

1.3.1 Types of MR Damper

The MR dampers are classified mainly into three types based on their construction, namely:

- Monotube damper
- Twin tube damper and
- Twin rod single tube damper
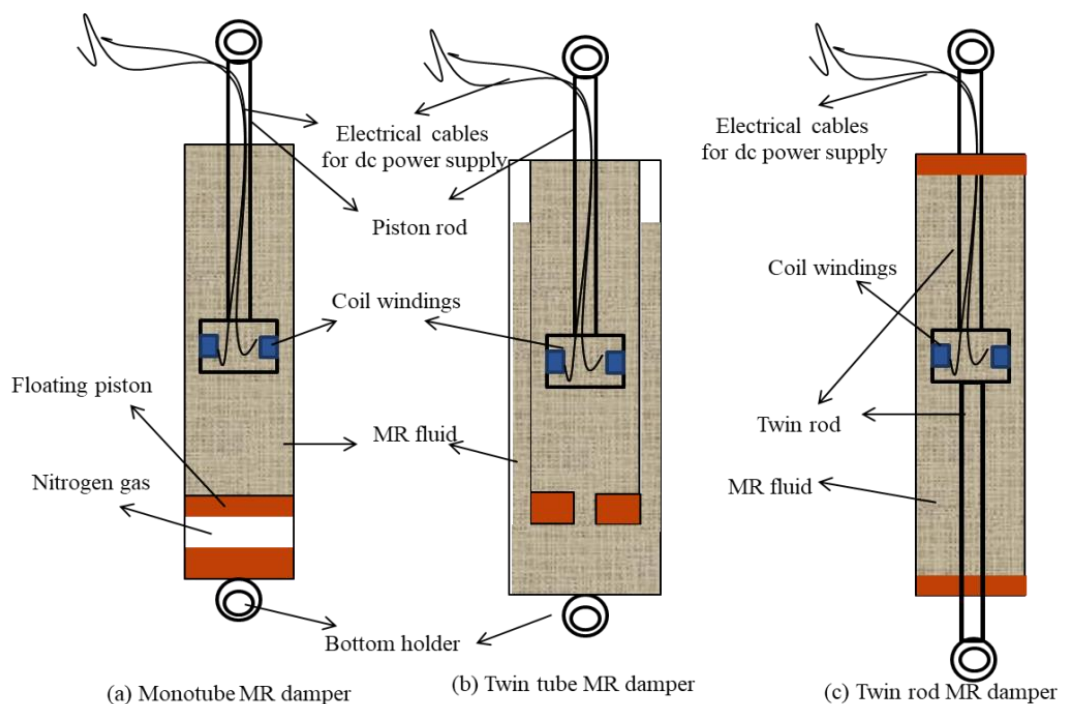
Figure 1.5 (a-c) MR dampers and their types

The monotube MR damper consists of a single cylinder for the piston, MR fluid and an accumulator for accommodating volume changes during piston rod movement. A floating piston separates the MR fluid from the accumulator chamber, which consists of high-pressure nitrogen gas, as shown in figure 1.5(a). An annular gap between the piston and cylinder permits fluid to flow between the chambers while the piston is in motion. When current is supplied to the piston coil, the MR fluid in the shear gap is subjected to a magnetic field, which offers more resistance to fluid flow, thus inducing more damping force. To avoid cavitation, high-pressure gas is necessary

for the accumulator below the floating piston. However, it requires a very high surface finish on the cylinder inner surface, sealing requirements and friction.

The twin-tube MR damper is shown in figure 1.5(b) and consists of two tubes arranged concentrically. MR fluid is filled in the inner tube while partially in the space between the inner and outer tube. Air at atmospheric pressure or some inert gas at high pressure occupies the remaining space in the outer tube. A base valve separates the inner and outer tubes. The inner tube houses the piston, and the volume changes occurring during the piston rod movement are accommodated by the MR fluid moving from the inner tube to the outer tube through the base valve. This configuration does not require high precision machining as in the case of a monotube MR damper. In the twin rod single tube MR damper, as depicted in figure 1.5(c), the piston has piston rods on either side and protrudes from either end of the cylinder. It does not need an accumulator as there are no volume changes during piston movement.

1.4 MAGNETORHEOLOGICAL BRAKE

Generally hydraulic brakes are used in contemporary mechanical systems. Nonetheless, conventional brakes have many disadvantages such as large size, increased temperature, less performance, more response time due to higher pressure build up etc. Alternatively, brakes with magnetorheological fluids will have higher performance, lesser temperature, less response time, lower mass, and lesser additional components etc. with quicker response time using optimal control strategies. Henceforth, brakes with magnetorheological fluids have immense probability to replace conventional brakes due to their inherent advantages.

The components of MR brake are outer casing, rotor discs, stationary stator disc, and copper coil on a bobbin and MR fluid gap. A schematic diagram of a single disc MR brake is given figure below. Fluid is filled in the gap between the stator and rotor disc where the copper coil is wound on the stator top surface which is having certain depth. The coil around the stator is supplied with electric current which generates magnetic flux density towards the rotor, through the MR fluid creating a braking effect. Avraam et al. (2010) and Attia et al., (2014) had discussed different types of MR brakes such as single plate brake, multiplate brakes, inverted drum brakes, and T-shaped brakes using different electromagnetic design to create higher

magnetic field in the fluid flow gap. Though, single rotor brake is compacted and very easy to manufacture different types of brakes design are needed to enhance the torque capacity. Figures 1.6-1.9 shows different types of MR brake

Figure 1.6 depict the disk type brake which is easier to fabricate but has higher inertia and lesser torque to volume proportion. The drum brake with inverted in shape which is compact and has hollow discs that encompas the coil which reduces the inertia of the disc than drum brake. Due to the larger availability of the area around the rotor disc T-shaped brake produces more torque.
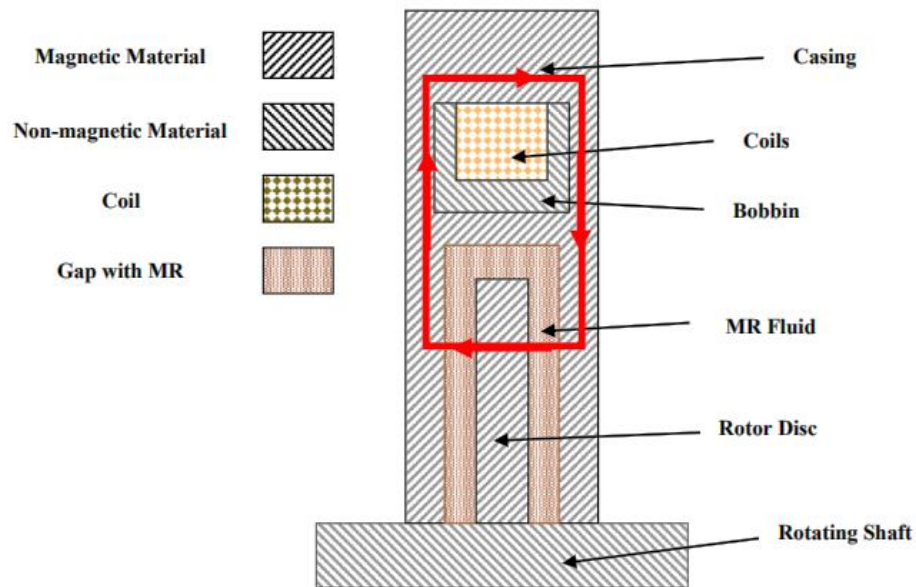
Figure 1.6 T-shaped MR brake

Figure 1.7 shows the disk type MR brake the drum type MR brake is also popular and in use. In this case, the rotor of the brake is a long cylinder and magnetic field is applied along the radial direction. The magnetic field is made majorly to flow radially and not around the end faces of the brake. Here, the coil is wound on the bobbin fixed to the housing.

Magnetic Material

Non-magnetic Material

Coil Windings

Gap with MR

Casing

Coils

MR Fluid

Rotor Drum

Rotating Shaft
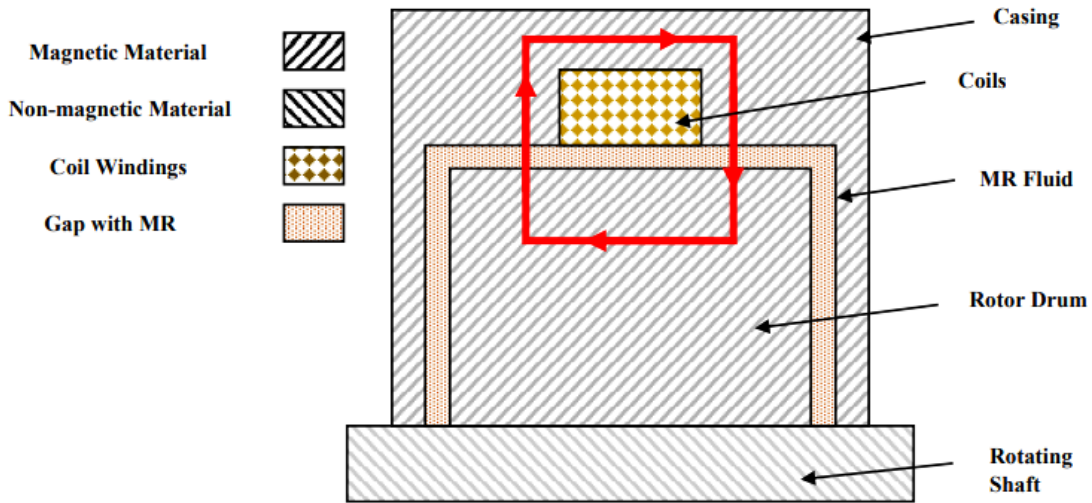
Figure 1.7 Drum type MR brake

Figure 1.8 shows the combination of disk type and drum-type MR brake. Here side housings are made of magnetic material unlike for drum-type MR brake. Thus, the magnetic flux caused by the coil flows in axial as well as radial directions.

Magnetic Material

Non-magnetic Material

Coil Windings

Gap with MR

Casing

Coils

Gap with MRF

Drum & Disk Type Rotor

Rotating Shaft
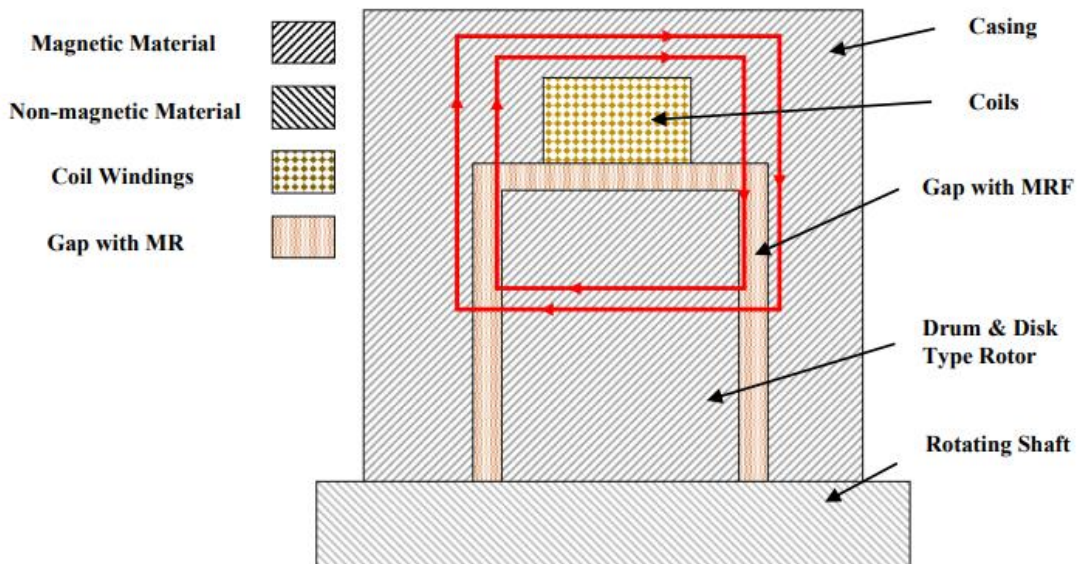
Figure 1.8 Hybrid MR brake

In the case of hybrid T-shaped MR brake, magnetic flux runs across both the outer and inner annular ducts of the T-flange and the radial ducts of the T-leg a large braking torque is expected. A typical configuration of the hybrid T-type MRB with different components is shown in figure 1.9.

10
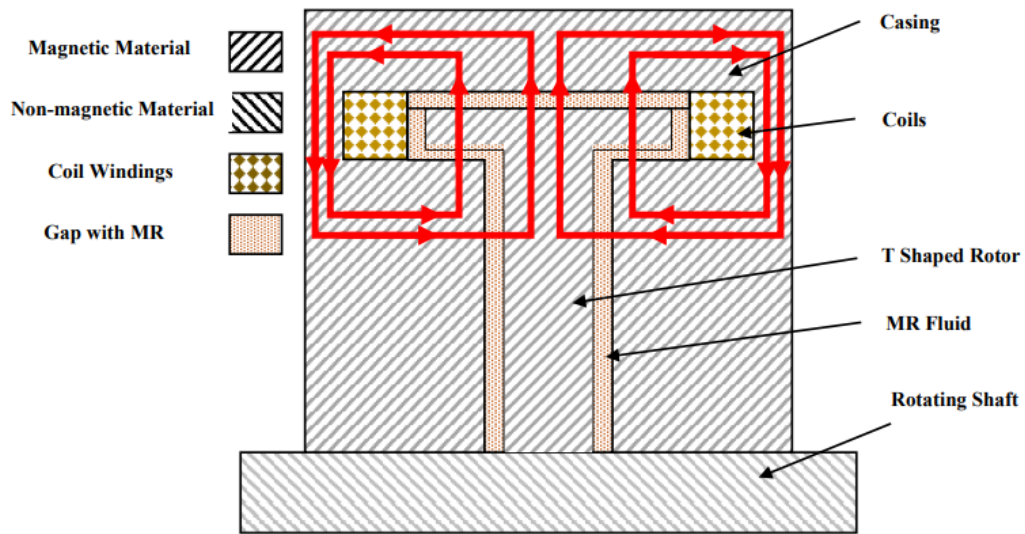
Figure 1.9 Hybrid T-type MR brake

However the complexity in fabrication is more than the other MR brakes. The simple disc MR brake was first used by Rabinow who invented MR fluid which he used as an application part. For high torque application such prosthetic knee, and automotive application multi disc MR brakes can be used. The design and fabrication are very highly complex and should be studied further to ease the design process of MR brakes to increase torque generation.

1.5 MR fluid damper in structural applications

MR fluid damper in structural applications was studied Dyke et al. (1998) for its effectiveness of MR damper for earthquake amplitude reduction. MR dampers subjected to random excitations when used in multiple storey building can reduce seismic vibrations coming from the ground. Yang et al. (2002) developed large scale (capacity 20 ton) MR damper for structural application and authenticated experimentally and analytically with the designs. The schematic diagram of the multi-stage MR damper is shown in figure 1.10. The requirement for low response time can be countered by the application of the large scale MR damper in structural implementations.
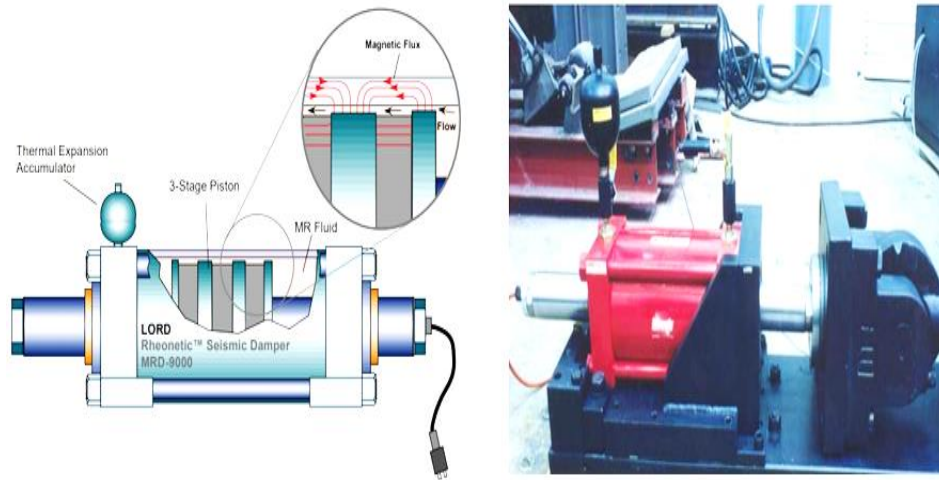
Figure 1.10 MR damper for civil engineering applications (Yang et al. (2004)

1.6 MR fluid mounts

Most of the chassis of the engine vibration can be controlled by the mount. However, hydraulic mounts having rubber and fluid with better controllability can reduce the vibration. The input to the MR mount will be high frequency and low amplitude signals which should be suppressed by effective use of MR mounts. One of the designs which was carried out by Do and Choi (2015) which is depicted in the figure 1.11 for higher load applications which operate in all the three modes of MR fluid operations. They also illustrated detailed guidelines for the development of the mount operated with shear and flow mode. Zhang et al. (2011) performed dynamic testing and modelling of MR fluid squeeze mount and found a good match between the mathematical and test results. Hong and Choi (2005) demonstrated through experiments that vibration levels of structural system employing controller can be effectively reduced by means of MR mounts.
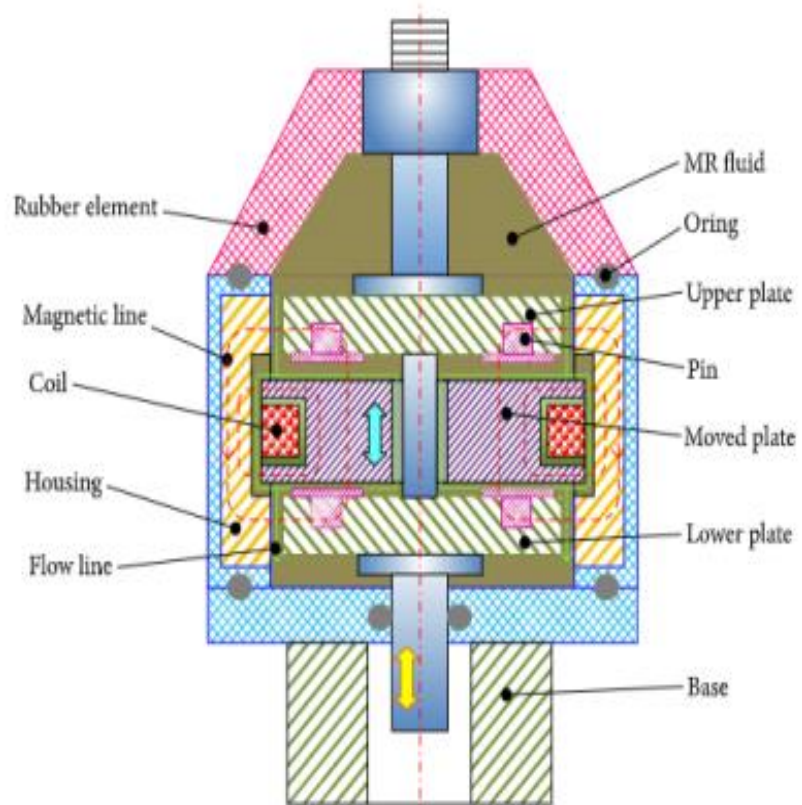
Figure 1.11 Magnetorheological mount (Do and Choi 2015)

1.7 Magneto-rheological fluid prosthesis

The schematic representation and image of the prosthetic knee damper are illustrated in figure 1.12. The design and development of prosthetic knee damper was carried out by Park et al. (2016) with an integrated controller and performance analysis was evaluated on different grounds. The results show that performance enhancement was seen at lower speeds than at higher speeds. The study related to the parameters of the prosthetic knee was evaluated by Jonsdottir at al. (2009). The torque generation and application of the magnetic field was calculated. Acharya et al. (2020) worked on MR brake for better torque generation using an optimal proportion of MR fluid. The idea can be further implemented to suit for the application in knee joints with reduced size and arranging multiple plates to increase the torque enhancement and to increase the applicability of the MR brake.
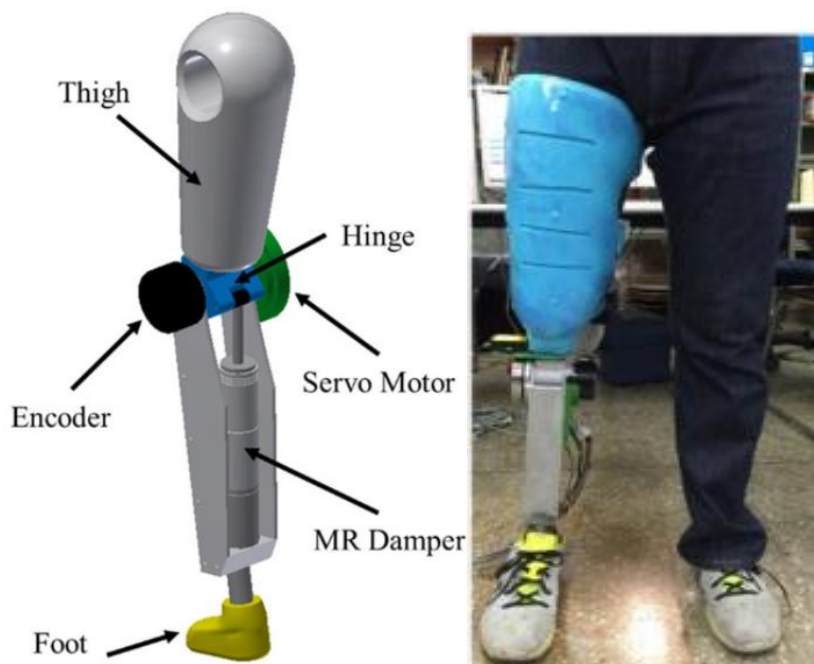
Figure 1.12 Prosthetic leg with MR damper and

schematic picture (Park et al. (2016)

1.8 MR fluid machining devices

Widespread work related to machining operations has been carried out to developing better finishing method using MR fluid. Song et al. (2011) investigated the tribology of aluminium, steel, and brass materials by using MR fluid (lord 132DG) for polishing in the existence and non-appearance of magnetic fields under various examination conditions. They observed that wear and friction loss is drastically come down with the application of magnetic field intensity. In another work, they observed that MR fluid effectively reduced roughness of steel surface while hard surface finish was obtained in case of brass and aluminium metals. MR fluid with higher particle concentration caused in better surface finish in case of hard job sample.
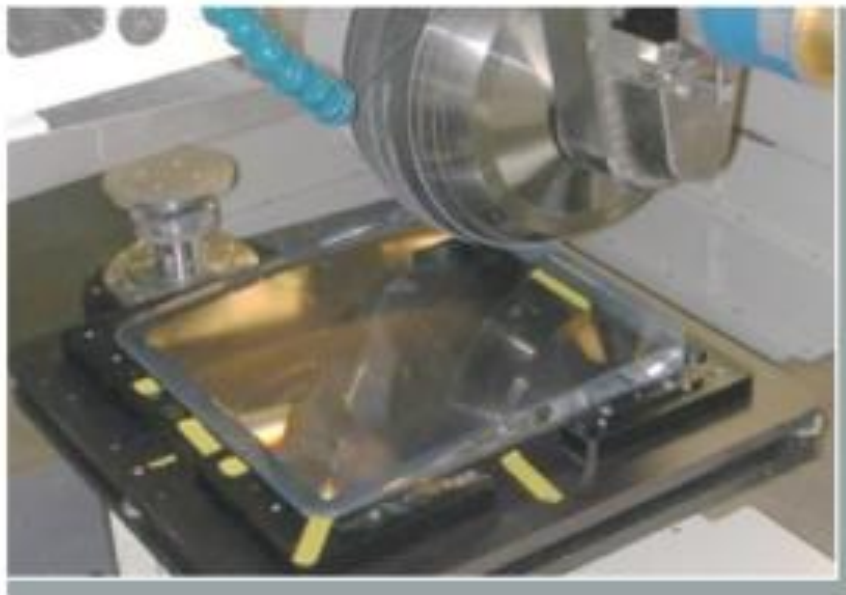
Figure 1.13 MR fluid operated polishing tool (lasermaterials.llnl.gov/focus-areas/optical-finishing))

1.9 SUMMARY

      In this chapter, a brief discussion on MR fluids and their models, MR dampers and their terminology and Multiplate MR brake and their terminology and categorizations have been presented. The current chapter provides the general terms necessary to know the remaining part of this study. Next chapter emphasizes the literature study related to the design of MR fluid-based devices in MR damper and MR brake applications.

1.10 ORGANIZATION OF THESIS

There are six chapters in this thesis i.e. Introduction, Literature study, MR fluid synthesis, sedimentation study, and characterization with temperature, performance analysis of the MR damper and two plate rotor MR brake to evaluate the temperature effect on damping force and torque generation and lastly the conclusions. Further, inspiration for research is reflected, trailed by defining the objectives and scope of research. The research methodology followed to carry out the outlined objectives is described.

Chapter 2. Brief literature on the synthesis of MR fluid, the effect of temperature sedimentation rate and flow characteristics of the MR fluids and the performance analysis of MR dampers and MR brakes.

Chapter 3. This chapter discusses the synthesis of different MR fluid samples of different carrier liquid and additives. Secondly, in this chapter sedimentation rate and characterization of the MR fluid to know the effect of temperature effect of settling rate and flow characteristics.

 Chapter 4. This chapter evaluates the effect of temperature on the performance of the MR damper by embedding a thermocouple in the damper to measure the temperature of the MR fluid inside the damper at various input parameters.

Chapter 5. This chapter details the design, development and characterization of the scaled down two plate rotor MR brake and, the current chapter also deals with the effect of sedimentation on torque generation.

Chapter 6. The last chapter deals with the contributions of the present work along with the important conclusions and future scope of work are presented.

CHAPTER 2

LITERATURE REVIEW AND METHODOLOGY

2.1 INTRODUCTION

The controllability and ease of the MR fluid applicability have gripped the thoughtfulness of the researchers. The distributed magnetic constituent part in the base fluid forms a series in the path of the applied magnetic field by changing the flow properties of the MR fluid. Settling is a common phenomenon observed in nature when particles of finite mass are dispersed in a fluid medium. Sedimentation stability determines the life and performance of MR fluid and disposing of it frequently has a detrimental environmental impact. Various works have been undertaken to find out parameters that impact the stability and improve the sedimentation stability of MR fluids. The application part of MR fluid consists of MR damper, MR clutch, MR brake etc. An evaluation of writings by some of the researchers was detailed in the following sections. A methodical literature study related MR fluid synthesis, characterisation, and design and development of MR damper and MR brake with the use of available lab setup by detailing the obtained results to practical applicability. Even though it can be reasoned that every part of the system shows a trivial role in the damping and torque generation process, from a real view it is essential to reflect the temperature effect on the performance of MR damper and torque generation capacity.

2.2 MAGNETORHEOLOGICAL FLUID

The primary constituents of MR fluids are magnetic particles, dielectric liquid medium, and additives to suspend the particles for a greater amount of time. The basic properties that affect the performance of any MR fluid application are particle size, particle shape, particle concentration, and magnetic saturation of the particle, carrier fluid viscosity, operating temperature of the fluid system and input parameters coming on to the system. The major problems associated with MR fluids were the sedimentation of the particles which decreases the performance of MR system when unused for longer period of time. Sarkar and Hirani (2015) and Sarkar and Hirani

(2013) synthesized MR fluid using three different particle sizes with three concentrations in-house and through characterization they showed the larger particle size have higher saturation magnetization point but mixed particles with the combination of particles have higher shear stress at higher shear rates. Zhu et al. (2021) studied the effect of nano particle doping on the carbonyl iron particles synthesized using dielectric arc discharge to synthesize bimodal MR fluid with various ratios of mixing. The outcomes show that there is an increase in chain strength and weak magnetic saturation in the MR fluid with the addition of nanoparticles and also they have shown that the rate of sedimentation reduces drastically with an increase in nanoparticle addition. Additionally, it has been pointed out the range of magnetic field strength, rheological behaviour, and sedimentation can be reasonably enhanced with optimal use of nanoparticles in carbonyl iron particles. The figure 2.1 shows the constituents in MR fluid.
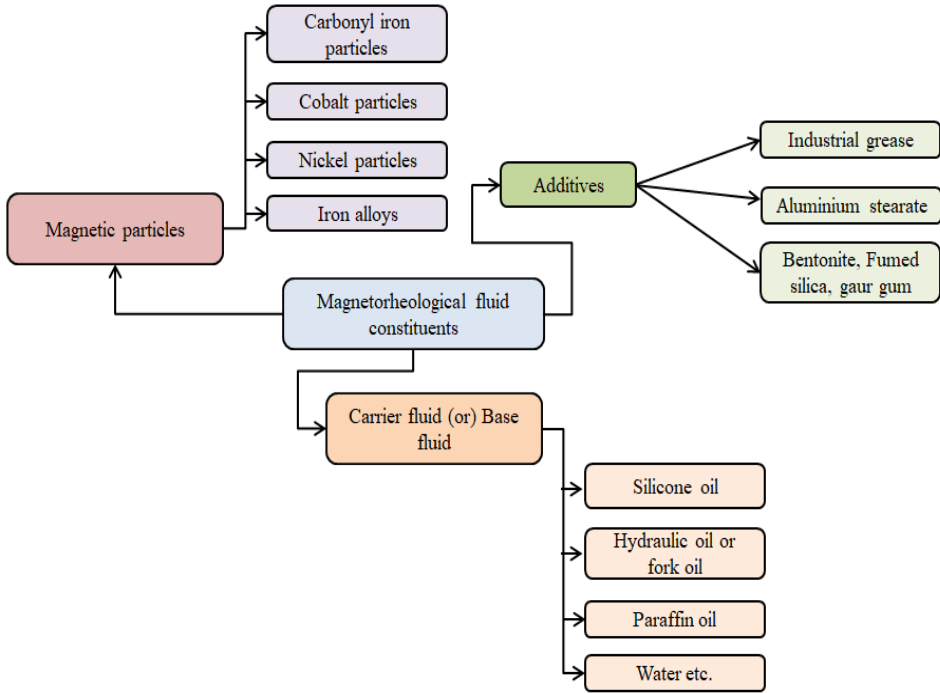
Figure 2.1 Constituents of MR fluid

Lately, has been shown by Ashtiani et al. (2015) that several methods have been adding additives and nanoparticles to the MRFs, coating particles, modifying the size and shape of the particles, etc. Among these methods, adding additives and

coating particles seems to improve MRFs' sedimentation stability; nevertheless, they generally deteriorate MR effects with increased sedimentation stability. Recently, Song et al. (2009) and Viota et al. (2007) experimented by replacing a few micro-particles with nano-particles has demonstrated a successful trade-off between stability and MR effect. However, using nanoparticles improved MRFs stability as Brownian forces overtook gravity forces at the cost of magnetic saturation was shown by Dong et al. (2015). Jönkkäri et al. (2015) prepared three MR fluid samples of 15% by weight with pure microparticles and other two samples were prepared by replacing 5 or 10% microparticles with nano particles to study the effect of nanoparticle concentration on sedimentation stability and yield behaviour of MR fluids. The results from the study reveals that 10% weight nanoparticles addition shows reduced settling rate by marginal yield stress trade off.

In particular, it was proved experimentally by de Vicente et al. (2010) that sphere, plate, and rod-like iron particles have no significant impact on magneto rheology but conversely it is results evaluates that rod like shape higher complex modulus than spherical and plate like structure. Guo et al. (2018) and Pu and Jiang (2005) prepared MR fluids using multi walled nanotubes and carbon nanotubes to study the influence of the coating on nanotubes in terms of sedimentation study and magnetic saturation. The results from the study indicate that sedimentation stability is increased significantly with the use of coated particles in the synthesis of MR fluid using ultra-sonication and mechanical stirring. Roupec et al. (2013) showed that temperature has a vital impact on decreasing viscosity and yield stress of the fluid from rheometer characterisation. The decrease in yield stress is due to less MR fluid quantity which decreases the viscosity in-turn reducing the inter-particle interactions. The enhanced thermal conductivity and reduced sedimentation rate are important parameters of MR fluid which was studied by Rahim et al. (2017). They prepared the MR fluid samples with hydraulic oil and additives by adding nano particles such as copper, aluminium, and fumed silica to reduce the sedimentation rate and enhance the thermal conductivity. The results show that there is an increase in thermal conductivity with a reduced sedimentation rate in comparison with commercially available MRF-132DG. They also concluded that shear yield stress increased in the

presence and absence of a magnetic field.

To study the effect of particle shape and sedimentation rate Shah et al. (2014) and Piao et al. (2015) used CI particles and plate like particles and synthesised the MR fluid using these particles. The results show increased sedimentation stability with nanoparticles with stable damping performance in small MR damper, and it is concluded that yield stress increases rapidly with increasing magnetic fields. Anupama et al. (2018) prepared the MR fluid and ER fluid to compare the effect of particle shape and saturation magnetization on the yield strength and viscosity of the fluid. The results indicate that deviation in yield stress after a certain magnetic field shows the importance of morphology and magnetic saturation of the particles in ther flow properties of the MR fluid. Zhang et al. (2018) prepared MR fluids from CI particles coated with polystyrene via dispersion polymerization to form core shell type particles. The results from reciprocating friction test and wear test shows that there is an enhanced Tribological property and also with this coating effect there is also an increase in the settling time with a compromising effect on shear yield stress. It is also shown by Liu et al. (2013) that coating has a significantly decreasing impact on performance of the damper and response time is shorter in the case of silica coated particles because of its affinity towards silicone oil than pristine coated particles.

Given the critical effect of carrier fluid on the rheological characteristics of MRFs, several works have been reported on using more viscous carrier fluid to overcome sedimentation problems. Kim et al. (2012) and Lim et al. (2004)synthesized MR fluids using carbonyl iron particles with poly ethylene oxide and fumed silica to study the sedimentation and density of the fluid. The results show that the medium viscosity carrier fluid will have a reasonable effect on MR fluid density and settling rate. Iglesias et al. (2015), López-López et al. (2006) and Fang et al. (2009) showed other methods of improving the sedimentation stability of MR fluids by synthesizing MR fluids with non-magnetic nanoparticles and additives such as oleic acid, aluminium stearate, silica particles. The results indicate that the sedimentation stability and flow properties have improved drastically with the additive of non-magnetic particles and additives, and also it has been proved that dispersion of particles in the case of silica nanoparticles is highly difficult after settling. Rankin et

al. (1999) studied the effect of an increase in the magnetic field on the flow properties of the MR fluid with various configurations of volume concentrations of particles. The results show that the sedimentation rate is decreased with an increase in particle concentration and inverse effect in case of yield stress is encountered with increased particle concentration. Sedlacik et al. (2011) studied the sedimentation and flow behaviour properties of the MR fluid by using carbonyl iron particles treated with 50% argon and 50% octafluorocyclobutane plasma. To confirm the surface modification X-ray photoelectron spectroscopy was used. The evaluation of the results shows that sedimentation rate was reduced drastically with moderate decrease in magnetic effect. Along the similar lines Zhang et al. (2012) and Fu et al. (2018) coated carbonyl iron particles with gelatine, grapheme oxide, multi walled nanotubes, and polystyrene to make shell type particles. The preparation of MR fluids with the shell CI particles was carried out. The results show an increased flow behaviour and decreased sedimentation rate due to low density and rough surface on the particle.

Particles size such as small and large particles and their combinations in different size ratios can significantly increase the rate of settling and mixing of smaller particles with larger particles will have good agreement with the theoretical models mentioned was studied by Hernando et al. (2015) by preparing three combination of size ratio for 30% volume concentration. Choi et al. (2016) and Gorodkin et al. (2000) synthesized MR fluids of various concentrations to study the effect of concentration on sediment velocity by visual observation. They concluded that an increase in particle concentration decreases the sedimentation velocity which was validated by vertical axis inductance monitoring system and also it is shown that increase in yield stress with particle concentration. The study of sedimentation and trade-off between the mixture of nanoparticles in microparticles was carried out by Ngatu and Wereley (2007), Butt (1996), Holdich (2014) and Zhu et al. (2019) by preparing the MR fluids of different concentrations and concludes that increase in nanoparticle concentration reduces the sedimentation but with decreased shear stress which was analysed by using Bingham plastic model.

Aruna et al. (2019) prepared five combinations MR fluid with the combination of clay, anti-friction agent and Palmolive oil to study the sedimentation effect and

concluded that clay as an additive will have vital impact on reducing settling rate than commercially available MR fluid. On the same lines Bombard et al. (2007) prepared MR fluid with hydrophilic silica and hydrophobic silica with phosphate coating on particles. The oscillatory tests show no particular interaction with phosphate coating. Through characterisation it is proved that hydrophilic silica has a greater interaction with the carrier fluid. Zuzhi et al. (2016) prepared MR fluid with silane coupling agent and bentonite as the additive with iron particles. They concluded that, 2.88% and 3.60% mass fraction of silane and bentonite shows the enhanced sedimentation, viscosity, and yield stress property of the MR fluid. Moreover, Anupama et al. (2018), Jiang et al. (2011), Morillas et al. (2018) worked on physical parameters of magnetic particles such as shape, size, concentrations, and particles with bidisperse in form and magnetic saturation. The interdependency of the all these parameters play an essential role in sedimentation and flow characteristics variation of the MR fluids.

Researchers have shown experimentally that temperature significantly influences sedimentation. Rabbani et al. (2015) prepared MR fluid with silicone oil and stearic and palmitic acid as the additive to study the effect of temperature on sedimentation and yield behaviour of the fluid. Adding of 3% by weight stearic acid can reduce the rate of sedimentation to a larger extent. The results from the study conclude that there was an accelerated sedimentation rate at higher temperatures with decreased shear stress. In addition, MR fluids viscosity is dependent on shear rate after attaining magnetic saturation.

Wong et al. (2001) and Zhang et al. (2004) proposed that particle size and high particle concentration can induce wear on the surface, and yield stress can be increased by applying external compression load and magnetic field on the fluid. Jha and Jain (2009) prepared the magnetorheological polishing fluid to study the size and volume concentration of the particle in finishing operations. The results show shear-thinning behaviour with a decrease in yield stress due to magnetic saturation at higher magnetic field strengths. And they also propose Herschel Bulkley and Casson model will show better fluid behaviour. Hato et al. (2011) prepared MR fluid samples with pure carbonyl iron particles and two combinations of organoclay nano additives to study the settling and flow behaviour of the fluids. The results from the study show

that pure carbonyl iron particle sample gives magnetic effect with higher rate of settling than nano additive organoclay MR fluids.

Madhavrao Desai et al. (2020) prepared MR fluids in-house and used a twin-tube MR damper designed based on finite element analysis. It was shown that the amplitude of vibration from the ground had been significantly reduced in four-wheeler applications. Hong et al. (2008) studied the effect of two modes of operation in MR dampers. The experimental results depict that the fluid gap and material properties play a significant role in increasing damping force and that combining the modes of operations has an enhanced performance than the single operating mode. El Wahed and McEwan (2011) and Yazid et al. (2014) developed mixed mode MR damper on the same lines. The experimental results show that shear mode and squeeze modes have increased performance when operated combined and also it's shown that squeeze mode has reduced performance than shear mode damper. Wang et al. (2014) worked on the effect of temperature on carrier fluid viscosity and particles. The experimental investigation shows that increased operating temperature for a longer time reduces the magnetic saturation, the coercivity of the particle, and viscosity of the carrier fluid. And also they conclude that lower activation energy base fluid should be selected for the synthesis of the MR fluid. Gurubasavaraju et al. (2017) used finite element analysis to model the shear mode damper and obtained the magnetic flux density in the flow gap which is in good relation with optimized results. Shivaram and Gangadharan (2007) fabricated a monotube MR damper to study the influential parameter among magnetic field, particle concentration, and plug thickness, frequency and vibration displacement. And they have obtained model equations of various input parameters using the response surface method. One of the recent applications of the damper in prosthetic leg is shown in figure 2.9(a) and 2.9(b).

However, the temperature has a significant effect on the properties of the MR fluid; experimentally, it was shown by Sahin et al. (2009) that yield stress of the MR greases decreases with an increase in applied magnetic field and temperature. Arief et al. (2016) and Bahiuddin et al. (2018) showed that the viscosity and dynamic yield stress of the fluid reduces due to thermal expansion property and the results shows that constitutive models along taking temperature and magnetic field can be

implemented to flow behaviour of the MR fluid. Singh et al. (2016) and Wiehe et al. (2013) synthesized MR fluids of three combinations of different particle concentrations to study the effect of particle concentration on viscosity of the MR fluid. It was concluded that settling decreases with increased particle concentration and also viscosity is reduced drastically with increased temperatures which affects the performance and life of the MR system.

The essential parameter that decides the performance of any MR fluid system is sedimentation stability and yield stress which is has more potential in industrial application such as brakes, clutches, dampers, prosthetic knee, and vibration tool chatter reduction etc. and also in biomedical applications such as cell treatment devices and pharmacy delivery systems. Typically, increasing the particle concentration, and size with higher saturation magnetization, and increasing current at a specific temperature increases the yield behavior of the MR fluid but it is also known that an increase in temperature decreases the yield stress and performance of the MR system was studied by Dogruoz et al. (2003), Gandhi and Bullough (2005), Goncalves et al. (2005), Guerrero-Sanchez et al. (2009), Li et al. (2021). McKee et al. (2018a) worked on the temperature effect on the properties of MR fluid and its performance in suspension system. Through rotational and oscillation characterization it was shown that flow properties and energy storage capacity in modulus reduced with rise in temperature and a similar effect is also observed with decrease in damping force with the suspension system.

2.3 MAGNETORHEOLOGICAL FLUID APPLICATIONS

MR fluids and their applications recently became popular, while Rabinow reported MR fluid applications decades ago. MR technology can be applied in applications where the systems work on semi-active control such as suspension systems, brakes, clutches, prosthetic knee etc. and several new potential applications. Wang et al. (2018) experimented on damping of thirty dampers which were used for control the amplitude of vibration on suspension bridges which is shown in figure 2.2 after an examination of ten years span. In these, twenty four dampers were provided substantial damping effect while other six failed to provide adequate damping. With this study they concluded that performance reduction is due to seepage of fluid and

rough irregular external texture of magnetic particles due to operation.

Figure 2.2 MR damper applied in structural damping (Wang et al. (2018))

Gudmundsson et al. (2010), Nikitczuk et al. (2007), and Shafer and Kermani (2011) studied the effect of an increasing number of rotor discs, limited dimensions, and weight optimization to increase the torque density in the fluid gap, and also the compactness. And they concluded that torque could be increased by increasing the number of plates and also the study reveals a trade-off between torque and weight reduction is required.
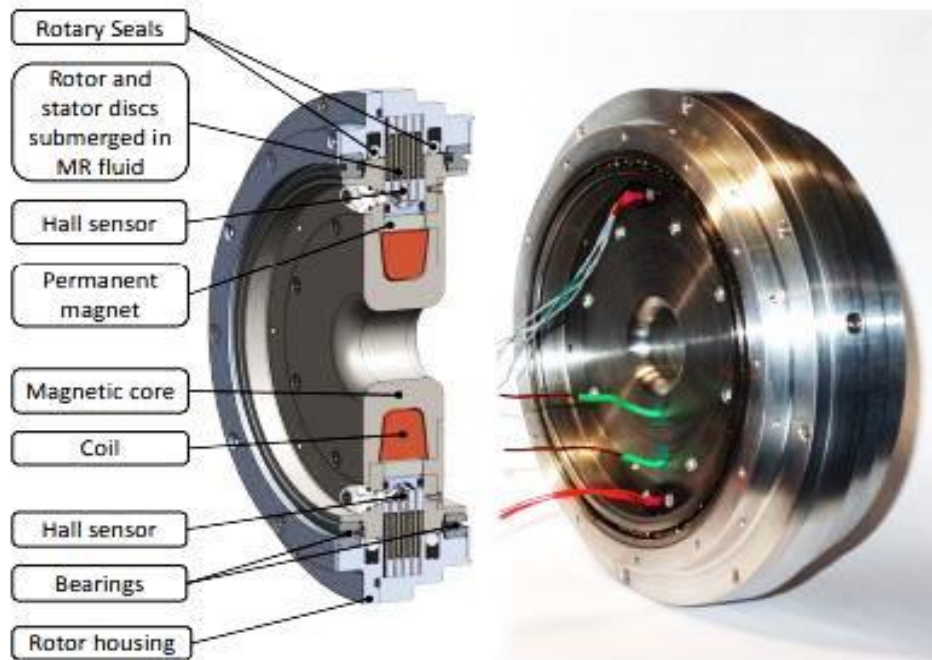
Figure 2.3 MR Clutch for vehicular application (Pisetskiy and Kermani (2018))

The present is focused on the temperature effect of MR fluid flow behaviour and its performance in MR dampers and two-rotor MR brakes. MR damper have seen positively implemented and it is available commercially but two-rotor MR brakes with miniature in size is not explored for many applications such as prosthetic knee while the topic of MR brake with the miniature size is underthe research stage. The following sections are concentrated on the literature review of MR damper and MR brake. Some of the applications of the magnetorheological fluid are shown in figure 2.2 to figure 2.7.
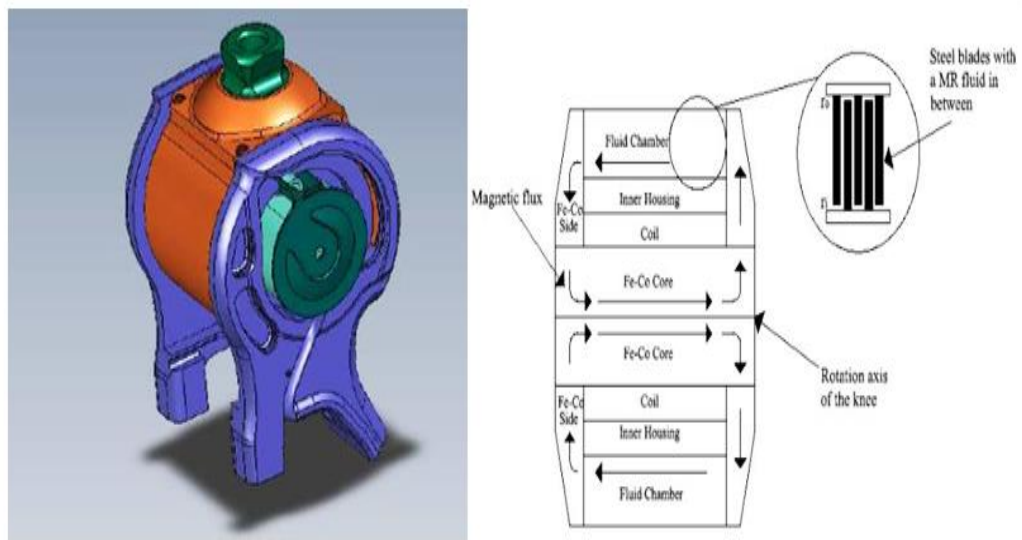
Figure 2.4 MR actuator (Gudmundsson, (2008))

Wong et al. (2001) and Zhang et al. (2004) proposed that particle size and high particle concentration can induce wear on the surface, and yield stress can be increased by applying anexternal compression load and magnetic field on the fluid. Jha and Jain (2009) prepared the magnetorheological polishing fluid to study the size and volume concentration of the particle in finishing operations. The results show shear-thinning behaviour with a decrease in yield stress due to magnetic saturation at higher magnetic field strengths. And they also propose Herschel Bulkley and Casson model will show better fluid behaviour. Hato et al. (2011) prepared MR fluid samples with pure carbonyl iron particles and two combinations of organoclay nano additives to study the settling and flow behaviour of the fluids. The results from the study show that pure carbonyl iron particle sample gives a magnetic effect with a higher rate of settling than nano additive organoclay MR fluids.
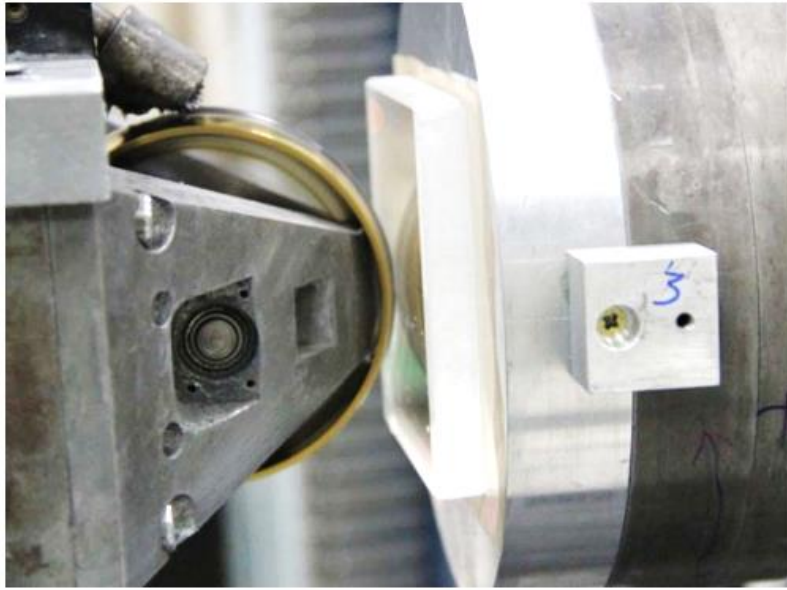
Figure 2.5 MR polishing tool (Chen et al. (2014))

Bompos and Nikolakopoulos (2016) planned and successfully executed the bearing operated with MR fluid. The developed bearing is depicted in figure 2.7. They also evaluated its effect on yield behaviour by coupling the finite element method and computational fluid mechanics. And concluded that nano particles along with the coating of the particles enhanced the performance of the bearing in. The active performance of bearing with MR fluid resulted in improved amplitude and frequency control.

Figure 2.6 MR bearing (Bompos and Nikolakopoulos (2014))

2.4 MAGNETORHEOLOGICAL DAMPERS

MR dampers are energy dissipating devices that generate heat when working at high shear rates. The two essential procedures involved in damper design are better material selection and optimal geometric dimensions and associated parameters for better performing damper. Figure 2.8 shows the general application of damper for vehicle suspension. The objective of the MR damper is to obtain higher damping forces by avoiding electromagnet saturation. The five parameters influencing damper performance are fluid gap, effective length, core length, number of coil turns, and applied current, which decides the magnetic flux density and damping force. Krishna et al. (2017) obtained design dimensions of the monotube MR damper through magnetostatic analysis and used response surface methodology compared with the genetic algorithm to increase the magnetic flux density in the fluid gap. Zhang et al. (2006) used finite element analysis to design the MR damper for its magnetic saturation. Also, experimental verification of the damper was carried out by fabricating the damper, which was entirely in agreement with the FE analysis. Along similar lines, Naserimojarad et al. (2018) proposed an optimal design method and finite element modelling to obtain higher flux density design dimensions. Results from the FE analysis are verified through experimental characterization for its agreement. Parlak et al. (2012) proposed using magnetostatic analysis and CFD analysis for optimal damper design and to obtain higher magnetic flux density in fluid flow gap. The results from the simulation are used for fabricating MR damper and verifying the feasibility of design optimization.

Parlak et al. (2013) also designed and fabricated the MR damper using Taguchi method for different configurations and obtained the optimal design of the damper. Li and Yang (2020) and Yang et al. (2021) developed three magnetorheological coil dampers with a sigmoidal microstructure model which significantly impacts control strategies and dynamic analysis of the dampers micro-macro mechanical model can give further details on optimisation and high-performance MR fluids. Wereley et al. (2013) fabricated MR damper to study the effect of temperature on damping performance by maintaining the required chamber temperature. The testing results show that the temperature of MRFs can reach up to

100oC beyond which mechanical components of MR dampers such as seals fail. The lumped parameter model showed that the physical of the fluid such as inertia and stiffness reduced at elevated temperatures. Yu et al. (2013) worked on the different nonlinear models like Bingham plastic model and Herschel-Bulkley model by comparing the damper experimental analysis force-velocity plots and concluding that the Bingham plastic model is easier than HB model for theoretical analysis and for unsteady velocity HB model is suitable than Bingham model. Sahin et al. (2009) showed that, temperature significantly influences MRF properties such as viscosity, yield stress, sedimentation stability, and thermal conductivity. Viscosity and shear stress reduces as the temperature of the MR fluid increases.

Figure 2.7 MR damper used two-wheeler vehicle Devikiran et al. (2021)

Dong et al. (2017) have shown that optimal design parameters using the six sigma optimal design algorithm can reduce the temperature effects on damping of the MR damper. McKee et al. (2018) conclude that the gap in fluid flow plays a vital role in the performance of the MR damper. Results based on a theoretical model developed by incorporating the temperature-dependent property of a CI and silicone oil-based MRF showed that with the increase in the temperature of MRF, there is a reduction in stiffness and dissipation energy. Bingsan (2017) studied the effect of temperature on MR damper performance over a temperature range of 0 to 100 °C through hydro mechanical analysis. The calculated pre-yield force and post-yield damping coefficient were reduced by almost 30% and 85%, respectively, as the temperature

reached 100 °C. Experimental results show that the MR damper performs better at low frequency and high load conditions than coupled rubber shock absorbers. Allien et al. (2020) synthesized MR fluids for composite sandwich structures. The results show that increased magnetic field increases yield stress, increasing the beams damping capability.
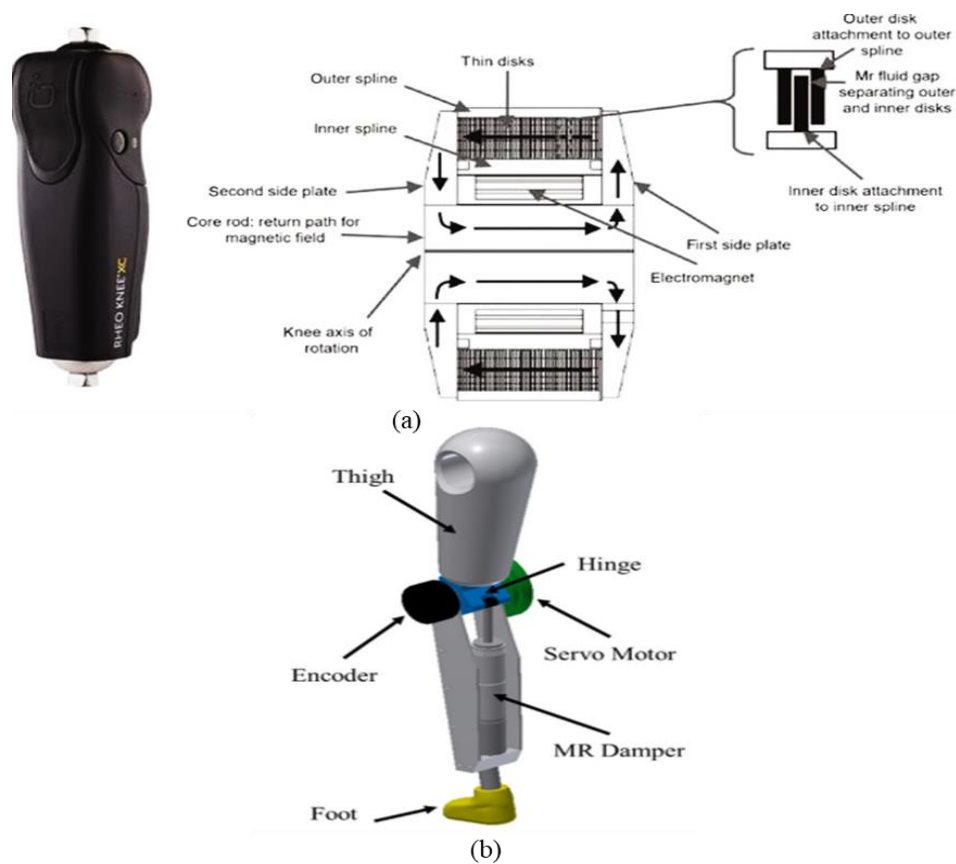
Figure 2.8 (a) Rheoknee (Bellman et al .2019)

(b) MR damper used in prosthetic limb

Bellmann et al. (2019) examined the practical performance of microprocessor-controlled with MR fluid and hydraulics based knee joints in day-to-day situations using biomechanical devices. A MR prosthetic knee consists of MR actuator, sensors and artificial intelligence. The viscosity of MR fluid is varied by the application of magnetic field and hence its flexion resistance. When the amputee walks, the stiffness of knee can be varied in real-time. Due to its inherent advantages compared to

hydraulic based prosthetic knees, it is being manufactured and marketed. Park et al. (2016) designed and manufactured MR prosthetic knee integrated with a controller and tested its performance on a level ground at different walking speeds.

Cheng et al. (2014) and Mistik et al. (2012) prepared different volume fraction MR fluids to study the influence of thermal conductivity behaviour. They proved that increased particle concentration increases thermal conductivity, which is also increased due to fluid compression. Wang et al. (2019) used finite analysis to show us that the piston rod dimension plays a significant role in distributing the magnetic flux to the gap and is studied through experimentation in twin-tube bypass, which gives higher damping force and can operate in fail-safe. A way to calculate the damping force of the damper is obtained through repeated experimentation and curve fit analysis. Kumbhar et al. (2015) and Nguyen and Choi (2009) obtained optimal parameters through finite element method and ANSYS parametric design language and showed that the damping force can be enhanced by increasing the applied current. Weiss (1994) studied through experimentation that temperature has vital effect on decreased performance by decreasing the yield stress of the fluid. Guerrero-Sanchez et al. (2009) studied heat generation inside the damper, which raises liquid temperature, decreasing the fluid's viscosity and reducing the MR damper's performance. Mangal and Kumar (2014) and Mangal and Kumar (2015) used finite element analysis to obtain the optimal dimensions through magnetic flux density in the flow gap. The experimental results were compatible with the design of damper from finite element analysis.

2.5 MAGNETORHEOLOGICAL BRAKE

Extensive research has been carried out on magnetorheological fluid systems that can be applied to suspension systems, seats, prosthetic legs, composite beam structures, etc. Apart from these MR fluid applications, MR brake with multiple rotors for torque generation can potentially replace existing brakes with better size and controllable torque. The MR fluid effect was studied by Rabinow and its torque behavior for replacements in exercise equipment by Webb (1998). The higher torque and its better controllability are vital for MR brake, which can be enhanced by a better selection of magnetic particles, rotor radius, and optimal design parameters of the gap,

stator length and better permeability materials. Optimal geometric dimensions of the MR brake, better permeability materials, and effective torque are important parameters to obtain higher torque. Maximization of torque and torque ratio; minimization of mass, temperature and the inductive time constant of the magnetic circuit and core arrangement for deciding the design parameters for higher torque generation was carried out by Jonsdottir et al. (2009), Nguyen and Choi (2010), Rossa et al. (2014), and Shamieh and Sedaghati (2017). Moreover Rossa et al. (2012) worked on disc brakes for betterment of actuators using better feedback control feedback is commonly used in various domains for better feedback.
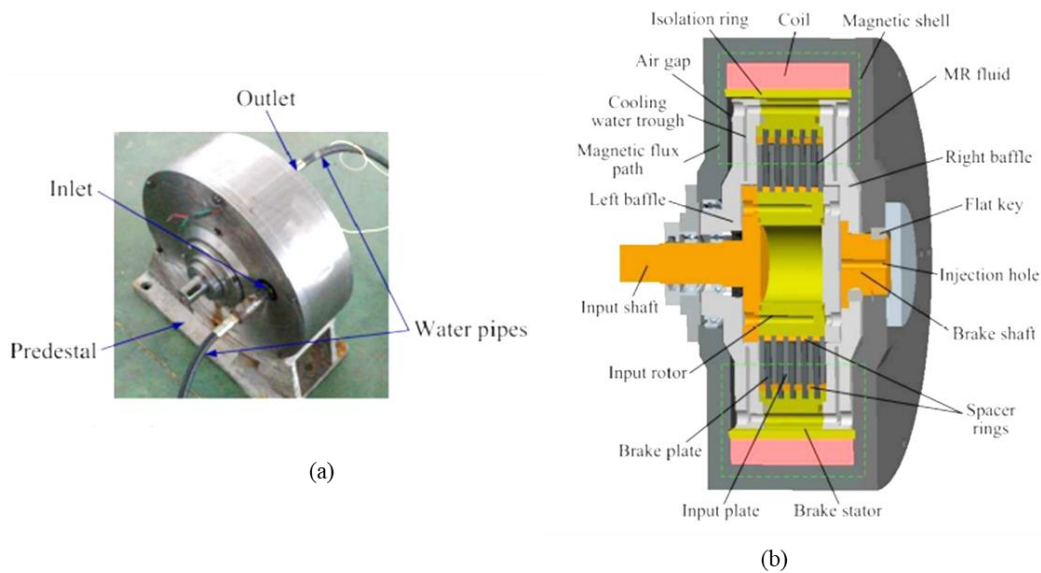
Figure 2.9 Multiplate Magnetorheological brake (Wang et al. 2013)

The power requirement for drum brake requires lower than for disc brakes, and reactivity is increased with increased fluid gaps. Li and Du (2003) show that torque variation is influenced by the viscosity and torque increases rapidly with increase in speed of rotation of the rotor. Wang et al. (2013) fabricated MR brake with multiples as shown in figure 2.9.
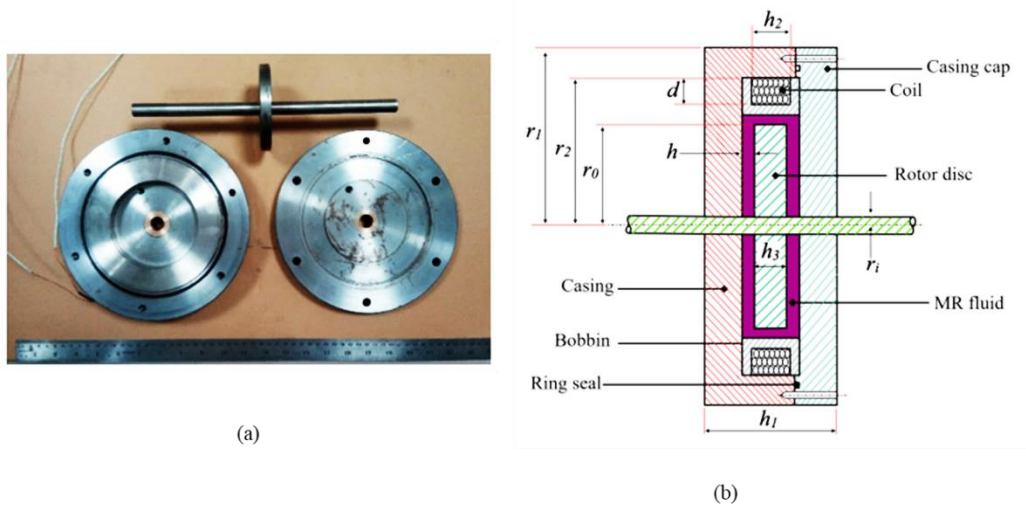
Figure 2.10 Single plate MR brake (Acharya et al. 2020)

Assadsangabi (2012) studied the disc brake through finite element analysis to study the maximization of magnetic flux density and by using genetic algorithm they optimized Multiplate brake. And they concluded that scaling down the size reduces torque generation. Li et al. (2007) developed a 2d MR joystick for virtual reality applications. They conclude that torque obtained from the joystick is about 10 Nm, which has a wide range of applications in virtual surgery and can be expanded to other application which is minimal in size. Avraam et al. (2010) worked on the development of active multi-pole core to increase the torque for rehabilitation with optimized mass and particle volume was evaluated. And Karakoc et al. (2008) has discussed the various types of MR brakes that can be studied for the replacements of MR brakes and applications which was discussed by Clair (1996) and Jolly et al. (1996).

The vital parameters which determine the torque characterization is fluid gap, the permeability of a material, rotor radius, and applied magnetic field. Using available industry fluid, Sukhwani and Hirani (2008) studied the torque characteristics and the characterization results evaluated the decrease in shear gap increases the torque generation and conclude the location of electromagnet play an important role in increasing the torque. It was shown by Poznic et al. (2017) that a combination of permeable and non-permeable materials has a significant influence on torque generation for one rotor brake than using commercially basonetic 5030. Through finite element analysis Zhou et al. (2007) and Zaifazlin Zainordin et al. (2018)

modelled two-rotor disc for higher torque capacity using commercially available fluid and they concluded that compactness and increasing rotor numbers increases the torque. Torque generation was calculated using analytical design equations by Acharya et al. (2019) for T-shaped MR brake shown in figure 2.11. Using MOGA technique they found the optimal design combinations of fluid combination and design dimensions of the brake. Using magnetostatic analysis Lijesh et al. (2018) studied the influence of various parameters on torque generation and suggested a method to calculate the highest torque using equations. However, temperature has a vital impact on the performance of any fluid system application. Carlson (2002) experimentally illustrates that the operating time and input parameters has higher impact on performance of MR damper and MR brake due to shear thickening effect of the fluid.

2.6 MOTIVATION

The temperature has a vital role in any MR fluid applications system and the performance and life of the system. It has been established from the literature that a large amount o MR damper applications mostly in the vehicular application. Lord Corporation (USA) is the top producers MR dampers for the truck seat and automobile damping in cars. Cost effectiveness and better performance in implementing the damper are the major requirements for any specific applications. The requirement in cost-effectiveness and performance is the basis for synthesis of MR fluid in-house and design development of MR damper for its performance analysis with respect to temperature function and finding out the relationship between damping force and temperature. The detail related to the present research which needs to be carried out is listed below.

- As a whole, the existing literature study shows single carrier fluid and single additive MR fluid studies. However, a comparative study has not been attempted using different carrier fluids and additives for stability and flow characteristics with varying temperatures and magnetic fields. Hence an effort was initiated in the present work to study various viscosity carrier fluids and combinations of additives.
- Six different MRFs have been prepared in-house and investigated their

sedimentation stability, viscosity, and yield stress variations at different temperatures and magnetic fields. Better MR fluid based on stability and yield stress was selected for performance analysis in MR damper, and the dynamic range of the two different viscosity fluids was discussed.

- A survey related to sedimentation rate at different temperatures and flow characteristics with varying temperature and magnetic fields is needed, along with the effect of temperature on the damper's performance while working and assessing the life of the fluid and particle through TGA and SEM of heat-treated CI particles after dynamic testing of the fluid.

- The selected fluid should be tested in the MR damper by connecting the thermocouple inside the damper

The literature study related to MR brakes is concentrated on the preparation of MR fluid and characterization for various applications such as automotive brakes and prosthetic applications. However, there is a need to analyze the performance of the miniature two-rotor MR brake to expand the application area of MR brakes with increased torque generation. The following research backdrops are outlined in the current work and listed below.

- To fabricate scaled down two rotor MR brakes and to study the torque generation performance. At the end of test, the temperature effect on settling and torque generation was carried out.

- Further the study was extended to carry out synthesis particles in-house using the chemical reduction method. The properties required for MR fluid preparation such as SEM, XRD and VSM of the sample was carried out. The modified design for the two-rotor MR brake were evaluated and incorporated in the context of the future scope of this study.

2.7 OBJECTIVES

1. To synthesize and study MR fluid sedimentation rate for different combinations of additives with varying temperatures.
2. To characterize MR fluid and to establish a relation between temperature, viscosity, and yield stress of MR fluid.
3. To design, develop, and perform dynamic characterization of monotube MR damper to study the temperature effect on damping force.
4. To study the torque generation capacity of two plate rotor magnetorheological brake and the sedimentation effect on torque generation.

2.8 SCOPE OF RESEARCH WORK

1. Preparation of MR fluid using carbonyl iron particles with two combinations of additives and carrier fluids.
2. Sedimentation stability study of various MR fluid combinations at different temperatures maintained in the incubator.
3. Rheological behaviour of different MR fluid combinations to know the yield behaviour of the MR fluids using non-linear model.
4. Development of monotube MR damper and thermocouple arrangement to measure the fluid temperature while damper is operating.
5. Finding the relationship between the damping force and temperature as the number of operating cycle's increases.
6. Characterizing the MR particles after operating the damper at higher temperatures and finding out the carrier fluid's destabilizing temperature point and magnetic particles through TGA and SEM analysis.
7. Development of miniature size two rotor MR brake for torque generation with varying currents.
8. Effect of sedimentation on torque generation after operating the MR brake for a certain amount of time.

2.9 METHODOLOGY

The present methodology section consists of particle characterization, synthesis and characterization of the MR fluid for flow characteristics. Secondly, design of MR damper and two rotor MR brake and its performance analysis using MR fluid. Finally, particle characterization before and after the MR fluid testing in MR damper and MR brake was carried out.

The following section illustrates the details of the methodology followed throughout the study, which is shown in figure 2.12. Before preparing the MR fluid sample, tests were carried out on particle size distribution and shape analysis using particle size analyzer and scanning electron microscope (SEM). The hysteresis curve and crystal structure study for the carbonyl iron (CI) (manufacturer: Sigma Aldrich, 44890) particles is obtained from the vibration sample magnetometer (VSM) (manufacturer: lakeshore) and X-ray diffraction (XRD). Studies on MR fluids' stability at different temperatures were carried out in an incubator, and characterization was carried out at the rheometer (manufacturer: Anton-Paar). After characterization, the results were analyzed for the damping force and dynamic range. The Bingham fluid model and Herschel-Bulkley model were used to analyze the flow behavior is given below.

$$\tau = \tau_o + \mu\,(\gamma) \qquad\qquad (2.1)$$

Where τ = shear stress (Pa), τ_o = Yield stress (Pa), μ = Viscosity (Pa-s) and γ = shear rate(s^{-1})

The best MR fluid which was found out from sedimentation study and higher yield stress is synthesized in the required quantity to fill the volume of the MR damper cylinder to study the performance characteristics of the MR fluid in damping and two-rotor MR brake for torque generation capacity for different input conditions such as amplitude, frequency, applied current and rotor speed. Finally after testing the damper particle analysis was carried out. The temperature of the MR fluid is measured using an embedded thermocouple while the damper is operating at different loading parameters. The theoretical model predicts the increase in temperature similar to that of the experimental values with an average error of 10.24 % in the on-state condition. Particle characterization on SEM and VSM was carried out after dynamic testing to

see the effect of temperature on morphology and magnetic saturation. It is tested using thermogravimetric analysis (TGA) the life of the fluid after dynamic testing of the fluid for approximately 85000 cycles. Finally, to imitate the temperature effect on the particle, particles were heat-treated at 200 °C, 400 °C, and 600 °C, and through SEM image, it is confirmed that deterioration of the particle starts after 200 °C, if the fluid is operated for a prolonged amount of time.

The second part of the study is related to miniature sized MR brake design, development and characterization. Largely the literature study is concentrated on preparation of MR fluid and characterization of MR brakes for various application such as automotive brakes. However, there is a need to analyze the performance of the miniature (total mass = 1.62 kg) two-rotor MR brake for various applications. Hence, an effort is initiated to fabricate miniature two rotor MR brakes and its performance analysis. Finally the temperature effect on settling and torque generation was carried out. Further the study was extended to carry out the synthesis of particles in-house using chemical reduction method. The properties required for MR fluid applications such as SEM, XRD and VSM of the sample was carried out and also the modified design for of the two-rotor MR brake was evaluated and incorporated in the context of the future scope of this study.
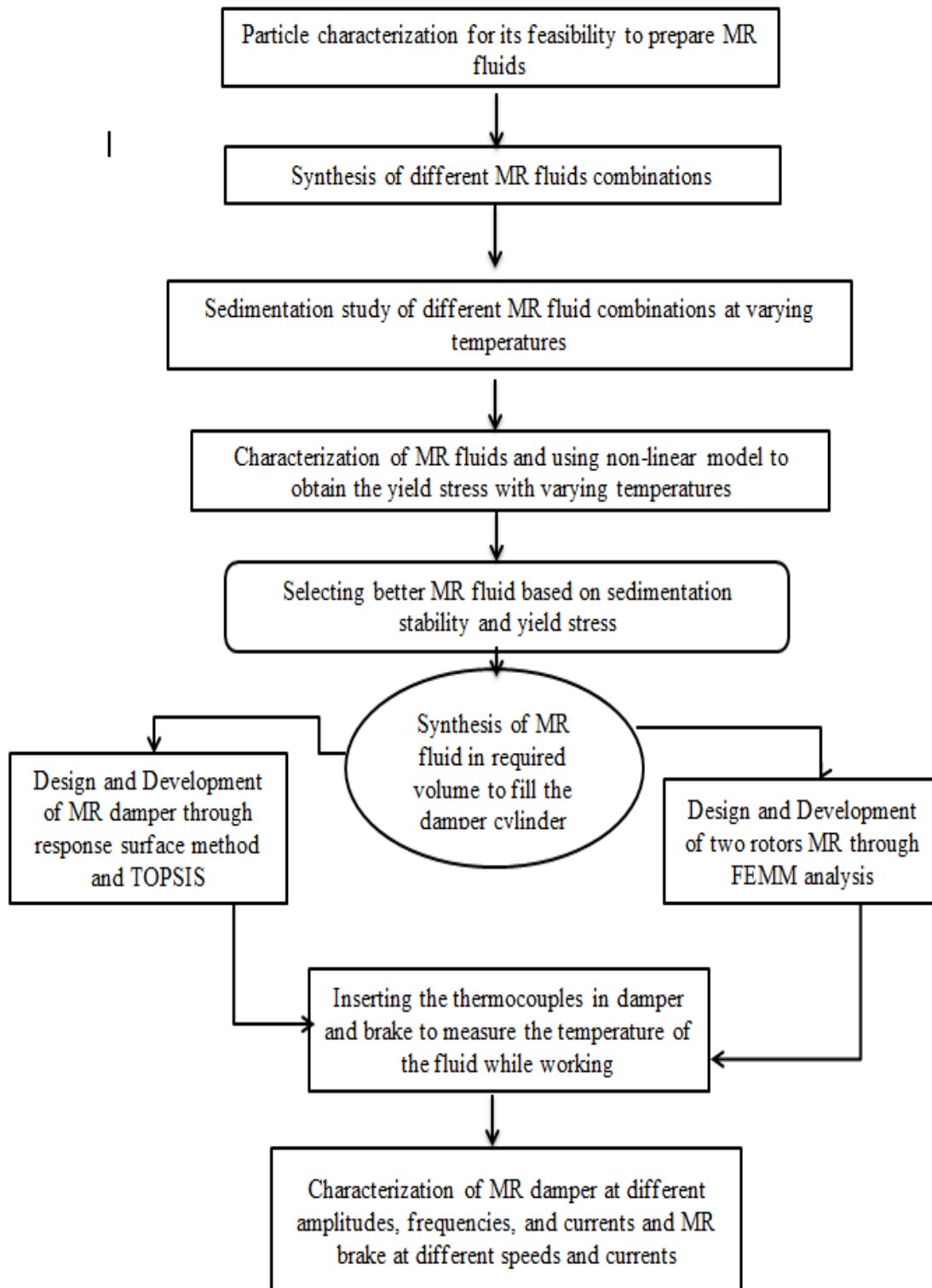
Figure 2.11 Methodology flow chart for the present study

2.10 SUMMARY

The current chapter shows the literature study related to synthesis and characterisation of MR fluids along with the design development of MR damper and two plate rotor MR brake. The literature discourses the stability of the MR fluid and its mode of operations in different applications. Later, an investigation on the use of MR fluid devices and the some device arrangements was informed. Several inadequacies connected with both the characterization and their performance studies the aims and scope of the current study have been projected. The successive chapters introduce the synthesis of MR fluids, and also design methodology to obtain the geometric dimensions of MR damper and MR brake for the fabrication process and finally arrive at the conclusions.

CHAPTER 3

EFFECT OF TEMPERATURE ON SEDIMENTATION STABILITY AND FLOW CHARACTERISTICS OF MAGNETORHEOLOGICAL FLUIDS WITH DAMPER AS THE PERFORMANCE ANALYSER

3.1 INTRODUCTION

Sedimentation stability and high yield stress of a magnetorheological fluid (MRFs) are essential parameters for better damping performance for any practical application. It has been proposed by the previous literature that the constituents of the MR fluid play a significant role in performance of any MR fluid application. The primary requirement for enhanced MR damper performance is sedimentation stability and higher yield stress of the MR fluid. Few researches have shown that carrier fluid viscosity and particle size have immense effect on the increased performance of the MR fluid. An increase in performance can be seen by increasing the particle concentration and base fluid viscosity of the fluid sample. This study synthesizes various MRFs from various commonly used carrier oils and additives. The MRF samples were prepared for 25 % volume fractions of carbonyl iron (CI) powder in either silicone oil (350 cSt) or hydraulic oil (50 cSt) and by using lithium and calcium-based additives or a combination of both the additives. The sedimentation stability and yield behaviour at different temperatures were carried out for all the MR fluid samples and based on this study higher stability and higher yield stress fluid are selected for performance analysis in the MR damper which is fabricated based on the dimensions obtained from the response surface optimization technique. Further, similar tests have been carried out by synthesizing MRF-7 with silicone oil (50 cSt) + lithium base grease as the additive. The sample's stability, yield stress and performance with temperature were carried out. Finally, temperature characteristics captured from the

thermocouple of the MR damper were analysed for the effect of temperature on dynamic range.

3.2 MATERIALS AND METHODOLOGY

Figure 3.1 gives brief details on the methodology followed in this work. Before preparing the MR fluid sample, tests were carried out on particle size distribution and shape analysis using particle size analyser and scanning electron microscope (SEM). The hysteresis curve and crystal structure study for the carbonyl iron (CI) (manufacturer: Sigma Aldrich, 44890) particles is obtained from the vibration sample magnetometer (VSM) (manufacturer: lakeshore) and X-ray diffraction (XRD). Studies on MR fluids' stability at different temperatures were carried out in an incubator, and characterization was carried out using a rheometer (manufacturer: Anton-Paar). After characterization, the results were analyzed for the damping force and dynamic range. Table 3.1 gives the details of particles used to synthesize six MR fluids. The Bingham fluid model used to analyze the flow behavior is given below.

$$\tau = \tau_o + \mu (\gamma) \qquad\qquad (3.1)$$

Where τ = shear stress (Pa), τ_o = Yield stress (Pa), μ = Viscosity (Pa-s) and γ = shear rate(s^{-1})
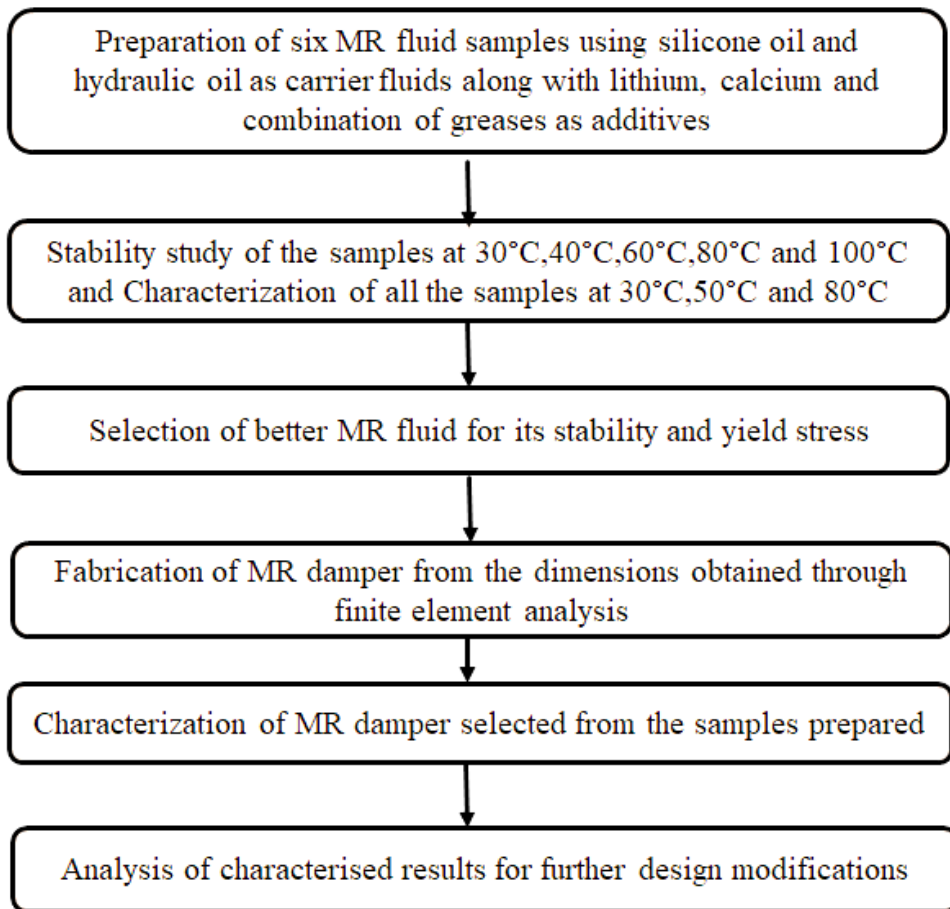
Figure 3.1 Methodology flow chart for this section of this study

3.2.1 Particle Characterization

Characteristics of carbonyl iron particles were studied by scanning electron microscope (SEM), Energy-dispersive X-ray spectroscopy (EDX), and particle size analyser as shown in figure 3.2 to figure 3.5. The reduction in saturation magnetization implies that the damping performance of MR fluid is reduced at higher temperatures. Table 3.1 gives a summary of the magnetic particle study.

Table 3.1 Summary of the material analysis.

Type of material	the shape of the particle	Size of the particle	purity of the powder	Deviation from standard purity
Carbonyl iron powder	Spherical	7.49 Microns	99.51%	0.48%
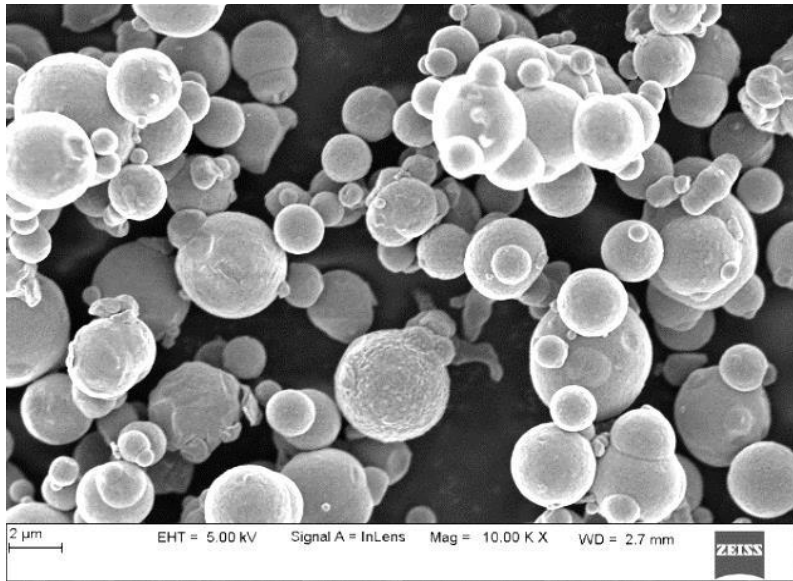
Figure 3.2 SEM image of CI particles

Figure 3.2 and figure 3.3 show the spherical shape of particles and the composition of the CI powder.
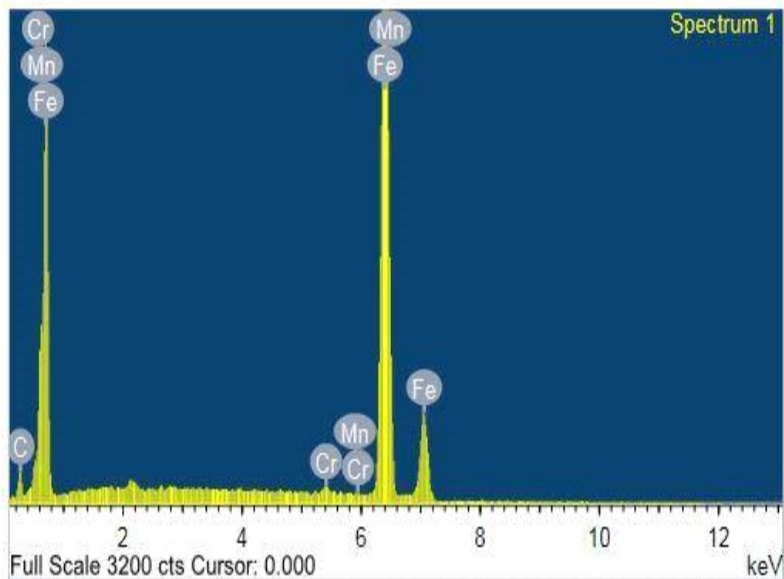
Figure 3.3 Elemental compositions in Carbonyl iron powder

Table 3.2 gives us the composition of the CI powder, which contains Iron (Fe), carbon(C), chromium (Cr), and Manganese (Mn) in 87.75%, 0 %, 0.41%, and 0.03% for a total of 88.18% respectively.

Table 3.2 Extracted powder composition

Element	Weight (%)	Atom (%)
Cr	0.41	0.49
Mn	0.03	0.03
Fe	87.75	99.48

The average size of the particle shown in figure 3.3 comes out to be 7.49μm, enough for the MR fluid preparation and applications. Since the magnetic dipolar moment in the particles grows with the volume fraction and the Brownian motion becomes insignificant in this particle range.
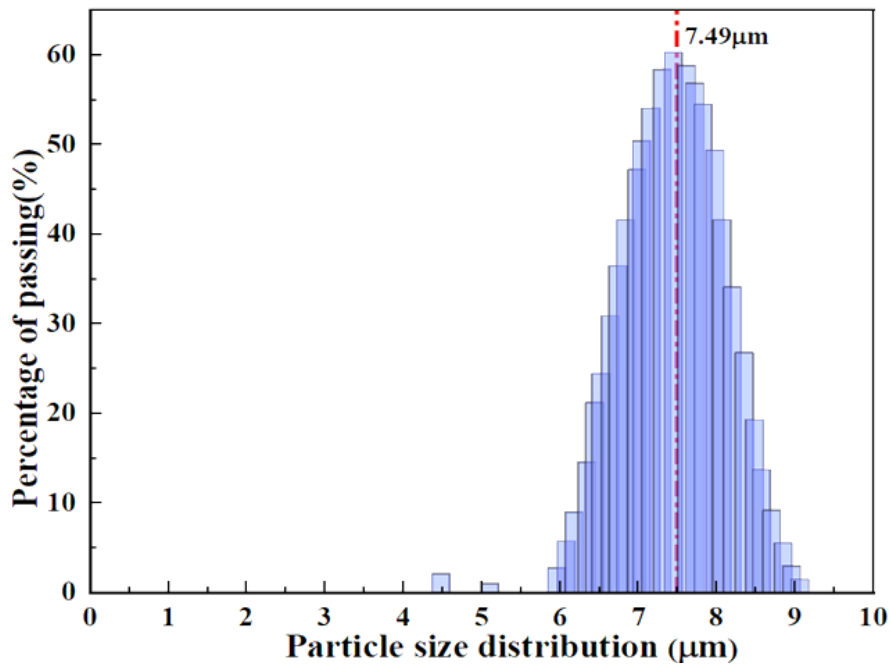
Figure 3.4 Particle size distribution of CI particles

The particle crystal structure of the CI particles was obtained using Advanced X-ray diffraction equipment. From figure 3.5, the peaks are obtained at 45.3°, 65.71°, and 82.94°, which correspond to 2θ at 110, 200, and 211 lattice planes which implies that the crystal structure is a body-centered cube (BCC) and gives confirmation to prepare the MR fluid for further studies in this work.
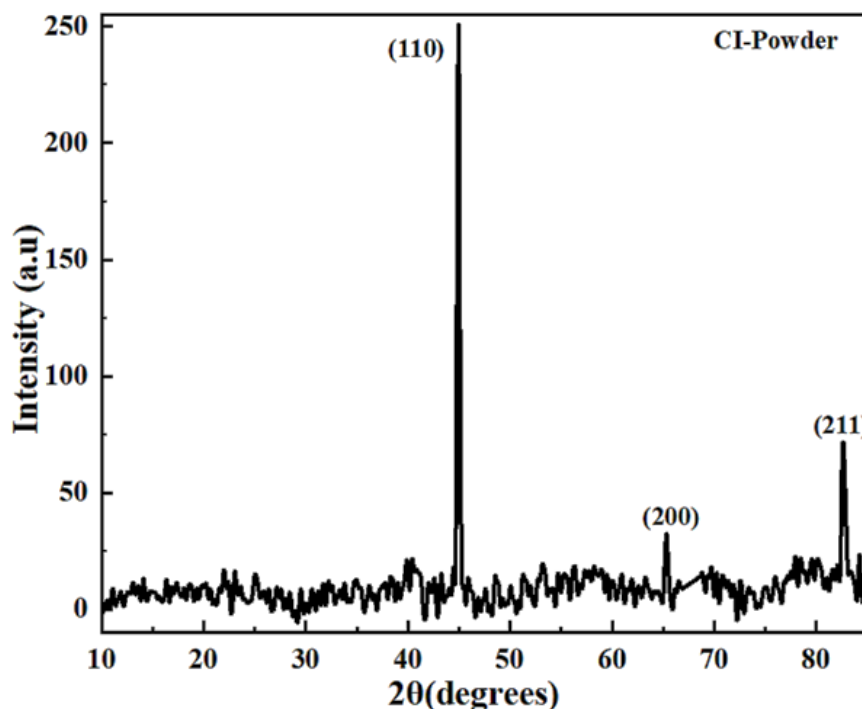
Figure 3.5 XRD plot of CI particles

Fourier Transform Infrared spectroscopy (FT-IR) analysis for the carbonyl iron particles is shown in figure 3.6. All individual samples were mixed to make pellets with KBr and tested in the weber number range of 500cm^{-1}-4000cm^{-1}. The analysis shows some of the elements present in the powder are discussed below. The presence of the hydroxyl group is shown by the peak at 3495.54cm^{-1}, which represents O–H stretching. The C-H band of stretching and triple bond of carbon-carbon is represented by wavenumber 2758 and 2289. The carboxyl group is shown by the peak 1548cm^{-1}. Asymmetric stretching and symmetric bonding are represented by the peak 1084cm^{-1}. A peak specifies the C–H bonds at 695cm^{-1}.

50
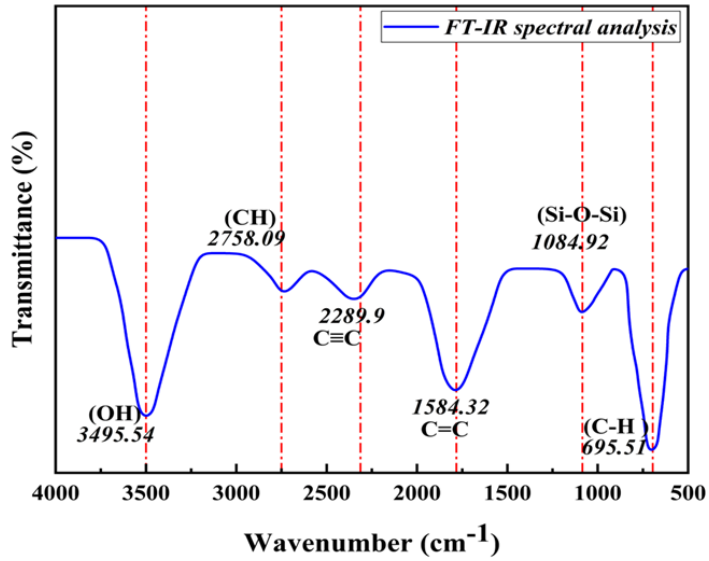
Figure 3.6 Fourier Transform Infrared spectroscopy of CI particles

The magnetic particles should possess higher magnetic saturation, lower remnant magnetization, and lower coercivity for better yield characteristics of the MR fluid and reversibility in magnetic effect. From the properties of particles, it is evident that 0.1464 emu/g retentivity, 0.59 Gauss coercivity, and 362 emu/g saturation magnetization at 300 K have better properties for MR fluid application. The saturation magnetization is reduced to 332 emu/g at 400 K shown in figure 3.7.
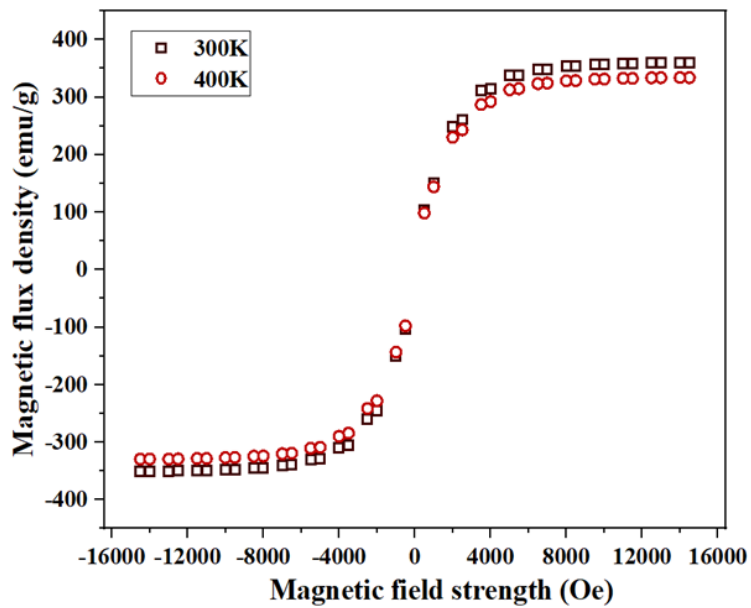
Figure 3.7 Vibration sample magnetometer of CI particles

Thermogravimetric analysis (TGA: PerkinElmer, TGA4000) was carried out quartz crucible to study the onset of degradation of two MRFs with an increase in temperature over time. As shown in figure 3.8, it is evident that weight loss of 21.64% at 323.37°C and 23.42% at 215.78°C for MRF-1 (sample taken: 20.38mg) and MRF-2(sample taken: 19.8mg) respectively. The evaporation of base fluid indicates the stability of the carrier fluid. As the temperature crosses the degradation temperature, the overall heat generated is transferred to the particles making the particles coagulate, as shown in figure 3.8 (insert image).
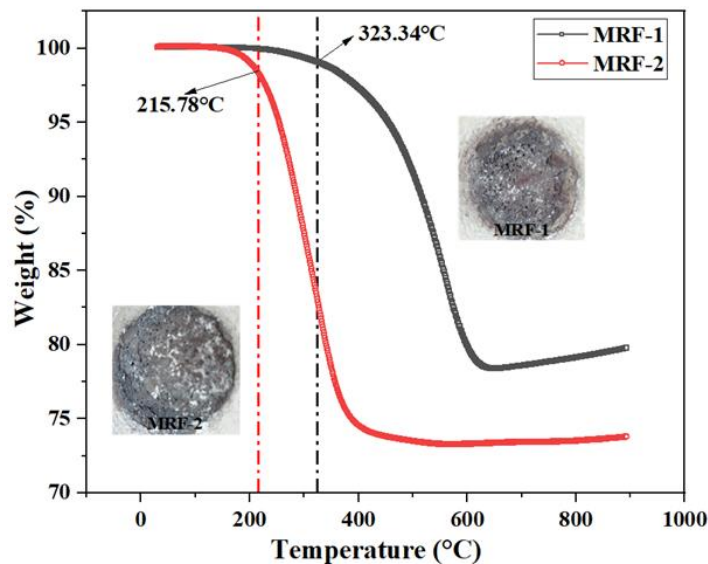
Figure 3.8 Thermogravimetric analysis of MR fluid samples

3.2.2 Synthesis of magnetorheological fluid

The primary step in characterizing the MR damper is to MR fluids were prepared by dispersing carbonyl iron particles (25 % by volume) in the carrier fluid (manufacturer: Sigma Aldrich, product number: 378372) with 2 % additive(s). Figure 3.9 shows the steps to synthesize MR fluids. First, a calculated amount of carrier fluid and additive was added, and the composition was stirred at 700 rpm for 12 hours. Finally, carbonyl iron particles were added to the mixture and stirred further for about 24 hours. The total time to prepare an in-house MR fluid was about 36 hours.
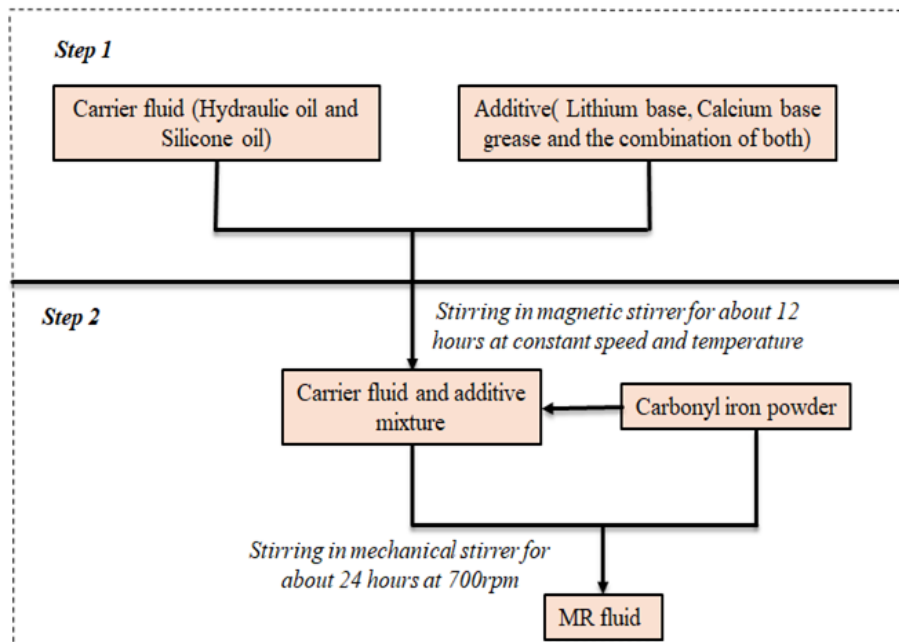
Figure 3.9 Steps to synthesize MR fluid

Figure 3.10 shows the instruments used to prepare MR fluids. Initially carrier fluid and additives were mixed using a magnetic stirrer with heating to completely homogenize the grease in the base fluid. Secondly, the primary mixture is stirred in mechanical stirrer. After the specified time of stirring the MR fluid sample is prepared.
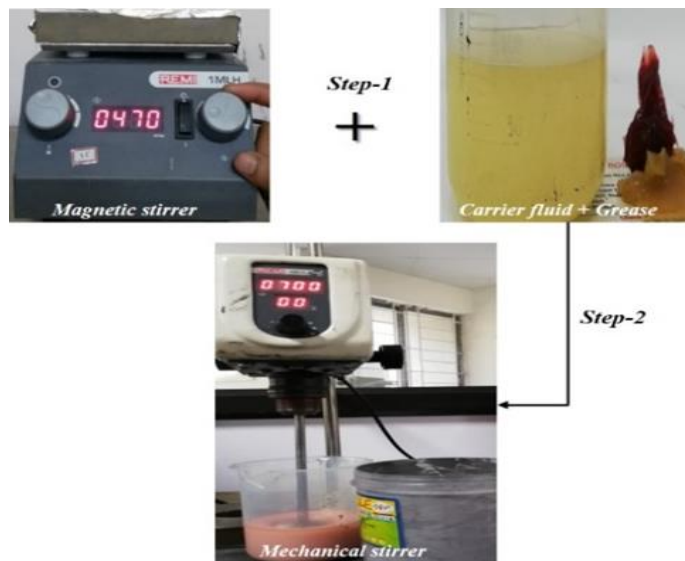
Figure 3.10 Instruments used to synthesize MR fluid

3.2.3 Sedimentation ratio of the MR samples

Generally, Carbonyl iron (CI) microparticles tend to settle down towards the bottom of the measuring cylinder due to gravity, leaving behind clear carrier fluid on top and forming a layer of particle-laden fluid at the bottom. The definition of sedimentation ratio is the volume of clear carrier fluid zone above the particle-laden layer to the total volume of the liquid in the cylinder before the settling process. The sedimentation ratio for all MR samples at ambient temperature and various higher temperatures was obtained through visual observation.

Figure 3.11 Particle size analyser (CILAS1064)

Figure 3.11 shows the equipment used to measure the average particle size of the particles. The temperature of samples was maintained in the laboratory incubator (2.5 % to 3 % error), as shown in figure 3.12. The time for settling particles is observed at five individual temperatures, and the sedimentation rate of the MR fluid layer is calculated.
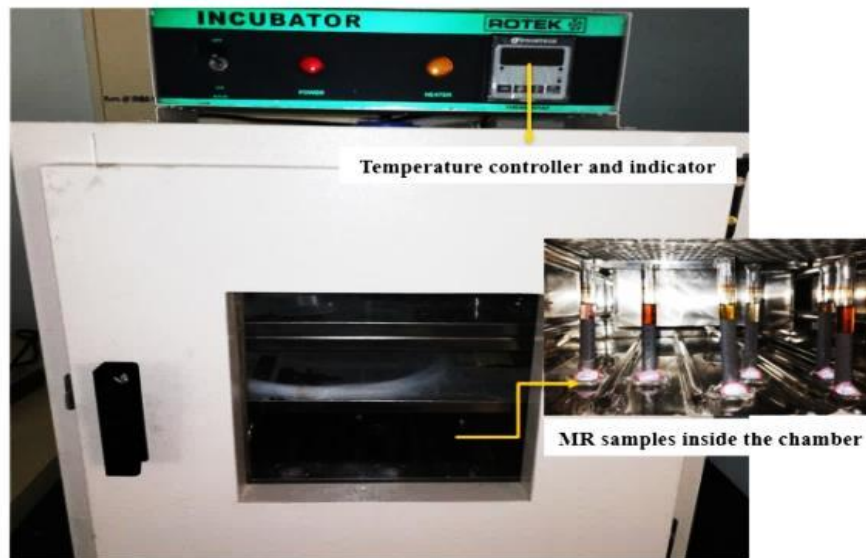
Figure 3.12 Incubator for constant temperature settling rate

The sedimentation rate is defined as the speed at which the interface between the clear liquid and particle-laden liquid comes down, which is more convenient in comparing the sedimentation stability of different MR fluids. The six MRFs after the settling of the particles are shown in figure 3.13.
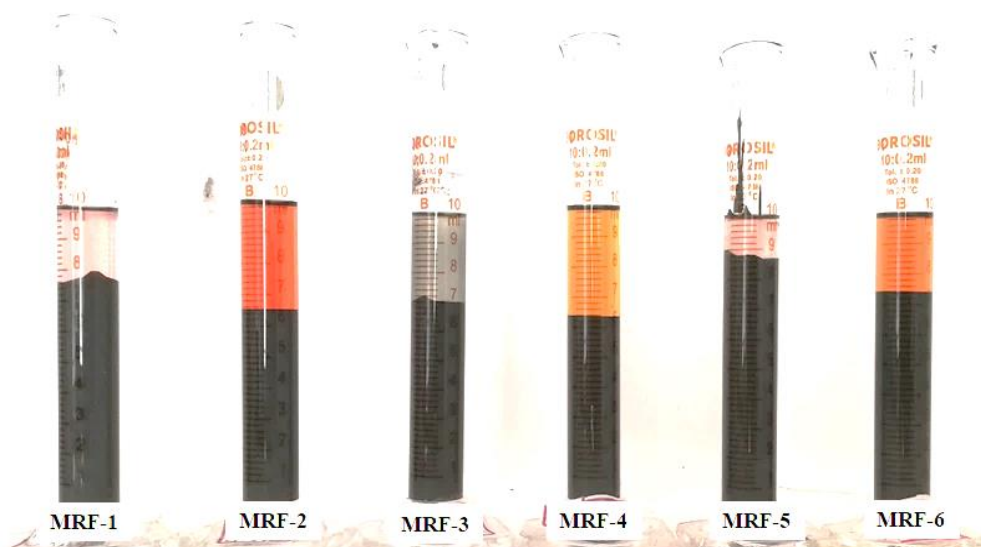
Figure 3.13 MR fluid samples after sedimentation study

In this study, silicon oil-based MR fluid (MRF-1, MRF-3, and MRF-5) gives higher stability than hydraulic oil (MRF-2, MRF-4, MRF-6) based MR fluids. Further to analyse the performance of the damper with temperature effect MRF-1 is selected

characterize the damper. Table 3.3 shows six different MR fluid samples synthesized from various carrier fluid and additives combinations.

Table 3.3 MR fluid samples with carrier fluids and additives

MR samples	CI powder (%)	Carrier fluid	Type of Additive
MRF 1	25	Silicone oil	Lithium grease
MRF 2	25	Hydraulic oil	Lithium grease
MRF 3	25	Silicone oil	Calcium grease
MRF 4	25	Hydraulic oil	Calcium grease
MRF 5	25	Silicone oil	Lithium+ calcium
MRF 6	25	Hydraulic oil	Lithium+ calcium

3.2.4 Characterization of the prepared MRF samples

The characterization of the MR fluid samples was carried out on a parallel plate rheometer with an MRD cell. The temperature of the MR fluid is kept constant (30 $^{\circ}$C, 50 °C, 80 °C) during the characterization of the sample. The rheometer has a shearing spindle which is pneumatically controlled with the air bearings. The shearing gap is maintained constant (1 mm) throughout the tests. The shear rate is applied from 0.1 s^{-1} to 500 s^{-1} at 0 A and 2 A currents, the plot of viscosity versus shear rate and shear stress versus shear rate were obtained. Figure 3.14 shows the rheometer setup used for characterization.
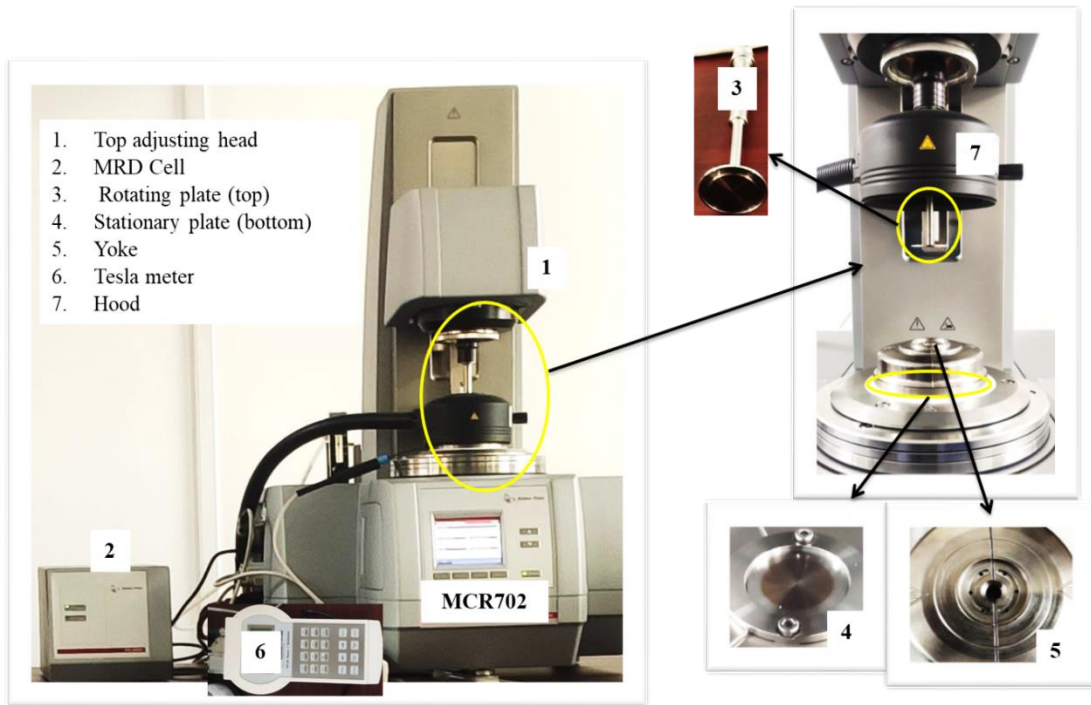
Figure 3.14 Rheometer setup for MR characterization

3.2.5 Geometric dimensions for fabrication

Optimizing the geometric dimensions for MR damper fabrication has been performed using the response surface method (RSM). The finite element (FE) analysis shows that the magnetic flux density increases with increased applied current up to some saturation point. The flux density is inversely proportional to the fluid flow gap width. The decrease in the magnetic saturation in the fluid is due to the effect additive effect on the particle.

Table 3.4 Geometric dimensions and their bounds

Geometric parameters	Lower bound	Upper bound
Flange length (mm) (L_f)	3	6
Core length (mm), (C_L)	15	27
Flow gap (mm), (g)	0.5	2.5
Number of Turns, (N)	100	500
Current Magnitude (I)	0.5	2.5

Magnetic core length increases the accommodation of the coils, which in turn increases the current supplied to the electromagnet. The geometric variables with lower and upper bounds are in Table 3.4. Figure 3.15 shows the flux lines between the effective length and the outer cylinder.
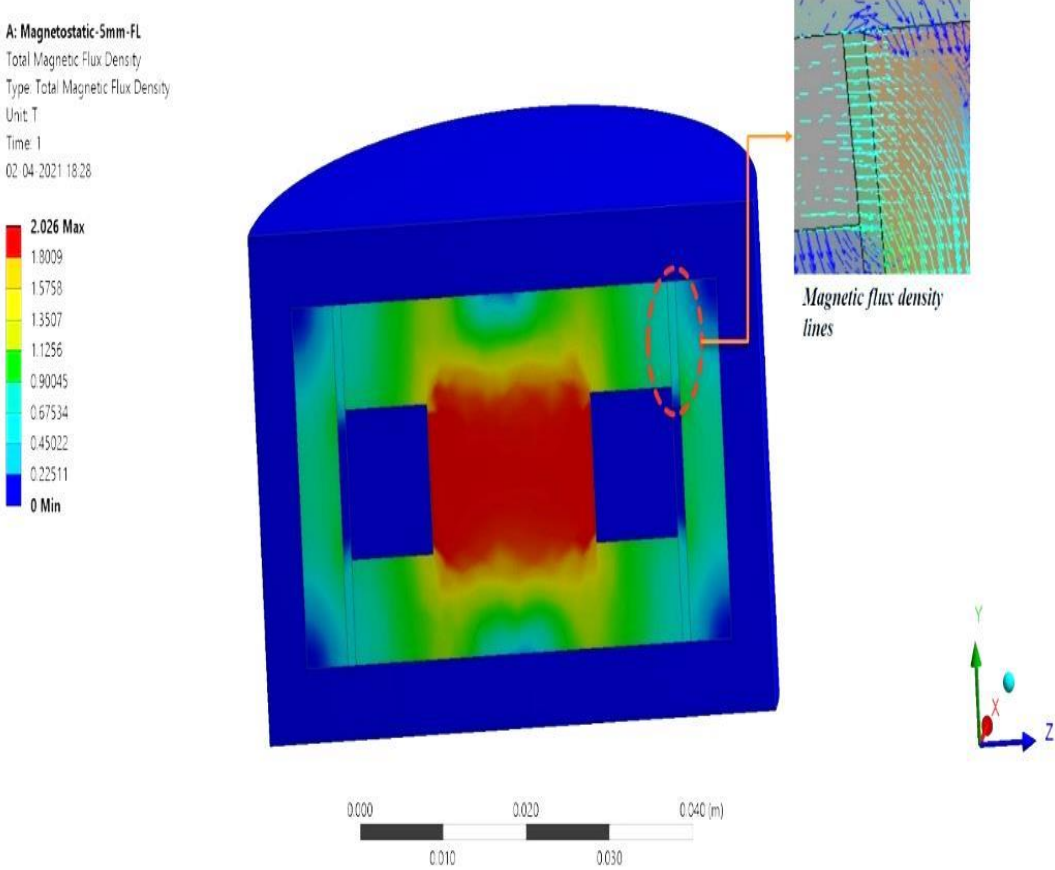
Figure 3.15 Magnetostatic analysis of MR damper model and flux lines

The two important parameters that influence magnetic flux variation in the damper are the effective length and fluid flow gap. The variation in magnetic flux density with an increase in effective length and fluid flow gap is depicted in figure 3.17. The decrease in the magnetic flux inside the fluid gap determines the yield stress of the fluid. The increase in yield stress increases the damping force and a decrease in yield stress decreases the damping force.
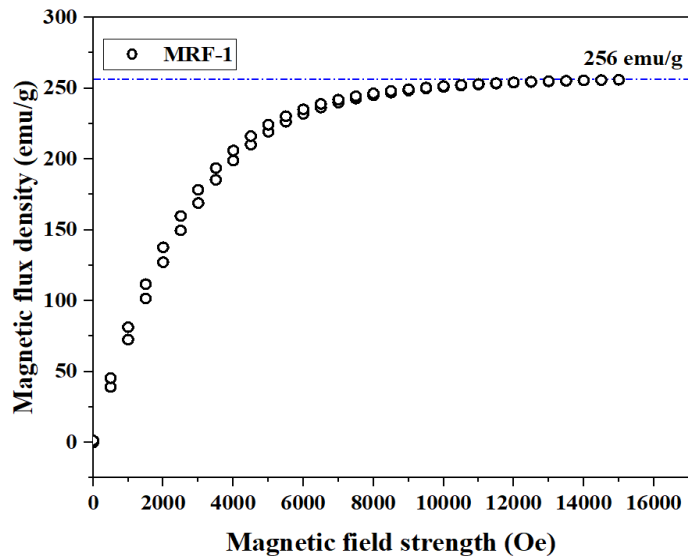
Figure 3.16 Saturation magnetization of MR fluid

The magnetic saturation curve used for MRF-1 is shown in figure 3.16. The decrease in the magnetic saturation point of the fluid when compared to the magnetic particle is due to the additive percentage which acts as a coating on the surface of the magnetic particle. The magnetic saturation point of the fluid is directly related to the yield stress of the fluid which decides the performance of the MR damper during the operation.
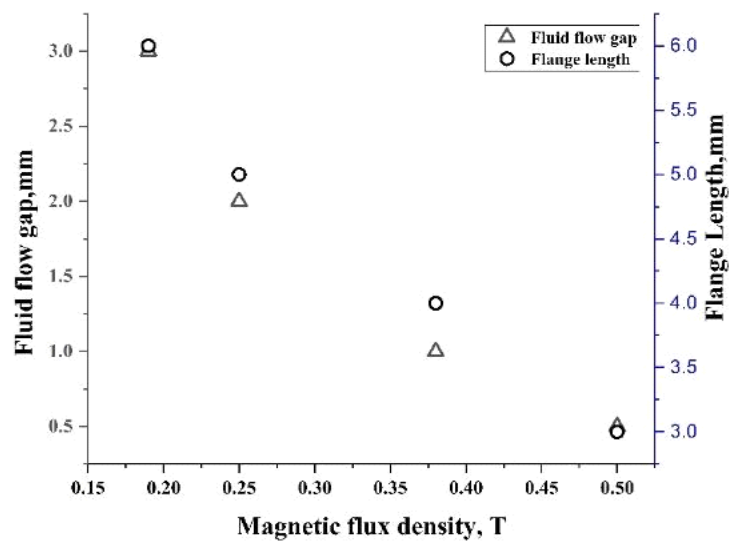
Figure 3.17 Effect of fluid gap and flange length in MR damper

The geometric dimensions that will give the highest magnetic flux density by the response surface optimization methodology (RSM) for MR damper fabrication are given in table 3.5. The upper bound and lower bounds were based on the literature and size requirements for the present study to measure force obtained by the mentioned fluid (MRF-1).

Table 3.5 Geometric dimensions selected for fabrication

	Flange length, mm	Corel length, mm	Flow gap, mm	Number of turns	Current, A
Points	5	21	1	350	1.5

3.2.6 Characterization of MR damper

The monotube MR damper consists of a cylinder filled with MRF-1 and an electromagnet consisting of a coil and electrical wires. The accumulator is not used in the fabrication process in the present study. Equation (1) shows that the damping force (F) has viscous force (F_v) and field-dependent force (F_τ).

$$F = F_\mu + F_\tau \tag{3.2}$$

The field-dependent damping force and viscous damping force are expressed by equations (3.3) and (3.4).

$$F_\tau = (2.07 + 12Q\mu/12Q\mu + 0.4 \times w \times g2 \times \tau y) \times (\tau_y L_f A_p/g) \text{ sgn } (v) \tag{3.3}$$

$$F_\mu = 1 + (w \times g \times v/2Q) (12\mu Q L_p A_p/w \times g^3) \tag{3.4}$$

$$Ap = \pi \times (D_p{}^2 - D_r{}^2)/4$$

$$w = \pi(g + D_p)$$

$$Q = v \times A_p$$

where L_p = length of the piston (mm), L_f = Pole length (mm), w = circumference gap (mm), D_p = piston diameter (mm), g = flow gap (mm), μ = apparent viscosity without current (Pa-s), τ_y = yield stress (Pa), D_r = Piston rod diameter (m), Q = flow rate (mm^3/s), and A_p = area of the piston (mm^2).

The dynamic range (DR) is the ratio of the overall damping force to the force which is uncontrollable which includes viscous force and accumulator force and negligible friction force.

$$DR = (F_\mu + F_\tau)/ F_\mu \qquad\qquad (3.5)$$

MR damper testing is performed on the damper testing machine, which is shown in figure 3.18. The damper testing machine consists of the hydraulic actuator, controlled by a portable test controller that controls the input parameters. The loading frames can be adjusted using vertical columns according to damper size. The force vs. displacement graphs was obtained by giving the required frequency and amplitude. The DC power supply gives external current to the coil whenever required. The characterization was carried out at three different frequencies (2 Hz, 3 Hz, and 4 Hz), three amplitudes (2 mm, 4 mm, and 6 mm), and five different currents (0 A to 1 A) to see the input parameter's effect on the performance of the damper. The dynamic range is calculated from the force obtained, and further results are evaluated.

Figure 3.18 Damper testing machine

The damper testing machine consists of the hydraulic actuator, controlled by a portable test controller that controls the input parameters. The loading frames can be adjusted using vertical columns according to damper size. The force vs. displacement graphs was obtained by giving the required frequency and amplitude. The DC power supply gives external current to the coil whenever required. The characterization was carried out at three different frequencies (2 Hz, 3 Hz, and 4 Hz), three amplitudes (2 mm, 4 mm, and 6 mm), and five different currents (0 A to 1 A) to see the input parameter's effect on the performance of the damper. The dynamic range is calculated from the force obtained, and further results are evaluated.

Figure 3.19 Exploded view of the MR damper

3.3 RESULTS AND DISCUSSION

This section deals results evaluation of the MR fluid sedimentation study and flow behaviour with temperature and magnetic field. To determine the performance of the MR fluid the damper is fabricated and through characterization the dynamic range of the fluid in the damper is obtained.

3.3.1 Sedimentation ratio of MR fluids

As the particles settle due to density difference, it leaves behind a clear volume of carrier fluid. The sedimentation ratio is defined as the clear carrier fluid volume on top of the particulate layer to the volume of the MR fluid sample before the start of settling. The viscosity of the carrier fluid also plays an essential role in the sedimentation of the particles. Since the viscosity of the silicone oil is five times more than the hydraulic oil, it is evident that the sedimentation is less in the case of silicone-oil MR fluid compared to hydraulic oil MR fluid. However, the choice of grease-based additives does not seem to affect the sedimentation ratio compared to the viscosity of carrier fluid irrespective of temperatures. Figure 3.14 (a)-(e) gives the visually measured sedimentation ratio as a function of time taken. It shows the volume of the clear liquid–suspension interface is dependent on time. The total time of the

experiment was 650 hours. In this section, the temperature effect on the sedimentation time, velocity of settling, and yield stress of the MR fluids was studied**.**
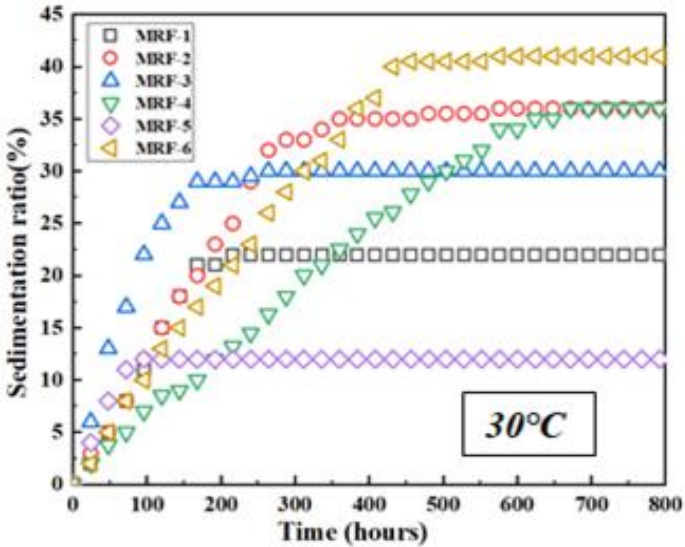
Figure 3.20 Sedimentation ratio of MRF-1 to MRF-6 at 30 °C

The sedimentation rate decreases with time as particles distance reduces, producing more particle contacts. By adding lithium and calcium base additives, there was a decrease in the sedimentation rate observed between the samples. MRF - 1 and MRF - 2 are prepared by adding lithium-based additives to silicone oil and hydraulic oil. MRF - 1 and MRF - 2 took 24 hours to form 0.2 ml and 0.3 ml and took eight days and 15 days to settle completely, respectively. Whereas for the same MRF - 1 and MRF - 2 samples at 100 °C, it took only 30 minutes to form 0.2 ml and 0.3 ml transparent layer, respectively. MRF - 3 and MRF - 4, which are prepared by adding calcium-based additive onto silicone and hydraulic oil respectively, took 24 hours to form 0.6 ml and 0.2 ml of clear liquid at ambient temperature. In contrast, the corresponding settlement happened in 30 minutes at 100 °C, respectively. It took seven days and 28 days, respectively to settle ultimately for MRF - 3 and MRF - 4.
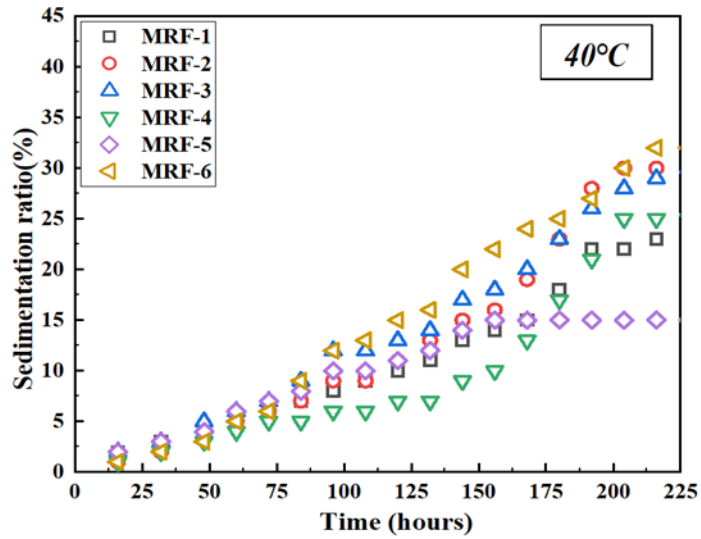
Figure 3.21 Sedimentation ratio of MRF-1 to MRF-6 at 40 °C

Finally, comparing MRF - 5 and MRF - 6 combinations of lithium and calcium-based grease additives mixed with silicone oil and hydraulic oil, respectively, it took 24 hours to form 0.2 ml and 0.4 ml of the transparent layer at ambient temperature. However, it took only 30mins to develop 0.1 ml and 0.3 ml of the transparent layer at 100 °C, and for complete settling, it took approximately 4 and 16 days, respectively. It is inferred from the above observations that the combination of carried fluid and additive significantly influences the stability of MR fluids.
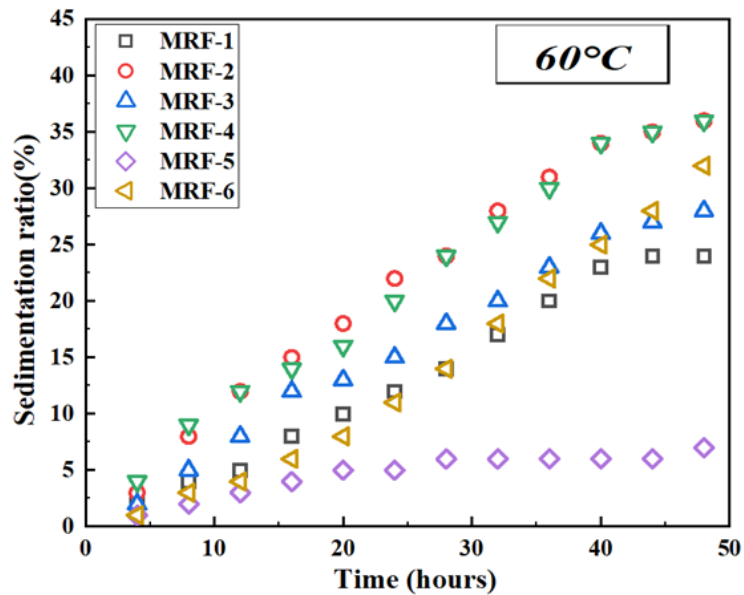
Figure 3.22 Sedimentation ratio of MRF-1 to MRF-6 at 60 °C
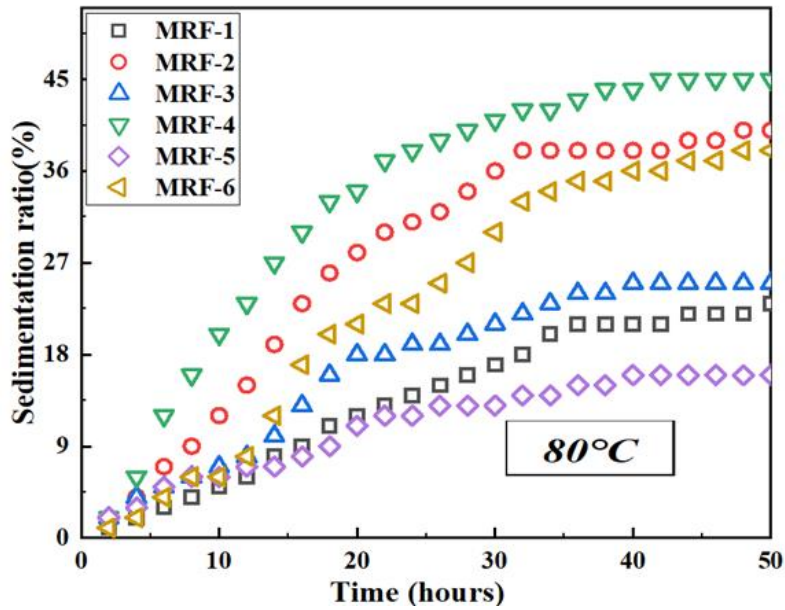
Figure 3.23 Sedimentation ratio of MRF-1 to MRF-6 at 80 °C

The temperature has a significant influence on particle settling. An increase in temperature makes the carried fluid viscosity and density decrease drastically, creating a higher density difference and particles settling faster. However, particle density is not affected by temperature rise. The sedimentation ratio of the silicone oil based MRF's is more than hydraulic oil based MRF. The increased sedimentation ratio is exponential as the temperature increases for all the MRFs considered in this study irrespective of the combinations of the fluid. In the characterization part MRF - 1 is selected for performance analysis of MR damper.
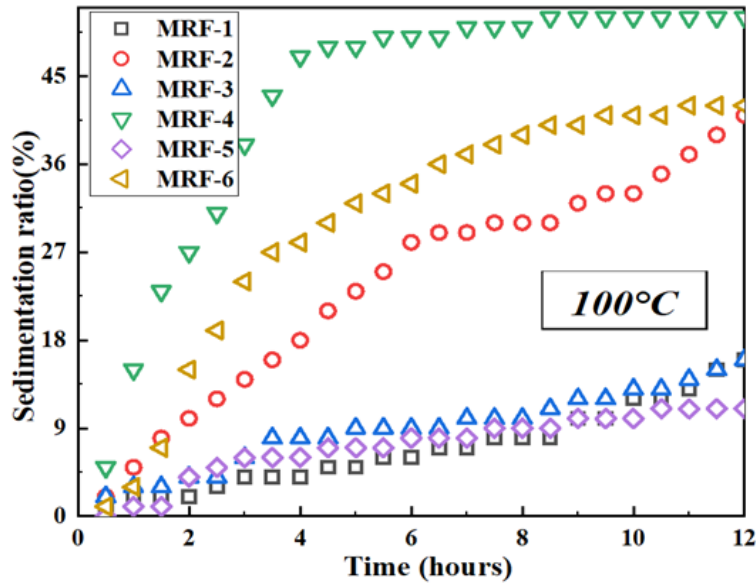
Figure 3.24 Sedimentation ratio of MRF-1 to MRF-6 at 100 °C

3.3.2 Sedimentation velocity of the MR fluid

The general formula for calculating Stoke's velocity for dilute suspensions is below.

$$v = g \times (\rho_p - \rho_f) \times d^2 / 18\mu \tag{3.6}$$

The particle concentration of the MR fluids is very dense such that interparticle forces hinder the settling. In the present study, settling velocity is calculated based on the sedimentation ratio and time function. The sedimentation velocity of all the samples is calculated at different temperatures, and the samples have been exponentially fitted by the curve fitting technique. This experiment shows that settling velocity is a function of temperature as the carrier fluid viscosity is also a function of temperature. The increase in velocity of MR fluid is that the viscosity of the carrier fluid and additive decreases drastically, making the particle holding stability of the grease weak in the carrier fluid. The sedimentation data of samples is converted to velocity data. The study shows that the silicone oil and lithium-based MR fluids have 0.00055 mm/min, and hydraulic oil and calcium-based MR fluids have 0.0011 mm/min at 30 °C for the same samples at 100 °C velocities are 0.0178 mm/min and 0.0356 mm/min. From the above comparison of velocities, the silicone oil and lithium-based MR fluids settle 0.5 times less fast than the hydraulic oil and calcium-based MR fluids at all temperatures up to 100 °C. From the analysis, it is evident that whatever the combination of MR

fluids used, the trend between the effects of the temperature on velocity remains the same, which is exponential in decay.

3.3.3 Characterization of the MR fluid

The flow properties of all the MR fluids were measured at 0 and 2 Amperes, respectively at 30 °C, 50 °C, and 80 °C temperatures. The viscosity variation for all the MRF samples is shown in figures 3.25 – 3.30. It is implied that; the viscosity decreases with an increase in temperature under both magnetic and non-magnetic exposures. However, the magnitude of reduction in viscosity concerning temperature decreases with a magnetic field. Figure 3.33 – 3.38 shows the Bingham fluid flow models shear rate versus shear stress flow curves. MR fluid yield stress increases with the applied field due to more particles coming in for chain formation. The percentage of viscosity recovered with varying shear rates with time is called as recovery rate.
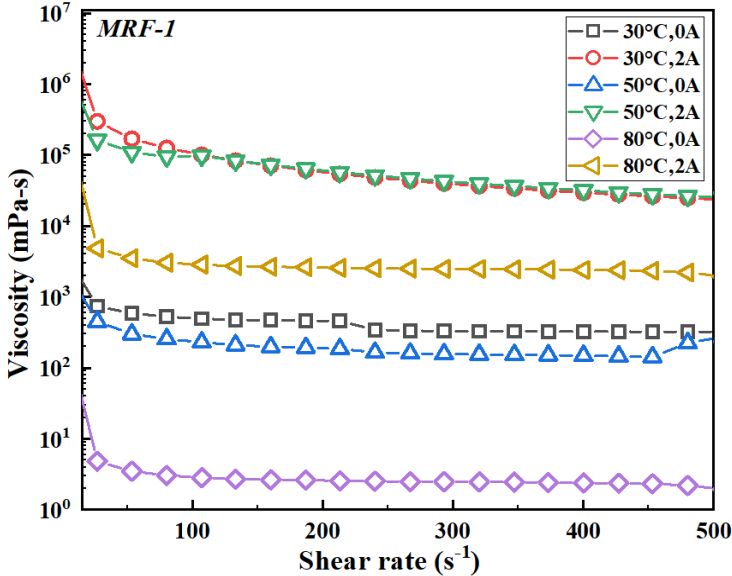
Figure 3.25 Viscosity curve for MRF-1 at different

temperatures and magnetic fields
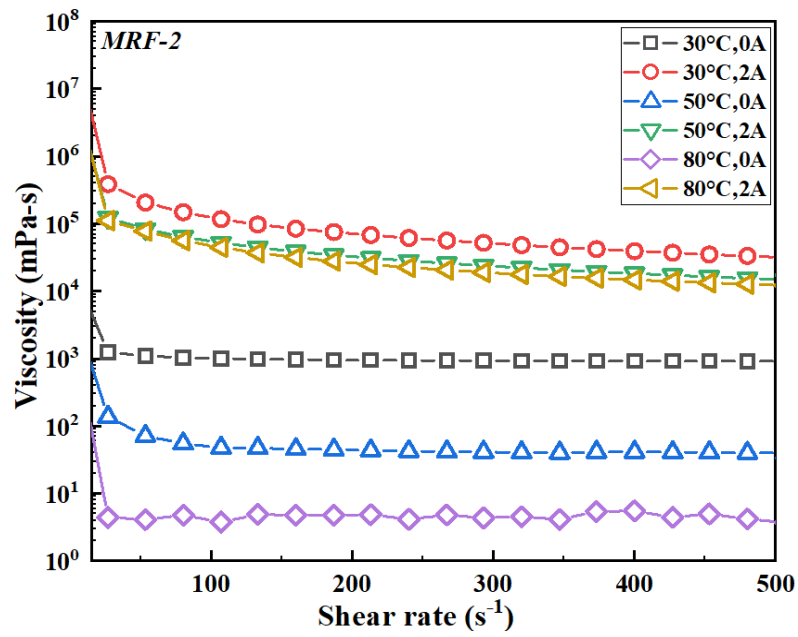
Figure 3.26 Viscosity curve for MRF-2 at
different temperatures and magnetic fields
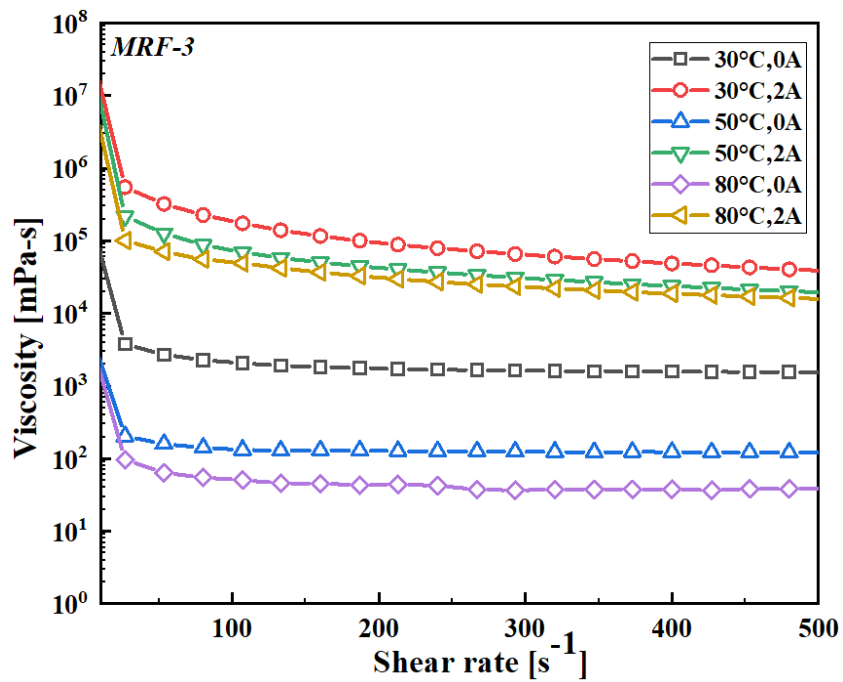
Figure 3.27 Viscosity curve for MRF-3 at
different temperatures and magnetic fields
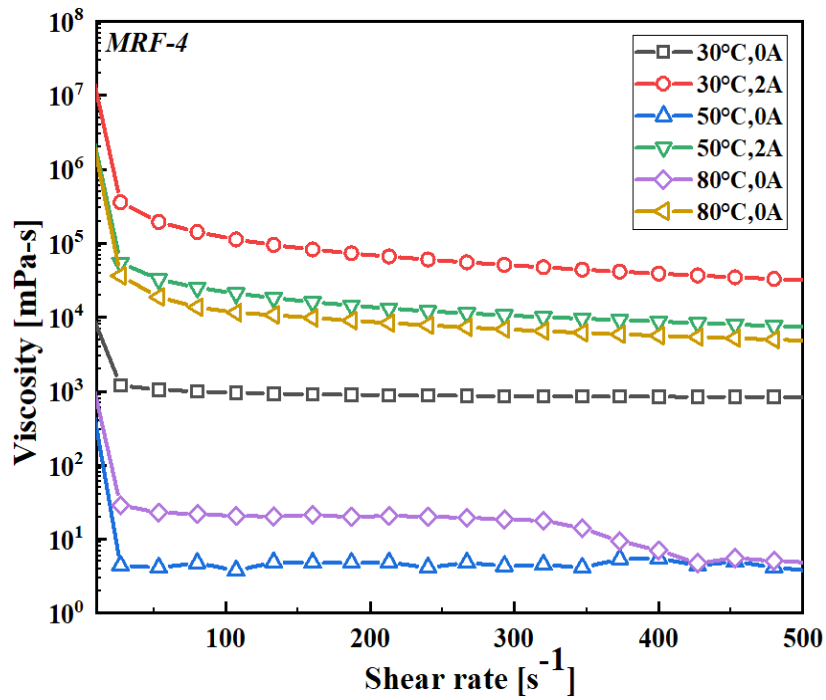
Figure 3.28 Viscosity curve for MRF-4 at

different temperatures and magnetic fields
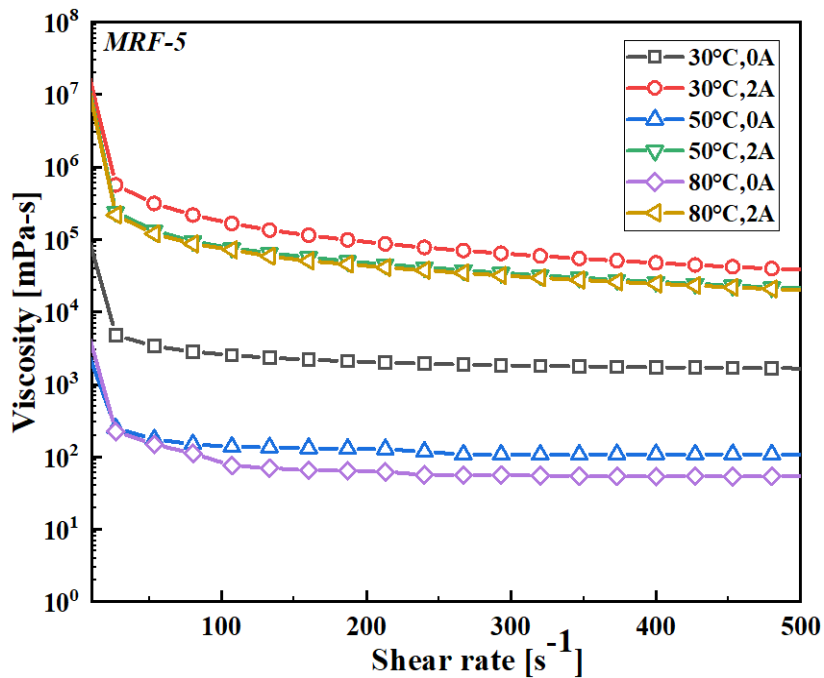
Figure 3.29 Viscosity curve for MRF-5 at

different temperatures and magnetic fields
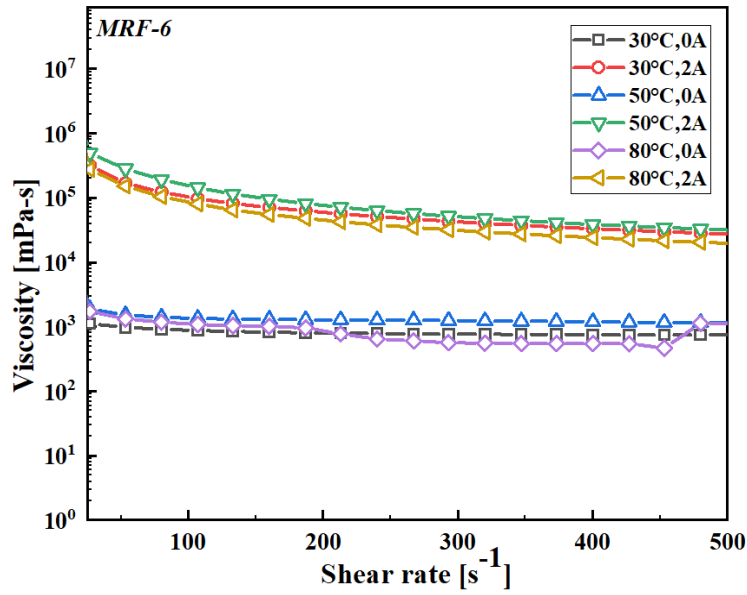
Figure 3.30 Viscosity curve for MRF-1 at

different temperatures and magnetic fields
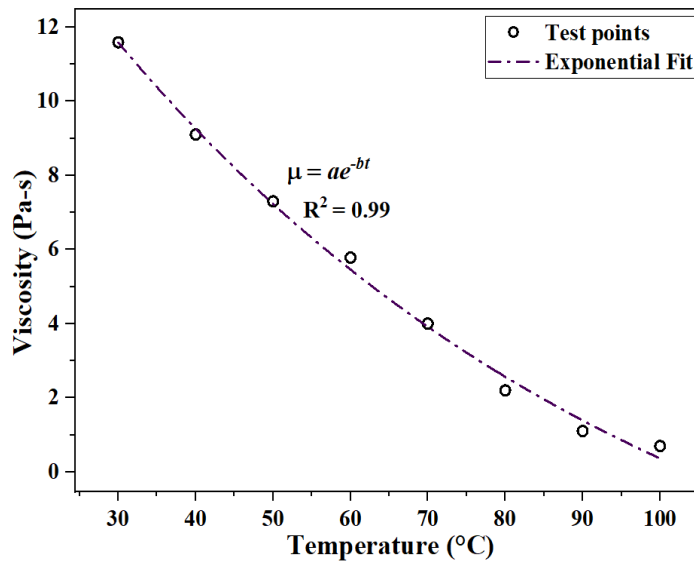
Figure 3.31 Viscosity curve for MRF-1 at different

temperatures and zero magnetic field

Figure 3.31 shows the influence of temperature on viscosity decrease and exponential model fit results with r-square value greater than 0.95. Viscosity variation was obtained at the different shear rates using a peak hold test in the rheometer at shear rates 1 s^{-1}, 300 s^{-1}, 1 s^{-1} for 30 s, 60 s and 150 s respectively. All the MRFs show

71

shear thinning behaviour with an increasing rate of shear. The viscosity recovery rate is 83.43 %, 60 % and 66.67 % of MRF - 1, MRF - 2, and MRF - 7, respectively. Figure 3.32 depicts the viscosity recovery rates of the MRF samples.
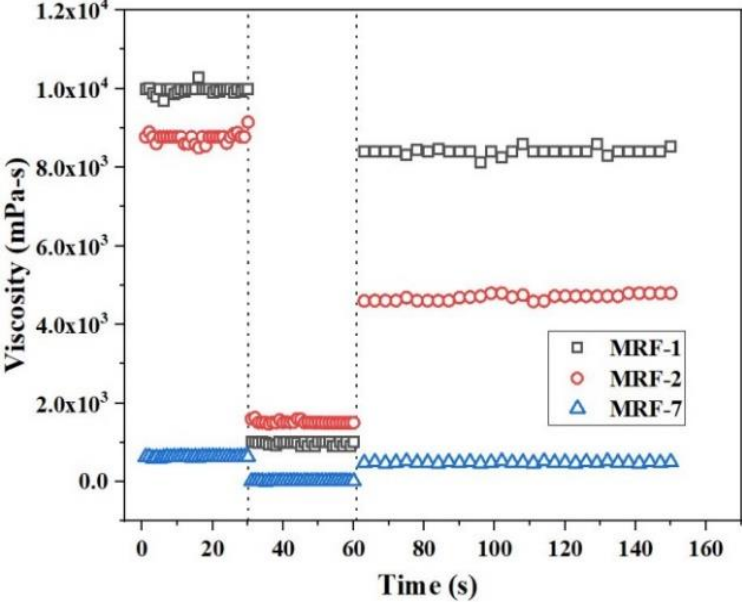
Figure 3.32 Viscosity recovery curve for MRF-1, MRF-2, and MRF-3
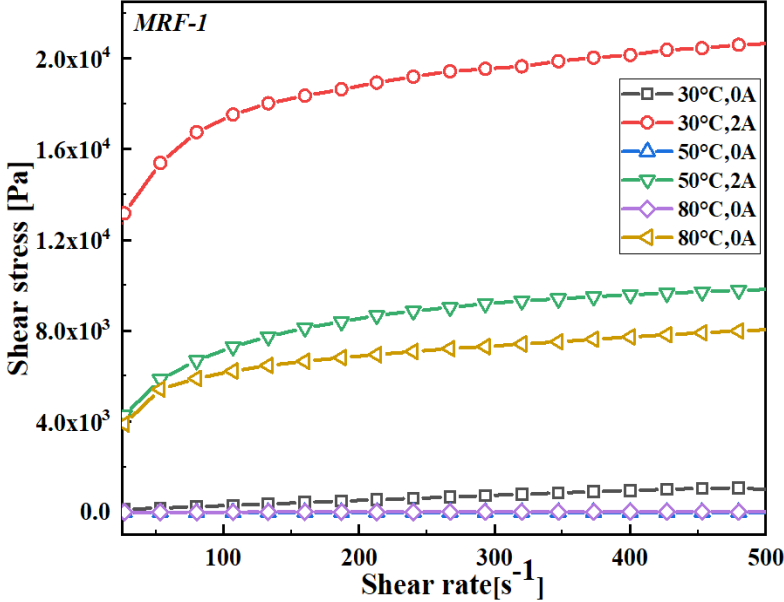
Figure 3.33 Shear stress variation curve of MRF-1 at

different temperatures and magnetic fields
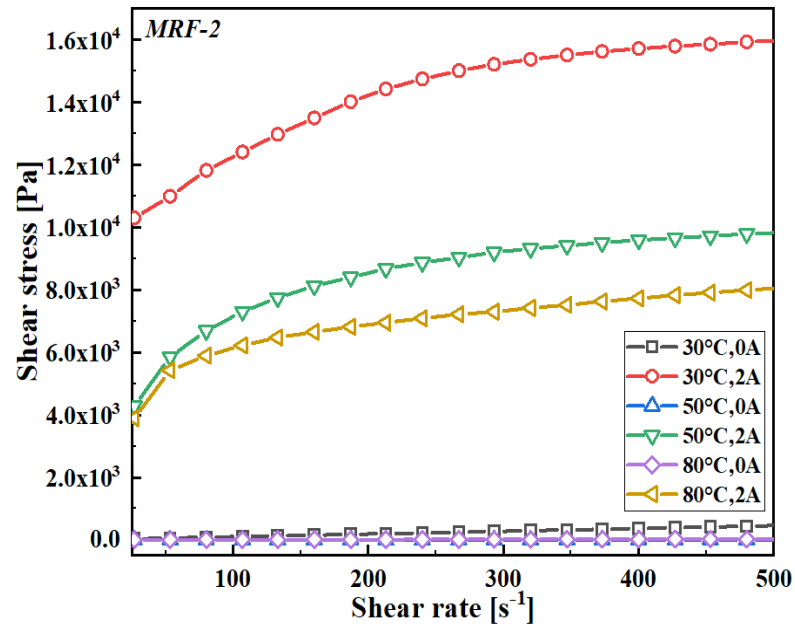
Figure 3.34 Shear stress variation curve of MRF-2 at

different temperatures and magnetic fields
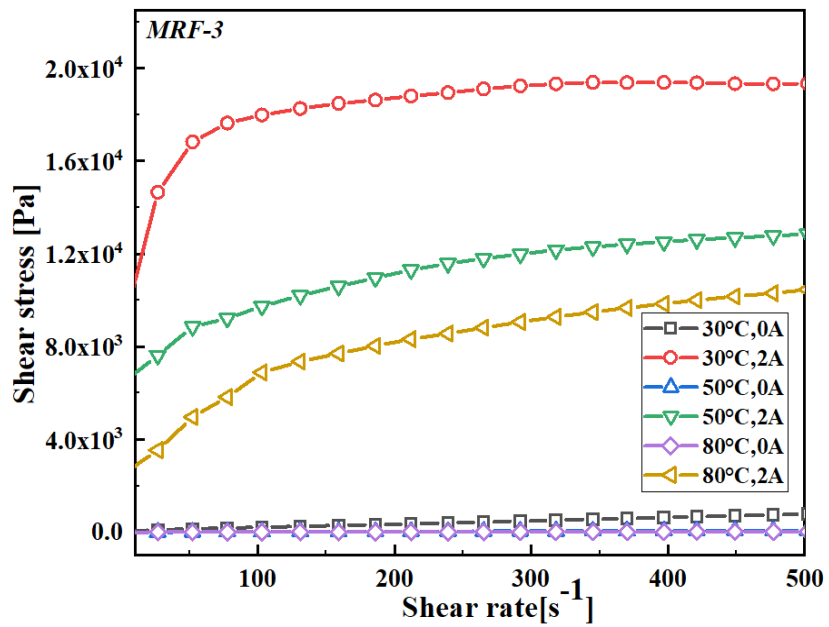
Figure 3.35 Shear stress variation curve of MRF-3 at

different temperatures and magnetic fields
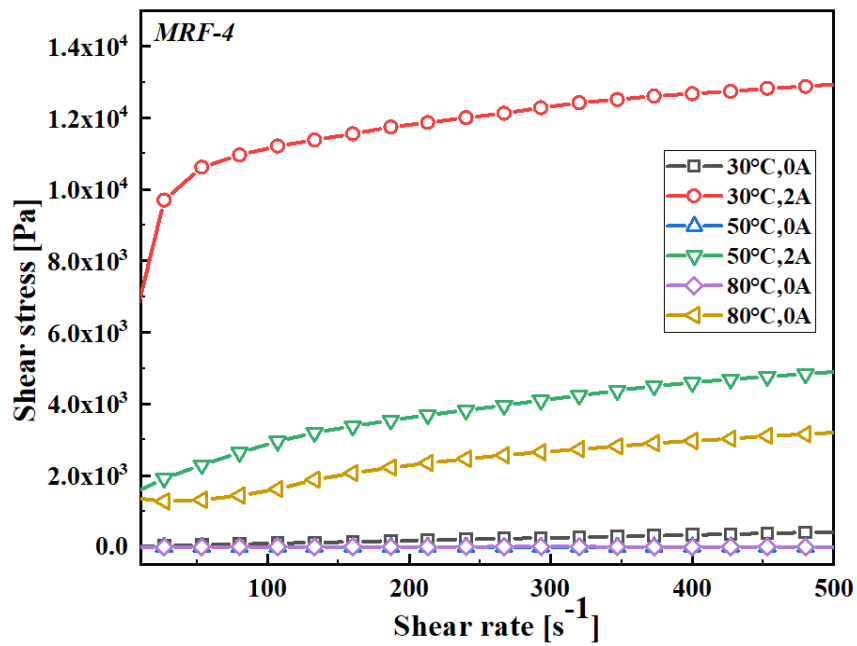
Figure 3.36 Shear stress variation curve of MRF-4 at

different temperatures and magnetic fields
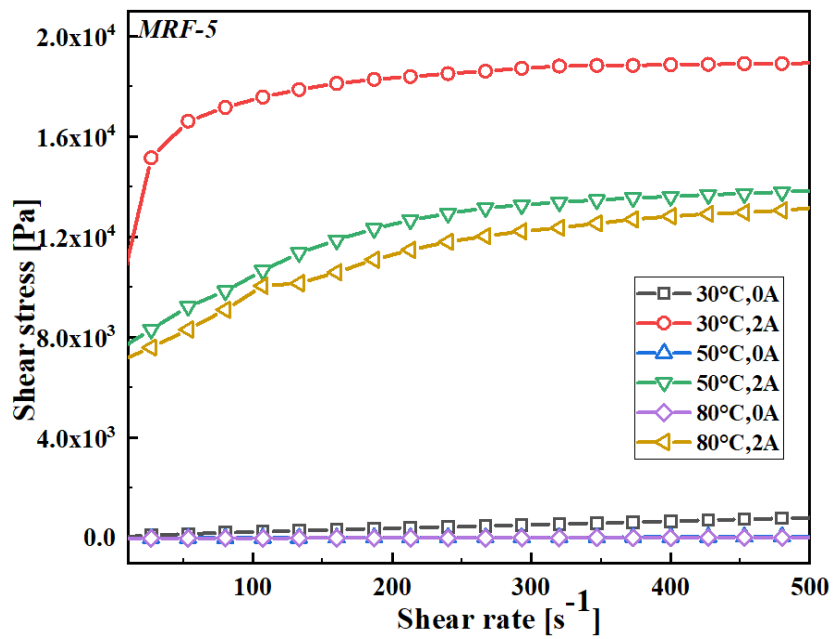
Figure 3.37Shear stress variation curve of MRF-5 at

different temperatures and magnetic fields
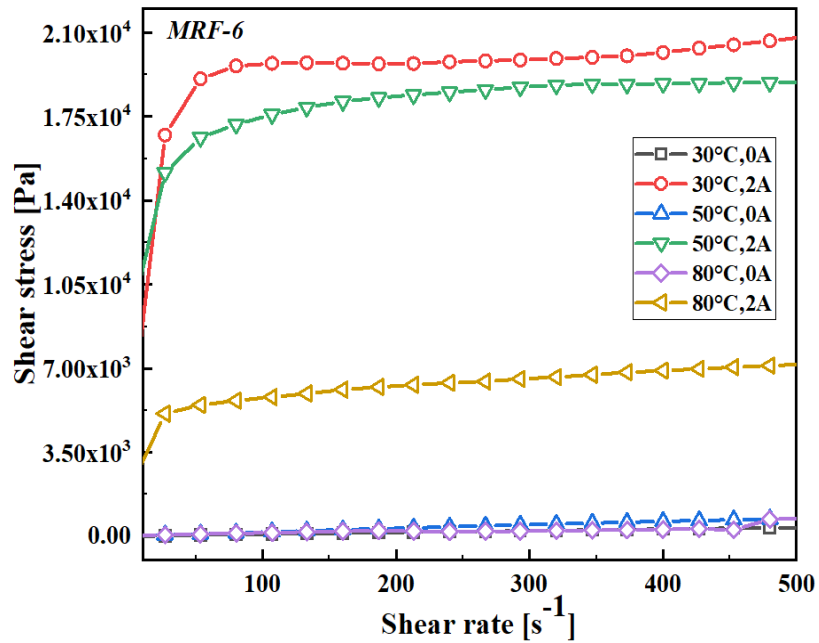
Figure 3.38 Shear stress variation curve of MRF-6 at

Different temperatures and magnetic fields

Figure 3.39 shows the behaviour of all the MRFs yield stress at various temperatures, and it is evident that for all the MRF, the yield stress decreases with increasing temperatures. The increase in the yield stress remains constant after a certain Ampere current due to the magnetic saturation of the CI particles.
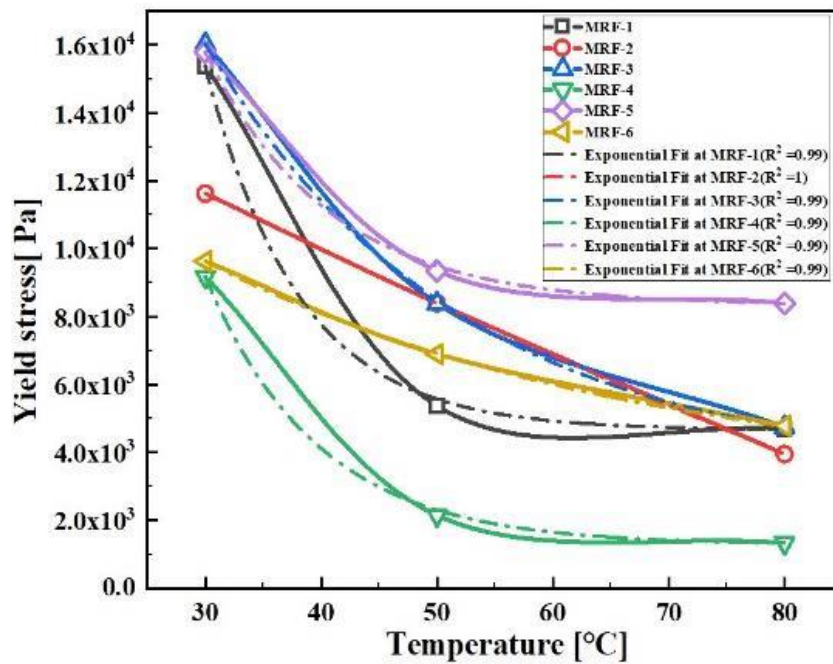
Figure 3.39 Decrease in yield stress of MR fluids at higher temperatures

3.3.4 Experimental test results of MR damper

MRF - 1 fluid selected based on better sedimentation stability and having the highest yield stress is used in a shear mode MR damper to study its damping characteristics. The force versus displacement curves for various amplitudes, frequencies, and currents are shown in figures 3.40 - 3.44. The sinusoidal input displacement is varied individually from 2 mm to 6 mm with an increment of 2 mm. The damper's expansion and compression from the mean position are positive and negative displacement. After testing for three inputs, i.e., frequency, amplitude, and applied current, three observations were made. The force versus displacement closed-loop graph area increases with input current representing an increase in the energy dissipated by the system in a single cycle. It is evident from the force versus displacement graphs that higher values of force are obtained at high amplitudes and increased frequency. But there is not much rise in the damping force at the lower amplitude and lower frequency.
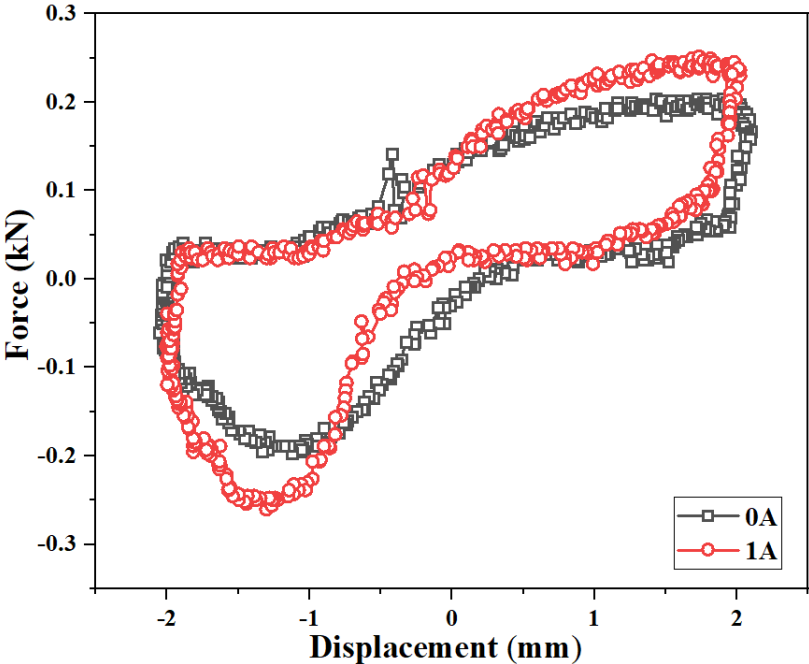
Figure 3.40 Force versus displacement curve at

2 mm amplitude and 2 Hz frequency

For 2mm amplitude at no current and 1 A, the force developed at frequencies 2 Hz and 4 Hz, respectively, which is a 34.6 % and 1 % increase in the damping force. At

6mm amplitude, for frequencies 2 Hz and 4 Hz at no current and 1 A, the force developed is 164.44 % and 138.36 % rise respectively, which is a significant rise compared to that for 2mm amplitude. Hence, the damping force is not sensitive to the vibration frequency and applied current (magnetic field) at low amplitude. However, the damping force is very sensitive to the vibration frequency at high displacement and not much to the applied current.
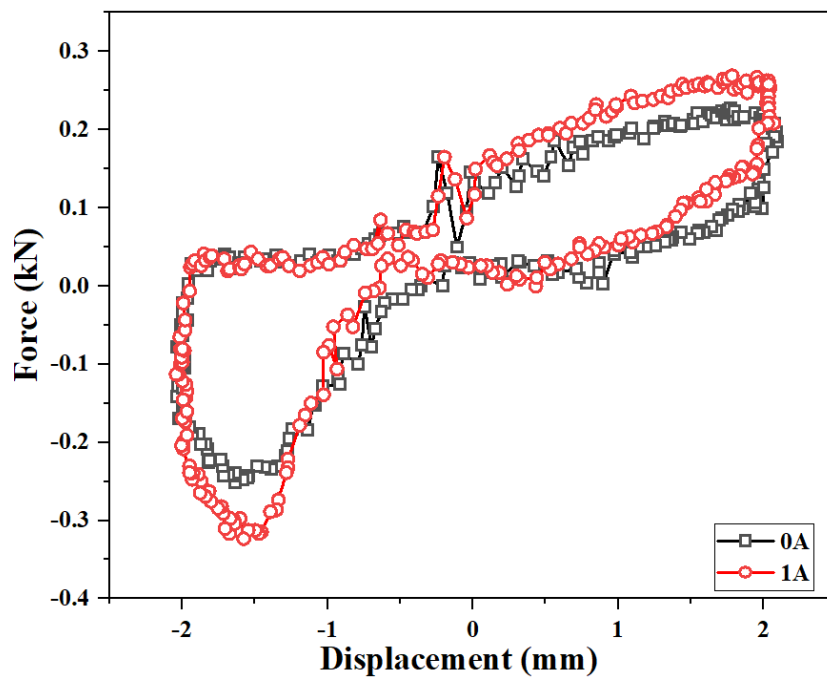
Figure 3.41 Force versus displacement curve at

2 mm amplitude and 4 Hz frequency

The force-displacement curves at constant lower amplitudes, varying frequencies and constant higher amplitudes and varying frequencies are illustrated in figures 3.40 and 3.41, respectively.   For a given frequency of 2 Hz under no current and 1A, the force developed at 2mm and 6mm amplitude is 186.9 % and 146.97 %, respectively. Nevertheless, at 4 Hz under no current and 1 A, the force developed at 2 mm and 6 mm amplitude is 463.43 % and 491.09 % more than 2 Hz. The percentage increase in damping force for a given increase in displacement amplitude is higher at higher frequencies when compared to values at low frequencies and low amplitudes. Hence, the damping force developed is sensitive to displacement amplitude, applied frequency and the applied magnetic field in decreasing order.
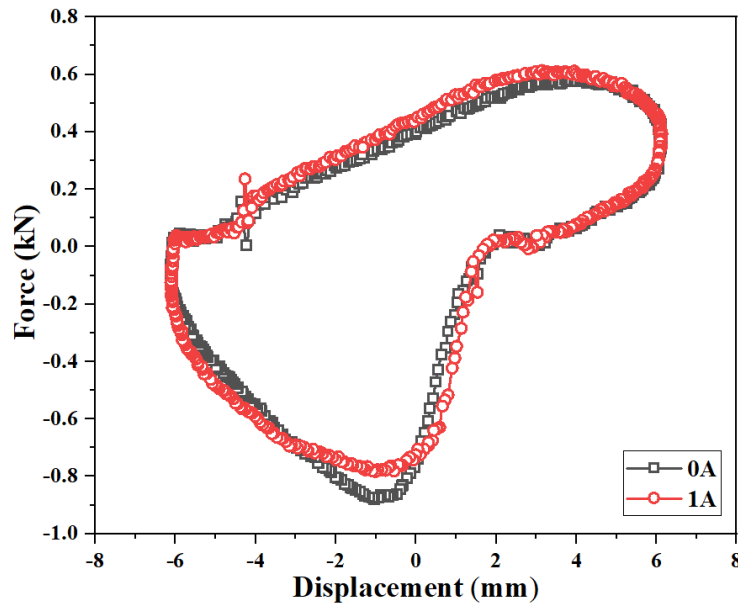
Figure 3.42 Force versus displacement curve

at 6 mm amplitude and 2 Hz frequency

Figures 3.42 and 3.43 depict force-displacement curves at constant 6 mm amplitudes and varying frequencies. Higher energy dissipation into the MR fluid increases the damping force at high amplitude, high frequency, and high currents. The distortion in the force-displacement diagram is due to the absence of an accumulator to compensate for the piston rod volume, which also leads to an increase in the compression load on the piston, and another reason for the change in the shape force-displacement diagram is the viscosity of the carrier fluid. The viscosity of the MR fluid increases with an increase in the viscosity of the carrier fluid.
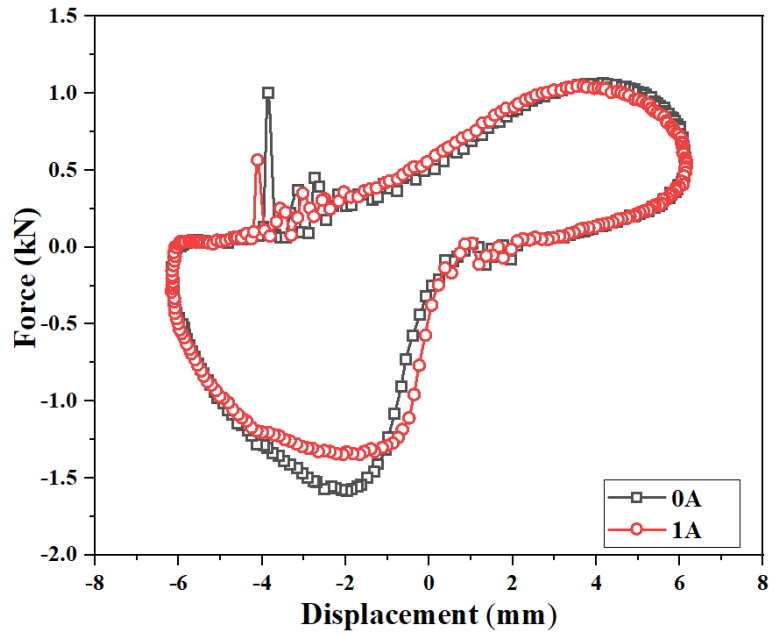
Figure 3.43 Force versus displacement curve at

6 mm amplitude and 4 Hz frequency

The performance of the MRF-1 was evaluated in MR damper by giving different input parameters and the force variations was obtained at various amplitudes, frequencies, and two currents. Figures 3.45 and 3.46 illustrate forces variations at three frequencies, three amplitudes, and 0 Ampere and 1 Ampere.
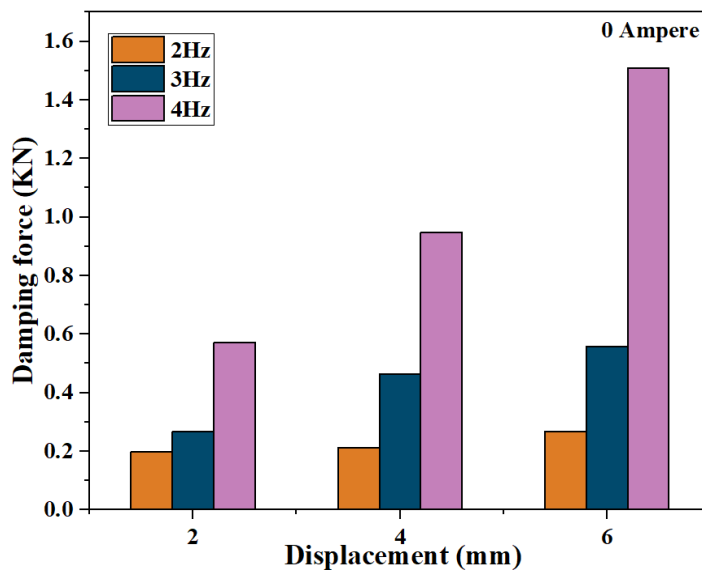
Figure 3.44 Damping force at various amplitudes,

frequencies, and currents for MRF-1 at 0A
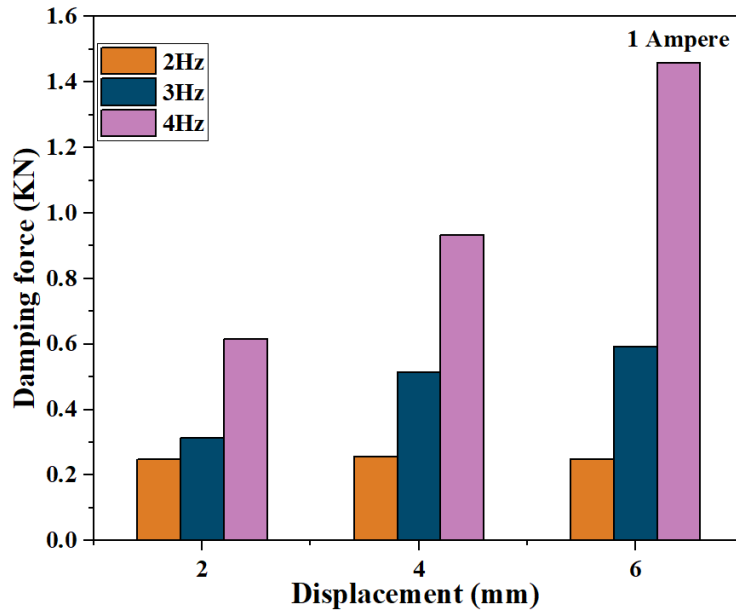
Figure 3.45 Damping force at various amplitudes,

frequencies, and currents for MRF-1 at 1A

Finally, to know the controllability of the MRF-1 in MR damper the dynamic range is calculated. The obtained dynamic range for MRF-1 is very less which is depicted in figure 3.46.
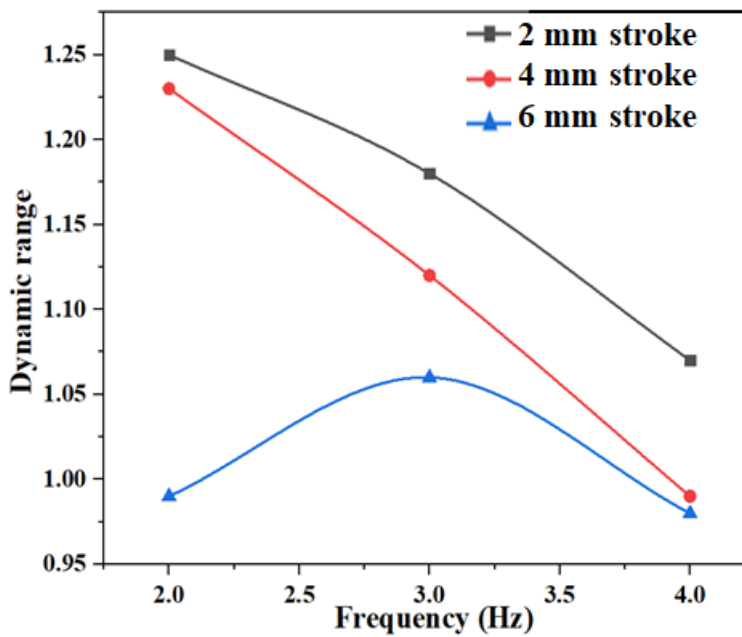
Figure 3.46 Dynamic range of MRF-1 with MR damper

After the fabrication of the MR damper, the flow characteristics of the MRF alone decide

the performance of the MR damper with varied input parameters such as amplitude, frequency, and current. Further, MRF-7 was prepared with silicone oil with viscosity (50 cSt) (manufacturer: sigma Aldrich, 378356) less than previously used MR fluids (MRF - 1 to MRF - 6) as the carrier fluid and 2 % of lithium base grease as the additive, 25 % by volume of carbonyl iron particles. The conditions (i.e., rotation speed and time) for MR fluid synthesis were kept the same as that of the first six MRF samples.

3.3.5 Stability, flow characteristics, and dynamic testing of MRF-7

The sedimentation study of new MR fluid is shown in figure 3.47 and 3.48, and it is evident from the graph that the sedimentation rate is very high than previous MRF samples. It takes nearly 40 hours and 7 hours to settle ultimately at 30°C and 100°C respectively, with 41 % settlement which is very much higher than the above six MRF samples. Characterization of MR fluid is carried out on a rheometer at different currents and temperature conditions. Figure 3.49 and 3.50 give the viscosity and shear stress variation of MRF-7. Figure 3.51 gives us the Bingham model fit analysis for the yield point of the prepared MR fluid sample at 30 °C. Figure 3.52 provide us with the increase in yield stress of the MR fluid at different currents at individual temperatures depicting a linear growth of yield stress at different applied currents.
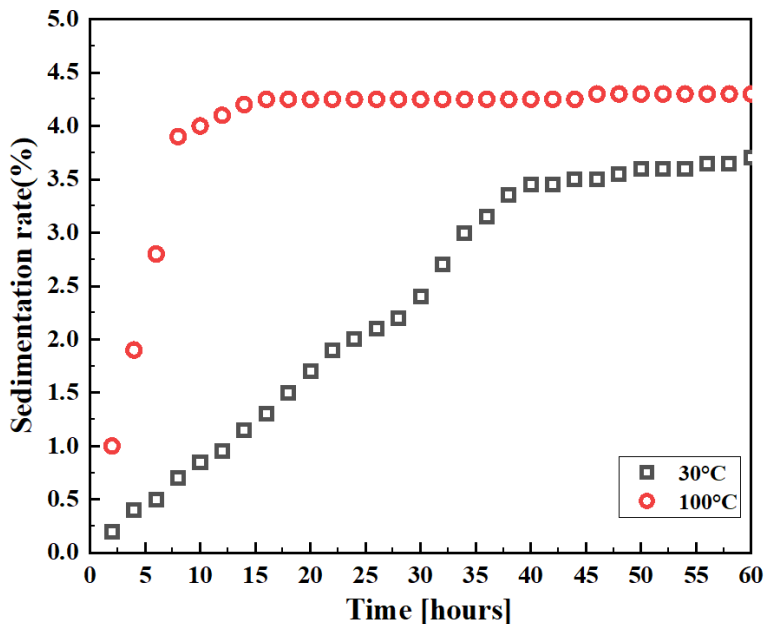
Figure 3.47 Sedimentation analysis of MRF-7
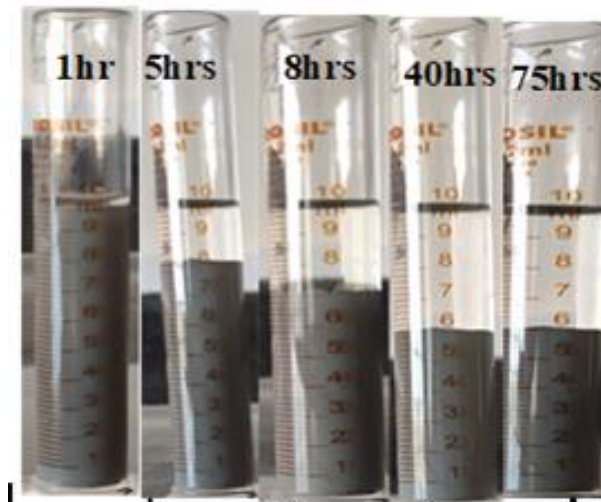
Figure 3.48 Settling study image of MRF-7

3.3.6 Conditions for characterisation of MR fluid

After the synthesis of MR fluid the fluid is to be characterised to study the flow behaviour of the MR fluid. The input conditions maintained at the time of testing is shown in table 3.6.

Table 3.6 Measuring conditions for characterisation of the MR fluid

Shear rate	0.1 s^{-1} to 500 s^{-1}
Currents	0.25 A, 0.5 A, 0.75 A, 1 A, 1.5 A, 2 A, 2.5 A.
Gap	1 mm
Temperature	30 °C, 50 °C, 80 °C
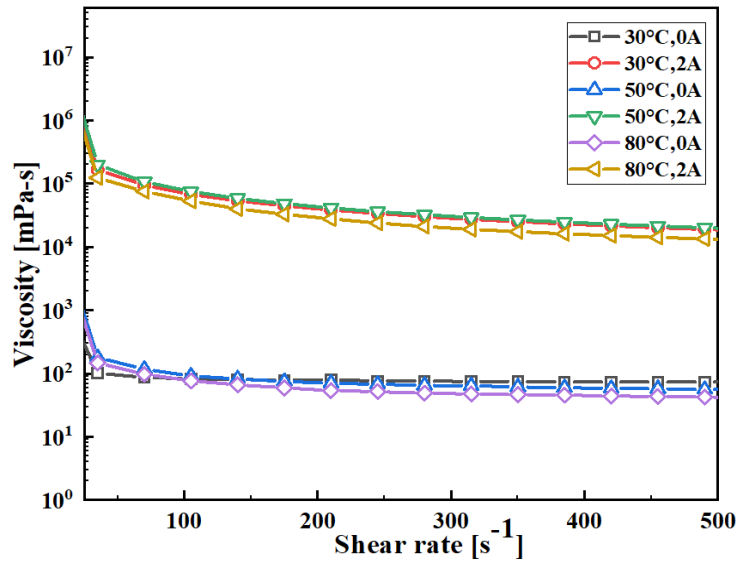
Figure 3.49 Viscosity variation of MRF-7

The flow properties of all the MR fluids were measured at 0 and 2 Amperes, respectively at 30 °C, 50 °C, and 80 °C temperatures. The viscosity and shear stress variation with temperature and magnetic field for all the MRF samples is shown in figures 3.49 – 3.50. It is implied that; the viscosity decreases with an increase in temperature under both magnetic and non-magnetic exposures. However, the magnitude of reduction in viscosity concerning temperature decreases with a magnetic field.
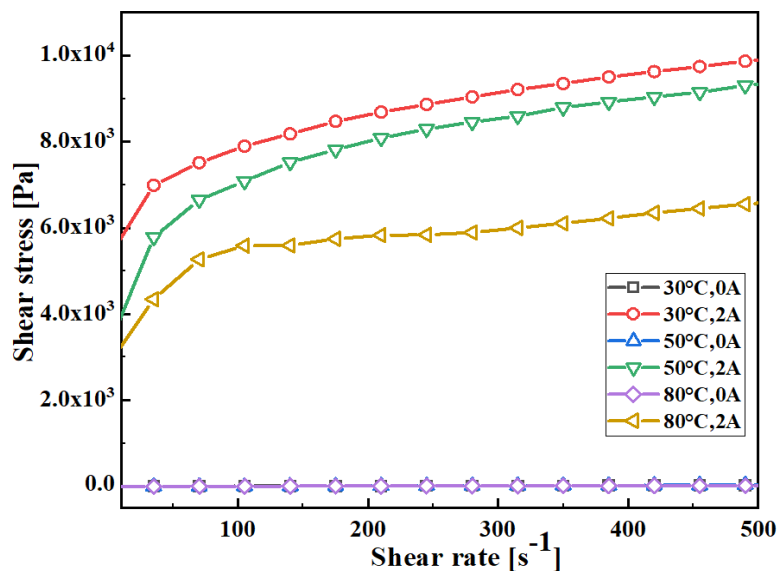
Figure 3.50 Viscosity variation of MRF-7
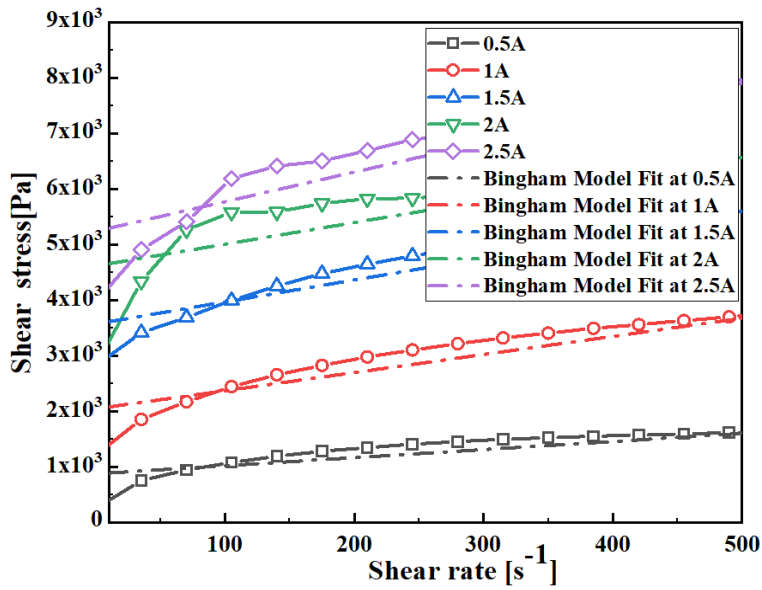
Figure 3.51 Bingham Model fit at 80 °C of MRF-7

The Bingham model fit of the shear stress variation curves is illustrated in the figure 3.51 and the yield stress obtained with the equation model equation at all the temperatures and magnetic fields were depicted in the figure 3.52. The Increase in yield stress is observed with increase in magnetic field. Yield stress increases linearly with the application of magnetic field. It is also observed that temperature increase decreases the yield stress significantly.
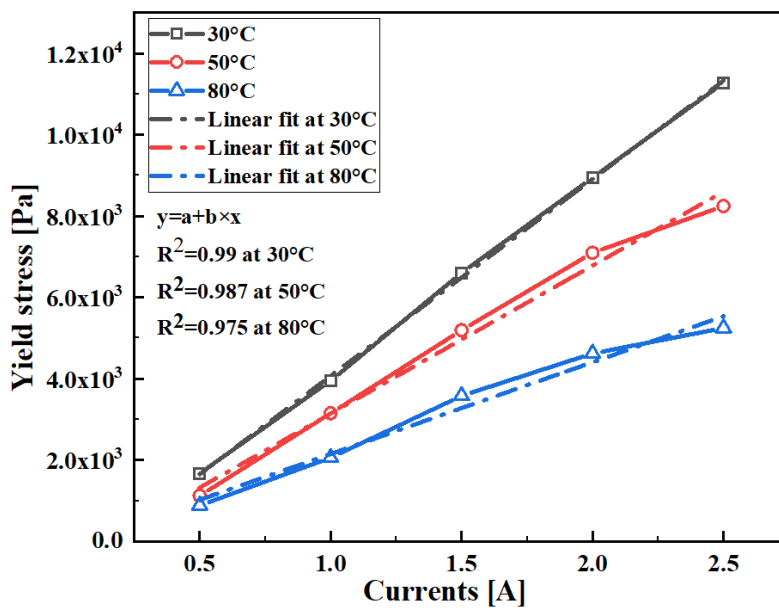
Figure 3.52 Yield stress variation of MRF-7 at 30 °C, 50 °C and 80 °C

3.3.7 Characterisation MR Damper

The dynamic characterization of the MR damper is also carried out on the same steps as that of the previous MR fluid (MRF-1) characterization. The input conditions to characterize the MR damper is given in table 3.7.

Table 3.7 Conditions used to characterize the MR damper

Frequency	2 Hz, 3 Hz, 4 Hz
Amplitude	2 mm, 4 mm, 6 mm.
Currents	0 A, 0.25 A, 0.5 A, 0.75 A, 1 A.

Figure 3.53 - 3.56 illustrates the force-displacement diagram for MRF-7. The peculiarity of the MRF is that area of the force versus displacement increases with an increase in the applied current, amplitude, and frequency.
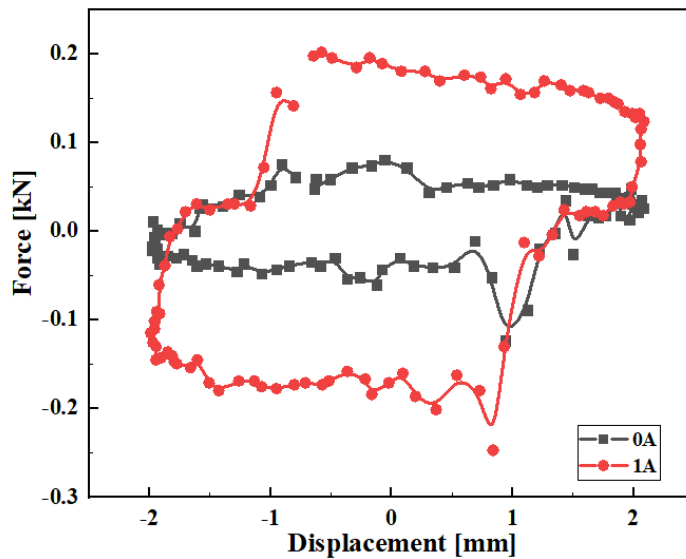
Figure 3.53 Force displacement curve for MRF-7 at 2 mm amplitude,

2 Hz frequency, and 0A and 1A currents

The maximum damping force obtained for MRF-7 is 0.245 kN, which is very much less than MRF-1. The shift in the upper part of the force-displacement graph is due to the absence of an accumulator, which is significantly minor in the case of MRF-7, indicating the effect of viscosity of the carrier fluid on the performance of the damper. The increase in the compression load in the case of MRF-7 is less than MRF-1, indicating

another effect of changing the carrier fluid on the distortion in the force-displacement curve.
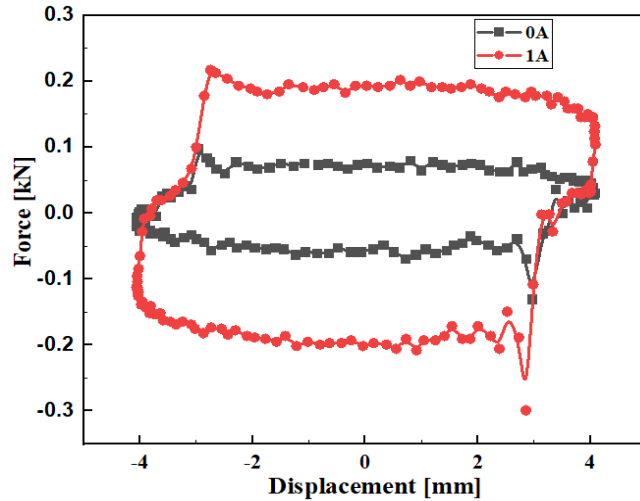
Figure 3.54 Force displacement curve for MRF-7 at 2 mm amplitude,

4 Hz frequency, and 0A and 1A currents

The force displacement curves depicted in figure 3.53 and 3.54 gives the force variation at 0 A, and 1 A at lower amplitude (2 mm) and varying frequencies (2 Hz and 4 Hz). The increase in force can be seen when the applied current is increased from zero to 1 Ampere. And also it is observed that an increase in frequency has very less impact on the damping force at specific amplitudes.
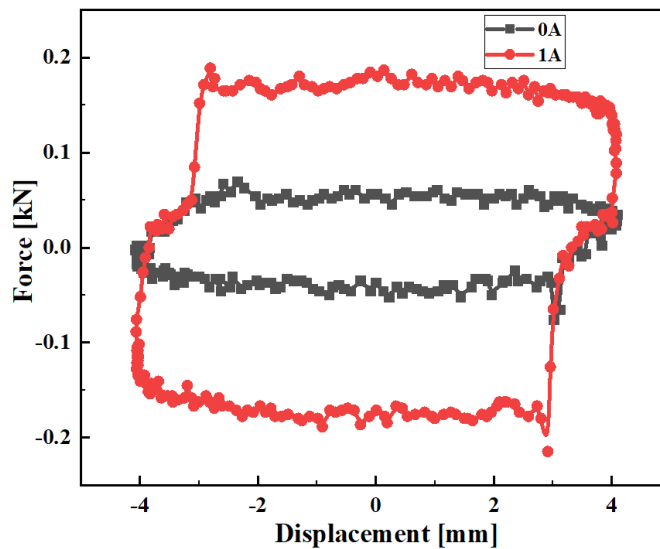
Figure 3.55 Force displacement curve for MRF-7 at 6 mm amplitude,

2 Hz frequency, and 0A and 1A currents

On the contrary, the damping force increases significantly with the increase in amplitude from 2 mm to 6 mm at a constant frequency. Figures 3.55 and 3.56 illustrate the increase in damping force. The increase in damping force at higher amplitudes increase because of larger energy dissipation in to the fluid making the force displacement curve increase in size.
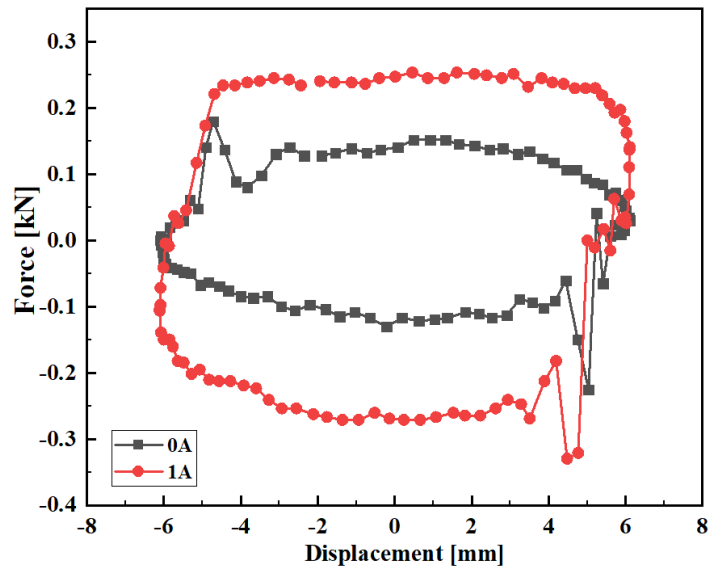
Figure 3.56 Force displacement curve for MRF-7 at 6 mm amplitude,

4 Hz frequency, and 0A and 1A currents

Figure 3.57 illustrates the overall damping force variation at all the input frequencies, amplitudes, and applied currents. The increasing trend is observed with an increase in the input parameters of the damper.
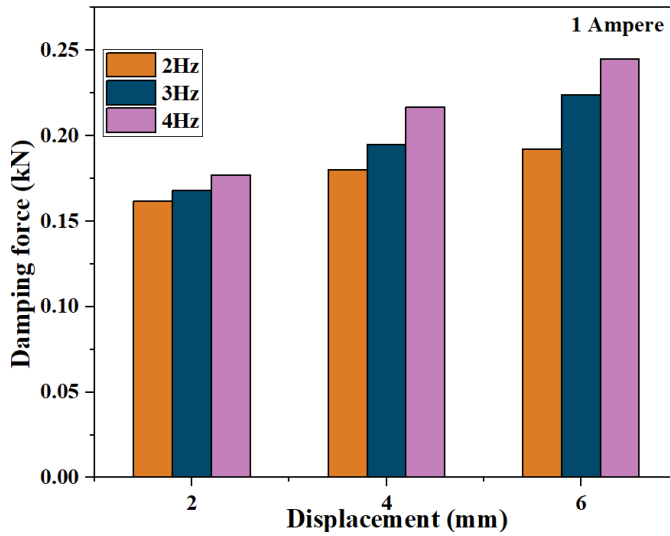
Figure 3.57 Damping force obtained at different input amplitudes,

frequencies, and 1A current

The dynamic range of the MRF-7 shows a decrease in variability with increasing amplitude and frequency, like MRF-1. The decrease in dynamic range is observed with an increase in amplitude, frequency, and current which indicates saturation magnetization of the MR fluids. The variation in dynamic range is the critical property of the MRFs reveals that carrier fluid viscosity plays a vital role in the dynamic range of the MR damper. The dynamic range of the MRF-7, which is decreasing in trend, contradicts the dynamic range of MRF-1.
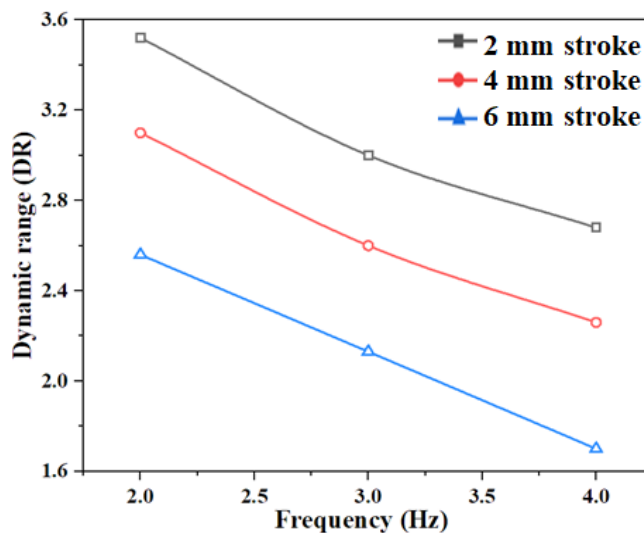
Figure 3.58 Dynamic range of MRF-7

If the MR system operates at constant amplitude, constant frequency and constant current higher viscosity oils can be selected. As in the case of artillery rebound displacement, firing rate and required current are constant and depend on the artillery range. But in the case of automobile application, displacements and frequencies impacting the damper are of various ranges, so the MR fluid's variability is very much needed. In this case, carrier fluid viscosity should be less than 350 cSt and above 50 cSt to obtain the required dynamic range.

3.4 TEMPERATURE EFFECT ON MR DAMPER PERFORMANCE

Figure 3.59 depict the experimental arrangement for temperature measurement. To measure the temperature of the damper, MRF-1 was prepared in calculated quantity and filled into the damper. Amplitude is set at 12 mm, frequency at 3 Hz, and 0 A and 0.4 A current. Two K-type thermocouples were attached to the damper cylinder's top and bottom surface, and NI9211 DAQ was used to capture the temperature readings. The test was carried out for 500 cycles to evaluate the temperature effect on the damping force.

Figure 3.59 Experimental setup to measure the temperature

of the damper while working

The Moog controller which controls the input parameters such as frequency, amplitude, and currents is shown in figure 3.60. At a particular loading parameters damper is tested and the results have been displayed on the pc and the data is acquired through the DAQ system which is inbuilt within the system. On the similar lines the thermocouples are connected to the surface of the damper. Thermocouples have been connected to the NI9211 DAQ system to acquire the temperature signals.
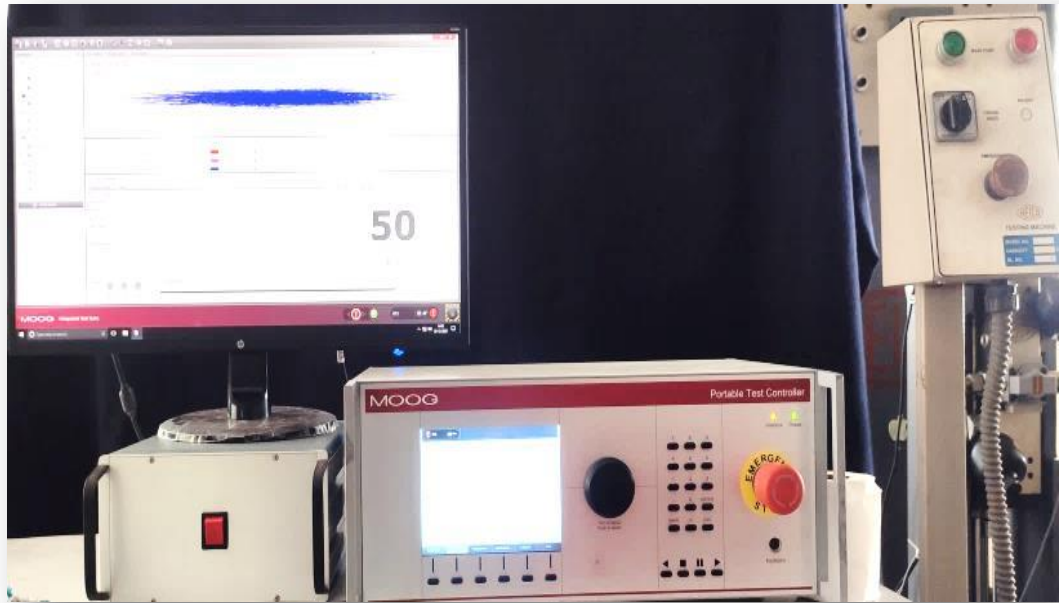
Figure 3.60 Moog controller and display unit
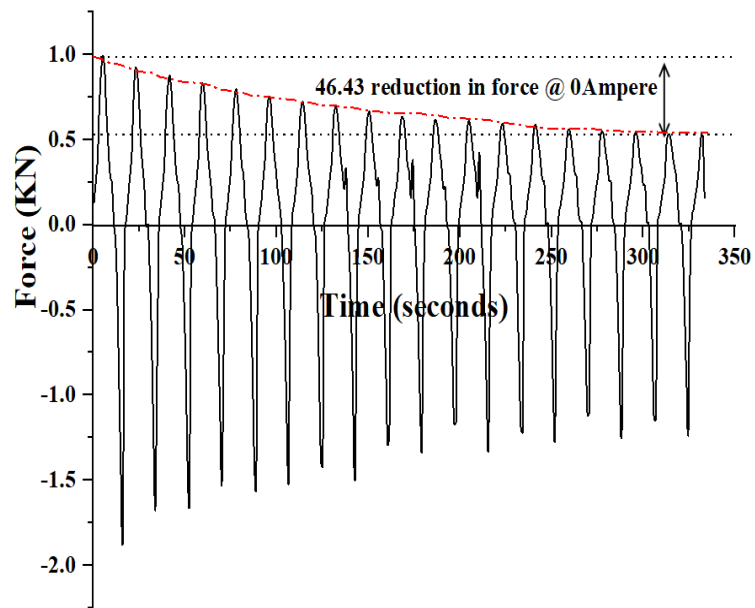
Figure 3.61 Force variation as a function of time at 0A

Force variation is plotted in the time domain to observe the decrease in damping force. The observations made during the analysis are that, the compression load is approximately 50 % more than the expansion load, and this is because of the absence of accumulator which will compensate for the piston rod volume of fluid

movement. Figures 3.61 and 3.62 illustrates the force variation as a function of time at 0 A and 1 A.
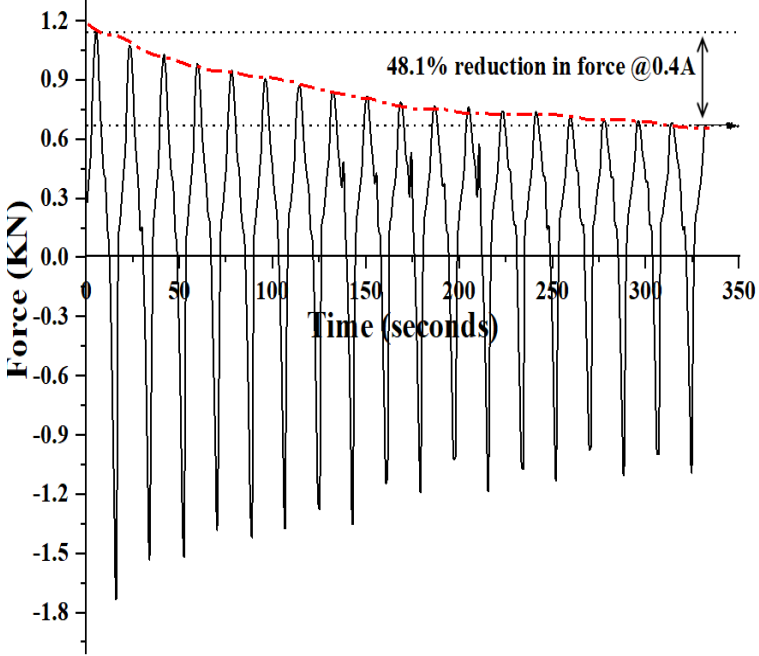
Figure 3.62 Force variation as a function of time at 0.4 A

Figure 3.63 shows that at zero current, the temperature rise is approximately 6.5 °C from atmospheric temperature. But the temperature rise in case of 0.4 A current is 19.5 °C from atmospheric which is significant. There is approximately 46.43 % and 48.1 % force reduction at 0 A and 0.4 A currents respectively. The second observation made is increase in the dynamic range of the damper. The temperature rise decreases the viscosity of the fluid causing less resistance to the flow of fluid. The decrease in damping force is exponential in trend and increasing the dynamic range. Figure 3.64 illustrates the increase in dynamic range of the MR damper as the temperature increases.
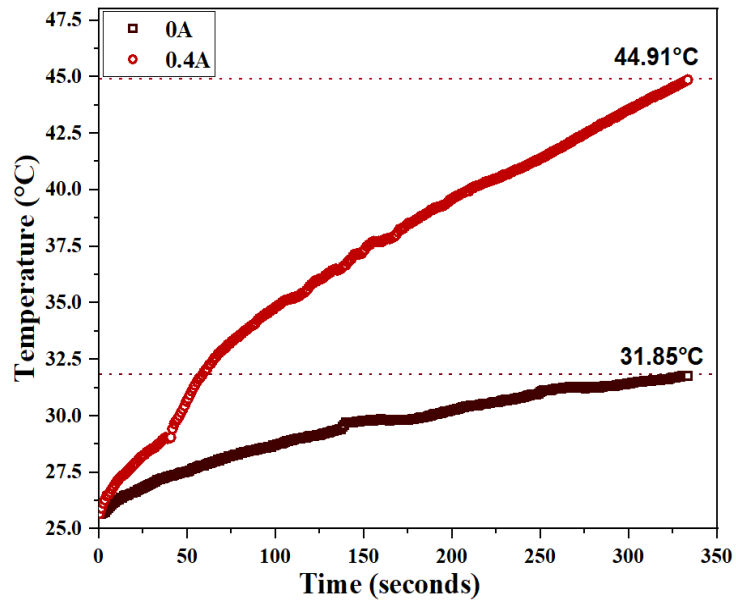
Figure 3.63 Temperature increase of the MR fluid during the testing
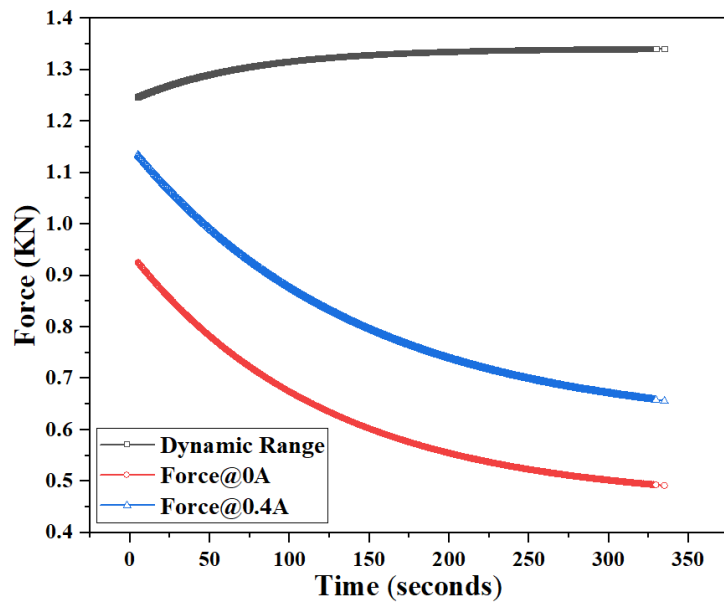
Figure 3.64 Temperature impact on damping force and dynamic range

3.5 SUMMARY

The Chapter-3 details confirmation of the CI particle size, and shape, which is of 7 microns in size and spherical in shape which is feasible for the synthesis of MR fluids. After verification of the particles shape and size six MR fluid samples have been prepared and studied for sedimentation stability and yield stress behaviour. Off six MR fluids MRF-1 gives better stability and yield stress which is selected for performance analysis in the next chapter-4.

CHAPTER 4

INFLUENCE OF TEMPERATURE ON MAGNETORHEOLOGICAL FLUID PROPERTIES AND DAMPING PERFORMANCE

4.1 INTRODUCTION

The MR fluid systems temperature plays a significant part in enhancing the performance of the system. As in the case MR damper, the operating temperature of the fluid inside the damper is very important in analysing the damping force and setting the limit for loading parameters to the MR damper. As per the authors knowledge very less research is available related to the temperature effect on damping performance by Dogruoz et al. (2003), Elsaady et al. (2021), Guo et al. (2019), McKee et al. (2018), Sahin et al. (2009) when the damper is operating. The present study aims to evaluate the temperature effect of MR fluid on performance while the damper is working. Before synthesizing MR fluid, scanning electron microscopy, X-ray diffraction, and particle size analysis verifies for the synthesis of MR fluid in-house. Characterization of the MR fluid at different temperatures and magnetic fields was carried out. The Herschel-Bulkley model is used to analyse the nonlinearity in the fluid by incorporating the temperature effect. The range of critical parameters used to fabricate the MR damper is selected using the Technique for Order of Preference by Similarity to Ideal Solution (TOPSIS) performance score. The temperature of the MR fluid is measured using an embedded thermocouple while the damper is operating at different loading parameters. The theoretical model predicts the increase in temperature similar to that of the experimental values with an average error of 10.24

95

% in the on-state condition. After characterisation of the damper particle characterization for morphology, saturation magnetization, and TGA has been carried out to see the effect of temperature on particle shape, and magnetic saturation and to analyse the life of the fluid through TGA after approximately 85000 cycles. Finally, to imitate the temperature effect on the particle, particles were heat-treated at 200 °C, 400 °C, and 600 °C, and through SEM image the deterioration of the particle is noted.

4.2 METHODOLOGY

This section of the study explains the process followed to attain the mentioned objective of temperature measurement and its effect on damping force while the damper is working.

4.2.1 Synthesis of MR fluid

Characterization of magnetic particles and steps to prepare magnetorheological fluids are presented in the following section shown in figure 4.1.

4.2.2 Particle characterization

Materials used for MR fluid preparation include carbonyl iron (CI) particles (manufacturer: sigma Aldrich, 44890), lithium grease (manufacturer: Permatex 80345) as an additive, silicone oil (manufacturer: Sigma Aldrich, 378372) as base fluid. Scanning electron microscope (SEM) and Particle size analyser (PSA) were used to obtain the shape (morphology) and average particle diameter of particles, respectively. The crystalline structure is analysed using X-Ray diffraction (XRD) at a 2 °/minute scanning rate with radiation of $\lambda=1.54$ Å. Precision electronic balance for weighing the required quantity of carrier fluid, stabilizer, carbonyl iron particles, and geared stirrer to disperse the particles in the carrier fluid are the instruments necessary to prepare the MR fluid. The properties of CI particles provided by the supplier are shown in table 4.1.

Table 4.1 MR fluid components and their properties

Carbonyl iron powder Properties	
Density	7.86g/ml
Shape	Spherical
Size	5-9microns
Properties of silicone oil	
Viscosity	350cst at 25°C
density	0.968g/ml
Boiling point	>=140°C
Properties of lithium base grease	
Viscosity	45100Cst at 40°C
Boiling point	>=250°C
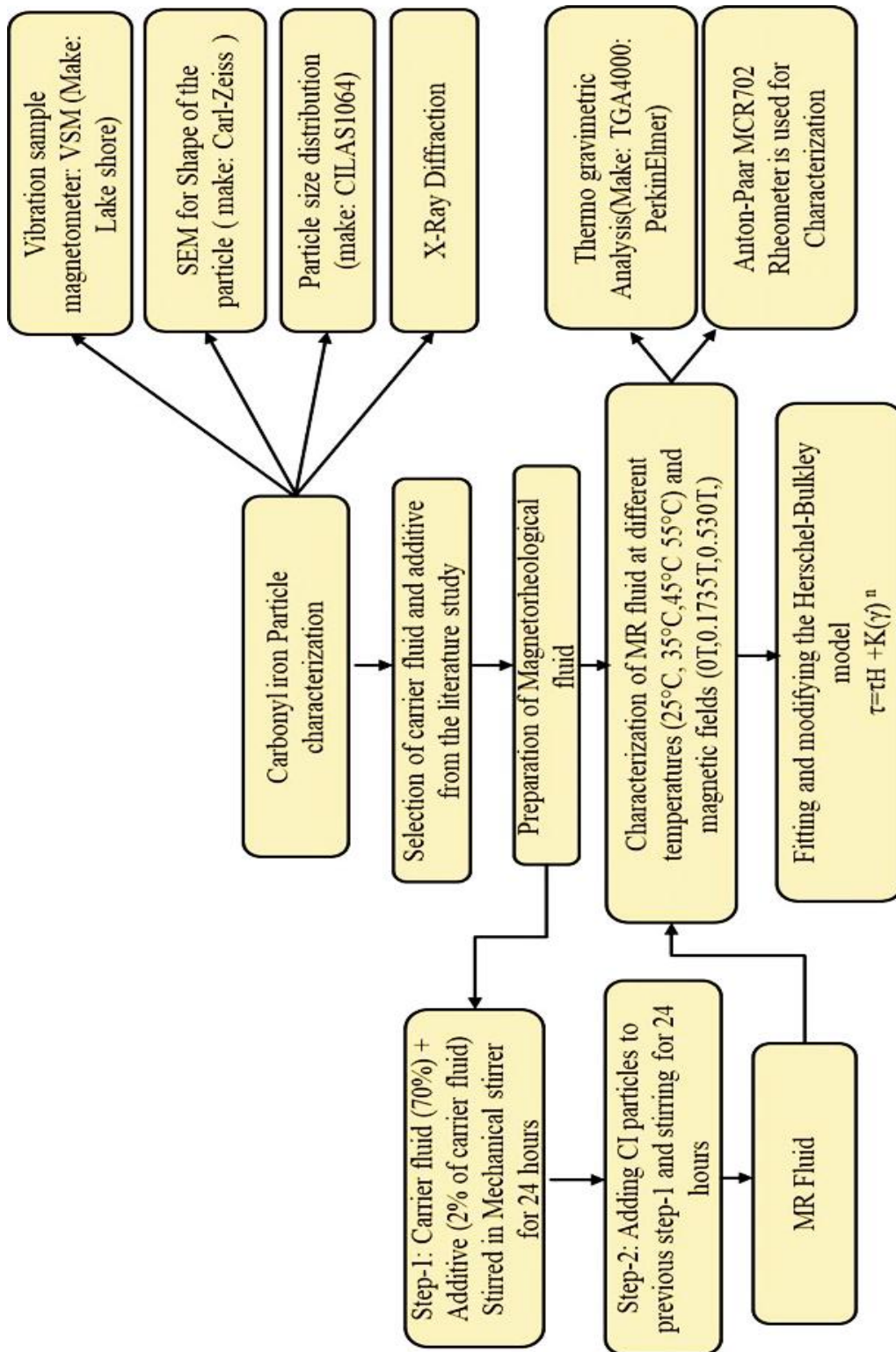
Figure 4.1 Methodology for particle analysis and characterization of MR fluid

The flowchart contains the following elements:

Top row boxes:
- Vibration sample magnetometer: VSM (Make: Lake shore)
- SEM for Shape of the particle (make: Carl-Zeiss)
- Particle size distribution (make: CILAS1064)
- X-Ray Diffraction
- Thermo gravimetric Analysis(Make: TGA4000: PerkinElmer)
- Anton-Paar MCR702 Rheometer is used for Characterization

Main flow boxes:
- Carbonyl iron Particle characterization
- Selection of carrier fluid and additive from the literature study
- Preparation of Magnetorheological fluid
- Characterization of MR fluid at different temperatures (25°C, 35°C,45°C 55°C) and magnetic fields (0T,0.1735T,0.530T,)
- Fitting and modifying the Herschel-Bulkley model $\tau = \tau H + K(\gamma)^n$

Bottom flow boxes:
- Step-1: Carrier fluid (70%) + Additive (2% of carrier fluid) Stirred in Mechanical stirrer for 24 hours
- Step-2: Adding CI particles to previous step-1 and stirring for 24 hours
- MR Fluid

4.2.3 Synthesis of MR Fluid

Table 4.2 refers to the materials used for MR fluid preparation. First, the silicone oil and stabilizing agent are weighed using the precision weighing balance and then transferred to a beaker. The silicone oil and stabilizer are stirred for about 24 hours by setting up the speed of a geared stirrer. Finally, after homogenizing the carrier fluid and stabilizer, CI particles were added to the same beaker and stirred for about 24 hours at 700 rpm. The volume fraction of silicone oil and carbonyl iron powder was taken in the ratio of 70 % and 30 %, respectively. Additives of 2 % by volume of silicone oil were added to the carrier fluid. Synthesized MR fluid is further characterized for sedimentation stability and flow behaviour discussed in the following sections.
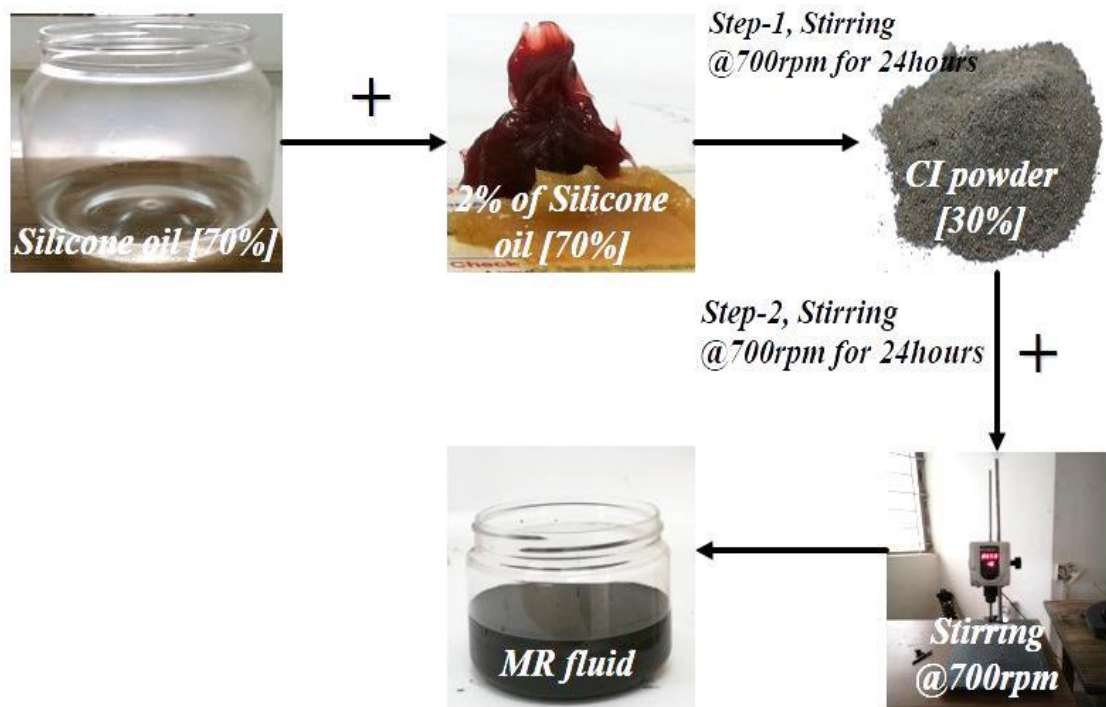
Figure 4.2 MR fluid synthesis

Table 4.2 Constituents used for preparing MR fluid

Materials	Quantity (Volume fraction in %)
Silicone oil	70
Carbonyl iron powder	30
Lithium white grease (% of total weight)	2

4.2.4 Stability of MR fluid

A high density of CI particles is a factor that influences the sedimentation of MR fluids when compared to base fluid density. The particles tend to settle towards the bottom of the measuring cylinder due to gravity, as the particles settle to the bottom, a volume of precise carrier fluid forms at the top of the measuring cylinder. The stability of MR fluid is measured as the ratio of the height of clear fluid after settling to the total volume of the MR fluid filled in the measuring cylinder before settling and is called the sedimentation ratio.

$$Sedimentation\ ratio\ (\%) = \frac{height\ of\ the\ clear\ fluid\ (ml)}{the\ total\ height\ of\ the\ fluid\ before\ settling (ml)} \times 100$$

The in-house MR fluid is taken in a 10 ml measuring cylinder. The measuring cylinder is provided with graduations of 0.2 ml, as shown in figure 4.3. The sedimentation is observed by measuring the height of the layer of particles settled with time. Many parameters affect the sedimentation rate, such as carrier fluid viscosity, shape, size of particles, stabiliser added, and carrier fluid temperature. All the parameters were kept constant except the fluid temperature in this work. To vary the temperature of the fluid, incubator is used that has a maximum temperature of 100 °C with 2-3 % error band.

Figure 4.3 MR fluid sample before and after settling

4.3 Rheological Characterization of In-house MR fluid

After settling studies of the prepared samples the fluid characterization is to be carried out to know the flow behaviour of the prepared sample to further analyse the performance of the damper. The measuring conditions to characterize the MR fluid are shown in table 4.3.

Table 4.3 shows the measuring conditions for MR fluid characterization

Shear gap	1 mm
Shear rate	$0.1\ s^{-1}$ -1000 s^{-1}
Magnetic fields	0 T, 0.1735 T, 0.530 T, 0.890 T
Temperature	25 °C, 35 °C, 45 °C, 55 °C

MR fluid rheological behaviour has been obtained using a rheometer (make: Anton-Paar MCR 702). The rotational rheometer can provide shear stress and viscosity values at the required magnetic field and temperatures which are shown in figure 4.4. Approximately 0.32 ml sample is loaded onto a bottom plate, and the shear gap is maintained at 1mm between the plates while testing. Obtained values might have an error of ±1-2 % due to sample loading of MR fluids with high viscosity. The rheometer has a temperature control unit that can heat the fluid to a maximum of 70 °C and cool the liquid to ambient temperature.

4.3.1 Temperature dependence of MR fluid Viscosity

Temperature and shear rate significantly influence the viscosity and affect the performance of MR fluid. Therefore, MR fluid viscosity varying with temperature and magnetic field was intended to be studied in the present work. MR fluid behaves as Newtonian fluid in zero magnetic fields, and when the field is applied, it shows a non-Newtonian fluid behaviour. Viscosity curves under the varying shear rates of 0.1 s^{-1} to 1000 s^{-1} at required magnetic fields and temperatures are determined.
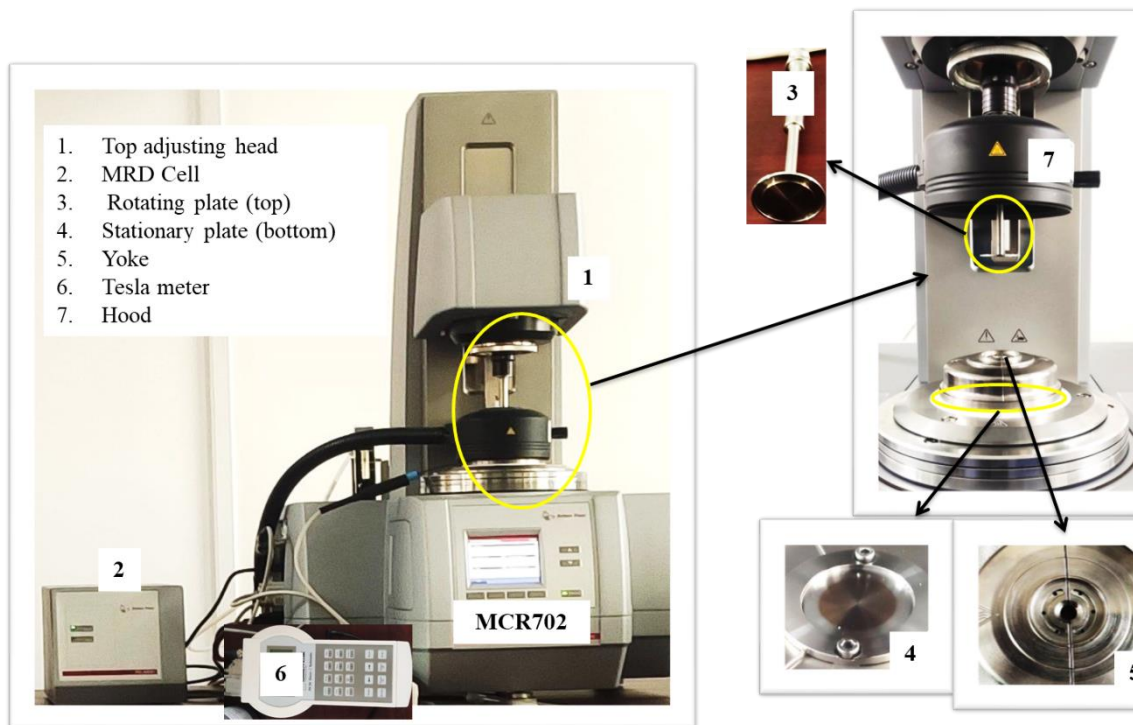
Figure 4.4 Rheometer for MR fluid property measurements

4.3.2 MR fluid yield stress

The fluid flow is restricted by CI particles arranged in a chain-like structure in the applied magnetic field, increasing MR fluid's yield point. It is also referred as the MR effect, and figure 4.5 represents the schematic representation of the MR effect.
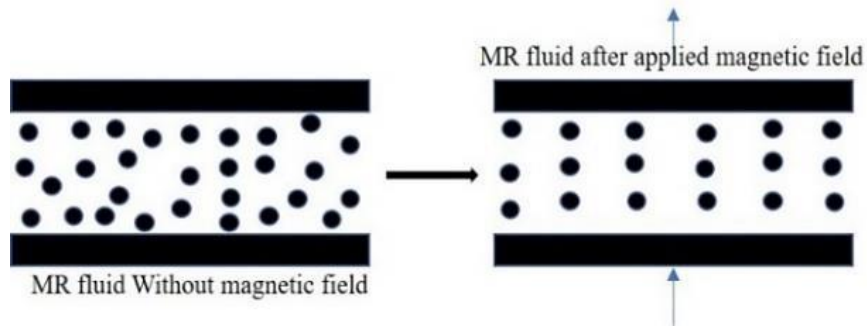
Figure 4.5 Magnetorheological effect with

the application of an external magnetic field

In this section, the behaviour of MR fluid for yield stress with and without magnetic field was studied at different individual temperatures. The shear stress behaviour with varying shear rates is observed at 25 °C, 35 °C, 45 °C and 55° C temperatures and at constant magnetic fluxes of 0 T, 0.1735 T, 0.53 T and 0.890 T. Under magnetic fields, yield stress increases at low shear rates compared to high shear rates. The variation in the yield stress with a supply of external magnetic field has been modelled based on Herschel-Bulkley (HB) model given by the equation below

$$\tau = \tau_H + K(\dot{\gamma})^n \qquad (4.1)$$

$$\dot{\gamma} = 0, \ \tau < \tau_H$$

Where τ = shear stress (Pa), τ_H = field (H)-dependent yield stress (Pa), $\dot{\gamma}$ = Shear rate(s^{-1}), K = consistency index and n = flow behaviour index.

4.4 Design and fabrication of MR damper

This section notes some essential performance parameters from the previous literature review and is optimised using the simple TOPSIS method for better performance. Following are the vital parameters listed below are considered.

- Fluid flow gap
- Effective pole length
- Core length to accommodate coil turns
- Number of turns of the coil
- Applied Current

Some of the above parameters and their relations were explained in section 4.7. Before going on to the actual fabrication process, the required dimensions have to be selected for the required size according to the raw material available. The material used for fabrication is selected from finite element (FE) analysis. Externally, the current supplied to the circuit can be controlled, but the other parameters should be decided before fabrication. The size (length, considering the maximum operating amplitude) and piston core must be fixed. Based on the limiting values, optimisation for geometric dimensions was carried out and the methodology for this study is given in figure 4.6. The primary step in this method is to convert all the parameter values into a normalised matrix using equation (2).

$$r_{ij} = \frac{xij}{\sqrt{\sum_{i=1}^{m} x_{ij}^2}} \qquad (4.2)$$

After selecting normalization weights, find out the weighted normalized matrix by multiplying the equation with weights chosen and given by equation (4.3).

$$a_{ij} = \omega_j r_{ij} \qquad (4.3)$$

The next step is to find out the ideal best (B^+ = increasing values among the parameters corresponding to given higher weights) and ideal worst parameters (B^- = decreasing values among the parameters corresponding to given lesser weights). Here, effective flange length and fluid flow gap are given weightage with 0.1 and 0.2 respectively, core length and a number of coil turns are given 0.1 each, and maximum weightage is given to magnetic flux density. They were used for finding the positive and negative Euclidian distance from equations (4.4) and (4.5).

$$Pi+ = \sum_{j=1}^{m} \sqrt{\left(B_{ij} - B_j^+\right)^2} \qquad (4.4)$$

$$Pi- = \sum_{j=1}^{m} \sqrt{\left(B_{ij} - B\bar{j}\right)^2} \qquad (4.5)$$

The performance score is calculated based on the magnitude of the magnetic flux density produced while calculating ideal best and ideal worst values. Equation (4.6) gives the formula for performance score calculation.

$$Pi = \frac{P_i^+}{p_i^+ + p_i^-} \tag{4.6}$$
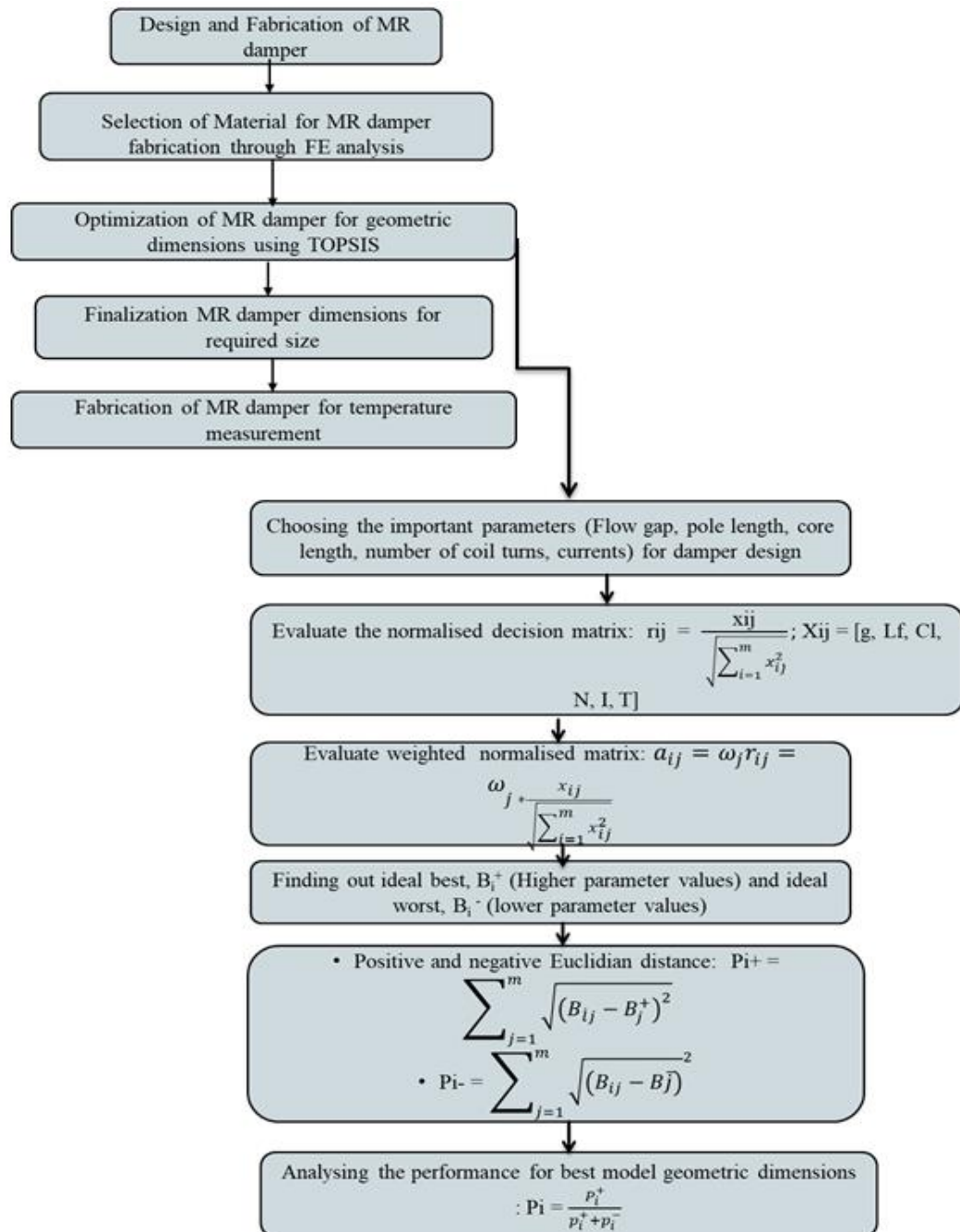
Figure 4.6 TOPSIS methodology flowchart

The overall goal line of this design of MR damper study is to get geometric dimensions for maximum magnetic flux density in the fluid flow gap and, in turn, to have a better damping force

Finite element analysis

The primary objective is to select a material for the fabrication of the damper through step-wise analysis of permeability of the materials in getting optimal damper. According to electromagnetic field theory, the magnetic induction line is almost parallel at the interface between the boundaries of the enclosure, fluid, piston core, and outer cylinder. The relation between magnetic flux and magneto-motive force in the piston core and cylinder can be obtained through Ohm's law which is given below

$$\Phi = NI / R_m \tag{4.7}$$

Where Φ is the magnetic flux, N= number of turns, I am the current, and R_m $(1/\mu A, \mu$ is the magnetic permeability of the material, and A is the cross-sectional area of the circuit) is the resistance offered by the magnetic circuit. Magnetic flux density (B) is computed from the current flux density (J) of the applied DC, and this current density is further used to evaluate the magnetic field intensity (H), which was developed using Ampere's law and Gauss law of magnetics and are given by

$$\nabla \times H = J + dD/dt \tag{4.8}$$

$$\nabla \cdot D = \rho$$

Magnetic flux density is given by(Nguyen et al. 2007)

$$B = \mu_o NI / 2 \times g \times \mu_r \tag{4.9}$$

Where ρ = free electric charge, J = I/A, current density, D = electric flux density, g = fluid flow gap (mm), μ_r = relative permeability of MR fluid, μ_0 = magnetic permeability of free space.

The material properties of the damper have been considered with the exact dimensions of fluid flow gap, pole length, and core length with non-magnetic materials for outer cylinder and piston rod for damper-1 and magnetic materials for the same cylinder and piston rod for damper-2.

4.4.1 Geometric dimensions for MR damper fabrication

Design dimensions for the fabrication of the damper are obtained from the TOPSIS method, which can be exclusively employed in many engineering applications where more than one objective is involved (minimising one parameter by maximising another parameter). The principle of operation is based on the user's requirements, which gives closeness to the ideal solution Pavić and Novoselac (2016). The advantage of this method is that the user can place the various magnitude of importance on the objectives that one wishes to employ that depends on application and interest and it is done by placing different weights on the objective functions.

In this section of the study, multiple parameters that decide the performance of the damper (contrary parameters) are studied based on weightage given to parameters given by the user on beneficial/non-beneficial terms. This method aims to see the importance of each parameter that contributes to the increase in the magnetic flux density in the fluid flow gap. As discussed earlier, the design parameters include effective length, core length, and the number of coils, currents, and fluid flow gap. The five models with different dimensions are selected within the required limits by assigning the weightage to each parameter and obtaining the parameters which give the highest magnetic flux density selected for fabrication. From the previous literature, study fluid flow gaps play a significant role in obtaining the highest magnetic flux density. Based on this literature, available weights are assigned. The model dimensions and the weights used to obtain the dimensions are given in table 4.4 - table 4.5.

Table 4.4 Models used for selection of MR damper dimensions

Models	Effective length	Core length	coils	Fluid gap	Magnetic flux density
Mod-1	3	15	300	0.5	0.671
Mod-2	4	18	450	2	0.842
Mod-3	5	21	400	1	0.906
Mod-4	6	24	350	2.5	0.549
Mod-5	7	27	500	1.5	1.01

Table 4.5 Weightage is given to each design parameter

Flange length (mm)	Core length(mm)	No of coil turns	Shear gap(mm)	Magnetic flux density
0.1	0.1	0.1	0.2	0.5

Taking the fluid gap as the non-beneficial criteria and giving more weightage to the magnetic flux density in the fluid flow gap by maintaining the applied current constant at 1.5 A, the performance scores of individual models are given in table 4.6. The dimensions obtained for fabrication are given in table 4.7.

Table 4.6 Performance score of all the models

Model-1	0.51858
Model-2	0.46935
Model-3	0.73768
Model-4	0.16195
Model-5	0.73016

Table 4.7 Selected dimensions for fabrication

Dimensions for fabrication MR damper	
Flange length	5mm
Shear gap	1mm
Core length	21mm
Number of copper turns	400
Maximum operating current	1.5 A

4.5 Fabrication of MR damper

After material selection, the fabrication process is carried out on traditional machining processes based on the dimensions obtained from the previous section. To vary the magnetic field electrical cables have to be passed through the hole drilled (3mm) in the piston rod and to measure the temperature thermocouple (K-type) is passed along with electrical cables until the top of the piston head. A copper coil is wound using the mechanical winding machine, which has a dial for counting the number of turns on the piston core material. Figure 4.7 shows the complete MR

damper arrangement for characterisation along with the thermocouple tip on the piston head.
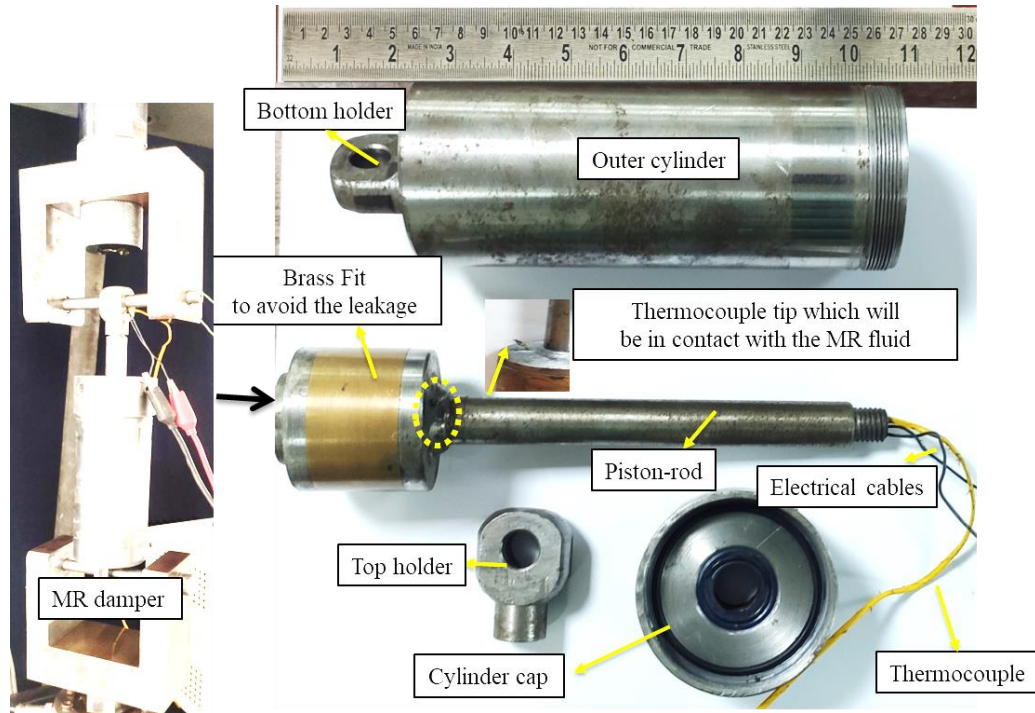
Figure 4.7 Thermocouple arrangement to measure

the temperature of the MR fluid inside the damper

4.5.1 Characterisation of MR damper

The complete arrangement to measure the temperature inside the damper is shown in figure 4.8. The structure consists of a damper testing machine fitted with an MR damper. The k-thermocouple is inserted where one side of the bead comes in contact with fluid on top of the piston head. During the continuous operation of the MR damper, the movement of the liquid from the flow gap comes in contact with the thermocouple bead, measuring the temperature of the fluid. Inline by measuring the fluid temperature inside, there were other two other thermocouples connected onto the surface of the outer cylinder, Ts_1-top surface, and Ts_2 bottom surface. Temperature and force-displacement data are acquired simultaneously with NI-9211 thermal DAQ and inbuilt data acquisition through the controller of the damper testing machine, respectively. The force data is acquired from the load cell attached at the bottom fixture. The displacement given to the damper is acquired from the displacement

transducer attached at the top and the hydraulic actuator. The current is supplied with the help of the dc power supply.

Figure 4.8 DAQ and controller setting for temperature characterisation

4.5.2 Theoretical study on heat generation in MR damper

The temperature of the MR fluid plays a significant role in the MR damper's performance and affects the life of the system operating under these fluids. A theoretical model was modelled and validated experimentally to study the model's applicability. Using lumped system analysis proved academic experimentation results for different damping forces. A control volume is selected within the damper where energy balance in rate form is applied upon solving the relation gives the temperature at any instant Breese and Gordaninejad (1999.). Converting the obtained model to nondimensional terms to get the heat leaving the system and heat generated from the applied current. The important assumptions in order to prove the applicability of the lumped phenomena were variation in yield stress of the MR fluid between atmosphere the and the system is not more than 5 % and that also Biot number should be less than 0.1 Dogruoz et al. (2014.). The energy balance is given by

110

$$Q\text{-}W = \frac{dU}{dt} \qquad\qquad (4.10)$$

Where Q = heat transfer rate, W = the work supplied and $\frac{dU}{dt}$ = internal energy of the system.

The heat is leaving the system through convection is given by the equation below

$$Q = h\, A_s\, [T(t)\text{-}T_0] \qquad\qquad (4.11)$$

Where h = convective heat transfer coefficient, A_s= External surface area of the damper, T_0= Ambient temperature, T (t) = temperature at any instant of time.

Work done in this equation (4.10) is given by two terms one is force-displacement, and another is electricity supplied and is given below

$$W = F\,(t) \times \frac{dx(t)}{dt} \text{-} I^2(t)R \qquad\qquad (4.12)$$

Where F(t) is the work input to the piston rod, $x(t) = \bar{x} \sin (\omega t)$, I = input current, R = resistance of the wire.

Constitutive law is used to represent the inherent nonlinearity in the MR damper is assumed to be equation (4.13).

$$F(t) = C \times \left|\frac{dX(t)}{dt}\right|^{\alpha} \text{sgn}(\frac{dX(t)}{dt}) \qquad\qquad (4.13)$$

C and α ($0 \le \alpha \le 1.5$, are the functions of current and temperature, and they are the damping coefficient and fractional exponent, which shows the inherent nonlinearity in the MR damper.

The internal energy within the control volume is given in equation 4.14.

$$\frac{dU}{dt} = \frac{dT(t)}{dt} \sum mc\hat{p} \qquad\qquad (4.14)$$

$\frac{dT(t)}{dt}$ = rate of temperature change in the system, $\sum mc\hat{p}$ = summation of all the internal energies. Substitution and rearranging of terms give

$$T(t) + \lambda\,[\,T(t) - T_0] = \frac{C\bar{x}\cos(\omega t)}{\sum mc\hat{p}}\,|\bar{x}\omega\cos(\omega t)|^{\alpha}\,\text{sgn}(\frac{dX(t)}{dt}) + \eta \qquad (4.15)$$

$$\text{Where } \lambda = \frac{hAs}{mc\hat{p}}, \quad \eta = \frac{I^2R}{\sum mc\hat{p}}$$

For MR fluid damper 4th order Runge-Kutta method is used to solve the equation 4.15 for any value of α.

4.6 Results and Discussion

The detailed results of particle analysis, synthesis, sedimentation study, characterisation, design, and characterization of the damper for thermal analysis are discussed in the following section.

4.6.1 Particle characterisation

The primary step before MR fluid preparation is to characterize the commercially available CI particles to verify the feasibility of preparing the MR fluid. Figure 4.9 shows the morphology of the particle which is spherical in nature. The mean particle size of CI particles is 7.42 µm when measured with a particle size analyser and is shown in figure 4.10. Shape and size play an essential role in magnetorheological fluids' stability and yield behaviour. As the particle size increases, the sedimentation rate also increases.
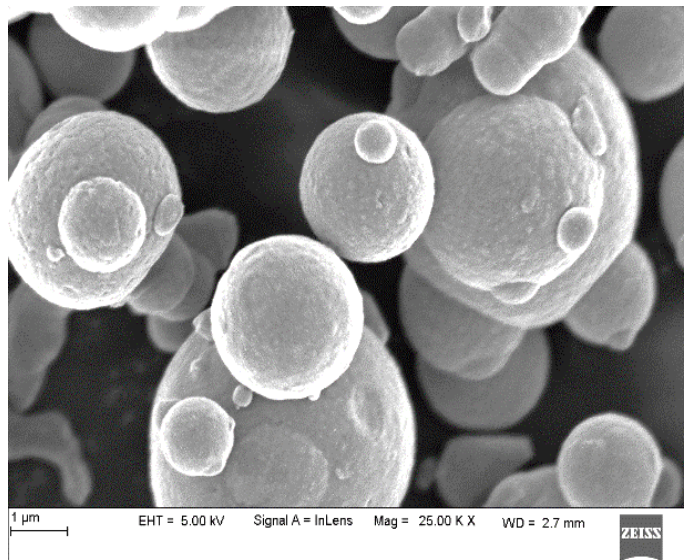
Figure 4.9 SEM image of CI particles
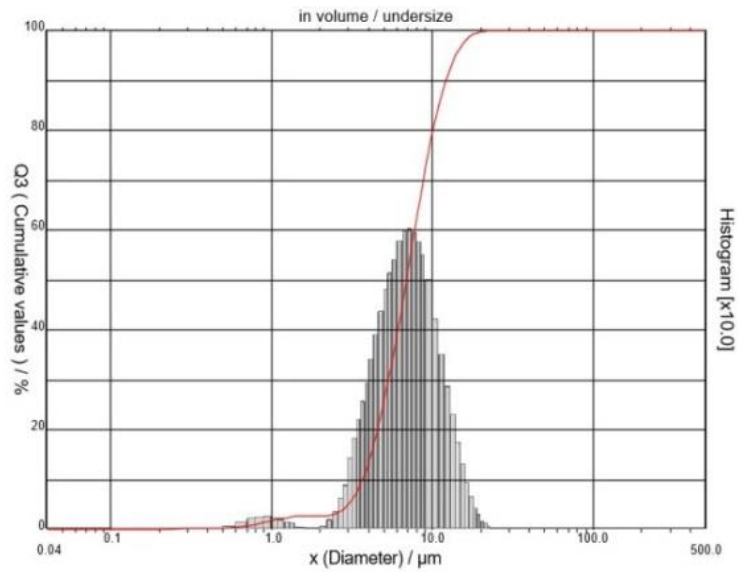
Figure 4.10 Particle size distribution of CI particles

From figure 4.11, the peaks are obtained at 45.3°, 65.71°, and 82.94°, which correspond to 2θ at 110, 200, and 211 lattice planes which imply that the crystal structure is a body-cantered cube (BCC).
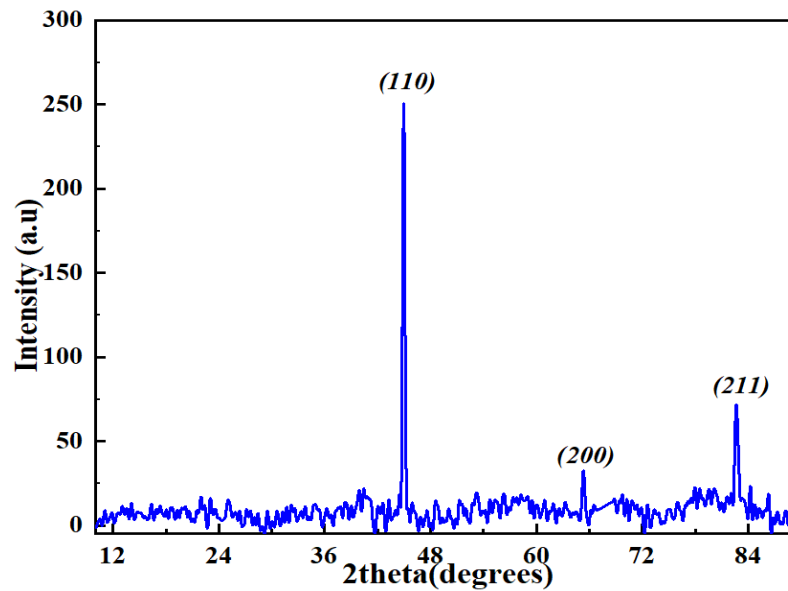
Figure 4.11 XRD of CI particles

4.6.2 Sedimentation stability

After synthesis of MR fluid the initial step is to test for the settling behaviour of the sample. Figure 4.12 shows the sedimentation study of the MR fluid at different temperatures. The sedimentation results show that, at 30 °C, 28 % of MR particles have been settled, and it takes nearly 336 hours to settle down completely. The fluid temperature is increased from 30 °C to 100 °C with an increment of 10 °C. At each temperature, the time corresponding to sedimentation is noted down.
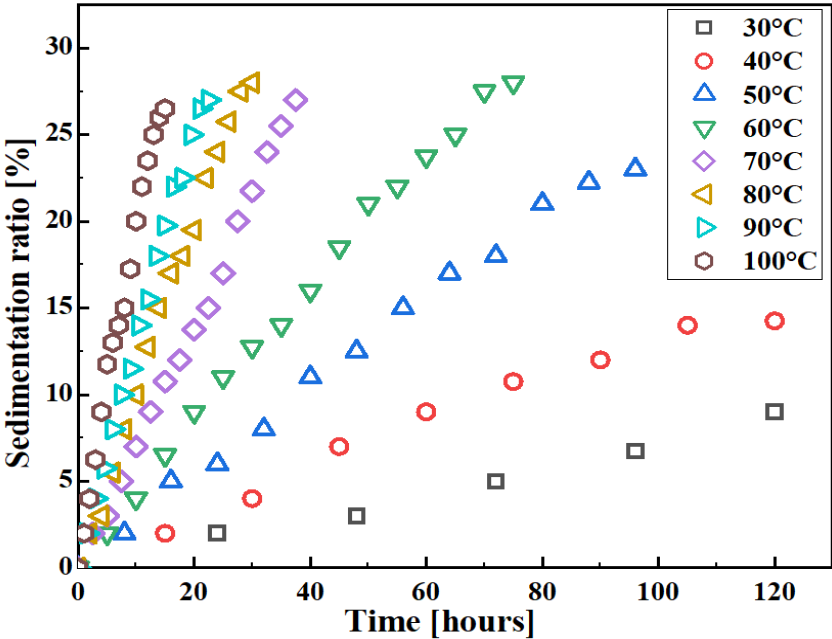
Figure 4.12 Sedimentation ratio of MR fluid at different temperatures

Figure 4.12 shows the details of the sedimentation ratio at individual temperatures. The variation of sedimentation rate at different temperatures was observed for 2 % sedimentation, i.e., time is taken for 2 % sedimentation at a particular temperature. The results were characterised using an exponential curve shown in figure 4.13. These results can be further explored to evaluate the time taken to settle at a particular settling rate to re-operate the MR fluid system.
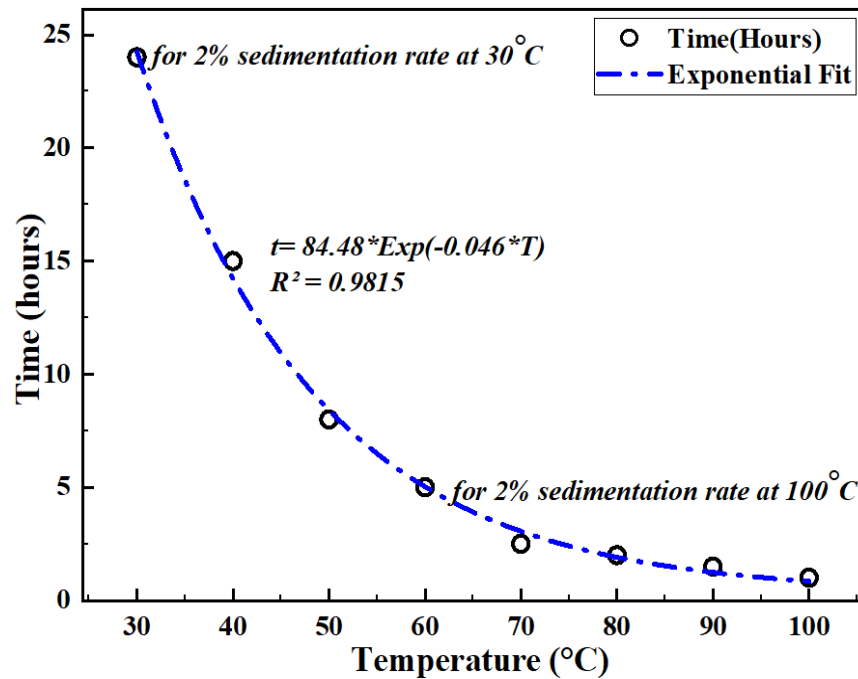
Figure 4.13 Time taken to settle at constant sedimentation rate

with varying temperatures

4.6.3 Temperature effect on the MR fluid viscosity

For various temperature and magnetic field strengths of MR fluid, shear rate versus viscosity were plotted from varying shear rates. MR fluid viscosity without magnetic field in between temperatures of 25 °C - 150 °C and with magnetic field in the temperature range of 25 °C-55 °C were obtained as shown in figures 4.14 - 4.17. Figure 4.18 illustrates the temperature effect on in-house MR fluid and commercially available MR fluid viscosity at zero magnetic field. The exponential decay model fit analysis illustrates that decrease in viscosity follows a similar pattern for both fluids with r-square value greater than 0.9, which is the reliability of the obtained values. The comparative study of in-house fluid viscosity with commercial fluid resembles the same trend at higher temperatures without magnetic field. However, the increase in viscosity with the magnetic field increase and the temperature of MR fluid up to 0.530 T. After 0.530 T magnetic fields, viscosity does not change significantly because of the magnetic saturation of particles. Nevertheless, the decrease in viscosity is exponential with the shear rate. The curve fitting method obtains the relationship between the viscosity and temperature, given by equation 4.16.
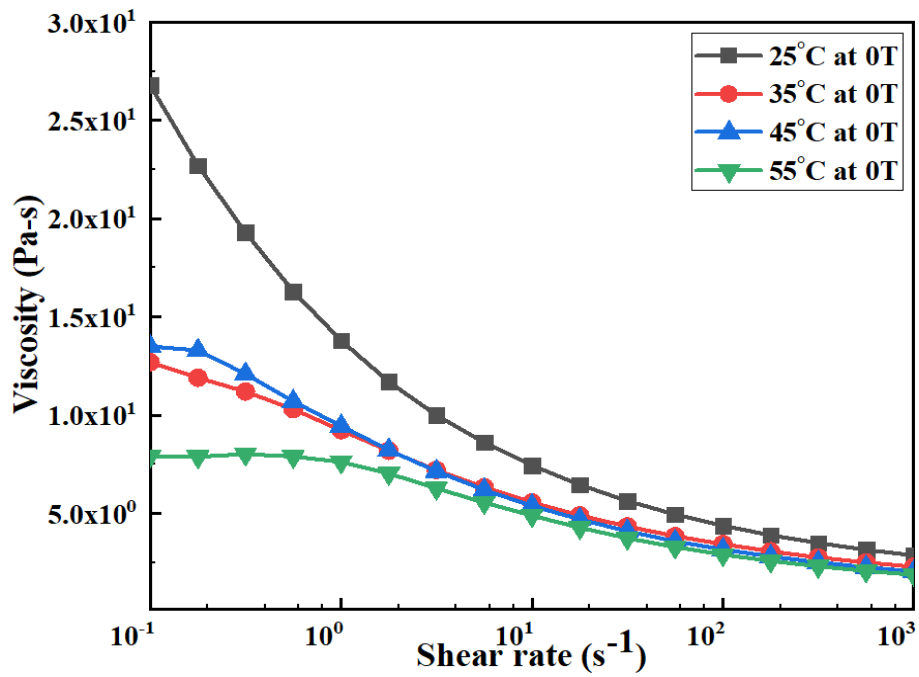
Figure 4.14 Viscosity versus shear rates at 0 T with varying temperatures
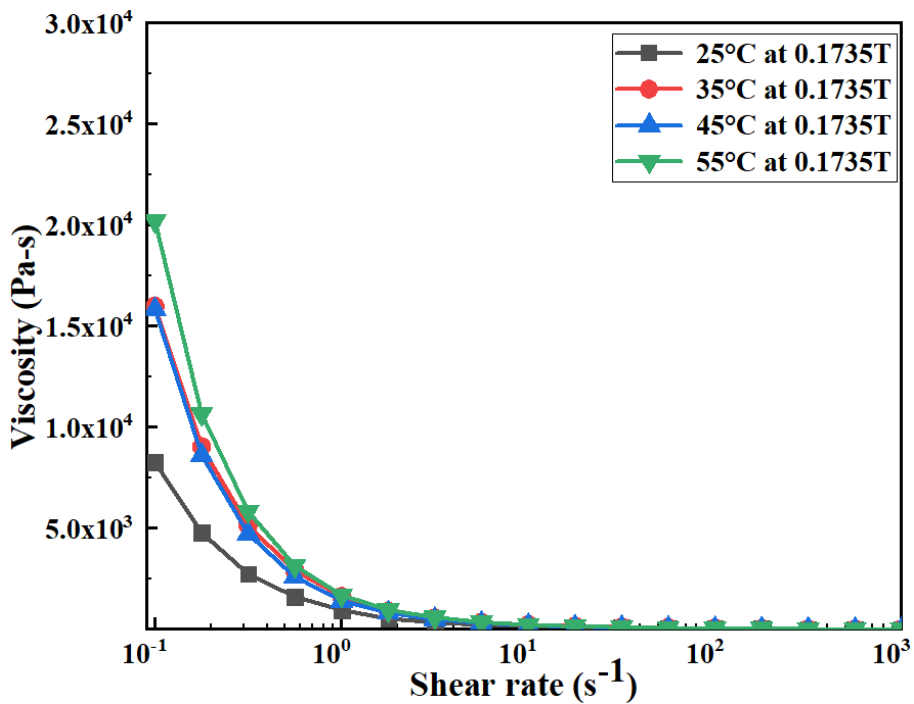
Figure 4.15 Viscosity versus shear rates at 0.1735 T with varying temperatures
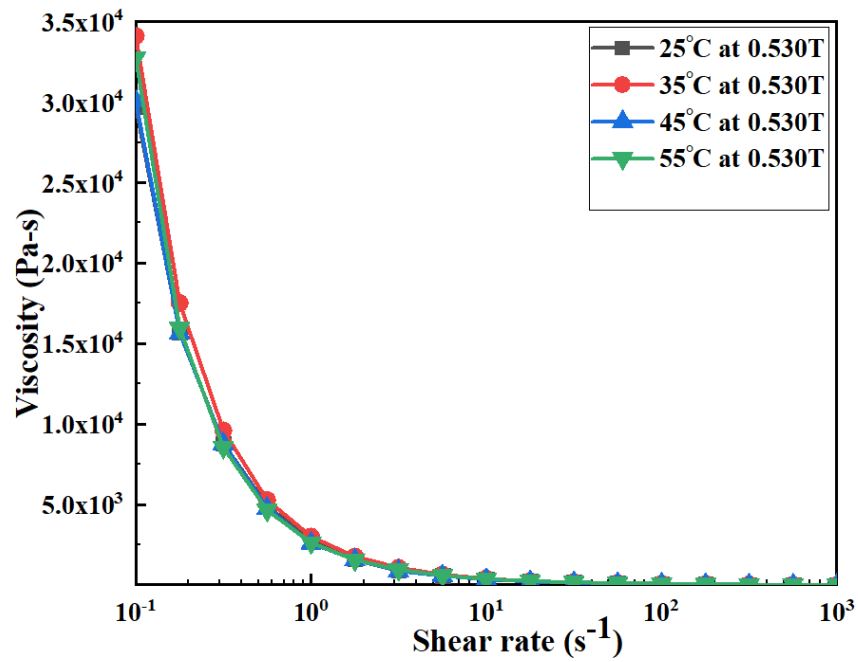
Figure 4.16 Viscosity versus shear rates at 0.530 T with varying temperatures
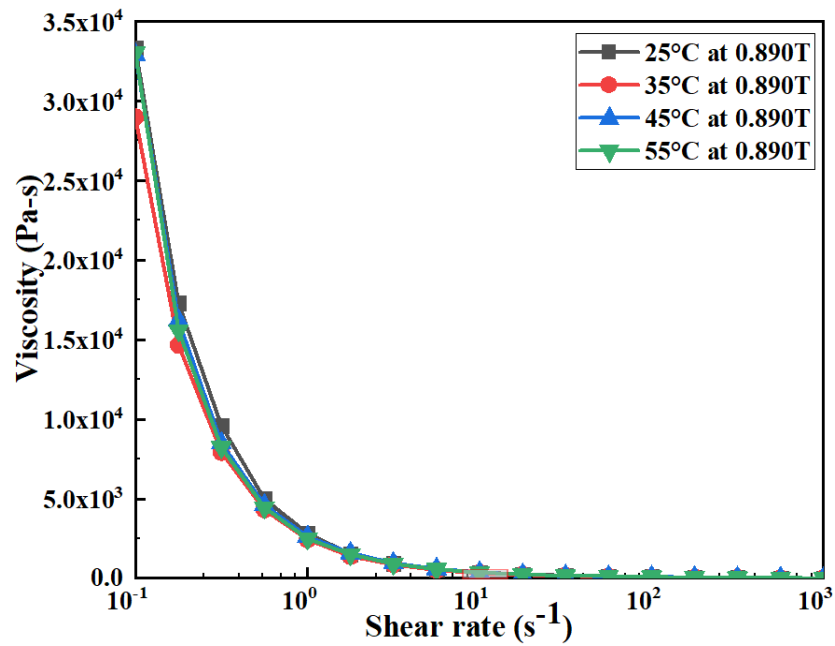
Figure 4.17 Viscosity versus shear rates at 0.890 T with varying temperatures

The comparative study to know the behaviour of the MR fluid viscosity for in-house and commercially available is illustrated in figure 4.18 with exponential model fit analysis.
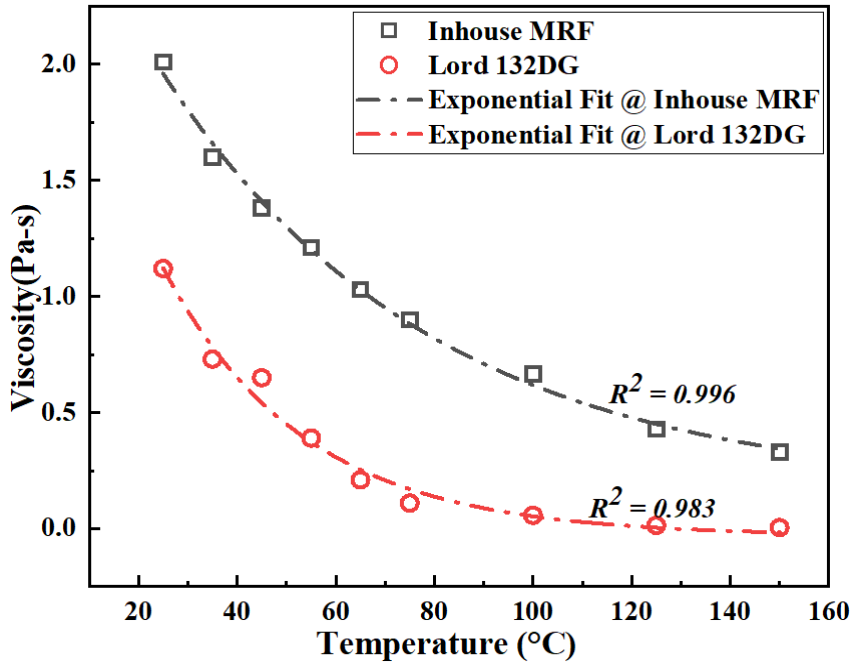
Figure 4.18 Temperature versus viscosity at zero magnetic field

The experimentation found it to decrease exponentially with the increased temperature at various magnetic fields.

The equation for the exponential curve is given below

$$\mu = a\, e^{-bT} \tag{4.16}$$

Where a and b are constants, T = temperatures, μ = viscosity (Pa-s).

4.6.4 Temperature effect on MR fluid yield stress

To describe the flow behaviour of MR fluid, HB model at varying shear rates and magnetic fields is used. The model comprises Newton's law, power-law, and Bingham plastic law and is expressed by equation (4.17).

$$\tau = \tau_B + K\,(\dot{\gamma})^n \tag{4.17}$$

Where τ = shear stress (Pa), τ_B = field (H)-dependent yield stress (Pa), $\dot{\gamma}$ = shear rate(s^{-1}), K = consistency index and n = flow behaviour index.

The flow behaviour of MR fluid at various temperatures and magnetic fields is obtained and is shown in figures 4.19 – 4.22. It is clear that when the external field is applied, the nonlinear Herschel Bulkley (HB) model fits the flow behaviour. The available literature study shows that MR fluid properties are mainly affected by

118

temperature. At zero magnetic fields, MR fluid has a yield stress of 4.27 Pa and 2.75 Pa at 25 °C and 55 °C temperatures, respectively, and there is a 35.59 % decrease in the yield stress. At a magnetic field strength of 0.890 T, the MR fluid has 2760.3 Pa and 2423.1 Pa dynamic yields stress at temperatures 25 °C and 55 °C, respectively. Approximately a 12.21 % decrease in the yield stress was detected at 25 °C to 55 °C with a magnetic field. Higher magnetic fields increase the yield stress at constant temperature up to the saturation point. An increase in temperature at a definite magnetic field reduces yield stress.
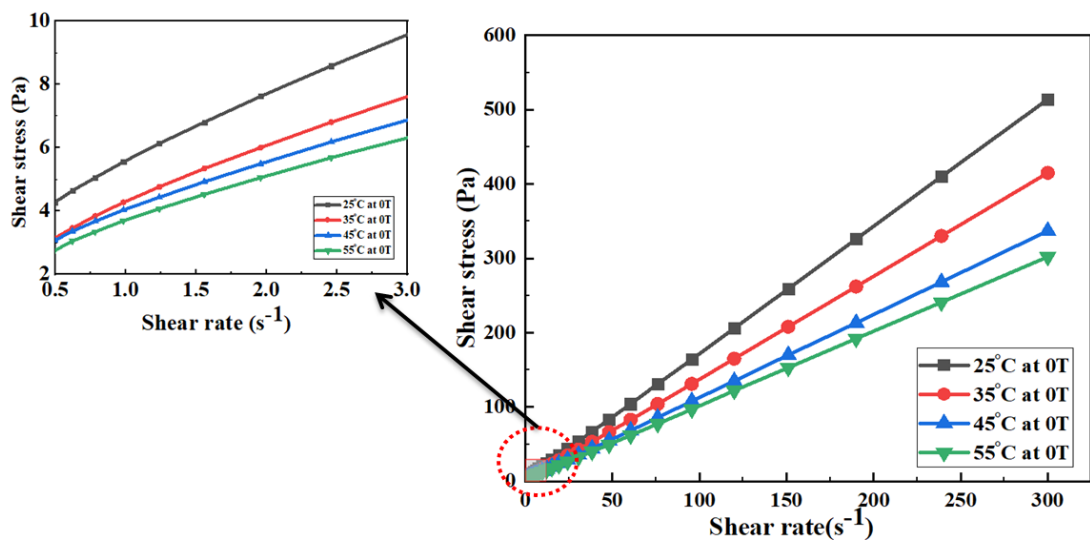
Figure 4.19 Shear stress versus shear rate at 0 T with varying temperatures
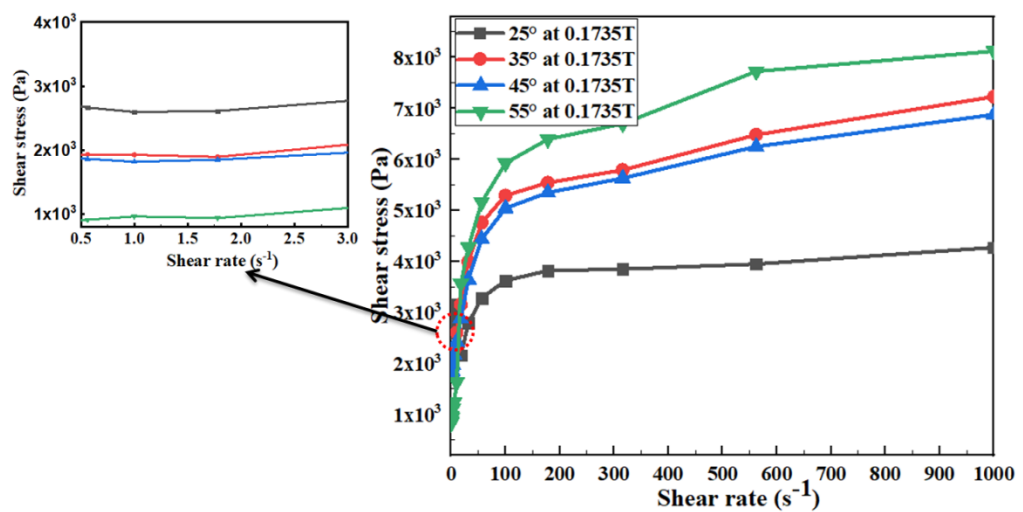
Figure 4.20 Shear stress versus shear rate at 0.1735 T with varying temperatures
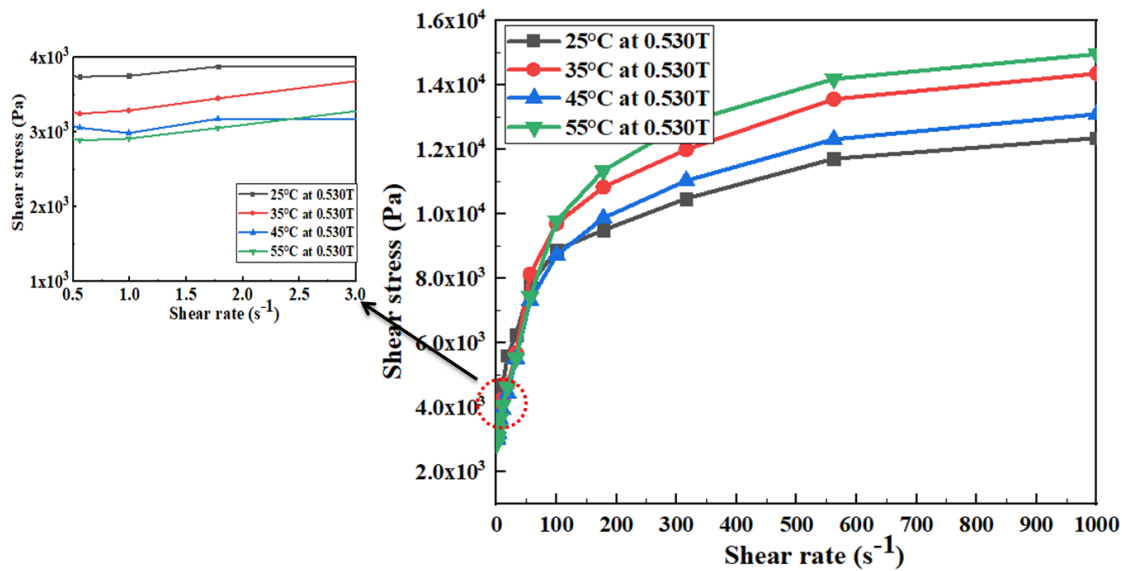
Figure 4.21 Shear stress versus shear rate at 0.530 T with varying temperatures
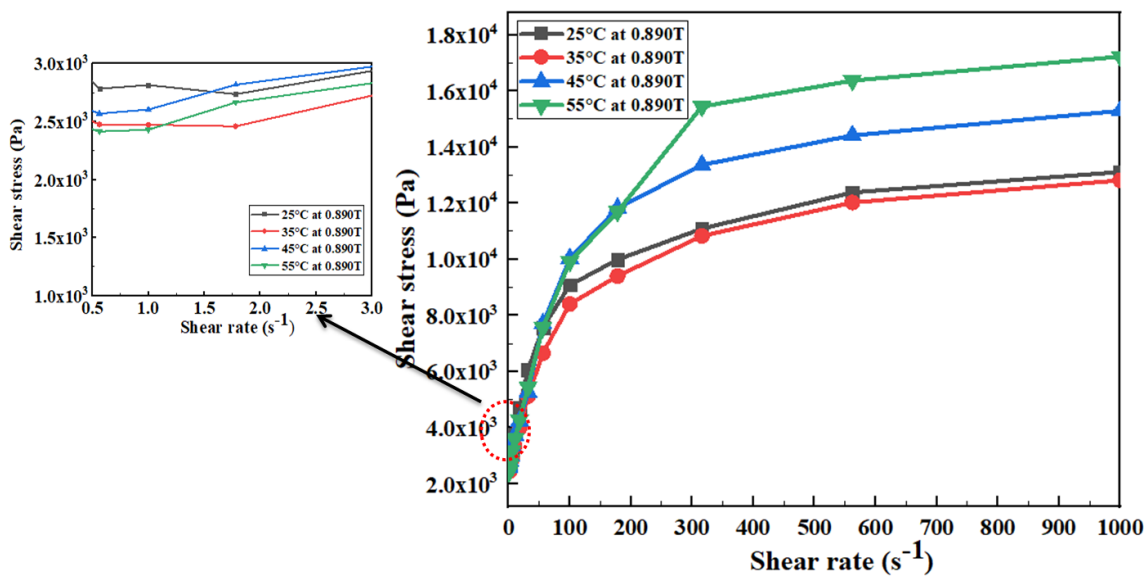
Figure 4.22 Shear stress versus shear rate at varying

temperatures and magnetic fields

Generally, microparticles will have high magnetic properties compared to nanoparticles. When the magnetic field increases, the chain formation filling gaps between the microparticles will increase the yield stress. To modify the HB model and include the temperature effect, the change in parameters has to be analysed at different temperatures. Figure 4.23 depicts the variation of yield stress with increase in magnetic field and the B-H curve for prepared MR fluid is also mentioned.

120
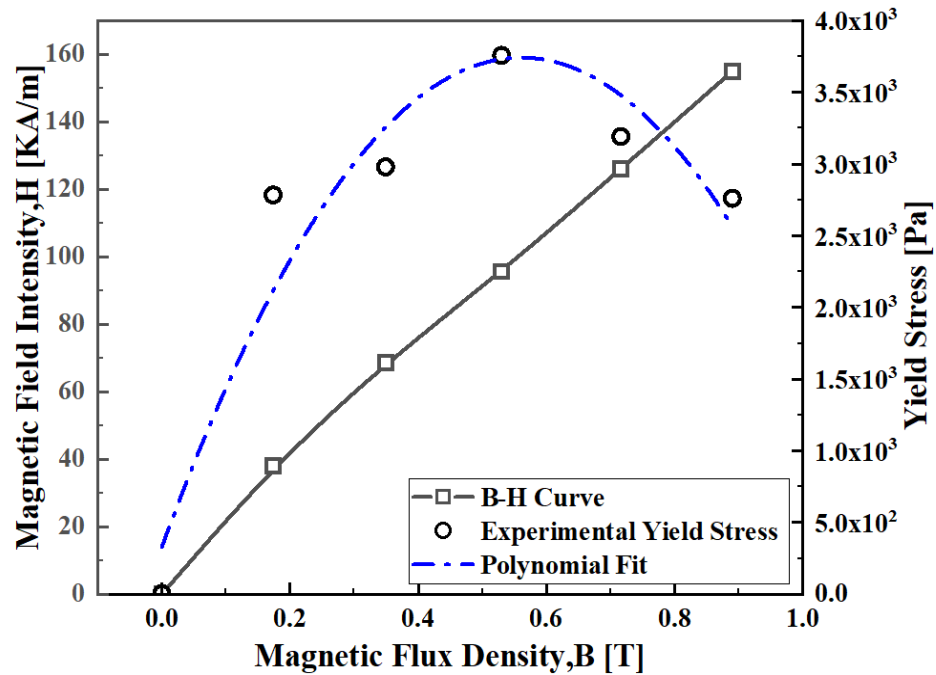
Figure 4.23 Yield stress variation concerning

the external magnetic field at 25 °C

The B-H curve for equipment shows us that a magnetic field passes through the fluid on the plate. The second-order polynomial equation is fitted over the data obtained and is expressed in equation (4.18).

$$\tau_B = a_o(B^2) + a_1(B) + a_2 \qquad (4.18)$$

Where a_o, a_1, and a_2 are constants, B = Magnetic flux density [T]

Figure 4.24 show the dependency of consistency index K on the applied magnetic field has been fitted with a 2nd order polynomial and given by equation (4.19).

$$K = -115.6(B^2) + 943.36(B) + 93.41 \qquad (4.19)$$
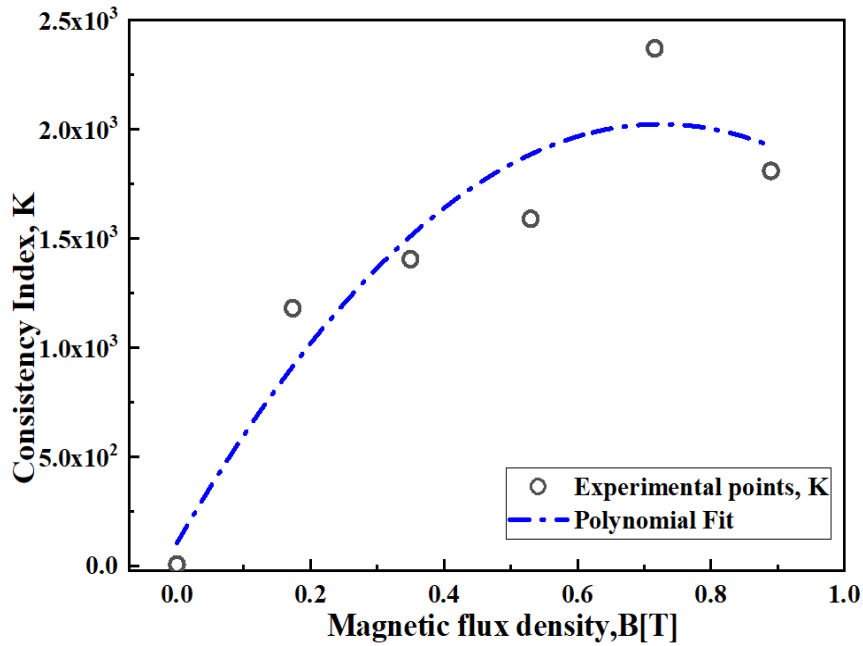
Figure 4.24 Magnetic field versus Consistency index

Table 4.8 HB model parameters and yield stress values at different magnetic fields (25 °C temperature)

Magnetic flux density(T)	τ_B (Pa)	K	n	R-Square
0	4.27	1.59	1	0.99
0.1735	2784.6	1179.8	0.202	0.94
0.530	3757	1588.64	0.276	0.97
0.890	2760.3	1808.19	0.285	0.960

Table 4.8, table 4.9, table 4.10, and table 4.11 show the model parameters at different temperatures. The analysis shows that temperature affected yield stress, consistency index, and fluid viscosity, which agrees with the research carried out in the previous studies. At lower shear rates, the flow behaviour curve slope is more than that at higher shear rates.

122

Table 4.9 HB model parameters and yield stress values at different magnetic fields (35 °C temperature)

Magnetic flux density(T)	τ_B (Pa)	K	n	R-Square
0	3.14	1.24	1	0.99
0.1735	1927.1	1407.49	0.227	0.965
0.530	3313.1	1571.81	0.312	0.96
0.890	2574.32	1491.52	0.31	0.967

From the tables it can be observed that at specific magnetic fields and increasing temperature, yield stress decreases significantly. The decrease in yield stress can be interpreted as a decrease in the damping force as the yield behaviour of the sample is directly related to on state damping of the MR damper.

Table 4.10 HB model parameters and yield stress values at different magnetic fields (45 °C temperature)

Magnetic flux density(T)	τ_B	K	n	R-Square
0	3.07	1.05	1	0.99
0.1735	1894.72	1104.26	0.252	0.96
0.530	3153.9	1426.13	0.312	0.967
0.890	2569.37	1786.05	0.315	0.957

The decrease in yield stress is also due to temperature rise and the Brownian motion of nanoparticles. The Brownian movement comes into the picture because of the existence of nanoparticles in smaller quantities that causes a reduction in yield stress (Wang et al. (2019)). The Brownian motion in the MR fluid can be minimised by increasing the particle size of which compromises the settling rate of the particles.

Table 4.11 HB model parameters and yield stress values at different magnetic fields
(55 °C temperature)

Magnetic flux density(T)	τ_B (Pa)	K	n	R-Square
0	2.75	0.98	1	0.99
0.1735	867.61	856.17	0.297	0.961
0.530	2979.32	1576.5	0.324	0.964
0.890	2423.18	1505.30	0.358	0.967

The decrease in yield stress of the MR fluid after a certain magnetic field depicts the fluid's saturation point in magnetic particles and is shown in figure 4.25. Figure 4.26 illustrates the decrease in yield stress with the temperature at specific magnetic field along with exponential decay model fit with r-square value greater than 0.9.
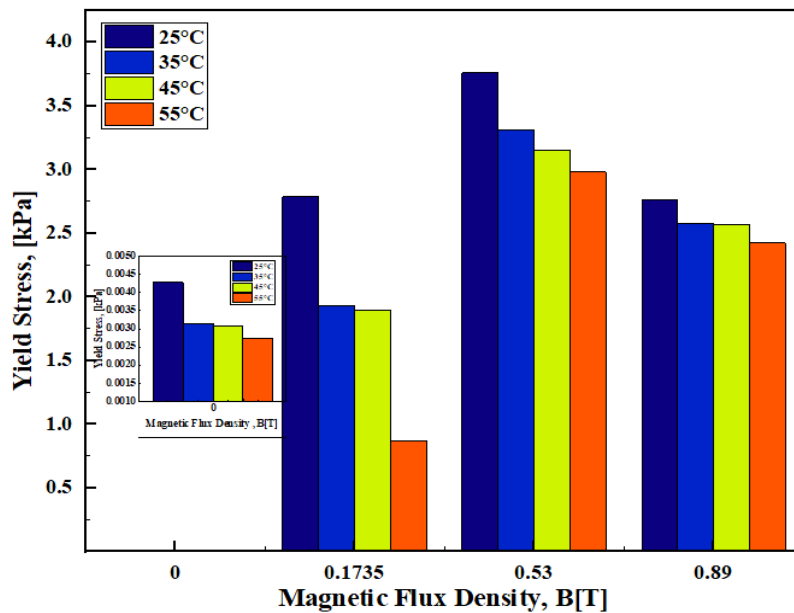
Figure 4.25 Yield stress variation with application

of magnetic field and temperature
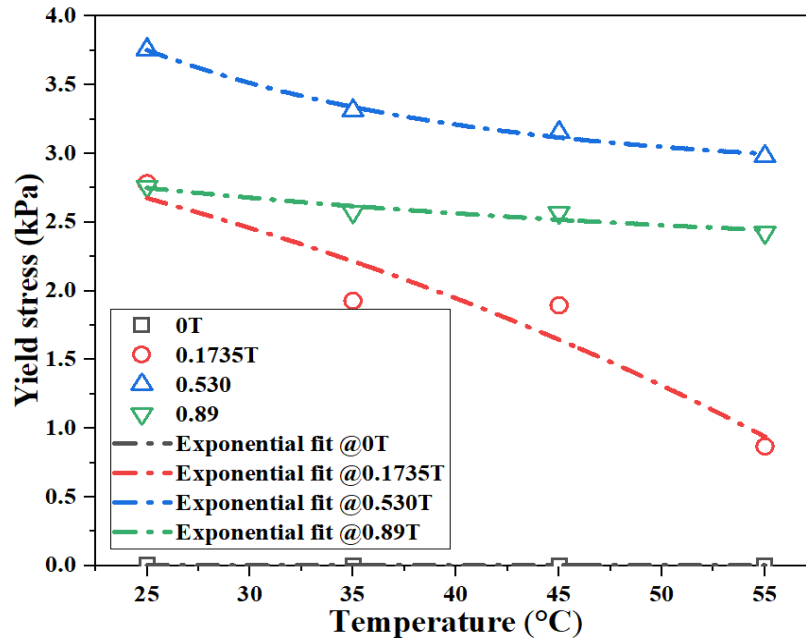
Figure 4.26 Yield stress variation with exponential model fit

Based on figure 4.26, a curve has been fitted considering the temperature and magnetic field effect; the HB model is incorporated by adding the Arrhenius equation (decaying impact) and is shown by equation (4.20). The parameters were calculated using the equation mentioned in table 4.11. This model will be further implemented in computational fluid dynamics (CFD) simulation work.

$$\tau\ (T,\ \dot{\gamma}) = \tau_B\ (B)\ A_1\ (T) + K(B)\ A_2(T)\ \dot{\gamma}^{\ n} \tag{4.20}$$

A_1 and A_2 are the exponential decay functions representing the temperature effect on MR fluid yield stress and viscosity.

$$A = A_o Exp\ (Ea./R.\ T) \tag{4.21}$$

Where A_o= pre-exponential parameter, Ea.=activation energy, R=universal gas constant=8.314 J/K.mol, T = temperature

Table 4.12 Parameters of the exponential decay function in various temperature

ranges are obtained using equation (4.20)

Magnetic flux density (T)	Temperatures (°C)	$E_{a.}(\tau_B)$	$E_a(\mu)$	$T_3(°C)$	R^2
0-0.890	25-55	2314.176	340.32	45	0.91

4.7 Design and fabrication of MR damper

Before fabrication, the materials used for fabrication are selected based on the finite element magnetostatic analysis and dimensions for fabrication were determined from the TOPSIS technique.

4.7.1 Selection of material for MR damper fabrication

The selection of materials for the fabrication of MR damper is studied through finite element analysis (FE) of ANSYS workbench and to find out the induced magnetic field in the fluid flow gap at different current inputs, which also decides the performance of MR damper. Figure 4.27 gives the schematic representation of the MR damper.
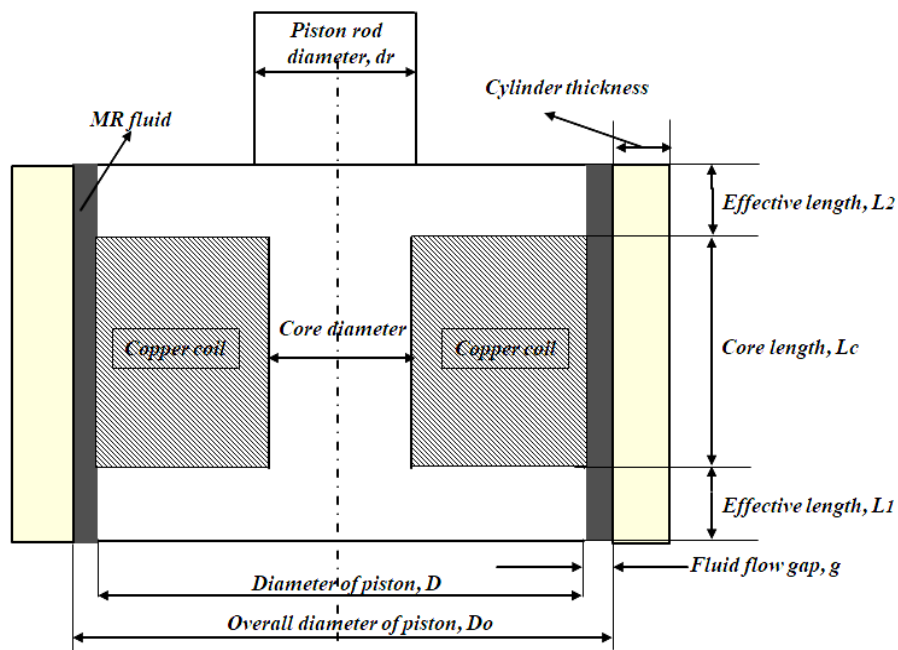
Figure 4.27 Schematic representation and terminology of the piston

The other vital parameters which enhance the magnetic flux density in the damper are the materials of a piston, cylinder, and design dimensions of the damper. The selected materials for the analysis are shown in table 4.13.

Table 4.13 Materials used for FE analysis

Models	Piston core	Piston-rod	Cylinder
Model-1	SA1018	Non-Magnetic	Non-Magnetic
Model-2	SA1018	SA1018	SA1018

4.7.2 Estimation of damping force from FE analysis

Theoretical damping force is calculated based on the magnetic flux density obtained in the gap between the effective length and the outer cylinder. Finite element analysis is employed to obtain the magnetic flux density in the gap and then substituting in equation (4.23) to find the yield stress of the fluid. The properties such as viscosity, density, specific heat capacity, and the permeability of the material are to be added in the equations below. The overall damping force induced in the damper is given by the three forces, i.e., frictional force (F_f), field-dependent yield stress (F_τ), and viscous force (F_μ), and is shown in equation 4.22 Xu et al. (2013). In this case, neglecting the friction force, the other two forces are considered for the study.

$$F = F_f + F_\tau + F_\mu \tag{4.22}$$

$$F_\tau = 2.07 + \left(\frac{12\mu Q}{12\mu Q + 0.4\omega g^2 \tau_B}\right)\frac{\tau_B L A p}{g} sgn(\dot{u}) \tag{4.23}$$

$$F_\mu = \left(1 + \frac{\omega g \dot{u}}{2Q}\right)\frac{12\mu Q L_t A p}{\omega g^3} \tag{4.24}$$

$$Q = \dot{u}Ap$$

$$\dot{\gamma} = \frac{Velocity}{2*Flow\ gap}$$

$$\mu = 0.0006\gamma^{.-0.6091}$$

$$w = \pi\left(\frac{g}{2} + \frac{g}{2} + D\right)$$

$$Ap = \frac{\pi(D^2 - d_0^2)}{4}$$

where L = effective length (mm), $L_t = L_1 + L_2$, total effective length (mm), w = Average circumference of flow gap (mm), D = diameter of piston (mm), g = gap thickness (mm), μ = apparent viscosity (Pa-s), τ = shear stress (Pa), d_o is the diameter of piston rod (mm), Q = volumetric flow rate (mm^2 /s), and u = relative velocity (mm/s).

The results from FE analysis show that the magnetic materials with high permeability give a higher value of magnetic flux density in the flow gap than the non-magnetic materials with less magnetic permeability. Figure 4.28 (damper-1) below shows us the leakage of a large amount of magnetic flux from the damper to the ambient, and figure 4.29 (damper-2) indicates no magnetic flux leakage from the ambient.
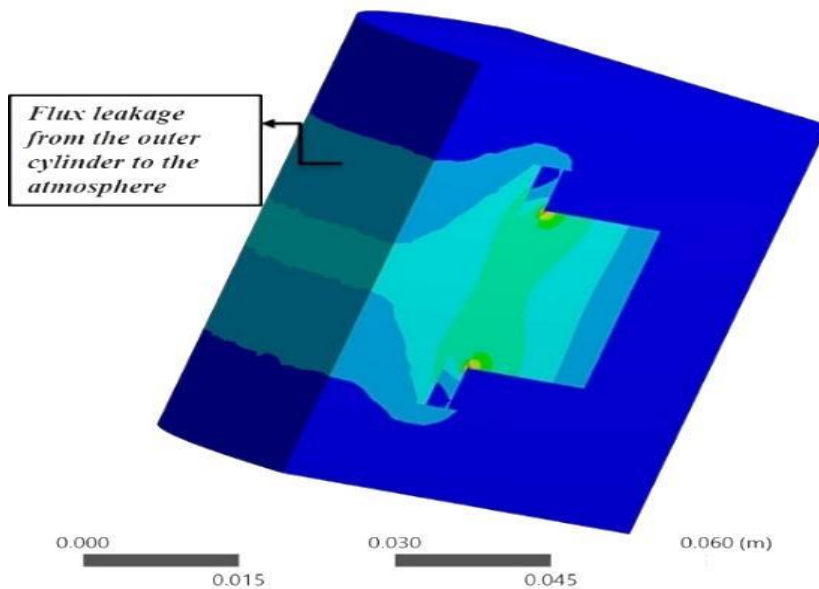
Figure 4.28 Magnetic flux density variation in damper-1
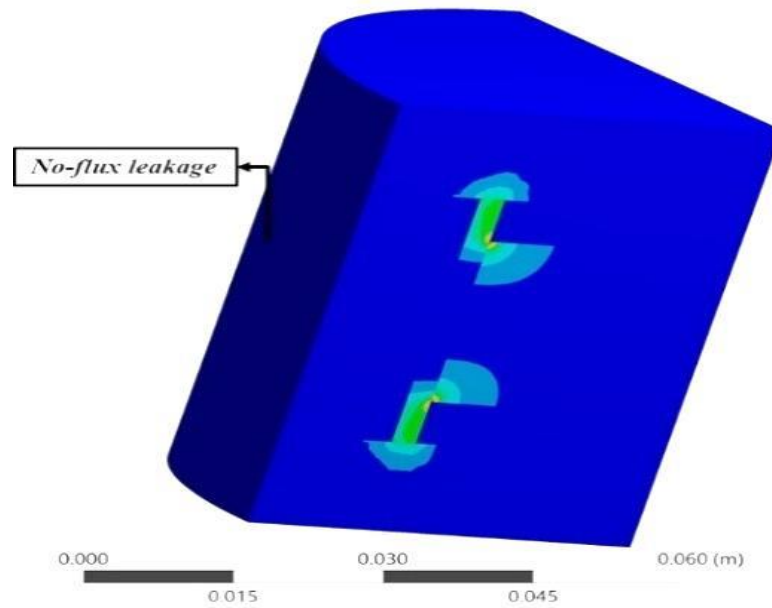
Figure 4.29 Magnetic flux density variation in damper-2

Figure 4.30 show us the magnetic material used for cylinder and piston material for MR damper fabrication. The materials used are SA1018 for piston core, SA1018 for cylinder and EN8 for piston rod.

Figure 4.30 Raw material for MR damper fabrication

4.7.3 Characterisation of MR damper

This work aims to determine the relationship between the temperature effects on the damping behaviour of the MR fluids in the damper. The first step in characterization was setting up the MR damper onto the damper testing machine.

Before fitting, MR fluid sample is kept in a desiccator vacuum pump to remove the air bubbles trapped in the fluid while stirring in the mechanical stirrer (to avoid air pressure on the piston) and then pouring the calculated fluid volume in the cylinder chamber. Checking the electromagnetic circuit for closeness using a multimeter and simultaneously connecting the thermocouple wires internally and externally to *NI-9211* thermal DAQ and this DAQ to the pc. Figure 4.31gives the MR damper characterisation flow charts.

By switching on the damper testing machine, some cycles at random amplitudes, frequencies, and current are operated to check the smooth operation. After checking with random conditions, the input conditions for the test on the damper are set. The amplitudes, frequencies, and currents selected are 8 mm, 10 mm, 12 mm, and 2 Hz, 3 Hz, 4 Hz, and 0 A, 0.25 A, 0.5 A, and 1 A, respectively. The plots were obtained at a particular amplitude, frequency, and varying currents. This step is repeated for different amplitudes and frequencies.
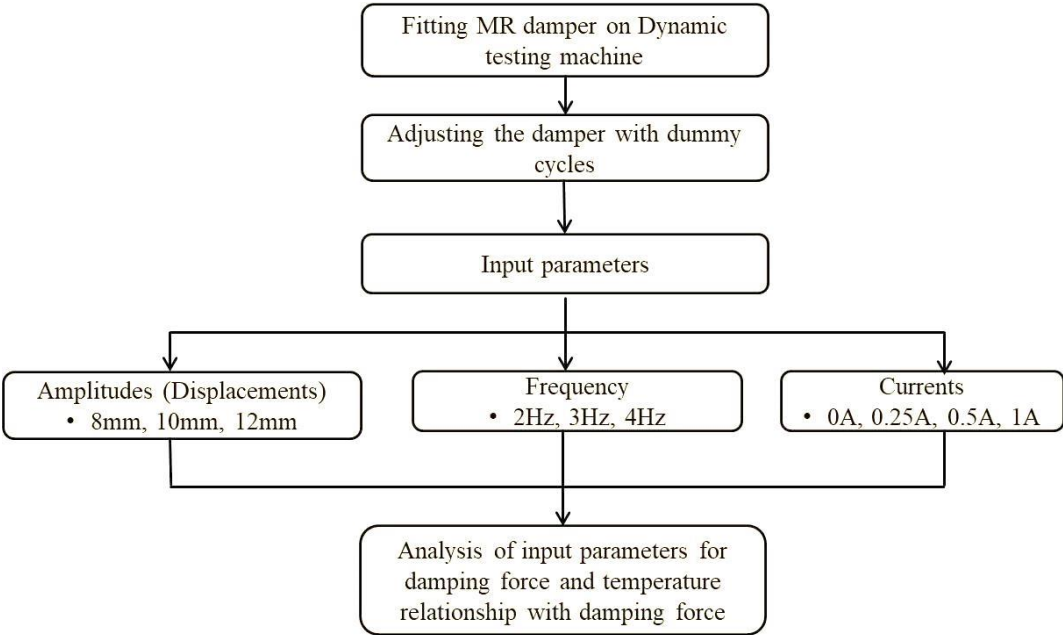
Figure 4.31 MR damper characterisation flowchart

The damping effect of suspension is usually described by force-displacement curves. The area covered by the force-displacement curve shows the damping effect of the damper in that period. The air bubble effect also adds to the distortion in force-displacement graphs at lower temperature. As the damper operating time increases, the

130

temperature of the fluid increases which reduces the viscosity of the fluid making the air escape from the MR fluid hence decreasing the distortion in force-displacement graph. The peak force shift towards the left of the force-displacement curve as shown in figure 4.32 which is similar to work done Guo et al. (2019). The plots shown below are for the 100th cycle and 1000th cycle to see the increase in temperature and decrease in the damping force at a single stretch for different currents was also carried out by Bharathi Priya and Gopalakrishnan (2019a).

Table 4.14 Parameter values for theoretical model analysis

Properties	Values
Heat transfer coefficient, h (w/m^2-k)	28
Surface area of the damper, A_s (m^2)	0.0336
Total heat capacity of system, $\sum_n mc_p$(J/K)	1905
Resistance of the electromagnet, Ohms (Ω)	22.4
T_{amb}(°C)	25-32

Figure 4.32 Force versus displacement curves at

8 mm amplitude, 2 Hz frequency, and 0 A

131
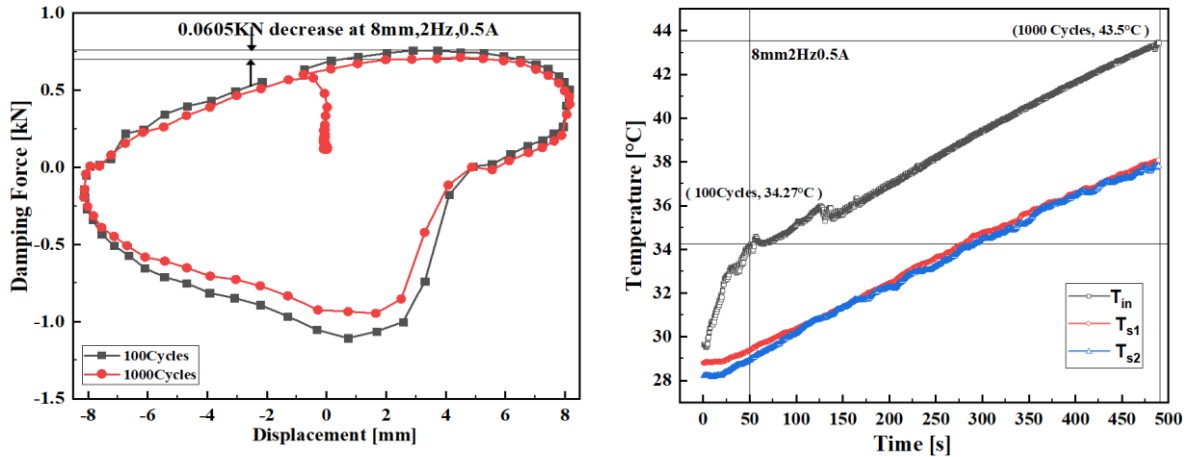
Figure 4.33 Force versus displacement curves at

8 mm amplitude, 2 Hz frequency, and 0.5 A

Figures 4.32- 4.35 shows the force-displacement measurement at 8 mm amplitude, 2 Hz, 3 Hz, 4 Hz frequencies at 0 A and 0.5 A. The test was been carried out for 1000 cycles to see the temperature rise in all the cycles. The distortion in force-displacement loop is caused due to the absence of accumulator and the presence of bubbles in high viscosity MR fluid which shifts the peak force towards the right side of the force-displacement graph. Atmospheric air gets trapped in the process of synthesizing MR fluid forming numerous bubbles in the process of mechanical stirring, due to high viscosity of the carrier fluid trapped air is not escaped easily at low temperatures. Along with the accumulator and air bubble effect and inertial and frictional effects also has a minimal impact on force reduction. The characterisation of MR damper in this study is carried out in the absence of the accumulator which is creating average compression load of 36.9 % more than the expansion stroke (Chooi and Oyadiji (2008), Elsaady et al. (2021).

Figure 4.34 Force versus displacement curves at

8 mm amplitude, 4 Hz frequency, and 0 A
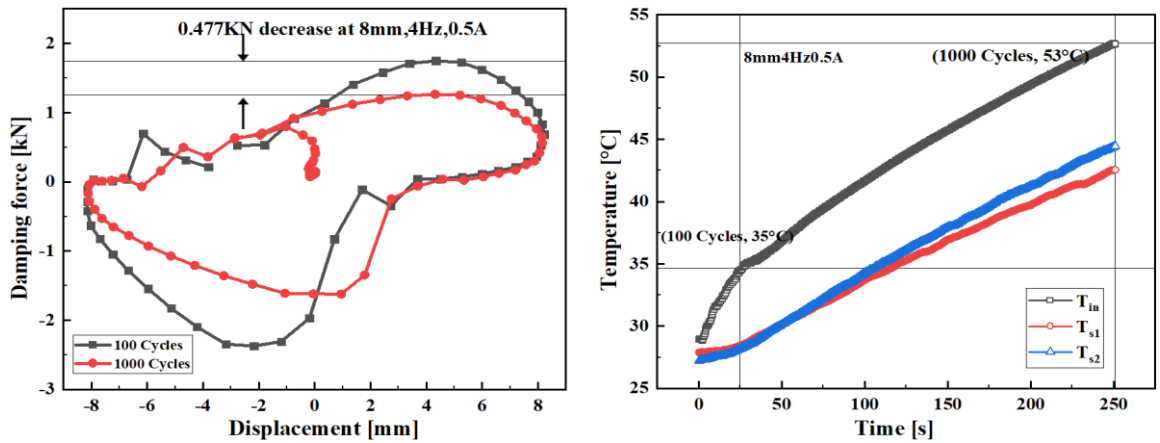
Figure 4.35 Force versus displacement curves at

8 mm amplitude, 4 Hz frequency, and 0.5 A

For instance, in figure 4.32 - 4.35, for 8 mm amplitude 2 Hz frequency, there is a decrease of 30 N force and 40.85 °C temperature at 0A and 60.5N force decrease and 43.5 °C temperature rise at 0.5 A current. At 10 mm amplitude 2 Hz frequency, there is a decrease in 153 N and 340 N decrease in force and 45.9 °C and 48.5 °C temperature increase at 0 A and 0.5 A currents, respectively.
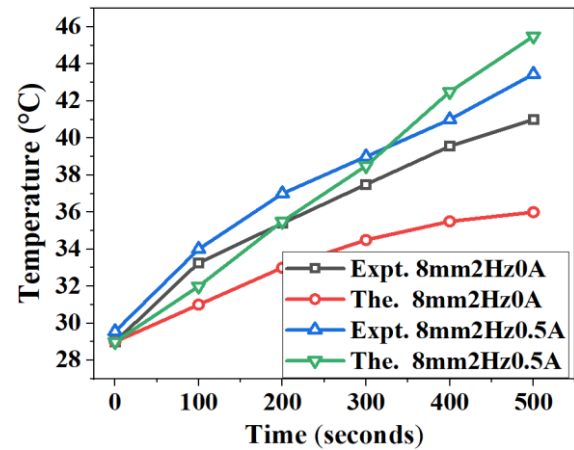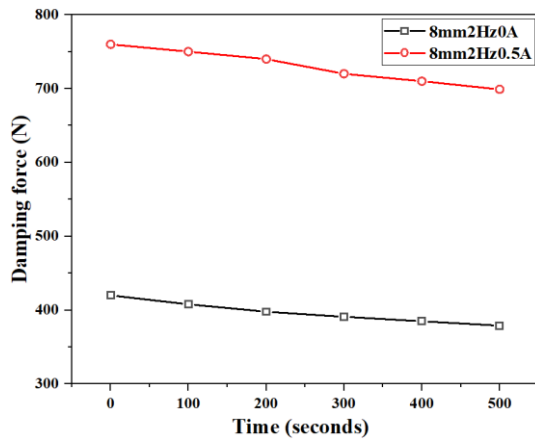
Figure 4.36 Force decrease with increase in time at

8 mm amplitude, 2 Hz frequency, and 0 A and 0.5 A

Figure 4.36 and 4.37 depicts the variation of damping force as function of time at 8 mm amplitude, 2 Hz and 4 Hz frequency at 0 A and 0.5 A currents. The insert in the figures show the theoretical validation of the experimental force values.
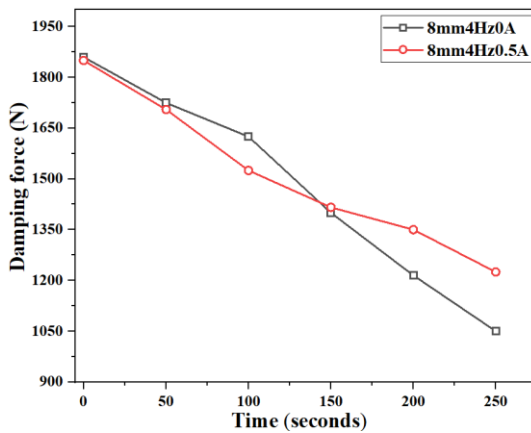
Figure 4.37 Force decrease with increase in time at

8 mm amplitude, 4 Hz frequency, and 0 A and 0.5 A

Figure 4.38 Force versus displacement curves at

10 mm amplitude, 2 Hz frequency, and 0 A
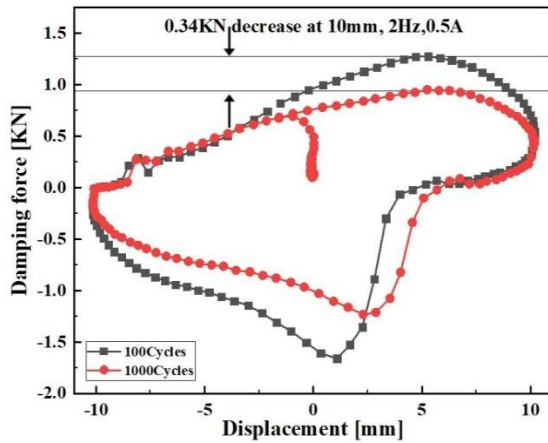
Figure 4.39 Force versus displacement curves at
10 mm amplitude, 2 Hz frequency, and 0.5 A
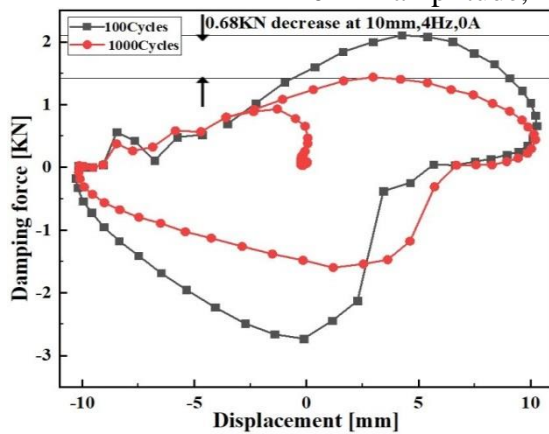
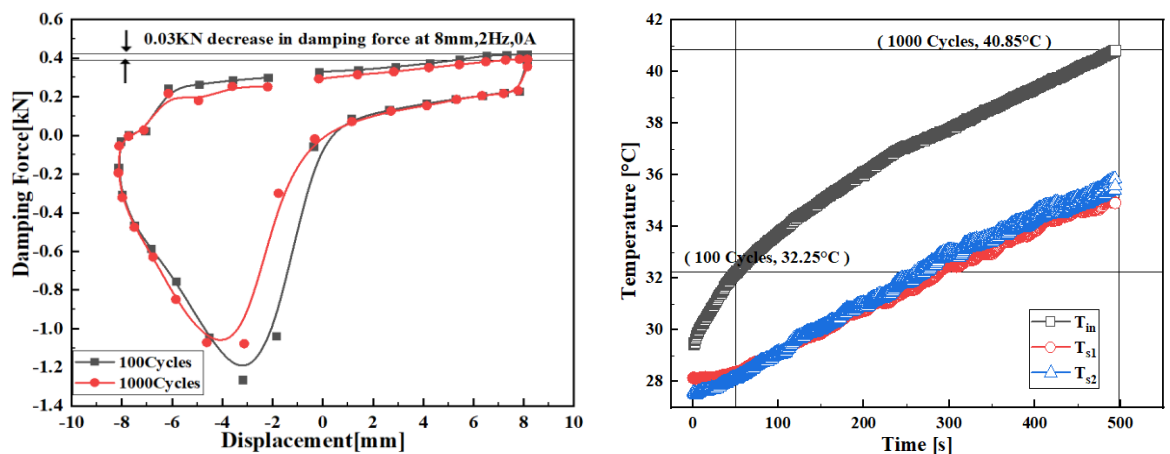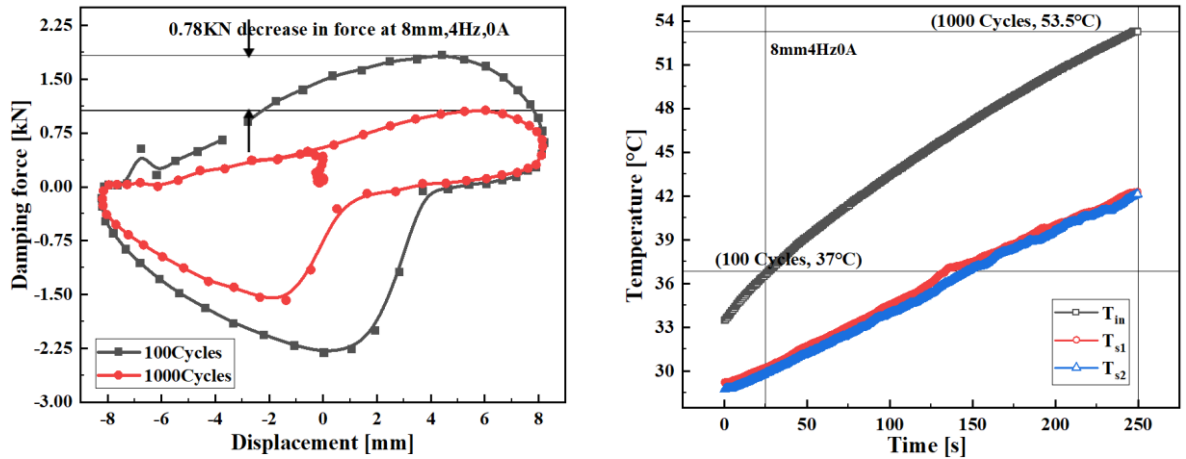

Figure 4.40 Force versus displacement curves at
10 mm amplitude, 4 Hz frequency, and 0 A
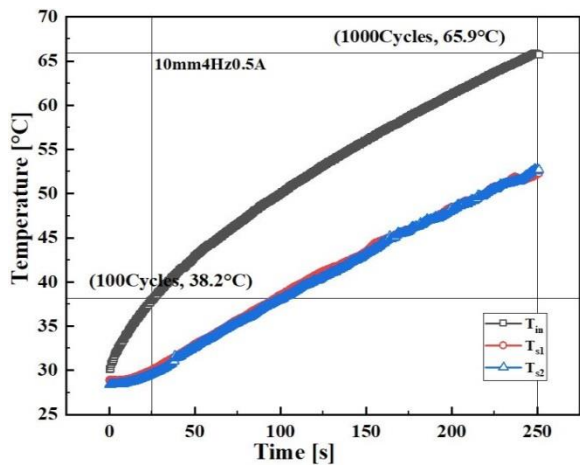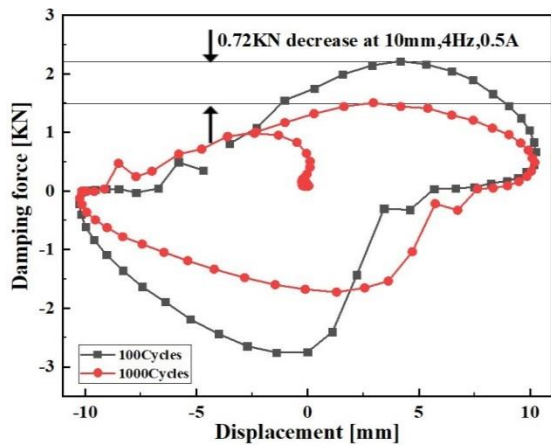
Figure 4.41 Force versus displacement curves at 10 mm amplitude,
4 Hz frequency, and 0.5 A
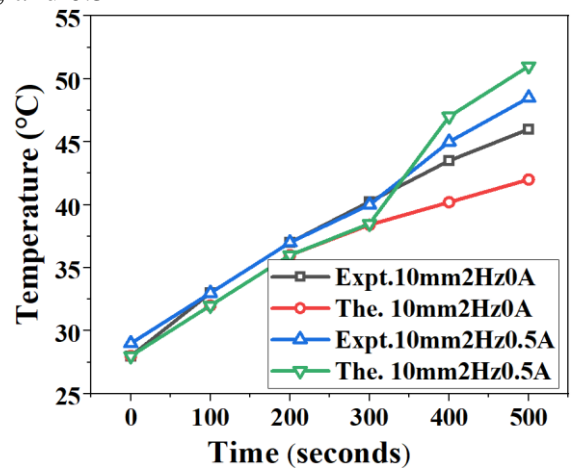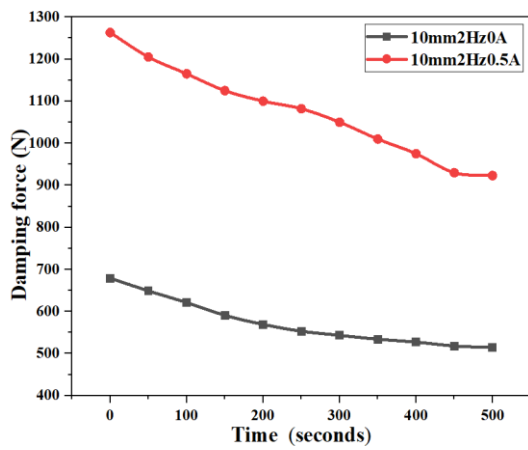
Figure 4.42 Force decrease with increase in time at 10 mm amplitude,
2 Hz frequency, and 0 A and 0.5 A
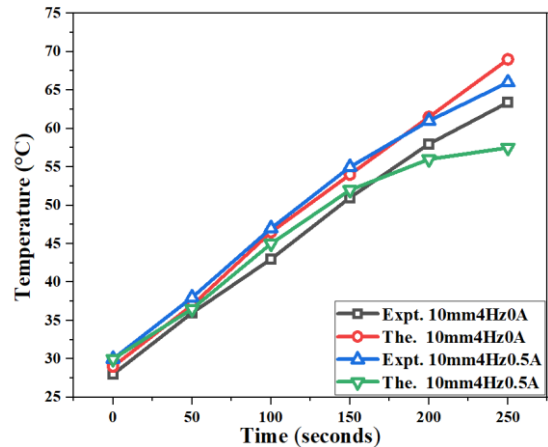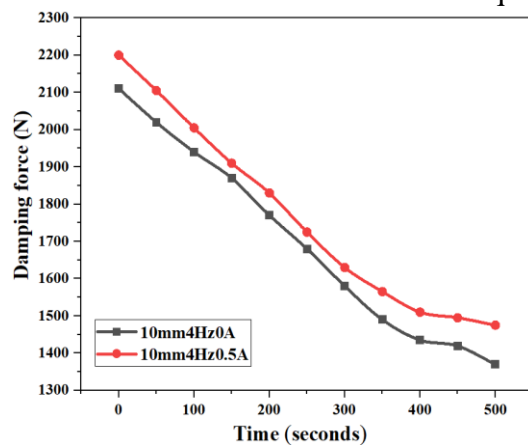
Figure 4.43 Force decrease with an increase in time at 10 mm amplitude,
4 Hz frequency, and 0 A and 0.5 A

For the 12 mm amplitude 2 Hz frequency, the force decrease was 200 N and 473 N, and the temperature increase was 42.65 °C and 53.57 °C at 0 A and 0.5 A currents, respectively. Taking another instance, at 8mm amplitude and 3 Hz frequency, there is a forced decrease of 375 N and 160 N, and the temperature increase is from 36.2 °C to 46.1 °C at 0 A and 0.5 A currents, respectively. At 10 mm amplitude and 3 Hz frequency, there is a 470 N and 440 N decrease in force and temperature increase from 54.9 °C to 56.76 °C at 0 A and 0.5 A currents, respectively. At 12 mm amplitude and 3 Hz frequency, there is a decrease of 797 N and 400 N force and temperature rise is from 57.28 °C to 65.76 °C at 0 A and 0.5 A, respectively. At 4 Hz frequency and 8 mm, 10 mm and 12 mm amplitude, there is a decrease of 780 N and 477 N, 680 N and 720 N, 868.4 N and 1070 N force and 53.5 °C to 53 °C, 63.2 °C to 65.9 °C, 74.2 °C to 79.36 °C temperature increase at 0 A and 0.5 A currents respectively. The critical observation is that, as the amplitude of vibration increases, the damping force at a particular frequency decreases, causing a temperature increase. And at a specific amplitude and increase in frequency, there is also enhancement in the damping force decrease and rise in temperature. The average temperature difference between off-state and on-state is approximately 8 °C which indicates the rise in temperature with application of current. The amplitude has a having a significant impact on temperature rise by three times more than that of the frequency. Figures 4.32 - 4.35, figures 4.38 – 4.41, and figures 4.44 – 4.47 shows the peak force decrease with the increase in temperature along with theoretical model results with experimental temperature values.

This section also deals with the prediction of the temperature inside a damper with the theoretical model mentioned in section 4.5 and compared with the experimental values obtained from the thermocouple which is in direct contact with the MR fluid in operation. The known temperature at different time periods and noting the corresponding peak force values, the theoretical temperatures were evaluated. The fluid temperature obtained as a function of time from thermocouple inside the damper is taken for theoretical comparison. Dogruoz et al. (2014.) Studies illustrates that varying convective heat transfer coefficient between 28 and 35 w/m^2-k has negligible impact on temperature difference for the dampers. The theoretical model analysis in this study, the

parameter values were taken is shown in table 4.13 and the Biot number is 0.007 which is less than 0.1 and satisfies the lumped parameter applicability. Theoretical model also gives the similar observation of an increase in temperature and decrease in force as that of the experimental results for amplitude, frequency, and currents with an average error of 7.92 % and 10.24 % at 0 A and 0.5 A currents respectively.
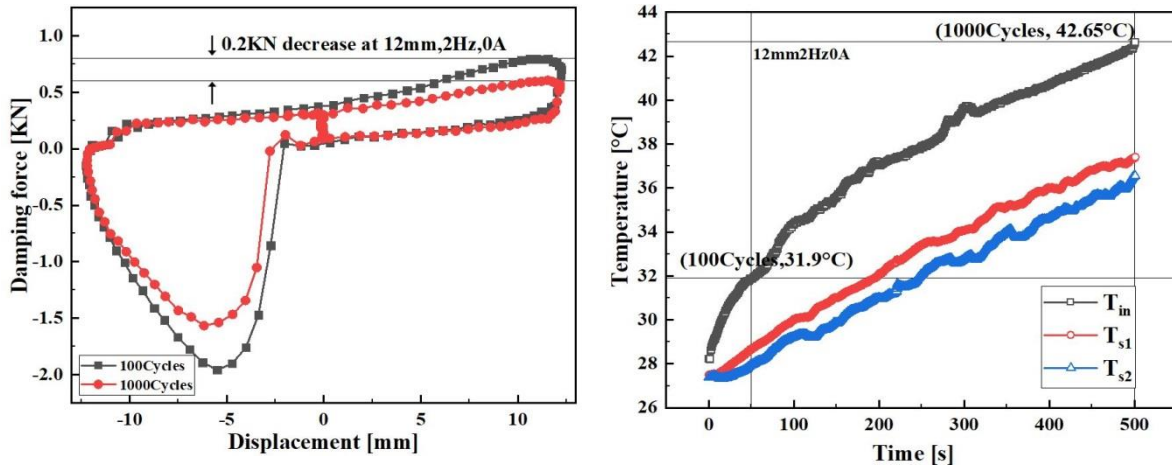
Figure 4.44 Force versus displacement curves at 12 mm amplitude,
Hz frequency, and 0 A
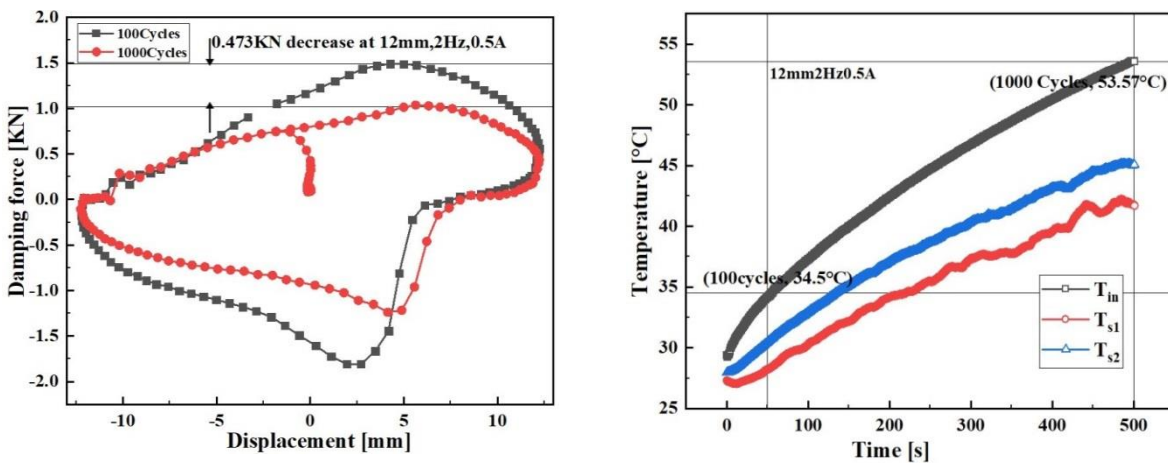
Figure 4.45 Force versus displacement curves at 12 mm amplitude,

2Hz frequency, and 0.5 A

138
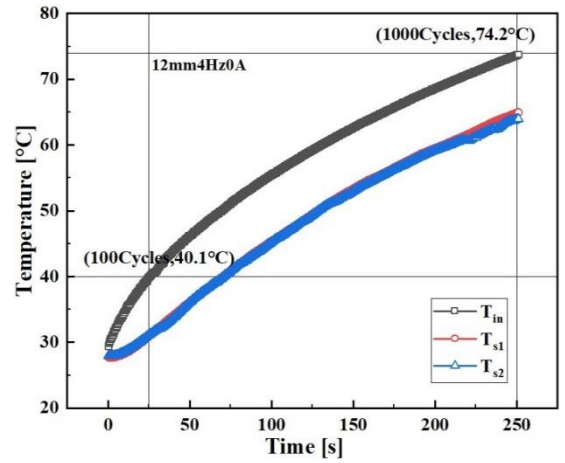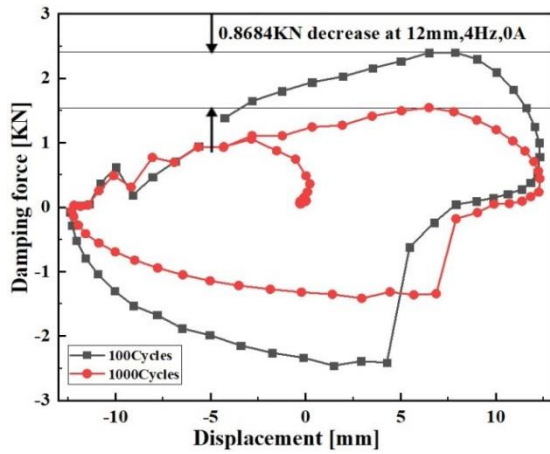
Figure 4.46 Force versus displacement curves at 12 mm amplitude,

4Hz frequency, and 0 A
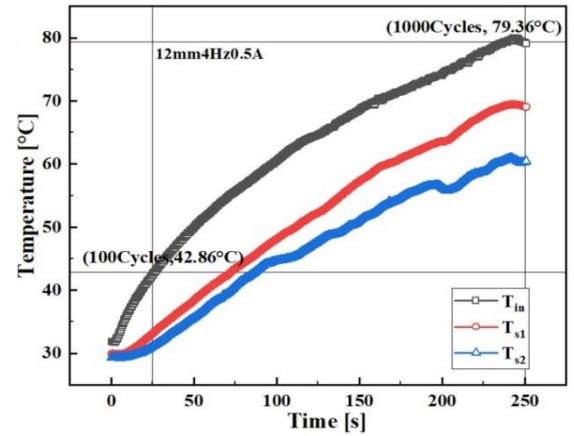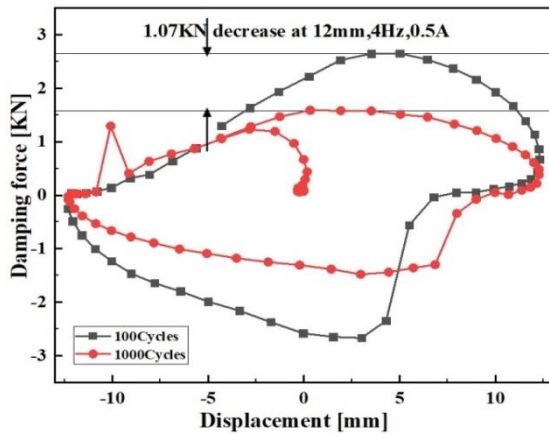
Figure 4.47 Force versus displacement curves at 12 mm amplitude,
4 Hz frequency, and 0.5 A
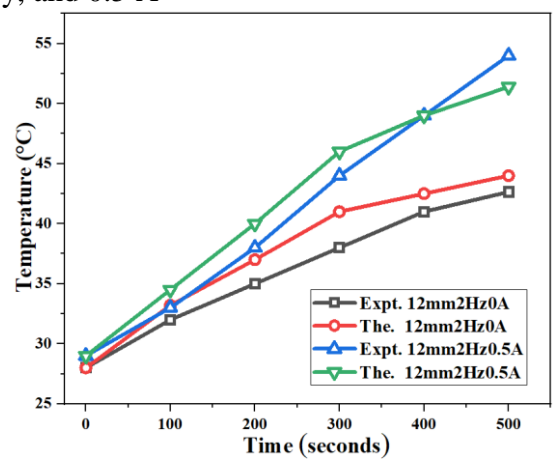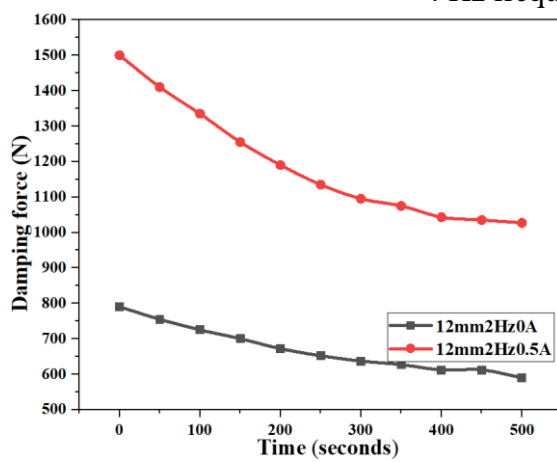
Figure 4.48 Force decrease with increase in time at 12 mm amplitude,
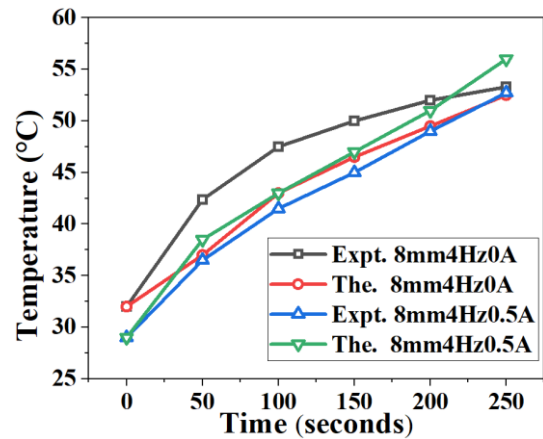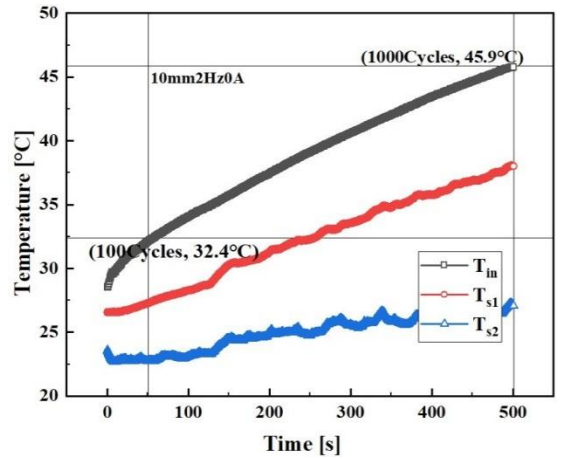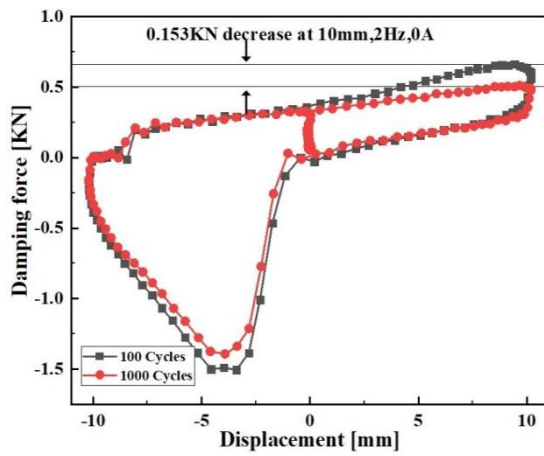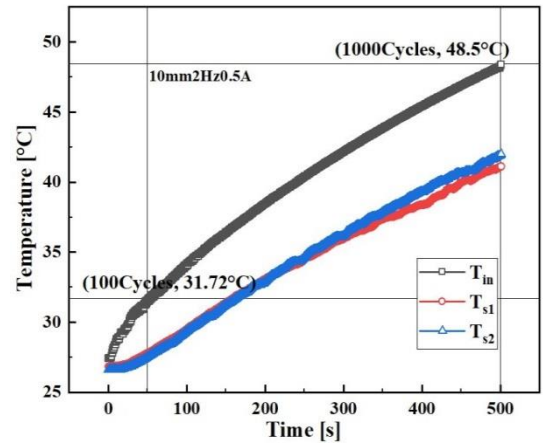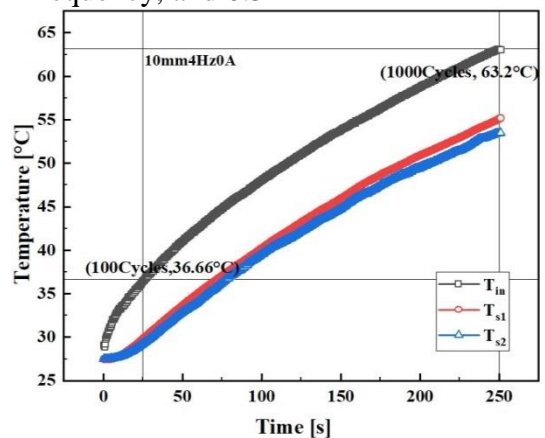2 Hz frequency, 0A and 0.5 A
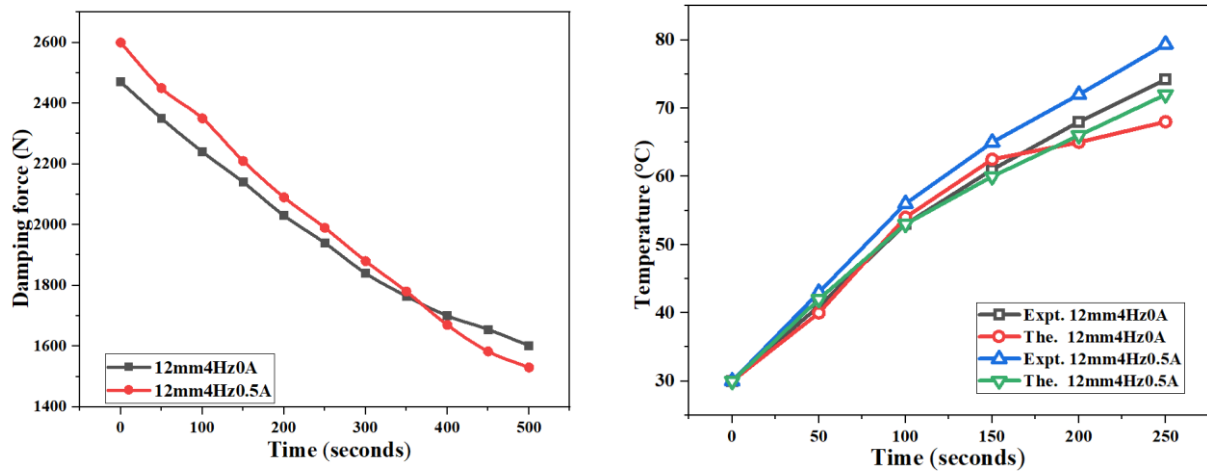
Figure 4.49 Force decrease with increase in time at 12 mm amplitude,

4 Hz frequency, 0A and 0.5 A
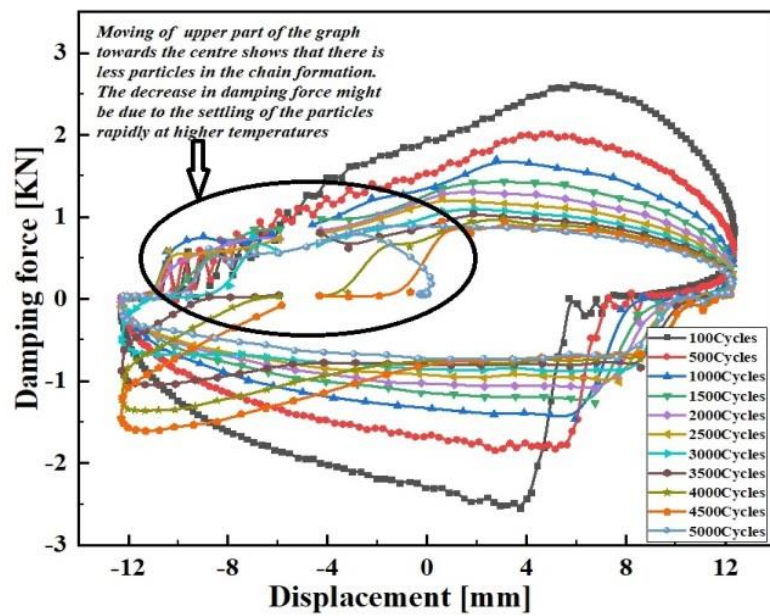
Figure 4.50 Force as a function of time for 5000 cycles
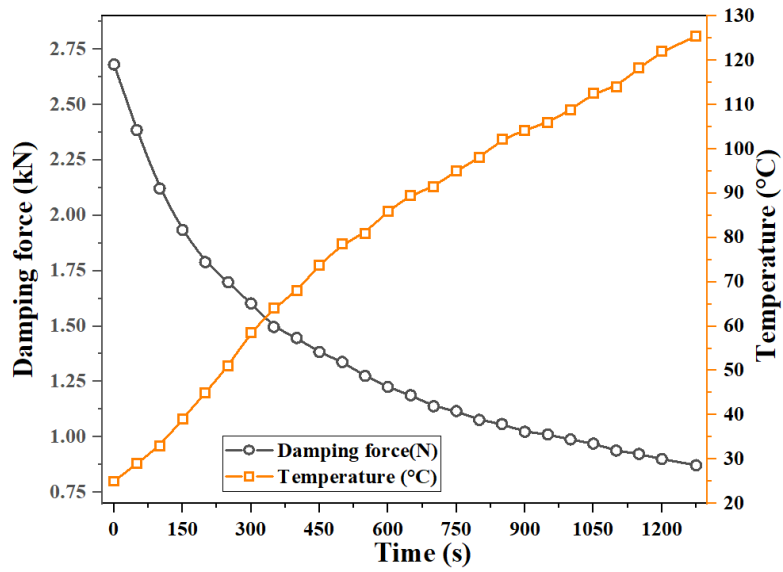
Figure 4.51 Force decrease and temperature rise relation

It is visible from figure 4.50 and 4.51 there is a decrease in the area of the force-displacement diagram indicating the rapid sedimentation of particles with formed chain breakages and energy dissipation into the fluid, making the fluid temperature rise. The relationship between damping force and temperature is obtained by running the damper at 12 mm amplitude 4 Hz frequency, 0.5 A current, and 5000 cycles which was also carried out by Bharathi Priya and Gopalakrishnan (2019b), Patel and Upadhyay (2018)
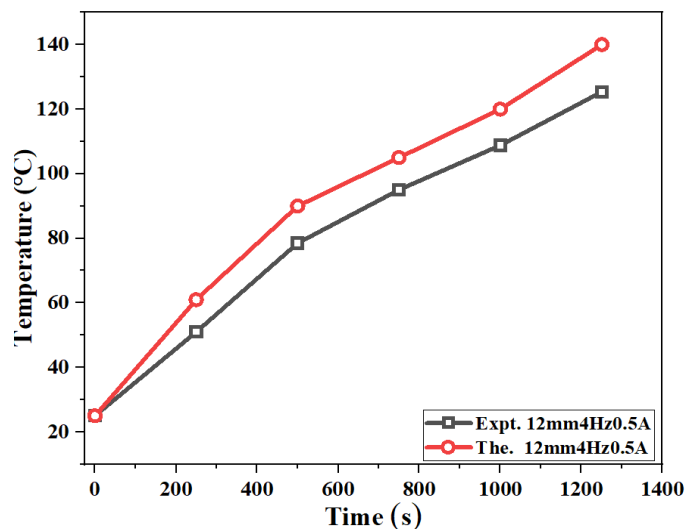
Figure 4.52 Experimental and theoretical model validation for temperature
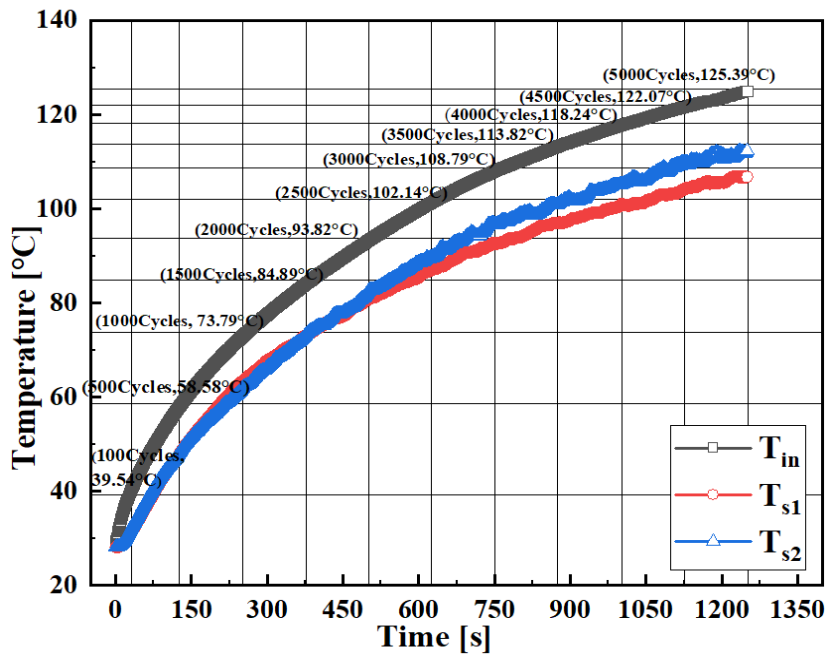
Figure 4.53 Temperature increase during the testing of the damper
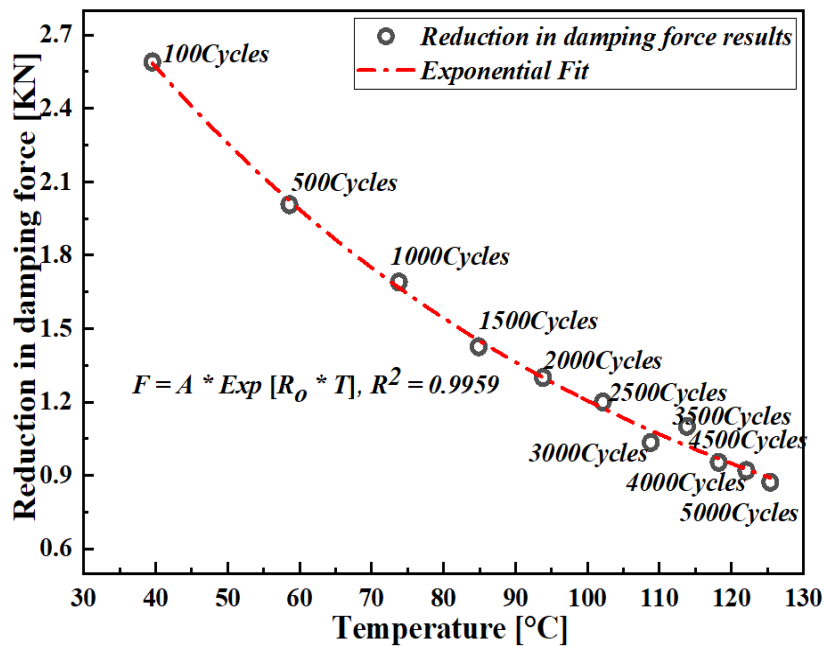
Figure 4.54 Relationship between force decrease and temperature

rise while damper in working

From figure 4.53 show the temperature increase during the testing of the damper, while figure 4.54 decreases in damping force as the temperature increases rapidly. One more observation is that there is an increase in the damping force upon

142

increasing the current up to a certain threshold point beyond which there is no increase in the force, which indicates the saturation point of the fluid. The above discussion on amplitude, frequency, currents, and temperature relation with damping force and decrease in temperature with insulation on the electromagnet is given in figure 4.55 and 4.56, respectively.
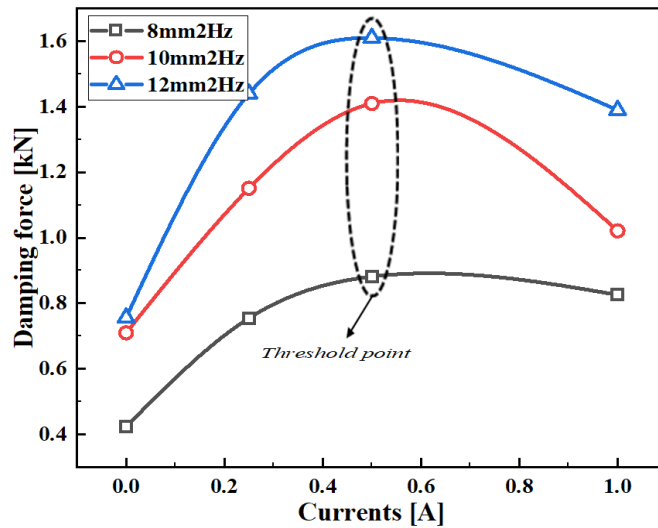
Figure 4.55 Damping force variation with different amplitudes and currents at 2 Hz frequency
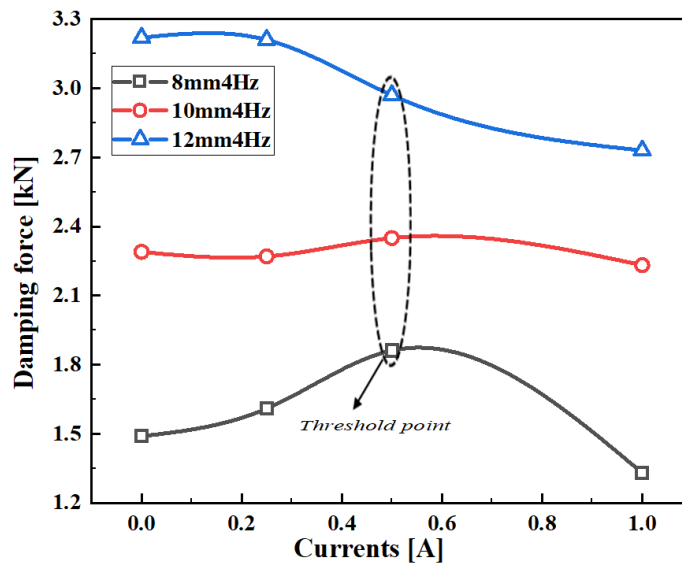
Figure 4.56 Damping force variation with different amplitudes and currents at 4 Hz frequency

4.8 Particle analysis after characterisation

After dynamic testing of MR fluid in the MR damper, the particle analysis is fundamental to see the effect of parameters on particle shape and saturation point of the particles. After operating the damper for approximately about 85000 cycles which include all test runs and dummy runs at different amplitudes, frequencies, currents, and temperatures, the MR fluid is taken out and cleaned for its carrier fluid and additive using filter paper and acetone and air-dried in the atmosphere for approximately 30 days. The particles sample was tested for particle shape on SEM and saturation magnetisation on the vibration sample magnetometer. The change in particle microstructure cannot be considered because of the particle melting point.
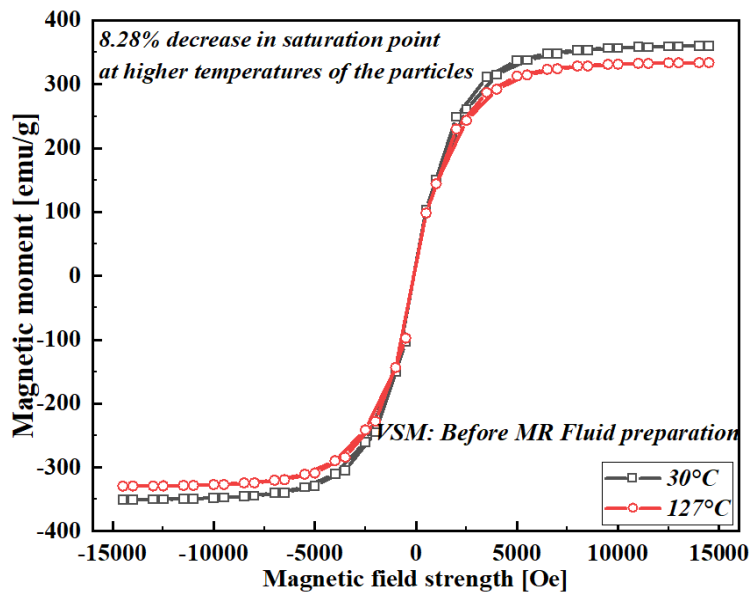
Figure 4.57 Magnetic saturation before synthesis of MR fluid

Figure 4.57 and 4.58 illustrate the saturation magnetization of the particles at room and higher temperatures before the preparation of the MR fluid and after testing the MR fluid in the damper. The results indicate that at room temperature (30 °C), the saturation point is 360 emu/g, and at higher temperature (127 °C), the saturation point reduces to 331emu/g, indicating the effect on the performance of the MR fluid. But when it comes to VSM testing after characterisation, at 30 °C, the saturation point is 270 emu/g, and 127 °C the saturation point is 145 emu/g. The reduction in saturation magnetisation is because of the remains of the additive

and carrier fluid, which acts as a coating on particles.
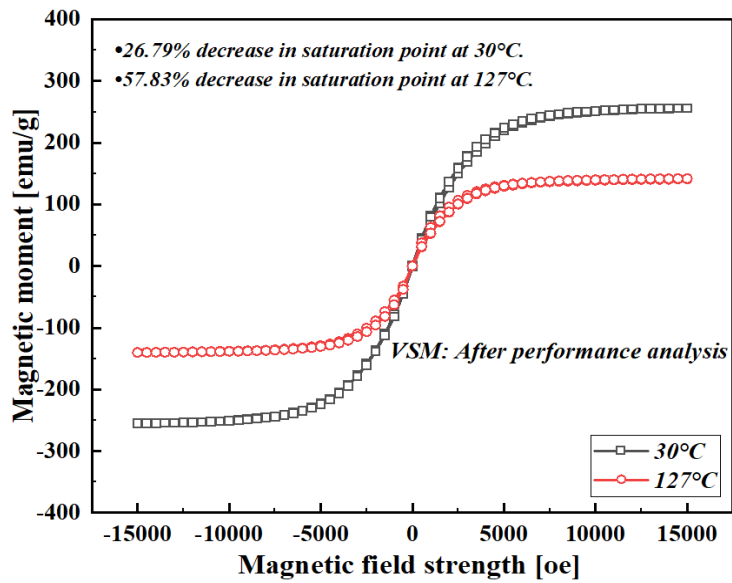
Figure 4.58 VSM of particles before and after characterization

Figure 4.59 shows the remains of additive and carrier fluid on the particles compared to particles before fluid preparation. SEM analysis shows no significant change in the shape of the particle after the characterisation.
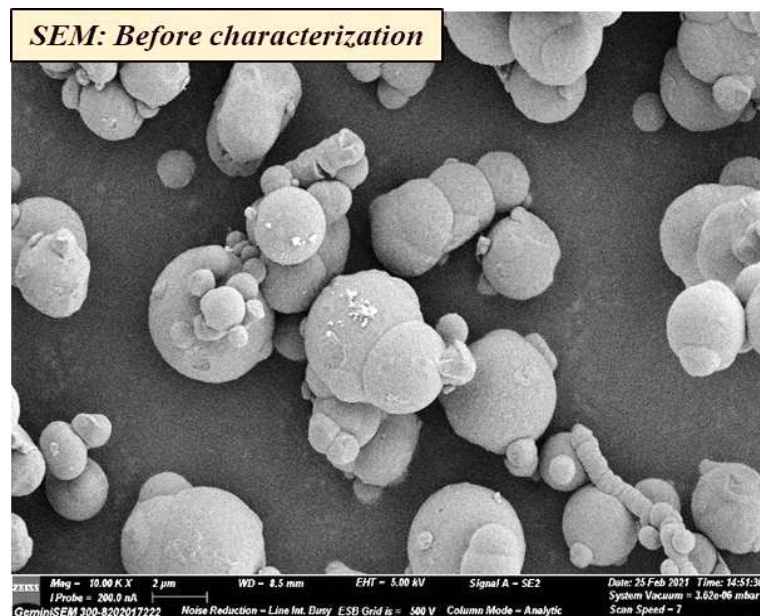
Figure 4.59 SEM images of particles before synthesis of MR fluid
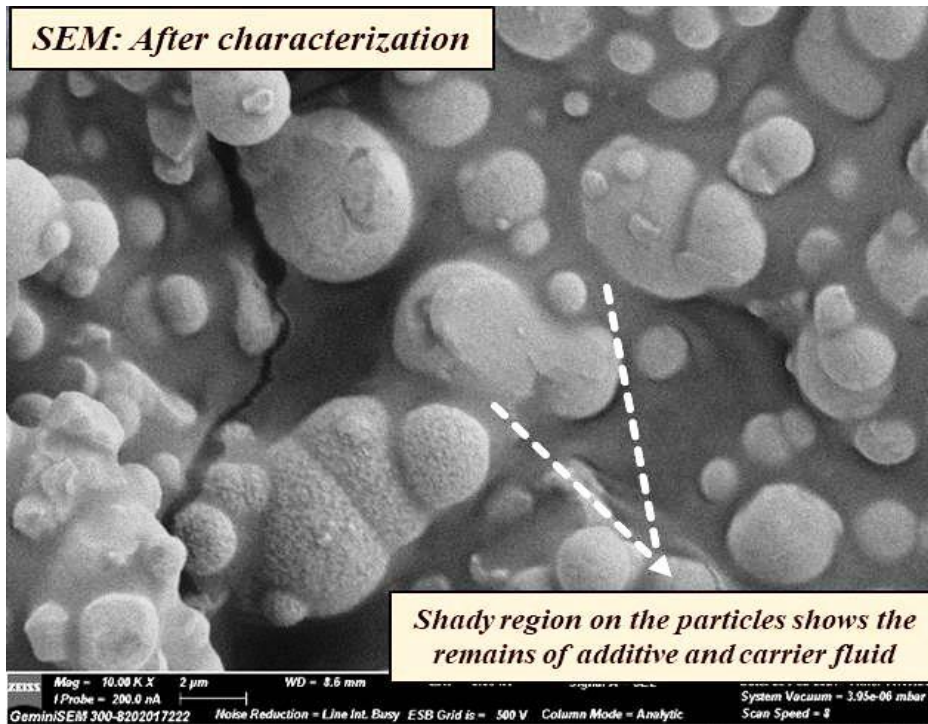
Figure 4.60 SEM images of particles before synthesis of MR fluid

Thermal stability of the MR fluid is carried out on thermogravimetric analysis (TGA) to study the carrier fluid's decrease in weight (%) before and after dynamic characterisation of the MR fluid in the MR damper. Figure 4.61 shows the TGA analysis of MR fluid before and after dynamic testing in the damper. The temperature at which the start of degradation of the MR fluid is 323.3 °C for before characterisation and 322.6 °C for after characterisation of the fluid, indicating the decrease in stability of the carrier fluid is negligible. The carrier's weight reduction is 0.249 %, implies that the silicone base MR fluid retains stability after this amount of cycles.
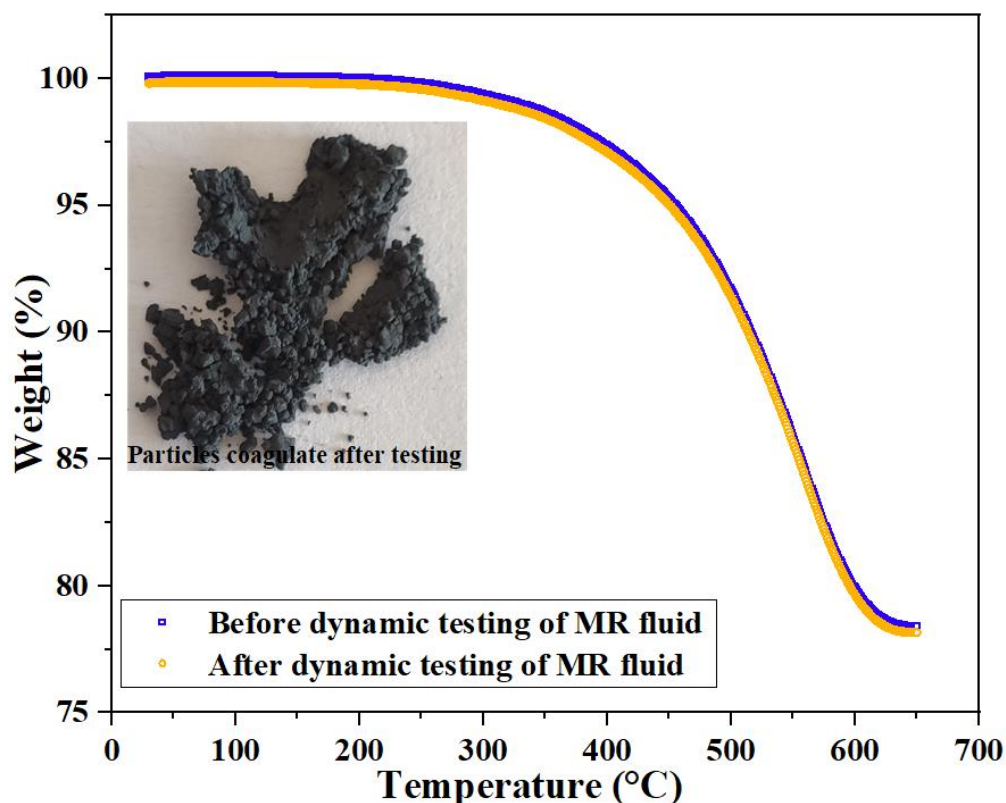
Figure 4.61 TGA of the MR fluid before and after characterization

The prolonged operation of the MR fluid makes the fluid temperature more, reducing the fluid's stability. After the complete destabilisation of the carrier fluid, the heat is transferred to the particles, making the particle change its shape. To imitate the heating effect, CI particles are heat-treated at 200 °C, 400 °C, and 600 °C in a furnace (with 3-4% error) for about 15mins after the furnace reaches steady-state temperature. The samples are tested for SEM images to see the distortion at different temperatures. The images show that, at 200 °C there is no change in the morphology but at 400 °C particle starts to fuse and at 600 °C, the particles start to melt, which is shown in figure 4.62.
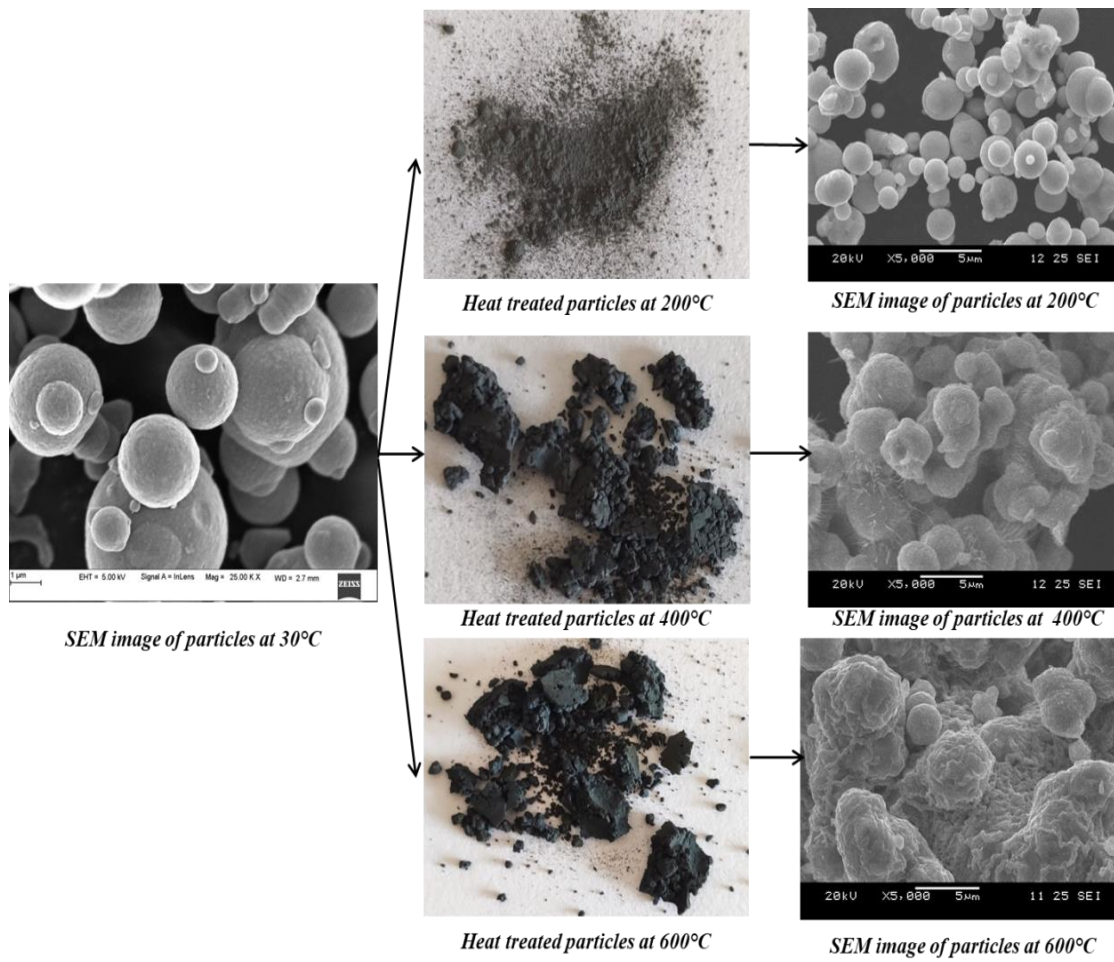
Figure 4.62 SEM images of heat treated particles

4.9 Summary

The present chapter deals with the temperature effect on the performance of the MR damper at various amplitudes, frequencies, and currents. In this study temperature of the MR fluid is measured by incorporating a thermocouple into damper through the piston and other two thermocouples were attached to the top and bottom surface of the cylinder surface. The exponential decrease in the force with the increase in temperature was obtained. After testing the MR fluid in the damper the, TGA and SEM images of the fluid and particles depicts no change in shape and life of the fluid, but VSM results illustrates a significant decrease in the saturation magnetization of the fluid. Finally, the heated treated particles SEM image shows that the destabilization point of the particles lies between 200 °C and 400 °C. The following chapter deals with the performance analysis of the two plate rotor MR brake with in-house prepared MR fluid.

CHAPTER 5

PERFORMANCE ANALYSIS OF TWO-ROTOR MAGNETORHEOLOGICAL BRAKE WITH IN-HOUSE MAGNETORHEOLOGICAL FLUIDS

5.1 INTRODUCTION

The torque generation capacity of a brake can be significantly enhanced by the use of MR fluids for their peculiar yield stress increase by increasing the external magnetic field. Increased torque in MR brake is a vital feature and can be appropriately enriched by the brake rotor radius and MR fluid gap in the design of MR brake. Attia et al. (2017), Li and Du (2003), Sohn et al. (2018), Song et al. (2018), Wu et al. (2020), Zhou et al. (2007) showed that the composition of MR fluid and size of particles, concentration and carrier fluid oil has a higher impact on the performance of MR fluid system. Acharya et al. (2021), Bucchi et al. (2015), Jonsdottir et al. (2009), Sohn et al. (2018) have carried out design development and characterization of MR brake of larger size (approximate 12 kgs) but the present study is concentrated on miniature size two-rotor magnetorheological (MR) brake (Total mass=1.62 kg) and its characterization for torque generation for in-house prepared MR fluid. The prepared MR fluids were studied for sedimentation rate at different temperatures and flow behavior at different currents and temperatures. The nonlinearity of the fluid is analyzed through Herschel-Bulkley model. The significant increase in sedimentation rate and decrease in yield stress shows the effect of temperature on the performance of the MR fluid. Finite Element Method Magnetics (FEMM) was used to design and fabricate two rotor MR brakes through magnetic flux density obtained in the MR fluid gap. Further tests have been carried out to identify the effect of sedimentation on torque generation at 52°C after 15 hours of sedimentation. TGA and SEM analysis of

151

the MR fluid and particles was carried out to see the saturation magnetization and destabilization point of the MR fluid at higher temperatures.

5.2 Methodology

Figure 5.1 show the methodology adopted to carry out the study. Firstly, preparation of the MR fluid using the commercialized magnetic particles (Sigma Aldrich: 44890, density: 7.86 g/cc) with silicone oil as the carrier fluid (Sigma Aldrich: 378372, 350 cSt, density: 0.96 g/cc). Secondly, the sedimentation study is carried out at two temperatures and characterization of the fluid samples for their flow behavior in the rotation is carried out on an MCR702 rheometer for different conditions of magnetic fields and temperatures. The inherent non-linearity in the MR fluid is studied through Herschel-Bulkley model. To analyze the performance of prepared fluid, two plates MR brake is designed and fabricated. The characterization of the MR brake is carried out on the test setup developed at various speeds and currents. Finally, the sedimentation effect on torque generation after 15 hours of sedimentation at 52 °C was carried out.
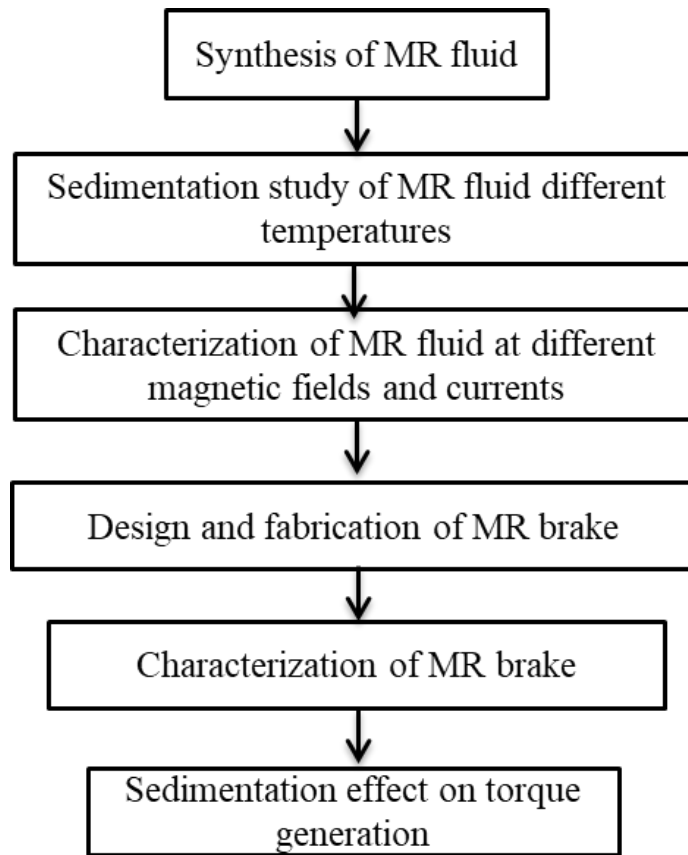
Figure 5.1 Flow chart for the present study

5.2.1 Synthesis and sedimentation study of MR fluids

MR fluids were prepared from the commercially available carbonyl iron particles (density: 7.86 gm/cc) with 30 % by volume in carrier fluid with density 0.960 gm/cc. The first step in the synthesis of MR fluid is homogenizing the aluminum stearate (3 % by volume of carrier fluid) additive in the carrier fluid for 12 hours. The second step is to add the CI particles in the homogenized primary fluid in steps of five minutes to avoid clogging of the particles at 750 rpm for 24 hours. The prepared sample has been tested for its sedimentation behavior at two different temperatures (30 °C and 75 °C). A laboratory incubator was used to study the temperature effect on the sedimentation of the particles. This increase in sedimentation rate at higher temperatures implies that there is a decrease in viscosity and density of the carrier fluid which allows the particles to settle at a faster rate.

5.2.2 Characterization of MR fluid

The flow resistance of the MR fluid was measured using parallel plate rheometer (MCR 702, Anton-Paar) in connection with MRD module. For characterisation of the fluid the parallel plate diameter used is 20 mm and a gap of 1mm was maintained. At the time of testing approximately 0.32 ml of fluid is poured at the center of the bottom plate. The magnetic circuit under the bottom plate generates the magnetic flux perpendicular accordingly with input current uniformly through the yoke which will also amplify. The experiments were carried out at two constant temperatures (30 °C and 50 °C). RheoCompass software is used to set the input parameters such as shear rate (s^{-1}), current (A) and to obtain the data of the testing through computer system. The testing is carried out at 0 kA/m, 44 kA/m, and 77 kA/m which give corresponding 0 T, 0.21 T and 0.401 T magnetic flux densities, respectively in the MRD cell of the rheometer. The flow behaviour of the MR fluid is tested for varying shear rates from 0.1 s^{-1} - 500 s^{-1} at an individual constant temperature with varying input currents.

5.2.3 Design and Fabrication of MR Brake through FEMM analysis

The design of MR brake with two rotors was carried out using finite element analysis using FEMM software. The fabrication of the brake is done with dimension that gives reasonable magnetic flux density in the fluid gap. The torque generated by two rotor brake is obtained by viscous toque (T_μ), field-induced torque (T_B) and frictional torque (T_f) which is given in equation (5.1).

$$T = T_\mu + T_B + T_f \tag{5.1}$$

Gudmundsson et al. (2010) and Park et al. (2008) calculated theoretical torque generation for single rotor MR brake using equation (5.2).

$$T_B = n\pi\eta\omega \ (r_1^4 - r_0^4)/(2g) + 2n\pi\int_{r0}^{r1} \tau(H,r) \ r^2 \ dr \tag{5.2}$$

Where, η = apparent viscosity (without magnetic field), n = number of surfaces in contact with fluid r_1 = Inner radius (mm), R = Outer radius (mm) ω = angular velocity of the rotor, τ_y = yield stress which is a function of magnetic field strength.
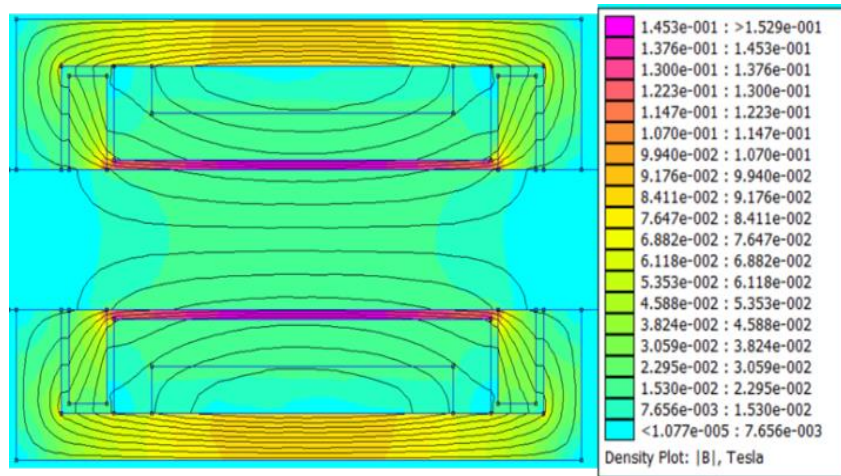
Figure 5.2 Magnetic flux lines in the shear gap of the MR brake

Figure 5.2 shows the MR brake model with magnetic flux passage through the gap. The variation along the length of the fluid gap is depicted in figure 5.3. In this study, the field induced and off-state torque generation, speed and torque ratio of MR brake were explored. The maximum amount of magnetic flux density obtained in the fluid gap is approximately 0.145 T.
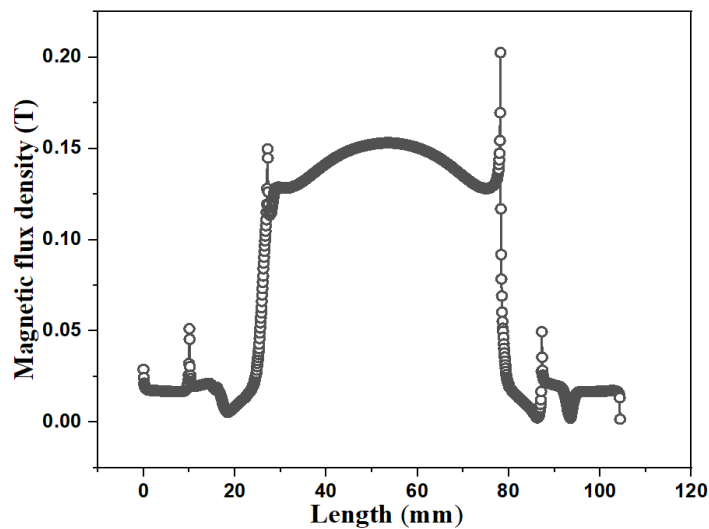
Figure 5.3 Variation of magnetic flux density along the length of shear gap

The schematic representation of the two-plate rotor MR brake is shown in figure 5.5. The MR brake consists of outer casing, bobbin on which the copper coil is wound, rotor discs, and rotor shaft. The magnetic field induced by the coil has to pass through the MR fluid in the gap between the casing and rotor for producing torque.

155

Hence, the casing, and rotor which form path for magnetic field should have high magnetic permeability to ensure concentration of flux density in the fluid gap. In order to prevent magnetic flux loss, the rotor shaft and bobbin is made of non-magnetic material which has less torque generation. Table 5.1 below depicts the dimensions of the MR brake and their materials

Table 5.1 Raw materials and their dimensions for fabrication of the brake

Parts of MR brake	Materials	Dimensions
Thickness of the casing (t)	SA1018	10mm
Bobbin(r_2)	SS316	30mm
Rotor radius (r_1)	SA1018	10mm
Shaft length (l)	EN8	180mm
Fluid gap (g)	MR fluid	1mm

Figure 5.4 shows the exploded view of the two-plate rotor MR brake. It consists of two rotors on the rotor rod at the end between which the fluid gap is provided. Filling of the MR fluid in the gap, the cover plates on both sides of the brake are covered with screws. Copper coils have been wound on the bobbin provided upon which the outer cylinder is fixed through which the electrical cables is taken and connected to the dc power supply.
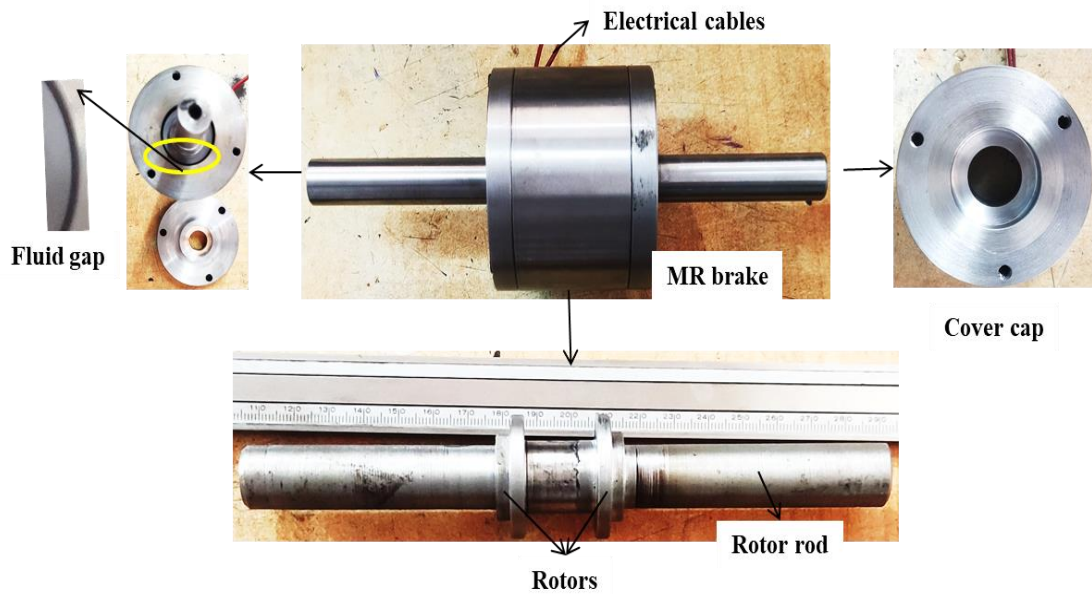
Figure 5.4 Exploded view of two plate rotor MR brake
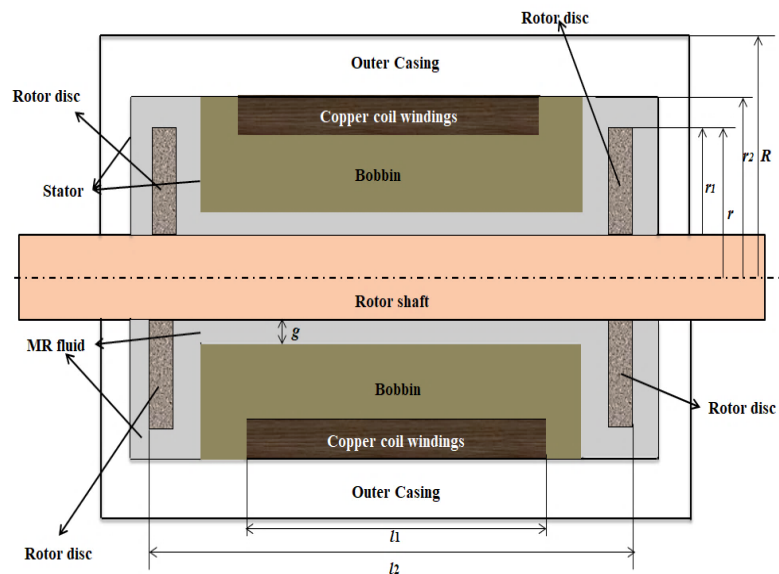
Figure 5.5 Schematic representation of the MR brake

5.2.4 Characterization of MR brake

Characterization setup comprises a DC Motor which acts as a speed controller (Maximum speed= 1440rpm) connected to the MR brake through a coupling, flywheel (19.6Kg), bellow couplings, and torque sensor (Max. Torque = 50 Nm). The speed controller is getting power from the dimmer stat. The output of the dimmer stat is linked to rectifier (RC) circuits which will convert AC to DC current and supply it to

the motor. A flywheel is connected between the torque sensor and motor to maintain a uniform rotation speed without many fluctuations. A torque sensor measures the difference in the torque between input and output shafts during operation. Generated torque is acquired through a torque transducer interface data acquisition system which is interfaced with datum software. The motor and other parts of the test setup were fixed to the base of the experimental setup. The figure 5.4 shows the experimental setup for testing MR brake.
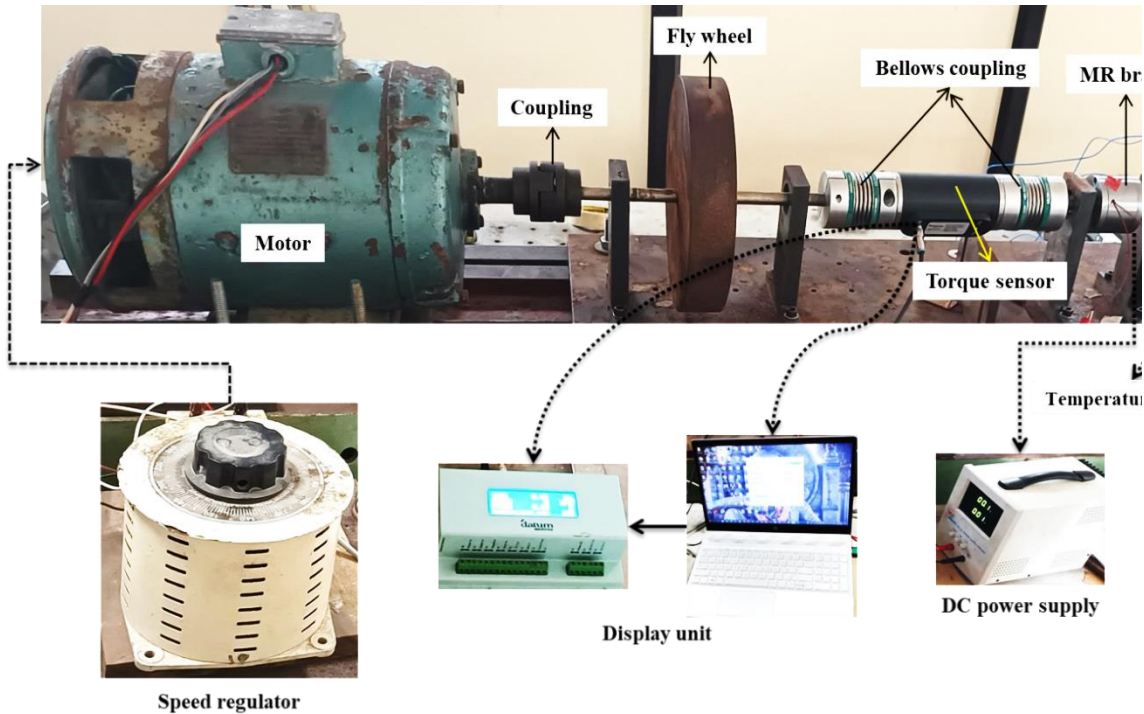
Figure 5.6 MR brake characterisation setup

Testing was carried out by filling the in-house prepared MR fluid (9 ml) in to the MR brake and fitting into the setup. The uniformity alignment of the setup was checked by running the setup for 5mins without acquiring data. Next, the motor speed was set to 50 rpm with a current of 0.25A, 0.5A, 0.75A, 1A, 2A, and 2.5A. Speed and torque data was obtained simultaneously using datum software. At every individual current and speed data were acquired at a rate of 100 points/sec. To maintain the repeatability and error in acquiring data experiments were carried out arbitrarily for various input conditions (Sukhwani and Hirani 2008). The tests were repeated for all the mentioned currents and speeds. For each test temperature was noted to evaluate the temperature effect on sedimentation at the end of the experiments. The

158

experiments were performed at different test speeds, and braking torque and speed reduction at different currents were acquired. The maximum torque generated in the case of in-house MR fluid is 2 Nm at a speed of 400 rpm and current of 2.5A. Tests were carried out to see the effect of the increase in speed. After completion of tests final temperatures of the system is noted and allowed it to cool for 15 hours. The test was repeated after 15 hours (at 52°C) of settling to see the Effect of sedimentation on torque generation.

5.3 Results and Discussion

Synthesis of the MR fluid sample and its settling and rheological behavior were carried out atdifferent temperatures and the performance of the MR fluid was tested in two-rotor MR brake for torque generation. Finally, the life expectancy of the MR fluid was studied through TGA and SEM analysis of a heat-treated CI particles.

5.3.1 Sedimentation rate of the MR fluids

Sedimentation is a general phenomenon that is considered a major factor in the study of MR fluids. When the density of the particles is dispersed in a low-density carrier fluid Jiang et al. (2011) which is the generally unavoidable disadvantage of the MR fluids. The sedimentation can be minimized by using additive such that the particles can be suspended state for a greater amount of time. Sedimentation is defined as magnetic particles settling (layer form) to the bottom due to the density difference between the carrier fluid and particles leaving behind clear fluid at the top. The figure shows the sedimentation study of the MR fluid at two different temperatures. Time was noted at intervals of one hour for ambient temperature and 15 minutes for higher temperature. The settling rate of the MR fluid at ambient and higher temperatures was 9 hours and 45 hours, respectively. It is evident that at higher temperatures settling rate of the particles increases rapidly due the decrease in the viscosity and density of the carrier fluid and similar studies has been carried by Kumar Kariganaur et al. (2022). After complete sedimentation of the particles the formation of cake is seen which will make particles difficult to disperse the particles. Figure 5.7 show the sedimentation rate of MR fluid at higher temperatures and the total time taken by the all the MR fluid samples to settle completely will be with in the 80 hours (atmospheric

settling). To avoid cake formation in MR fluid the particles have to be dispersed before completly settling.
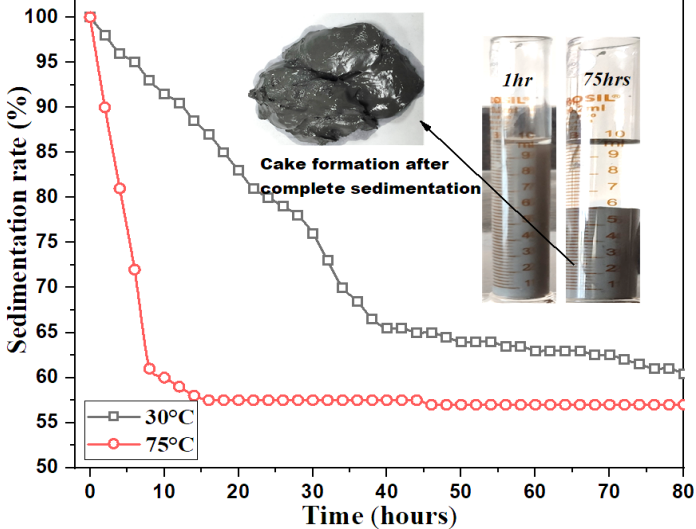
Figure 5.7 Settling study of MR fluid sample at two temperatures

Figure 5.8 show the temperature effect on the sedimentation rate of the MR fluid at constant sedimentation ratio. It is observed from the study that as the temperature of the fluid increases the settling of the particles increases reducing the time of settling. From this study, the reoperation time can be evaluated for the specific MR fluid system.

$t = 84.48e-0.046(T)$, $R^2 = 0.9815$
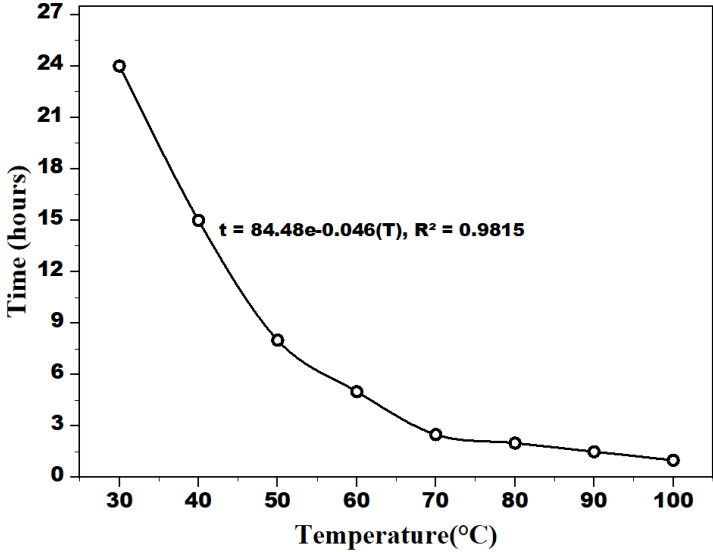
Figure 5.8 Settling time for varying temperatures at constant settling rate

5.3.2 Rheological characterization

Rheological studies on the fluid are carried out on the Anton-Paar MCR702 rheometer. A fluid gap of 1mm is maintained between the plates of 20 mm diameter, and the temperature is varied at constant magnetic fields. The homogenized MR fluid is poured onto the stationary bottom plate, and the top plate is moved down with RheoCompass software to maintain the gap between the plates. The fluid is subjected to a shear rate of $0.1s^{-1}$- $1000s^{-1}$. The flow curves were determined for the gaps at zero current and with currents at 0KA/m, 44KA/m, and 77KA/m. Nonlinearity is inherent in the MR fluids, which are visible when the external magnetic field is applied. The viscosity variation with an increase in temperature is shown in figure 5.9.
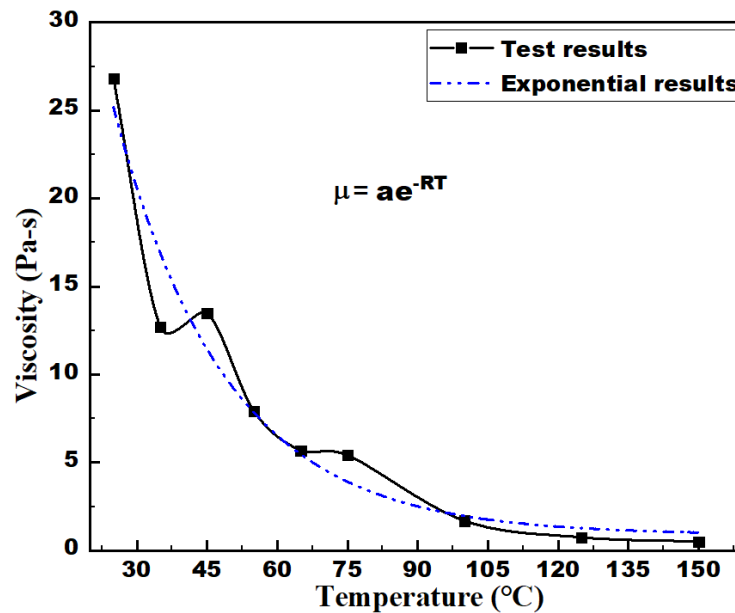
Figure 5.9 Temperature effect on viscosity of the MR fluid

The figure shows the flow characteristics of the MR fluid at different currents and temperatures. Form figure 5.9 it is shown that the viscosity of the fluid decreases with increase in temperature at zero input current and figure 5.10 it is shown that increase in shear stress and viscosity of the MR fluid with an increase in the applied current but the shear stress decreases with increase in temperature at constant current. The relationship between viscosity and yield stress as a function of temperature and current is given by equation 5.3.
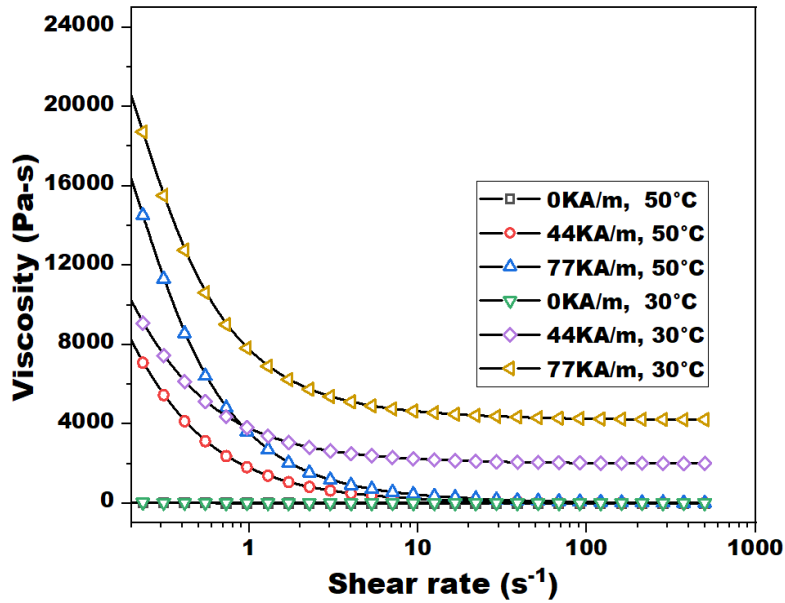
Figure 5.10 Viscosity variation at different magnetic fields and temperatures
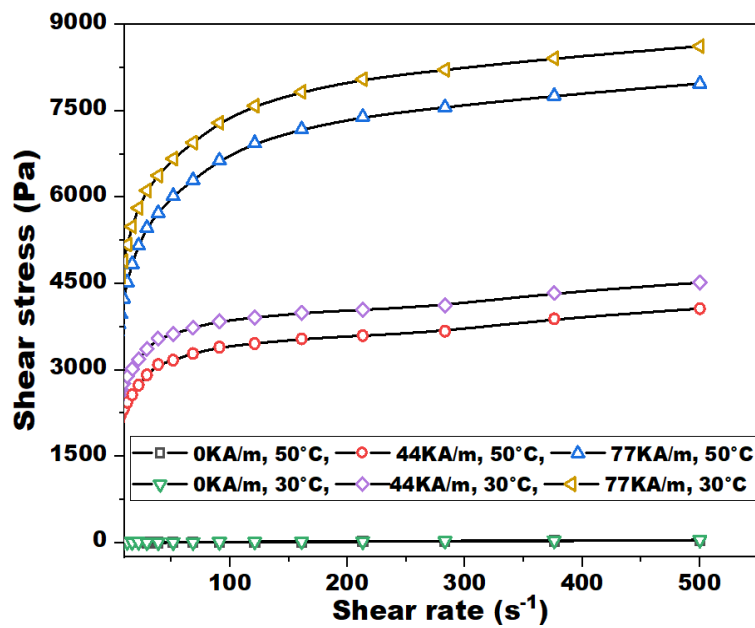
Figure 5.11 Shear stress variation at different magnetic fields and temperatures

The magnetic field's dependency on the yield stress is given in equation 5.3.

$$\tau_y = a_0 + a_1 \times B + a_2 \times B^2 \qquad (5.3)$$

Where a_0, a_1 and a_2 are constants, B = magnetic flux density (T), τ_y = yield stress

5.3.3 Magnetorheological Brake characterization

Torque and speed characterization of the MR brake was carried out for the in-house prepared MR fluid. The torque generated at different currents and speeds provided to MR brake containing in-house MR fluid and temperature rise during the operation of the brake as shown in figure 5.22 - 5.25. MR fluid composition is 25 % by volume with a 3 % aluminium stearate additive. The total volume of MR fluid filled in the brake was 9 ml. Lower torque generation in this study is due to the miniature size of the MR brake, which is of mass = 1.6 Kg with a radius of the rotor 10mm, and also the volume of the fluid-filled is also very less (i.e., 9 ml). Torque obtained by Acharya et al, 2020 (single rotor) and Chen and Liao, 2010 (multiple plates) were 14.5 Nm and 20 Nm respectively where plate radius and the number of plates are more compared to the present study [5, 6]. The geometric dimensions for the present study have been reduced drastically to evaluate the miniature size and volume of MR fluid which further reflects in weight optimisation which will impact the prosthetic knee application. To increase the torque generation the number of rotor plates can be increased in miniature design (Chen and Liao 2010) and also design modification can be done such that all the rotors should be within the bobbin.
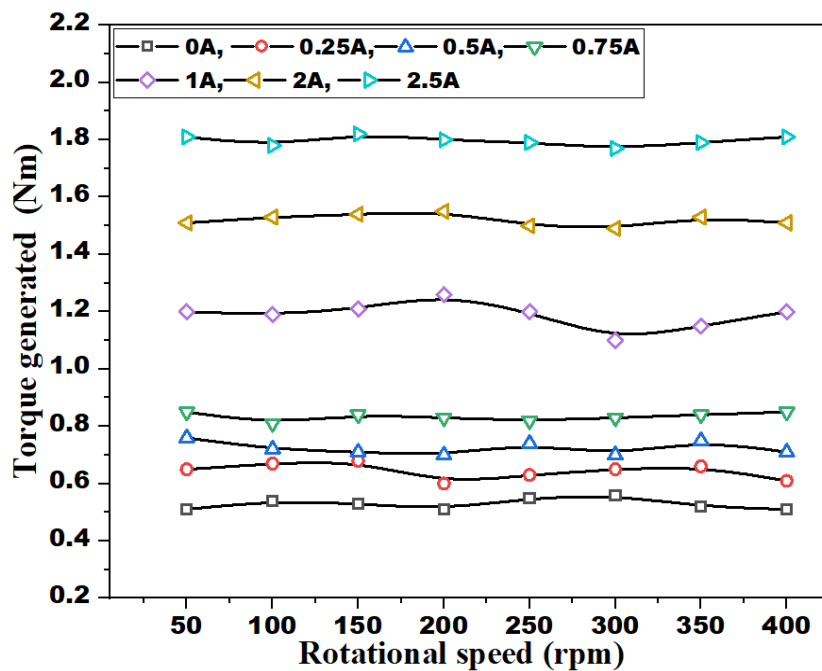
Figure 5.12 Torque generation with varying current and speeds.

The gap maintained for fluid filling is 1mm gap. An increase in generated torque with the increase in current remains almost constant for a particular current, shown in figure 5.22. The maximum generated torque in this study is approximately 1.9 N-m. Readings of the generated torque are noted every ten seconds and at each speed. From figure 5.23 the temperature rises during the operation from the thermocouple connected on top of the outer casing. Torque generation is slightly reduced after 450 rpm because of the viscosity reduction of the carrier fluid (shear thinning) during operation with an increased shearing rate of the fluid and temperature rise simultaneously. The test was repeated three times to see the decrease in torque at a higher speed. The decline in torque is gradual for repeat-1, 2, and 3 indicating the decrease in yield stress (viscosity reduction) of the MR fluid.
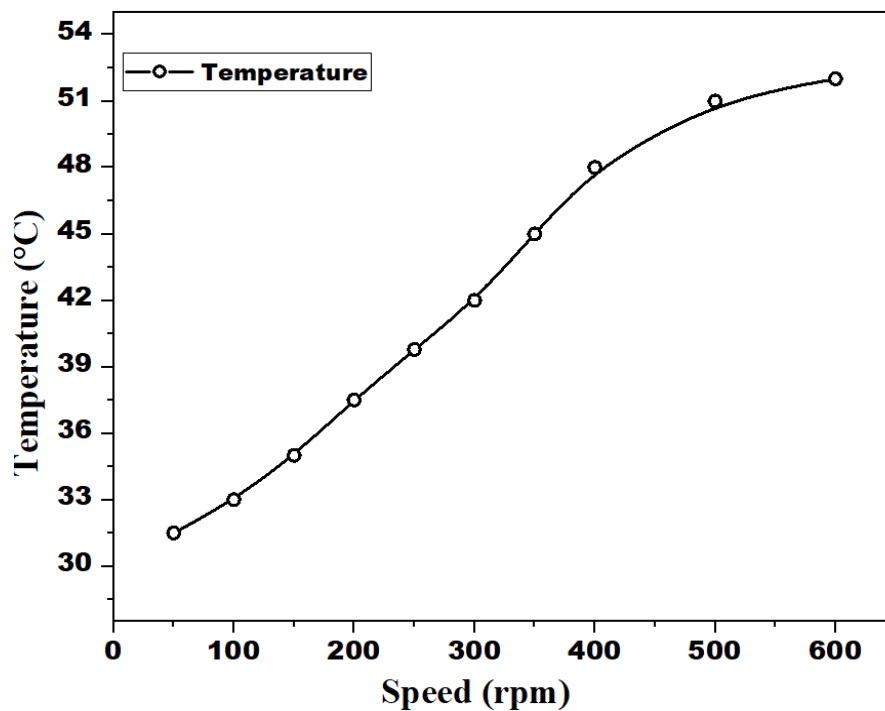
Figure 5.13 Temperature increase while operating

The other observation made in this study is that decrement in torque is taking place at higher currents and speeds, as shown in figure 5.14. At higher currents, more heat dissipates into the fluid, which makes the fluid temperature rise by decreasing the torque. The decrease in torque is possible at a lower current

164

if the brake is operated for a higher period of time. At the end of the testing the temperature of the fluid has reached 52.5 °C and the setup is allowed to cool. After 15 hours of cooling the MR brake is tested for torque generation and is about 1.05Nm which increases with speed up to 1.25 Nm.
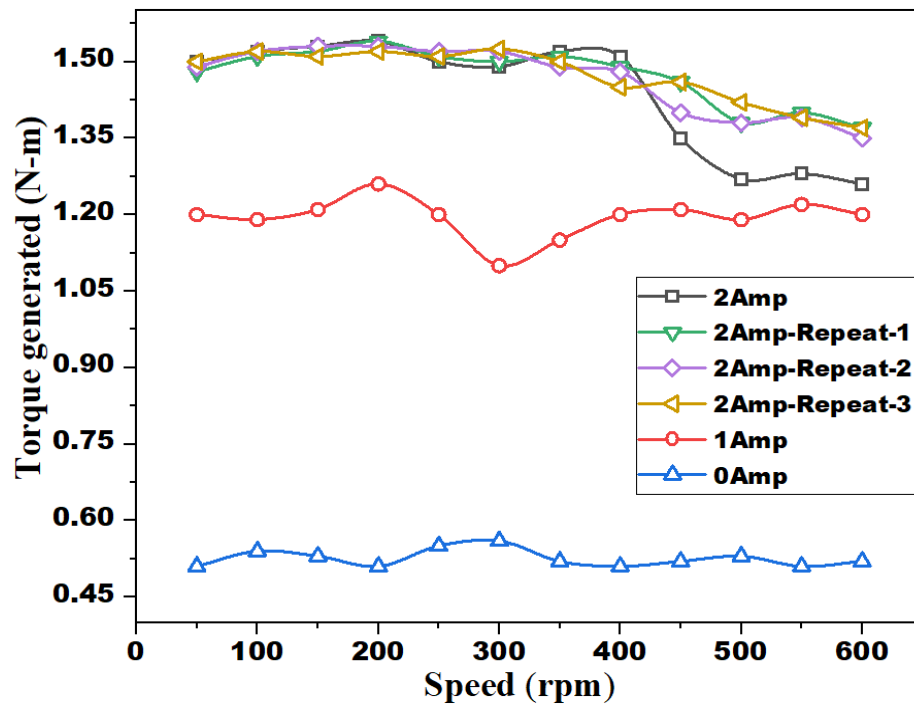
Figure 5.14 Torque generation after three repetitions

The gradual increase in torque indicates the dispersion of the particles which is shown in figure 5.15. This particular test has been repeated seven times to check the recovery rate of the torque to its original state and the results indicate that the torque generation has not reached its original state (1.51 Nm) because of permanent stiffness loss in viscosity of the MR fluid has under gone during the process of operation.
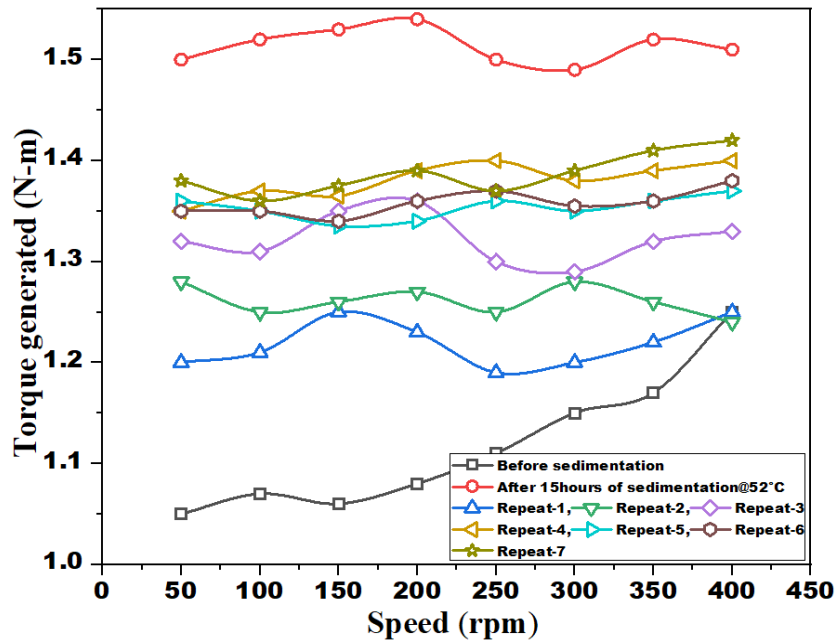
Figure 5.15 Sedimentation effect on torque generation

After completion of the tests the MR fluid was collected (figure 5.16) and tested for rheological flow behaviour and the results indicate that yield stress has increased by approximately 6% and 11% at 30°C and 50°C, respectively implying the peculiar shear thickening behaviour after testing of the fluid which is shown in figure 5.17.
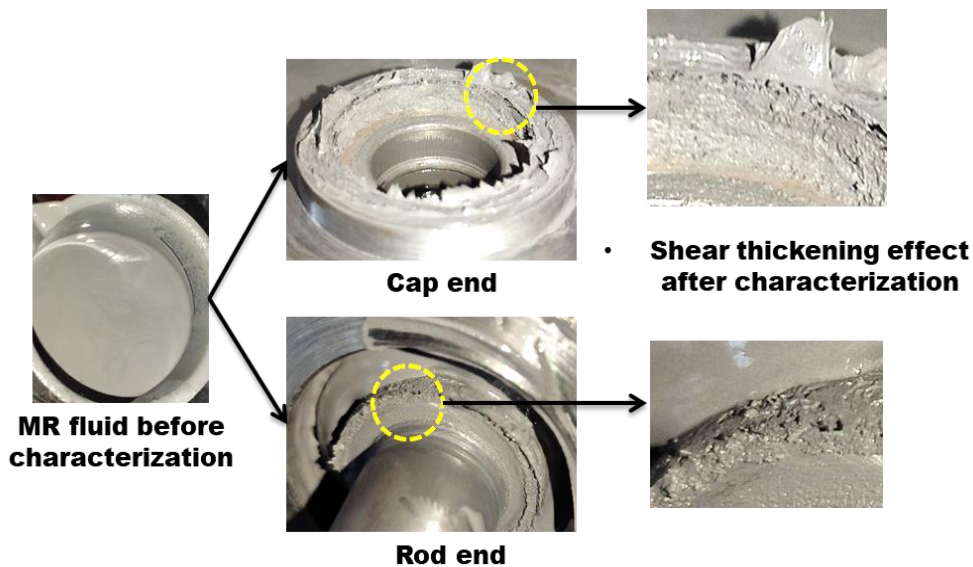
Figure 5.16 Shear thickening after testing the brake

The shear thickening behaviour of the fluid was observed at the end of the rotor and cover plate of the brake. The shear thickening behaviour of the fluid can be avoided by decreasing the particle concentration and carrier fluid viscosity. The optimal proportions of the fluid composition should be selected such that the flow ability of the fluid is ensured.
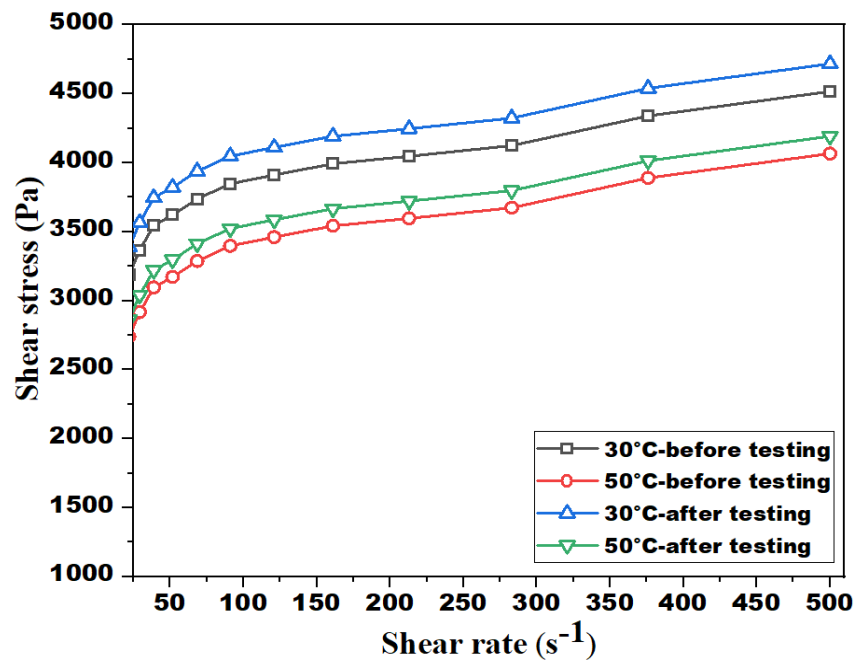
Figure 5.17 Flow characterization after shear thickening

Finally the fluid has been tested on TGA to study the critical temperature points for carrier fluid and magnetic particles to see the upper operating limits of the MR fluid to maintain MR system stable. The results from the TGA indicate that the temperature of the MR fluid should not cross 321 °C in order to avoid the destabilization of the MR system.
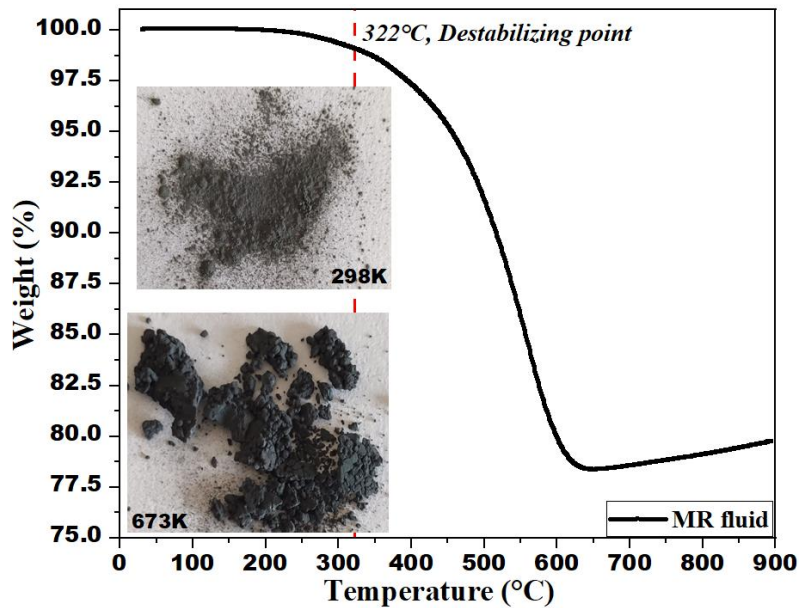
Figure 5.18 TGA of MR fluid

And also, the results from the SEM analysis heat treated particles for ten minutes shows that particles starts to change their shape at 200°C and starts melting at 400°C. The results of TGA and SEM are shown in figures 5.28 and 5.29. These gravimetric results can be used as critical points to evaluate the life expectancy of the MR fluid and its replacement in MR system.
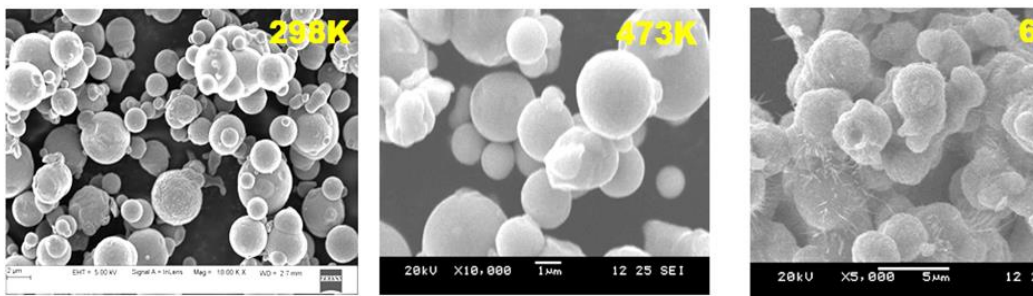
Figure 5.19 SEM images of the MR particles

5.4 Experimental procedure to prepare iron particles

0.1 Molar of Fe $(NO_3)_3$ ·9H2O(make: Loba chemie pvt. ltd, 03829) solution was mixed with 25 mL of distilled water (make: Loba chemie pvt. ltd. 6483C) to form a solution, then 5 mL of NH_3 in 40 ml of water was added intermittently into the mixture under dynamic stirring at 450 rpm in magnetic stirrer for 12 minutes. After

the composition was stirred the mixture was added with 6g of ascorbic acid (make: Loba chemie pvt. ltd, 01549) in 40 ml ethylene glycol and stirred for 15 minutes with heating at 65°C to form a consistent solution before it was moved into a glass plate. The product was collected by centrifugation, washed in ethanol several times, and lastly dried at 80°C using a laboratory incubator. The ready products were characterized using a scanning electron microscope (SEM) (make: Carl Zeiss) and energy-dispersive X-ray (EDS) committed to the SEM. Figure 5.20 -5.22 shows the fabricated particles shape and composition.
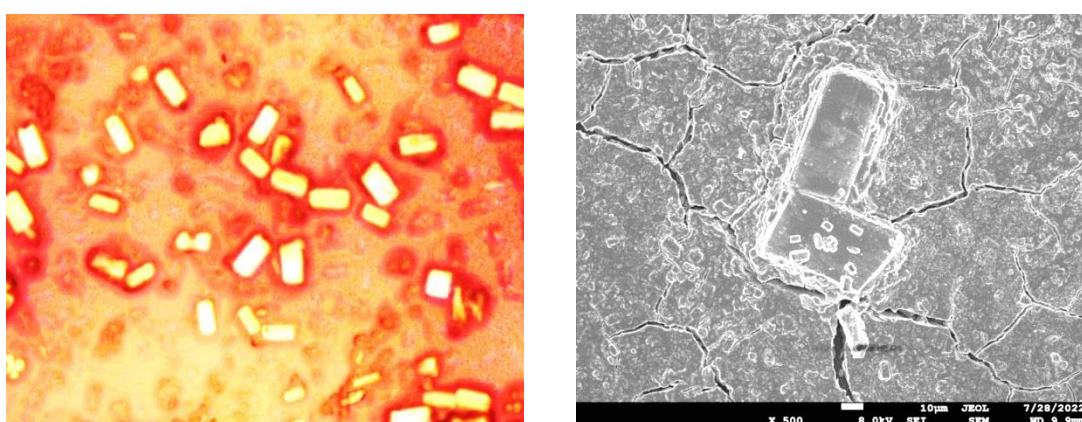
Figure 5.10 Optical microscopic images
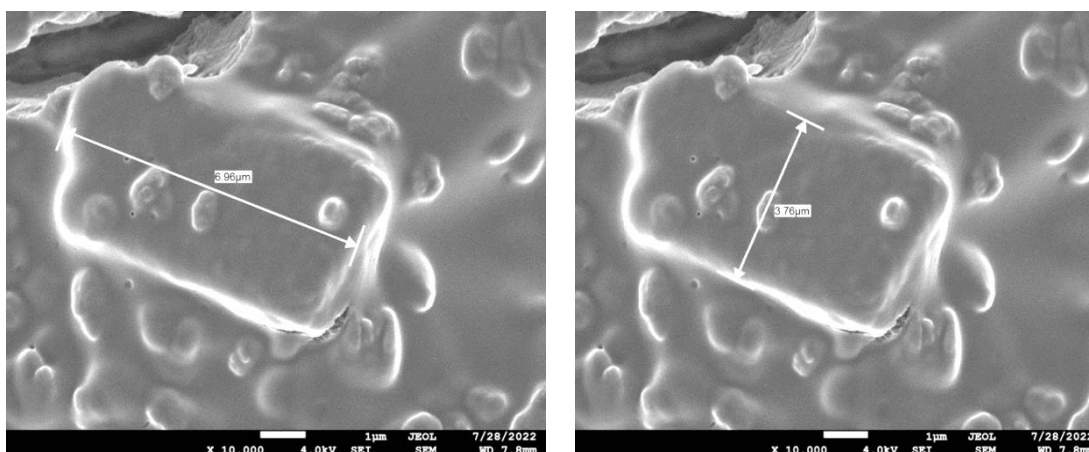
Figure 5.11 Size of the particle
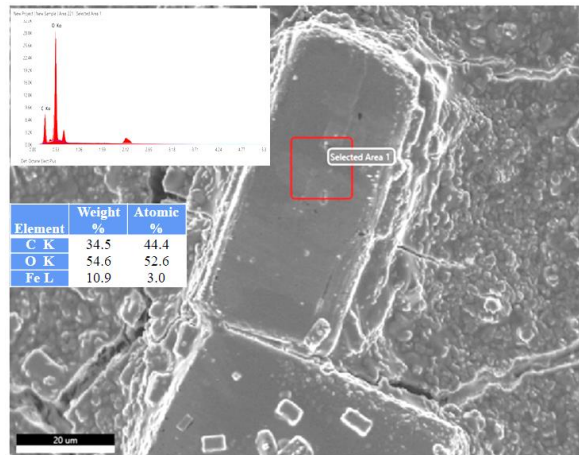
Figure 5.12 EDS of the synthesized particles

Figure 5.23 show the modified design of the MR brake through FEMM analysis for further study using the MR fluid synthesized using the prepared MR particles through a chemical process. The variation in the magnetic field throughout the fluid flow gap is illustrated in the below figure. The maximum magnetic field obtained in the fluid gap is 2.45 times more than that of the earlier design which is depicted in the below figure.
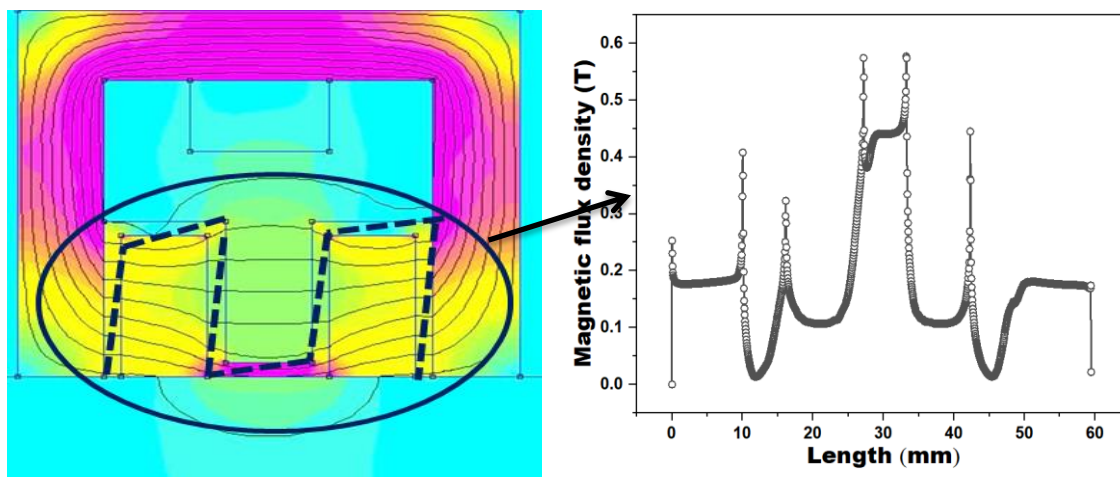
Figure 5.13 Modified design of MR brake and flux density

Variation throughout the length of the gap

5.5 Summary

Better MR fluid (MRF-1) based on stability and yield stress studied in chapter-3 is selected to find the torque generation in the two plate rotor MR brake which is discussed in chapter-5. The results illustrates that the torque generation is increased with increase in current and also results shows the decrease in torque after 450 rpm indicates the shear thinning effect during the testing of the brake. Through characterization of the MR brake it is observed that shear thickening behaviour at the rotor end because lower shearing gap. After completion of the synthesis of MR fluid, characterisation of MR fluid, and testing of MR fluid in the damper and brake the conclusions of all the study are discussed in chapter   6.

CHAPTER 6

SUMMARY AND CONCLUSIONS

6.1 Summary

In this work, CI particles were characterised for their morphology, size, composition, and saturation magnetization using SEM, particle size analyser, XRD, and VSM respectively to verify the feasibility of synthesizing MR fluid. After particle characterisation the synthesis of MR fluid was carried out to study the sedimentation rate and flow characterisation with the application of a magnetic field and temperature. Better MR fluid in terms of settling rate and yield stress was selected to study the effect of the temperature of the MR fluid in the damper on the performance of the damper and two rotor plate MR brakes. The geometric design dimensions of MR damper and brake was chosen from the TOPSIS and FEMM. To measure the temperature of the fluid, a thermocouple was embedded such that the tip of the thermocouple was in contact with fluid and in brake thermocouple was fixed on to the surface of the casing. During the testing of the MR damper and brake the results have been discussed in chapter 3, 4, and 5 respectively. The conclusions and contributions from this work are discussed in the section below.

6.1.1 Effect of Temperature on flow properties of Magnetorheological Fluids

Sedimentation stability and high yield stress of a magnetorheological fluid (MRFs) are essential parameters for better damping performance for any practical application. Preliminary investigations have been carried out on carbonyl iron particles to determine the morphology, particle size, crystal structure, and saturation magnetization for their feasibility of synthesizing magnetorheological fluids in-house. This study synthesizes various MRFs from various commonly used carrier oils and additives. The MRF samples were prepared for 25% volume fractions of carbonyl iron

(CI) powder in either silicone oil (350cSt) or hydraulic oil (50cSt) and by using lithium and calcium-based additives or a combination of both additives. The sedimentation stability and yield behaviour at different temperatures show a remarkable drop in sedimentation rate and yield stress for all the MR fluid samples. The characterization of the prepared MR fluids reveals that MRF-1, MRF-3, MRF-5 are more stable and have high-yield stress values. MRF-1 is selected to further characterize its dynamic performance in magnetorheological damper fabricated based on geometric dimensions obtained from the response surface optimization technique. The results indicate a 164.45% and 135.48% increase in damping force at higher amplitude and higher frequencies at 0A and 1A currents. Further, similar tests have been carried out by synthesizing MRF-7 with silicone oil (50cSt) + lithium base grease as the additive. The sample's stability and yield stress with temperature are carried out, and performance analysis shows a remarkable change in damping force than MRF-1. The dynamic range obtained is more practically viable in MRF-7 than MRF-1, with less variability. Finally, temperature characteristics captured from the thermocouple of the MR damper reveal an average of 43.78% reduction in damping force when the temperature is increased by 19.5 ∘C with increased dynamic range.

6.1.2 Effect of temperature on MR damper Performance

The magnetorheological (MR) system's performance depends on the MR fluid's temperature in operation. This study aims to evaluate the temperature effect of MR fluid on performance while the damper is working. Before synthesizing MR fluid, scanning electron microscopy, X-ray diffraction, and particle size analysis verifies for the synthesis of MR fluid in-house. Characterization of the MR fluid at different temperatures and magnetic fields was carried out. The Herschel-Bulkley model is used to analyse the nonlinearity in the fluid by incorporating the temperature effect. The range of critical parameters used to fabricate the MR damper is selected using the Technique for Order of Preference by Similarity to Ideal Solution (TOPSIS) performance score. The temperature of the MR fluid is measured using an embedded thermocouple while the damper is operating at different loading parameters. The results reveal that the fluid temperature rises significantly from atmospheric to 125.39°C with a decrease in damping force by 66.32% at higher loading parameters. The theoretical model predicts an increase in temperature similar to that of the

174

experimental values with an average error of 10.24% in the on-state condition. Particle characterization after dynamic testing reveals particle morphology has not changed but the saturation magnetization of the particles reduced by 57% at higher temperatures (127°C). It is observed through thermogravimetric analysis (TGA) that the life of the fluid is reduced by 0.25%, which is negligible after dynamic testing of the fluid for approximately 85000cycles. Finally, to imitate the temperature effect on the particle, particles were heat-treated at 200°C, 400°C, and 600°C, and through SEM image, it is confirmed that deterioration of the particle starts after 200°C, if the fluid is operated for a prolonged amount of time.

6.1.3 Performance Analysis of Two-rotor Magnetorheological Brake

The objective of this study is to characterize a two-rotor magnetorheological (MR) brake (Total mass=1.62Kg) for its torque generation for in-house prepared MR fluid. The prepared MR fluids were studied for sedimentation rate at different temperatures and flow behavior at different currents and temperatures. The nonlinearity of the fluid is analyzed through Herschel-Bulkley model. The significant increase in sedimentation rate and decrease in yield stress shows the effect of temperature on the performance of the MR fluid. Finite Element Method Magnetics (FEMM) shows that there is approximately of about 0.145T magnetic flux density in the gap to fabricate the MR brake. The characterization of the MR brake shows that there is an increase in torque with increase current and speed. Further tests have been carried out to identify the effect of sedimentation on torque generation at 52°C after 15 hours of sedimentation. TGA and SEM analysis of the MR fluid and particles shows that 322°C is the start of destabilization of the fluid and after complete destabilization, the particle starts to melt at 400°C which acts as critical points in controlling the MR fluid system input parameters.

6.2 Conclusions

Following are the conclusions drawn from the present study

➢ A combination of lithium base grease additive and silicone oil carrier fluid shows better particle holding ability at higher temperatures for an extended

period. The settling velocity of MR fluid with silicone oil as carrier fluid and lithium grease as an additive (MRF-1) is found to be 50 % lesser in comparison with MR fluid based on hydraulic oil as carrier fluid with calcium base additive (MRF-2).

➢ Characterization of all the MR fluid samples at a higher temperature reveals that MRF-1 gives higher yield stress which is 29.2% more compared MRF-2 at higher temperatures. The variability in controlling the MR damper is obtained from the lower viscosity MR fluid.

➢ The sedimentation rate is accelerated by the temperature of the fluid. The current study results can be utilized to determine the resting time between two subsequent operations of devices to avoid temperature accelerated sedimentation.

➢ The yield stress is affected by temperature and magnetic field, the HB model has been modified to incorporate yield stress as a function of the magnetic field, shear rate, and temperature using the measured data.

➢ The carrier fluid viscosity is a prominent factor in the MR fluid sedimentation stability and the performance of the MR fluid system. Higher carrier fluid viscosity results in higher damping force with less variability to control. Irrespective of input parameters the rise in temperature is observed, while the damper is in operation.

➢ The increase in temperature of the MR fluid from 30 °C to 127 °C decreases the magnetic saturation point by 30 %.

➢ Based on the normal operating conditions of the MR damper, the safety factor can be set for MR damper operating temperature using TGA and SEM results to avoid destabilization of the MR fluid system and increase the life of MR system.

➢ Firstly, in MR brake characterization, an increase in current increases the torque generation. Secondly, keeping a constant current with varying speeds has no impact on torque generation. Further operating MR brake for a prolonged period of time at various speeds make the fluid temperature rise reducing the torque generation.

6.3 Scope for Future Work

- The concentration of particles in synthesizing MR fluids should be set such the preparation of MR fluids should have a standard procedure.

- The design of MR damper can be modified by incorporating heat transfer enhancement devices accordingly to compensate temperature effect and to increase the performance of the damper.

- The non-linear model fitting can be modified by incorporating temperature effect to compensate for the damping force reduction.

- Better control strategies can be designed to compensate for the temperature effect on decreasing damping force by increasing the current supply.

- Miniature MR Brake (Mass $\leq$ 1kg) with increased torque generation can be further carried out to increase the applicability of the MR brake system.

- Real time strategy to control can be employed in MR damper and MR brake by including temperature effect into the required domain.

REFERENCES

Acharya, S., Saini, T. R. S., and Kumar, H. (2019). "Determination of optimal magnetorheological fluid particle loading and size for shear mode monotube damper." *J. Brazilian Soc. Mech. Sci. Eng.*, 41(10).

Allien, J. V., Kumar, H., and Desai, V. (2020). "Semi-active vibration control of MRF core PMC cantilever sandwich beams: Experimental study." *Proc. Inst. Mech. Eng. Part L J. Mater. Des. Appl.*, 234(4), 574–585.

Anupama, A. V., Kumaran, V., and Sahoo, B. (2018). "Magneto-mechanical response of additive-free Fe-based magnetorheological fluids: Role of particle shape and magnetic properties." *Mater. Res. Express*, 5(8).

Arief, I., Sahoo, R., and Mukhopadhyay, P. K. (2016). "Effect of temperature on steady shear magnetorheology of CoNi microcluster-based MR fluids." *J. Magn. Magn. Mater.*, 412, 194–200.

Aruna, M. N., Rahman, M. R., Joladarashi, S., and Kumar, H. (2019). "Influence of additives on the synthesis of carbonyl iron suspension on rheological and sedimentation properties of magnetorheological (MR) fluids." *Mater. Res. Express*, 6(8), 086105.

Ashtiani, M., Hashemabadi, S. H., and Ghaffari, A. (2015). "A review on the magnetorheological fluid preparation and stabilization." *J. Magn. Magn. Mater.*, Elsevier B.V.

Assadsangabi. (2012). "Optimization And Design Of Disk-Type Mr Brakes." *Int. J. ...*, 13(2), 293–300.

Avraam, M., Horodinca, M., Romanescu, I., and Preumont, A. (2010). "Computer controlled rotational MR-brake for wrist rehabilitation device." *J. Intell. Mater. Syst. Struct.*, 21(15), 1543–1557.

Bahiuddin, I., Mazlan, S. A., Shapiai, I., Imaduddin, F., Ubaidillah, and Choi, S. B. (2018). "Constitutive models of magnetorheological fluids having temperature-dependent prediction parameter." *Smart Mater. Struct.*, 27(9).

Bingsan, C. (2017). "Design and Experimental Research on Magnetorheological Rubber Coupled Shock Absorber of Rollers." 32, 202–210.

Bombard, A. J. F., KNOBEL, M., and ALCÂNTARA, M. R. (2007). "Phosphate Coating on the Surface of Carbonyl Iron Powder and Its Effect in Magnetorheological Suspensions." *Int. J. Mod. Phys. B*, 21(28n29), 4858–4867.

Butt, G. (1996). "Pergamon line illustrating how sedimentation type may vary during process ZONE SETTLING CHANNELLING suspension i n t h e f o r m of : separate flocculent f porous media." 9(1), 115–131.

Cheng, H., Hong, W., and Liu, C. (2014). "Study on preparation and thermal conductivity of high stability magnetorheological fluids." *J. Chinese Adv. Mater. Soc.*, 2(2), 130–137.

Choi, Y.-T., Xie, L., and Wereley, N. M. (2016). "Testing and analysis of magnetorheological fluid sedimentation in a column using a vertical axis inductance monitoring system." *Smart Mater. Struct.*, 25(4), 04LT01.

Clair, C. catanzarite and. (1996). "Commercial magnetorheological fluid devices." *Syria Stud.*, 10(23), 2857–2865.

Dogruoz, M. B., Wang, E. L., Gordaninejad, F., and Stipanovic, A. J. (2003). "Augmenting Heat Transfer from Fail-Safe Magneto-Rheological Fluid Dampers Using Fins." *J. Intell. Mater. Syst. Struct.*, 14(2), 79–86.

Dong, X., Tong, Y., Ma, N., Qi, M., and Ou, J. (2015). "Properties of cobalt nanofiber-based magnetorheological fluids." *RSC Adv.*, 5(18), 13958–13963.

Dong, X., Yu, J., Wang, W., and Zhang, Z. (2017). "Robust design of magneto-rheological (MR) shock absorber considering temperature effects." *Int. J. Adv. Manuf. Technol.*, 90(5–8), 1735–1747.

Fang, F. F., Choi, H. J., and Jhon, M. S. (2009). "Magnetorheology of soft magnetic carbonyl iron suspension with single-walled carbon nanotube additive and its yield stress scaling function." *Colloids Surfaces A Physicochem. Eng. Asp.*, 351(1–3), 46–51.

Fu, Y., Yao, J., Zhao, H., Zhao, G., Wan, Z., and Qiu, Y. (2018). "Bidisperse Magnetic Particles Coated with Gelatin and Graphite Oxide: Magnetorheology, Dispersion Stability, and the Nanoparticle-Enhancing Effect." *Nanomaterials*, 8(9), 714.

Gandhi, F., and Bullough, W. A. (2005). "On the phenomenological modeling of electrorheological and magnetorheological fluid preyield behavior." *J. Intell. Mater. Syst. Struct.*, 16(3), 237–248.

Goncalves, F. D., Ahmadian, M., Baird, D., Carlson, D., Inman, D., Kasarda, M., and Leo, D. (2005). *Characterizing the Behavior of Magnetorheological Fluids at High Velocities and High Shear Rates*.

Gorodkin, S. R., Kordonski, W. I., Medvedeva, E. V., Novikova, Z. A., Shorey, A. B., and Jacobs, S. D. (2000). "A method and device for measurement of a sedimentation constant of magnetorheological fluids." *Rev. Sci. Instrum.*, 71(6), 2476–2480.

Gudmundsson, K. H., Jonsdottir, F., and Thorsteinsson, F. (2010). "A geometrical optimization of a magneto-rheological rotary brake in a prosthetic knee." *Smart Mater. Struct.*, 19(3), 035023.

Guerrero-Sanchez, C., Ortiz-Alvarado, A., and Schubert, U. S. (2009). "Temperature effect on the magneto-rheological behavior of magnetite particles dispersed in an ionic liquid." *J. Phys. Conf. Ser.*, 149, 012052.

Guo, Y.-Q., Sun, C.-L., Xu, Z.-D., and Jing, X. (2018). "Preparation and Tests of MR Fluids With CI Particles Coated With MWNTs." *Front. Mater.*, 5(August), 1–8.

Gurubasavaraju, T. M., Kumar, H., and Arun, M. (2017). "Optimisation of monotube magnetorheological damper under shear mode." *J. Brazilian Soc. Mech. Sci. Eng.*, 39(6), 2225–2240.

Hato, M. J., Choi, H. J., Sim, H. H., Park, B. O., and Ray, S. S. (2011). "Magnetic carbonyl iron suspension with organoclay additive and its magnetorheological properties." *Colloids Surfaces A Physicochem. Eng. Asp.*, 377(1–3), 103–109.

Hernando, L., Omari, A., and Reungoat, D. (2015). "Experimental investigation of

batch sedimentation of concentrated bidisperse suspensions." *Powder Technol.*, 275, 273–279.

Holdich, R. (2014). "Solid / liquid separation by sedimentation This item was submitted to Loughborough ' s Institutional Repository (https://dspace.lboro.ac.uk/) by the author and is made available under the following Creative Commons Licence conditions . For the full text ." 1996 (February 1997).

Hong, S. R., Wereley, N. M., Choi, Y. T., and Choi, S. B. (2008). "Analytical and experimental validation of a nondimensional Bingham model for mixed-mode magnetorheological dampers." *J. Sound Vib.*, 312(3), 399–417.

Iglesias, G. R., Roldán, A., Reyes, L., Rodríguez-Arco, L., and Durán, J. D. G. (2015). "Stability behavior of composite magnetorheological fluids by an induction method." *J. Intell. Mater. Syst. Struct.*, 26(14), 1836–1843.

Jha, S., and Jain, V. K. (2009). "Rheological characterization of magnetorheological polishing fluid for MRAFF." *Int. J. Adv. Manuf. Technol.*, 42(7–8), 656–668.

Jiang, W., Zhang, Y., Xuan, S., Guo, C., and Gong, X. (2011). "Dimorphic magnetorheological fluid with improved rheological properties." *J. Magn. Magn. Mater.*, 323(24), 3246–3250.

Jolly, M. R., Carlson, J. D., and Muñoz, B. C. (1996). "A model of the behaviour of magnetorheological materials." *Smart Mater. Struct.*, 5(5), 607–614.

Jönkkäri, I., Isakov, M., and Syrjälä, S. (2015). "Sedimentation stability and rheological properties of ionic liquid–based bidisperse magnetorheological fluids." *J. Intell. Mater. Syst. Struct.*, 26(16), 2256–2265.

Jonsdottir, F., Thorarinsson, E. T., Palsson, H., and Gudmundsson, K. H. (2009). "Influence of parameter variations on the braking torque of a magnetorheological prosthetic knee." *J. Intell. Mater. Syst. Struct.*, 20(6), 659–667.

Karakoc, K., Park, E. J., and Suleman, A. (2008). "Design considerations for an automotive magnetorheological brake." *Mechatronics*, 18(8), 434–447.

Kim, M. S., Liu, Y. D., Park, B. J., You, C. Y., and Choi, H. J. (2012). "Carbonyl iron

particles dispersed in a polymer solution and their rheological characteristics under applied magnetic field." *J. Ind. Eng. Chem.*, 18(2), 664–667.

Krishna, H., Kumar, H., and Gangadharan, K. (2017). "Optimization of Magneto-Rheological Damper for Maximizing Magnetic Flux Density in the Fluid Flow Gap Through FEA and GA Approaches." *J. Inst. Eng. Ser. C*, Springer India.

Kumbhar, B. K., Patil, S. R., and Sawant, S. M. (2015). "Synthesis and characterization of magneto-rheological (MR) fluids for MR brake application." *Eng. Sci. Technol. an Int. J.*, 18(3), 432–438.

Li, G., and Yang, Z. B. (2020). "Modelling and Analysis of a Magnetorheological Damper with Nonmagnetized Passages in Piston and Minor Losses." *Shock Vib.*, 2020.

Li, W. H., and Du, H. (2003). "Design and experimental evaluation of a magnetorheological brake." *Int. J. Adv. Manuf. Technol.*, 21(7), 508–515.

Li, W. H., Liu, B., Kosasih, P. B., and Zhang, X. Z. (2007). "A 2-DOF MR actuator joystick for virtual reality applications." *Sensors Actuators, A Phys.*, 137(2), 308–320.

Li, Y., Luo, Y., Wang, Y., Luo, J., and Chen, Y. (2021). "Research on characterization method and influencing factors of sedimentation stability of magnetorheological fluid." *Korea Aust. Rheol. J.*, 33(4), 309–320.

Lijesh, K. P., Kumar, D., and Gangadharan, K. V. (2018). "Design of magneto-rheological brake for optimum dimension." *J. Brazilian Soc. Mech. Sci. Eng.*, 40(3).

Lim, S. T., Cho, M. S., Jang, I. B., and Choi, H. J. (2004). "Magnetorheological characterization of carbonyl iron based suspension stabilized by fumed silica." *J. Magn. Magn. Mater.*, 282(1–3), 170–173.

Liu, Y. D., Lee, J., Choi, S. B., and Choi, H. J. (2013). "Silica-coated carbonyl iron microsphere based magnetorheological fluid and its damping force characteristics." *Smart Mater. Struct.*, 22(6).

López-López, M. T., Zugaldía, A., González-Caballero, F., and Durán, J. D. G. (2006). "Sedimentation and redispersion phenomena in iron-based

magnetorheological fluids." *J. Rheol. (N. Y. N. Y).*, 50(4), 543–560.

Madhavrao Desai, R., Acharya, S., Jamadar, M. E. H., Kumar, H., Joladarashi, S., and Sekaran, S. R. (2020). "Synthesis of magnetorheological fluid and its application in a twin-tube valve mode automotive damper." *Proc. Inst. Mech. Eng. Part L J. Mater. Des. Appl.*, 234(7), 1001–1016.

Mangal, S. K., and Kumar, A. (2014). "Experimental and Numerical Studies of Magnetorheological (MR) Damper." *Chinese J. Eng.*, 2014, 1–7.

Mangal, S. K., and Kumar, A. (2015). "Geometric parameter optimization of magneto-rheological damper using design of experiment technique." *Int. J. Mech. Mater. Eng.*, 10(1), 1–9.

McKee, M., Gordaninejad, F., and Wang, X. (2018a). "Effects of temperature on performance of compressible magnetorheological fluid suspension systems." *J. Intell. Mater. Syst. Struct.*, 29(1), 41–51.

McKee, M., Gordaninejad, F., and Wang, X. (2018b). "Effects of temperature on performance of compressible magnetorheological fluid suspension systems." *J. Intell. Mater. Syst. Struct.*, 29(1), 41–51.

Mistik, S. I., Shah, T., Hadimani, R. L., and Siores, E. (2012). "Compression and thermal conductivity characteristics of magnetorheological fluid-spacer fabric smart structures." *J. Intell. Mater. Syst. Struct.*, 23(11), 1277–1283.

Morillas, J. R., Bombard, A. J. F., and Vicente, J. De. (2018). "Enhancing magnetorheological effect using bimodal suspensions in the single-multidomain limit." *Smart Mater. Struct.*, 27(7).

Naserimojarad, M. M., Moallem, M., and Arzanpour, S. (2018). "A comprehensive approach for optimal design of magnetorheological dampers." *J. Intell. Mater. Syst. Struct.*, 29(18), 3648–3655.

Ngatu, G. T., and Wereley, N. M. (2007). "Viscometric and sedimentation characterization of bidisperse magnetorheological fluids." *IEEE Trans. Magn.*, 43(6), 2474–2476.

Nguyen, Q. H., and Choi, S. B. (2009). "Optimal design of a vehicle magnetorheological damper considering the damping force and dynamic range." *Smart Mater. Struct.*, 18(1).

Nguyen, Q. H., and Choi, S. B. (2010). "Optimal design of an automotive magnetorheological brake considering geometric dimensions and zero-field friction heat." *Smart Mater. Struct.*, 19(11).

Nikitczuk, J., Weinberg, B., and Mavroidis, C. (2007). "Control of electro-rheological fluid based resistive torque elements for use in active rehabilitation devices." *Smart Mater. Struct.*, 16(2), 418–428.

Parlak, Z., Engin, T., and Çalli, I. (2012). "Optimal design of MR damper via finite element analyses of fluid dynamic and magnetic field." *Mechatronics*, Elsevier Ltd, 890–903.

Parlak, Z., Engin, T., and Şahin, I. (2013). "Optimal magnetorheological damper configuration using the taguchi experimental design method." *J. Mech. Des. Trans. ASME*, 135(8).

Piao, S. H., Bhaumik, M., Maity, A., and Choi, H. J. (2015). "Polyaniline/Fe composite nanofiber added softmagnetic carbonyl iron microsphere suspension and its magnetorheology." *J. Mater. Chem. C*, 3(8), 1861–1868.

Poznic, A., Miloradovic, D., and Juhas, A. (2017). "A new magnetorheological brake`s combined materials design approach." *J. Mech. Sci. Technol.*, 31(3), 1119–1125.

Pu, H., and Jiang, F. (2005). "Towards high sedimentation stability: Magnetorheological fluids based on CNT/Fe3O4 nanocomposites." *Nanotechnology*, 16(9), 1486–1489.

Rabbani, Y., Ashtiani, M., and Hashemabadi, S. H. (2015). "An experimental study on the effects of temperature and magnetic field strength on the magnetorheological fluid stability and MR effect." *Soft Matter*, 11(22), 4453–4460.

Rahim, M. S. A., Ismail, I., Choi, S. B., Azmi, W. H., and Aqida, S. N. (2017).

"Thermal conductivity enhancement and sedimentation reduction of magnetorheological fluids with nano-sized Cu and Al additives." *Smart Mater. Struct.*, 26(11).

Rankin, P. J., Horvath, A. T., and Klingenberg, D. J. (1999). "Magnetorheology in viscoplastic media." *Rheol. Acta*, 38(5), 471–477.

Rossa, C., Jaegy, A., Lozada, J., and Micaelli, A. (2014). "Design considerations for magnetorheological brakes." *IEEE/ASME Trans. Mechatronics*, 19(5), 1669–1680.

Rossa, C., Lozada, J., and Micaelli, A. (2012). "A new hybrid actuator approach for force-feedback devices." *IEEE Int. Conf. Intell. Robot. Syst.*, 4054–4059.

Roupec, J., Mazůrek, I., Strecker, Z., and Klapka, M. (2013). "The behavior of the MR fluid during durability test." *J. Phys. Conf. Ser.*, 412(1).

Sahin, H., Wang, X., and Gordaninejad, F. (2009). "Temperature dependence of magneto-rheological materials." *J. Intell. Mater. Syst. Struct.*, 20(18), 2215–2222.

Sarkar, C., and Hirani, H. (2013). "Synthesis and characterization of antifriction magnetorheological fluids for brake." *Def. Sci. J.*, 63(4), 408–412.

Sarkar, C., and Hirani, H. (2015). "Effect of Particle Size on Shear Stress of Magnetorheological Fluids." *Smart Sci.*, 3(2), 65–73.

Sedlacik, M., Pavlinek, V., Lehocky, M., Mracek, A., Grulich, O., Svrcinova, P., Filip, P., and Vesel, A. (2011). "Plasma-treated carbonyl iron particles as a dispersed phase in magnetorheological fluids." *Colloids Surfaces A Physicochem. Eng. Asp.*, 387(1–3), 99–103.

Shafer, A. S., and Kermani, M. R. (2011). "On the feasibility and suitability of mr fluid clutches in human-friendly manipulators." *IEEE/ASME Trans. Mechatronics*, 16(6), 1073–1082.

Shah, K., Phu, D. X., Seong, M. S., Upadhyay, R. V., and Choi, S. B. (2014). "A low sedimentation magnetorheological fluid based on plate-like iron particles, and verification using a damper test." *Smart Mater. Struct.*, 23(2).

Shamieh, H., and Sedaghati, R. (2017). "Multi-objective design optimization and

control of magnetorheological fluid brakes for automotive applications." *Smart Mater. Struct.*, 26(12).

Shivaram, A. C., and Gangadharan, K. V. (2007). "Statistical modeling of a magnetorheological fluid damper using the design of experiments approach." *Smart Mater. Struct.*, 16(4), 1310–1314.

Singh, H., Singh Gill, H., and Sehgal, S. S. (2016). "Synthesis and Sedimentation Analysis of Magneto Rheological Fluids." *Indian J. Sci. Technol.*, 9(S1).

Song, K. H., Park, B. J., and Choi, H. J. (2009). "Effect of magnetic nanoparticle additive on characteristics of magnetorheological fluid." *IEEE Trans. Magn.*, 4045–4048.

Sukhwani, V. K., and Hirani, H. (2008). "Design, development, and performance evaluation of high-speed magnetorheological brakes." *Proc. Inst. Mech. Eng. Part L J. Mater. Des. Appl.*, 222(1), 73–82.

Vicente, J. de, Vereda, F., Segovia-Gutiérrez, J. P., Puerto Morales, M. del, and Hidalgo-Álvarez, R. (2010). "Effect of particle shape in magnetorheology." *J. Rheol. (N. Y. N. Y).*, 54(6), 1337–1362.

Viota, J. L., González-Caballero, F., Durán, J. D. G., and Delgado, A. V. (2007). "Study of the colloidal stability of concentrated bimodal magnetic fluids." *J. Colloid Interface Sci.*, 309(1), 135–139.

Wahed, A. K. El, and McEwan, C. A. (2011). "Design and performance evaluation of magnetorheological fluids under single and mixed modes." *J. Intell. Mater. Syst. Struct.*, 22(7), 631–643.

Wang, D., Zi, B., Zeng, Y., Hou, Y., and Meng, Q. (2014). "Temperature-dependent material properties of the components of magnetorheological fluids." *J. Mater. Sci.*, 49(24), 8459–8470.

Wang, H., Li, Y., Zhang, G., and Wang, J. (2019). "Effect of temperature on rheological properties of lithium-based magnetorheological grease." *Smart Mater. Struct.*, 28(3).

Weiss. (1994). "Controllable fluids: Temperature dependence of post-yield propereties."

Wereley, N. L., Hu, N. M., and Hiemenz, W. J. (2013). *Analysis of a magnetorheological damper incorporating temperature dependence*. *Int. J. Veh. Des.*

Wiehe, A., Kieburg, C., and Maas, J. (2013). "Temperature induced effects on the durability of MR fluids." *J. Phys. Conf. Ser.*, 412(1).

Wong, P. L., Bullough, W. A., Feng, C., and Lingard, S. (2001). "Tribological performance of a magneto-rheological suspension." *Wear*, 247(1), 33–40.

Yang, Y., Xu, Z. D., Guo, Y. Q., Sun, C. L., and Zhang, J. (2021). "Performance tests and microstructure-based sigmoid model for a three-coil magnetorheological damper." *Struct. Control Heal. Monit.*, 28(11), 1–22.

Yazid, I. I. M., Mazlan, S. A., Kikuchi, T., Zamzuri, H., and Imaduddin, F. (2014). "Design of magnetorheological damper with a combination of shear and squeeze modes." *Mater. Des.*, 54, 87–95.

Yu, M., Wang, S., Fu, J., and Peng, Y. (2013). "Unsteady analysis for oscillatory flow of magnetorheological fluid dampers based on Bingham plastic and Herschel-Bulkley models." *J. Intell. Mater. Syst. Struct.*, 24(9), 1067–1078.

Zaifazlin Zainordin, A., Priyandoko, G., and Mohamed, Z. (2018). *Performance Simulation Analysis for Magnetorheological Damper with Internal Meandering Flow Valve*. *Int. J. Automot. Mech. Eng.*

Zhang, H. H., Liao, C. R., Chen, W. M., and Huang, S. L. (2006). "A Magnetic Design Method of MR Fluid Dampers and FEM Analysis on Magnetic Saturation." *J. Intell. Mater. Syst. Struct.*, 17(8–9), 813–818.

Zhang, P., Dong, Y. Z., Choi, H. J., and Lee, C. H. (2018). "Tribological and rheological tests of core-shell typed carbonyl iron/polystyrene particle-based magnetorheological fluid." *J. Ind. Eng. Chem.*, 68, 342–349.

Zhang, W. L., Liu, Y. D., and Choi, H. J. (2012). "Field-responsive smart composite particle suspension: Materials and rheology." *Korea Aust. Rheol. J.*, 24(3), 147–153.

Zhang, X. Z., Gong, X. L., Zhang, P. Q., and Wang, Q. M. (2004). "Study on the mechanism of the squeeze-strengthen effect in magnetorheological fluids." *J. Appl. Phys.*, 96(4), 2359–2364.

Zhou, W., Chew, C. M., and Hong, G. S. (2007). "Development of a compact double-disk magneto-rheological fluid brake." *Robotica*, 25(4), 493–500.

Zhu, W., Dong, X., Huang, H., and Qi, M. (2019). "Iron nanoparticles-based magnetorheological fluids: A balance between MR effect and sedimentation stability." *J. Magn. Magn. Mater.*, 491.

Zhu, W., Dong, X., Huang, H., and Qi, M. (2021). "Enhanced magnetorheological effect and sedimentation stability of bimodal magnetorheological fluids doped with iron nanoparticles." *J. Intell. Mater. Syst. Struct.*, 32(12), 1271–1277.

Zuzhi, T., Fei, C., Xiangfan, W., and Jian, W. (2016). "A Novel Preparation Process for Magnetorheological Fluid with High Sedimentation Stability." *Mater. Manuf. Process.*, 31(15), 2030–2036.

List of publications

International Journals

1. **Ashok Kumar Kariganaur**, Hemantha Kumar, and Arun M, "Effect of Temperature on Sedimentation Stability and Flow Behaviour of Magnetorheological Fluids with Damper as the Performance Analyser". *Journal of Magnetism and Magnetic Materials*, (Elsevier, IF: 3.097). *https://doi.org/10.1016/j.jmmm.2022.169342*

2. **Ashok Kumar Kariganaur**, Hemantha Kumar, and Arun M, "Influence of Temperature on Magnetorheological Fluid properties and their performance", *Smart Materials and Structures* (IOP, IF: 4.131). *https://doi.org/10.1088/1361-665X/ac6346*

3. **Ashok Kumar Kariganaur**, Hemantha Kumar, and Arun M, "Impact of Particle concentration on Magnetorheological Fluid Properties and Damping performance", *Korea-Australia Rheology Journal* (Springer, IF: 1.446). *https://doi.org/10.1007/s13367-022-00029-8*

4. **Ashok Kumar Kariganaur**, Hemantha Kumar and Arun Mahalingam, "Experimental Investigation on Dual Particle Magnetorheological Fluid and their Performance", *Heat Transfer Engineering*, (Taylor's and Francis, IF: 2.1, *(Under Review)*

5. **Ashok Kumar Kariganaur**, Hemantha Kumar and Arun Mahalingam, "Limiting the Upper Bound of Flow Gap and Effective Length of Magnetorheological Damper through Dynamic Characterisation for Optimal Design and Performance", **Frontiers of Materials**, (Frontiers, IF: 3.960), *(Under review)*

6. **Ashok Kumar Kariganaur**, Hemantha Kumar and Arun Mahalingam, "Effect of reduced geometric dimensions on torque generation in two plate rotor magnetorheological brake with in-house magnetorheological fluid", **Smart Materials and Structures (IOP, IF: 4.1)**. *https://doi.org/10.1088/1361-665X/acb871*

7. **Ashok Kumar Kariganaur**, Hemantha Kumar and Arun Mahalingam, "Experimental Investigation on Feasibility of Using Stokes Settling Law for Batch Settling at Different Temperatures and performance analysis for Magnetorheological fluids using Magnetorheological Damper", *Advances in materials and Processing Technologies (Taylor's and Francis, Scopus journal)* **(Under review)**

International Conferences

1.   **Ashok Kumar Kariganaur**, Hemantha Kumar, M. Arun (2019, December), "Effect of magnetic permeability, shearing length, and shear gap on magnetic flux density of the magnetorheological damper through finite element analysis", 2nd International Conference on Recent Trends in Metallurgy, Material Science and Manufacturing (*IMME2019*), NIT Tiruchirappalli, Tamilnadu. (Materials Today: Proceedings) *https://doi.org/10.1016/j.matpr.2020.05.714*

2.   **Ashok Kumar Kariganaur**, Hemantha Kumar and Arun Mahalingam, (2020, August), "Comparative study on the effect of single coil and multi coil magnetorheological damper through finite element analysis", 1st International Conference on Advances in Physical Sciences and Materials (*ICAPSM2020*), SNSIT Coimbatore, Tamilnadu. (JPCS: Proceedings). *doi:10.1088/1742-6596/1706/1/012193*

1. **FESEM (Field emission scanning electron Microscope) (Make: Carl Zeiss-sigma)**

Specification: Electron Source: Schottky Thermal Field Emitter, Resolution* at 30 kV (STEM): 1.0 nm, Resolution* at 15 kV : 1.0 nm, Resolution* at 1 kV: 1.6 nm, Resolution* at 30 kV (VP Mode) :2.0 nm, Maximum Scan Speed :50 ns/pixel, Accelerating Voltage :0.02 – 30 kV Magnification: $10\times$ – $1,000,000\times$, Probe Current: 3 pA - 20 nA (100 nA (optional), Image Frame store 32 k $\times$ 24 k pixels.

2. **CILAS 1064 Particle size analyser**

Specification: Particle size range: 0.04 to 500 µm, Number of lasers: 2, Laser source: Fibre and collimated laser diodes, Wavelength: 635 and 830 nm, Power :3/7 mW, Beam diameter: 2 and 20 mm, Repeatability :$\pm$ 0.5 %, Reproducibility: < 2 %.

3. Lakeshore:7407- Vibration sample Magnetometer (VSM)

Specification: Make and Model: Lakeshore, USA, Model 7407, Max. Magnetic field: 2.5 T, Dynamic moment range: 1x10e-6emu – 10e3emu.

Vibrating Sample magnetometer feasible measurements

- M Versus H at Room Temperature.
- M Versus T at constant H (Selected Field) M Versus H at constant Temperature (Low Temperature range 20-300K and High Temperature range 300 -1270K

4. **Weighing balance**

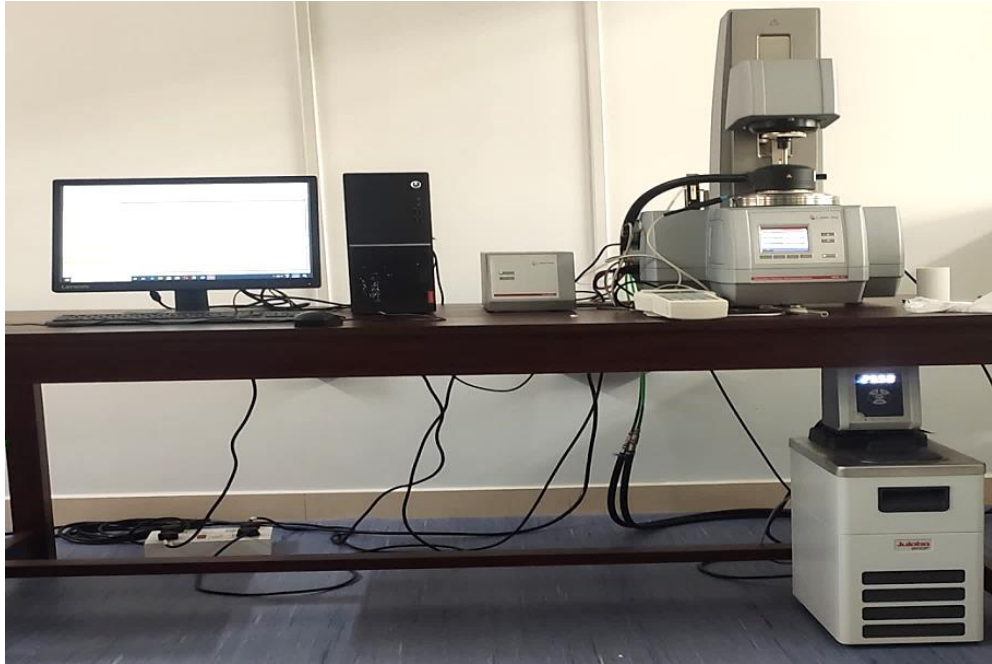**Specification:** Maximum capacity: 1 Kg, Accuracy: 0.1g, Power: 230V AC, 50Hz

5. **Mechanical stirrer (Make: Remitek)**
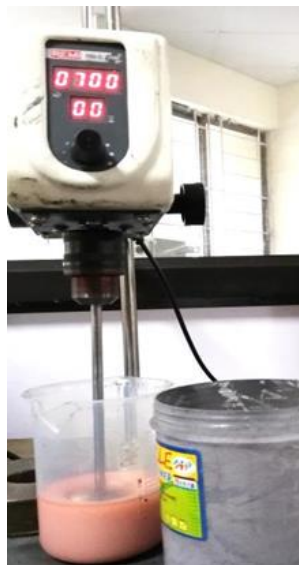
Parameter Specification: Max. Capacity: 5litres, Speed range: 50-1500 rpm, Power: 10W Voltage: 220-240V, frequency: 50 Hz

6. Rheometer MCR702(Make: Anton-Paar, Austria)

Specification: Minimum torque, rotation: 1nNm, Maximum torque, rotation: 230mNm Minimum torque, oscillation: 0.5nNm, Maximum angular frequency: 628 rad/s, Normal force: 0.005 to 50 N, Maximum temperature:160°C to 1000°C, Pressure: up to 1000bar Rheometer Software: RheoCompass, MRD Cell: 1Tesla, Temperature range: -10 to 170°C (Peltier Heating/Cooling), Oil free Motor Power: 0.55 kW, Output (5 bar): 55 l/min max., Pressure: 8 bar, Tank Volume: 10, Weight: 59 kg Power Supply Magneto Cell 230V HCP 14-12500,12.5,1 mA.

7. Damper testing machine (DTM)(Make: Heico India)

Force transducer

Actuator

Load cell

Damper testing machine
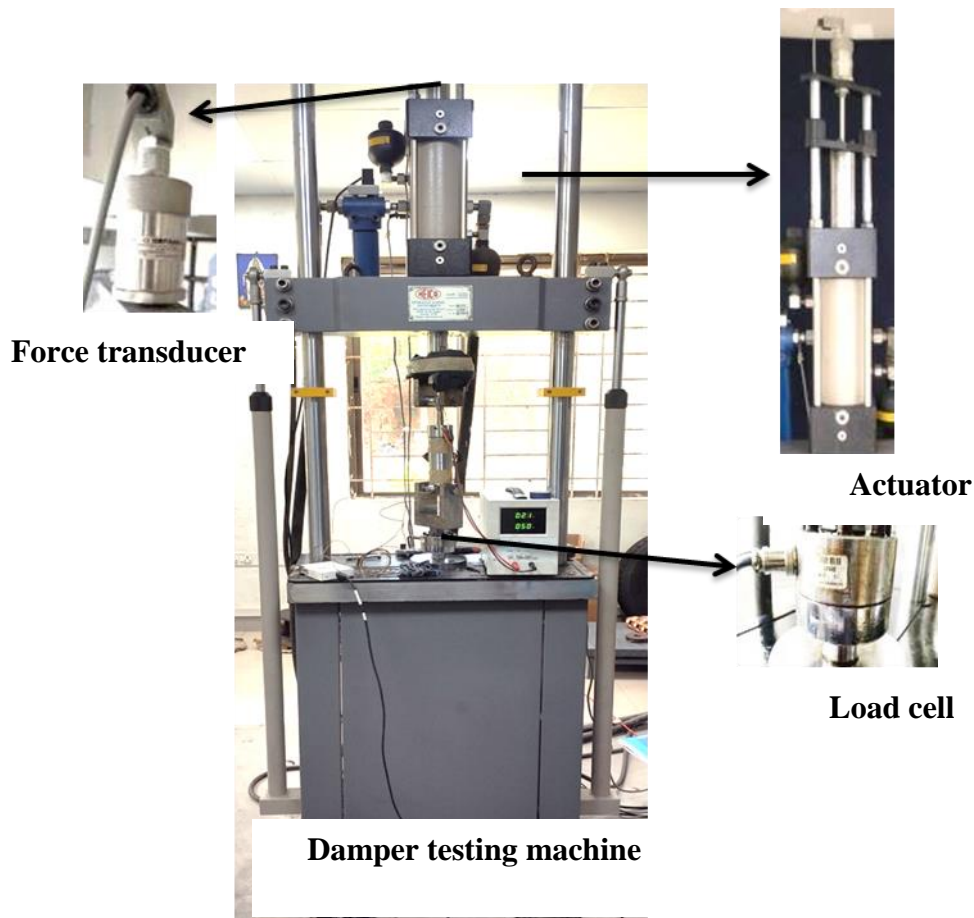
Actuator: Capacity: +/- 20 kN, Stroke: 150 mm (+/- 75 mm) Max., working pressure: 210 bar Max., Velocity: 0.8 m/s- 1.2 m/s, Servo valve: 63LPM, Pressure line filter 180 LPM, Accumulator (2 No.) 0.36 ltr. Capacity

Displacement sensor: Range 200 mm Full scale output 10 volts sampling rate: 2 kHz, Operating temperature: -30 to +75 deg. C

Load cell: Capacity +/- 30kN, Resolution: 0.001kN, Excitation Voltage 10 Volts DC, Operating temperature 0 to +60 deg. C

8. Moog Controller and display unit
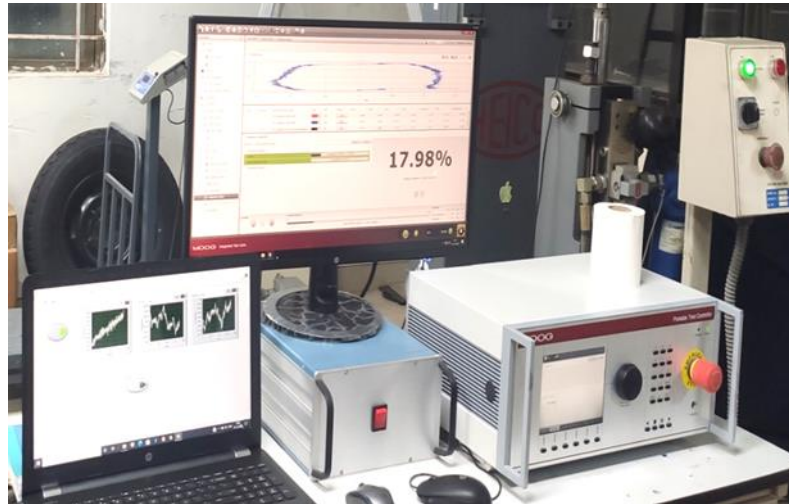
Specifications: Auto PID operation, Digital signal processing based closed loop servo controller with 10 kHz. Number of control channels – 4, Demand wave generation - Sine, Triangular, Square and ramp signal.

9. Hydraulic power pack

Specifications: Flow rate: 64Litres/min,. Operating Pressure: 210 bar,

Capacity: 200 litres, power supply: 440V

10. DC power supply

Specifications: Output: 0 to 30V / 5A, resolution: 10mV, Current: 5 mA Load , Regulation: <= +/-(0.05% + 10 mV), Input Supply: 230 AC +/- 10% / 50-60 Hz, resistance: <=10 milli Ohms

11. NI9211 Thermal DAQ

Specifications: 4-Channel, 14 S/s/ch, ±80mV C Series Temperature Input Module

12. Datum M425 Torque sensor with universal interface

Specifications: Range: 0-50 Nm, Accuracy: 0.1%, Non-Linearity: 0.1%: Repeatability: 0.05%, Sample Rate: 4k samples/sec, Temperature range: -10 to +70˚C, Power supply: 10-24Vdc 250mA.

13. Display unit (Make: Datum electronics)

Specifications: Universal Torque Transducer Interface, Power Supply: 15-24V DC

14. Dimmer stat for speed control

Specifications: Rated Input voltage: 230V, Voltage range: 0– 260V, Max Load: 12.21 kVA Max Current: 15Ampere

15. Motor

Specifications: Power: 3HP, Rated Voltage: 230V DC, Max. Current: 12Ampere, Max speed: 1440 rpm

<center>**BIO-DATA**</center>

Name   Ashok Kumar K.

Date of Birth   30-03-1989

Mobile Number +91 7760938603

Email Id   ashokk.nitk@gmail.com

Address   S/o Gopalappa K., Opposite Amba Mutt, D. No. 64, Pattanaseragu village,   Orvai (post), Kurugodu (taluk), Bellary – 583 113.

Qualification

1   National Institute of Technology Karnataka [Coursework Grade: 7.93] Doctor of Philosophy, (Mechanical Engineering), [2018 – 2022]

2   University Vishweshwaraya College of Engineering, Bangalore (Bangalore University) [Percentage: 86.45 %] Master of Engineering, Thermal Science and Engineering (Mechanical Engineering) [2014 – 2016]

3   National Institute of Engineering, Mysore (Autonomous) [Grade: 8.32] Bachelor of Engineering – B.E., Mechanical Engineering [2008 – 2012]

Work Experience

1   Worked has project associate in mechanical engineering department of Indian Institute of Science, Bangalore for the project "Thermal analysis of Energy efficient aeroponic chamber."
March, 2017 – November, 2017 (09 months, [Position - Project Associate]

2   Worked has junior research fellow (JRF) at NITK Surathkal, Mechanical Engineering, under the project title "CFD analysis of magnetorheological dampers." [November, 2017- September, 2019] [01year 09 months]

3   Worked has full time research fellow at NITK Surathkal, Mechanical Engineering, Under the topic title "Effect of temperature on Magnetorheological fluid and its performance in magnetorheological damper and two plate rotor magnetorheological brake"

<center>202</center>

(Experimental investigation) [October, 2019-October, 2022] [03 Years]

Journal Publications: 05
International Conferences: 03